



University
of Glasgow

Moreton, Fiona Catherine (2016) *The pathophysiology of CADASIL: studies in a Scottish cohort*. PhD thesis.

<http://theses.gla.ac.uk/7533/>

Copyright and moral rights for this thesis are retained by the author

A copy can be downloaded for personal non-commercial research or study

This thesis cannot be reproduced or quoted extensively from without first obtaining permission in writing from the Author

The content must not be changed in any way or sold commercially in any format or medium without the formal permission of the Author

When referring to this work, full bibliographic details including the author, title, awarding institution and date of the thesis must be given

The Pathophysiology of CADASIL: Studies in a Scottish cohort

Fiona Catherine Moreton
BSc (Hons), MBChB (Hons), MRCP (UK)

Submitted in fulfilment of requirements for the Degree of Doctor of Philosophy
Institute of Neuroscience and Psychology
University of Glasgow
January, 2016

“For what purpose humanity is there should not even concern us: why you are there, that you should ask yourself: and if you have no ready answer, then set for yourself goals, high and noble goals, and perish in attempting the great and the impossible.”

Friedrich Nietzsche

Abstract

Since identification that mutations in *NOTCH3* are responsible for cerebral autosomal dominant arteriopathy with subcortical infarcts and leukoencephalopathy (CADASIL) in the early 1990s, there has been extensive characterisation of the clinical and radiological features of the disease. However therapeutic interventions remain elusive, partly due to a limited understanding of the vascular pathophysiology and how it leads to the development of strokes, cognitive decline and disability. The apparent rarity and heterogeneous natural history of CADASIL potentially make conducting any longitudinal or therapeutic trials difficult. The role of disease biomarkers is therefore of some interest.

This thesis focuses on vascular function in CADASIL and how it may relate to clinical and radiological markers of disease. Establishing the prevalence of CADASIL in the West of Scotland was important to assess the impact of the disease, and how feasible a trial would be. A mutation prevalence of 10.7 per 100,000 was demonstrated, suggesting significant under diagnosis of the disease across much of Scotland.

Cerebral hypoperfusion is thought to be important in CADASIL, and it has been shown that vascular abnormalities precede the development of brain pathology in mouse models. Investigation of vascular function in patients, both in the brain and systemically, requires less invasive measures. Arterial spin labelling magnetic resonance imaging (MRI) and transcranial Doppler ultrasound (TCD) can both be used to obtain non-invasive and quantifiable indices of vascular function. Monitoring patients with MRI whilst they receive different concentrations of inspired oxygen and carbon dioxide can provide information on brain function, and I reviewed the practicalities of this technique in order to guide the design of the studies in this thesis.

22 CADASIL patients were recruited to a longitudinal study. Testing included peripheral vascular assessment, assessment of disability, neurological dysfunction, mood and cognition. A CO₂ reactivity challenge during both TCD and arterial spin labelling MRI, and detailed MRI sequences were obtained.

I was able to demonstrate that vasoreactivity was associated with the number of lacunes and brain atrophy, as were carotid intima-media thickness, vessel stiffness, and age. Patients with greater disability, higher depressive symptoms and poorer processing speed showed a tendency to worse cerebral vasoreactivity but numbers were small. This observation suggests vasoreactivity may have potential as a therapeutic target, or a biomarker.

I then wished to establish if arterial spin labelling MRI was useful for assessing change in cerebral blood flow in CADASIL patients. Cortical grey matter showed the highest blood flow, mean (SD), 55 (10) ml/100g/min and blood flow was significantly lower within hyperintensities (19 (4) ml/100g/min; $p < 0.001$). Over one year, blood flow in both grey matter (mean -7 (10) %; $p = 0.028$) and deep white matter (-8 (13) %; $p = 0.036$) declined significantly. Cerebrovascular reactivity did not change over one year.

I then investigated whether baseline vascular markers were able to predict change in radiological or neuropsychological measures of disease. Changes in brain volume, lacunes, microbleeds and normalised subcortical hyperintensity volume (increase of 0.8%) were shown over one year. Baseline vascular parameters were not able to predict these changes, or those in neuropsychological testing.

NOTCH3 is found throughout the body and a systemic vasculopathy has been seen particularly affecting resistance vessels. Gluteal biopsies were obtained from 20 CADASIL patients, and *ex vivo* myography investigated the response to vasoactive agents. Evidence of impairment in both vasodilation and vasoconstriction was shown. The addition of antioxidants improved endothelium-dependent relaxation, indicating a role for oxidative stress in CADASIL pathology. Myography measures were not related to *in vivo* measures in the subgroup of patients who had taken part in both studies.

The small vessels affected in CADASIL are unable to be imaged by conventional MR imaging so I aimed to establish which vessels might be responsible for lacunes with use of a microangiographic map overlaid onto brain images registered to a standard brain template. This showed most lacunes are small and associated with tertiary arterioles.

On the basis of this thesis, it is concluded that vascular dysfunction plays an important role in the pathophysiology of CADASIL, and further assessment of vascular measures in longitudinal studies is needed. Arterial spin labelling MRI should be used as it is a reliable, non-invasive modality that can measure change over one year. Furthermore conventional cardiovascular risk factor prevention should be undertaken in CADASIL patients to delay the deleterious effects of the disease.

Table of Contents

Abstract	3
Author's declaration	11
Acknowledgement	12
List of Tables	13
List of Figures	14
Publications and Presentations	16
Definitions/Abbreviations	18
Chapter 1 - Introduction	20
1.1 Introduction	20
1.2 Clinical characteristics of CADASIL patients	20
1.2.1 Subcortical ischaemic events	22
1.2.2 Migraine	22
1.2.3 Psychiatric disturbance	23
1.2.4 Cognitive impairment	23
1.2.5 Other clinical manifestations	24
1.2.6 Natural history and phenotypic variability in CADASIL	25
1.2.7 Factors influencing disease progression in CADASIL	26
1.2.8 Health burden of CADASIL	27
1.2.9 The need for biomarkers in CADASIL	28
1.3 The molecular basis of CADASIL	28
1.3.1 The NOTCH3 receptor	28
1.3.2 <i>NOTCH3</i> mutations causing CADASIL	29
1.4 The vascular basis of CADASIL and disease biomarkers	31
1.4.1 The role of NOTCH3 in vascular development	31
1.4.2 Histological abnormalities in CADASIL	32
1.4.3 Putative mechanisms of vascular dysfunction	34
1.4.4 The effect of CADASIL on the vascular system	39
1.4.5 Role of vascular abnormalities as biomarkers	41
1.5 Imaging in CADASIL	41
1.5.1 Anatomical MRI markers	41
1.5.2 Imaging brain function <i>in vivo</i>	49
1.5.3 Imaging perfusion, haemodynamics and metabolism	53
1.5.4 Positron Emission Tomography (PET) and Single Photon Emission Computed Tomography (SPECT)	56
1.5.5 Transcranial Doppler ultrasound (TCD)	59
1.6 Summary and aims of thesis	60
Chapter 2 - Materials and Methods	63
2.1 Funding	63
2.2 Ethics	63
2.3 Patient recruitment	63
2.3.1 Inclusion criteria	63
2.3.2 Exclusion criteria	64
2.3.3 Withdrawal of participants	64
2.4 Management of participants	65
2.4.1 Study Protocol	65
2.5 Clinical assessment	66
2.5.1 Clinical definitions	67
2.6 Clinical Scales	67

2.6.1	National Institute of Health Stroke Scale (NIHSS)	67
2.6.2	Modified Rankin Scale (mRS)	69
2.6.3	Hospital Anxiety and Depression Scale (HADS).....	70
2.7	Neuropsychological Testing	72
2.7.1	General Testing Conditions	72
2.8	Vascular Studies	74
2.8.1	Training of the Investigators.....	74
2.8.2	General testing conditions	74
2.8.3	Pulse Wave Analysis.....	75
2.8.4	Pulse Wave Velocity	77
2.8.5	Flow-mediated dilatation of the brachial artery (FMD)	78
2.8.6	Peripheral artery tonometry.....	81
2.8.7	Carotid intima-media thickness (CIMT)	83
2.9	Transcranial Doppler Ultrasound	86
2.9.1	General Testing Conditions	86
2.9.2	Procedure	86
2.9.3	Analysis	87
2.10	Magnetic Resonance Imaging.....	88
2.10.1	General Testing Conditions	88
2.10.2	MRI screening	88
2.10.3	MRI procedure	88
2.10.4	Imaging protocol	89
2.10.5	Gas administration and equipment	92
2.11	MRI image processing	93
2.11.1	Lesion definitions	94
2.11.2	Visual examination of scans	94
2.11.3	Lacune number and volume	96
2.11.4	Subcortical lacunar lesions	97
2.11.5	Cerebral microbleeds.....	97
2.11.6	Subcortical hyperintensity segmentation	99
2.11.7	Other imaging processing	102
Chapter 3	Epidemiology of CADASIL in the West of Scotland	103
3.1	Introduction	103
3.2	Methods	104
3.2.1	Identification of cases.....	104
3.2.2	Population and Geographical area.....	104
3.2.3	Statistics.....	105
3.3	Results.....	105
3.3.1	Disease prevalence.....	105
3.3.2	Mutation prevalence	108
3.3.3	Projected affected cases in Scotland	109
3.4	Discussion	109
3.5	Conclusion	112
Chapter 4	Respiratory Challenge MRI: Practical Aspects	113
4.1	Introduction	113
4.2	Rationale.....	114
4.2.1	Gases.....	115
4.2.2	Carbon dioxide.....	117
4.2.3	Oxygen	119
4.2.4	Acetazolamide	121
4.3	Technique.....	122
4.3.1	Preparation.....	122
4.3.2	Standardisation of testing conditions	123

4.3.3	A trial run	124
4.3.4	The respiratory challenge	125
4.3.5	The Environment and equipment	130
4.4	MRI sequences and examples of use in cerebrovascular disease	133
4.4.1	BOLD signal	133
4.4.2	Cerebral blood flow	134
4.4.3	Dual echo imaging (BOLD and perfusion)	135
4.4.4	Cerebral blood volume	135
4.5	Recommendations	136
4.6	Conclusion	137
Chapter 5 - Impaired cerebral and peripheral vasoreactivity are associated with higher numbers of lacunes in CADASIL.		138
5.1	Introduction	138
5.2	Methods	139
5.2.1	Study cohort	139
5.2.2	Study procedures	139
5.2.3	MRI analysis	140
5.2.4	Statistical analysis	147
5.3	Results	148
5.3.1	MRI markers at baseline	150
5.3.2	Blood flow and reactivity	150
5.3.3	Is peripheral and cerebral vessel function associated with conventional MRI markers?	153
5.3.4	Does vasoreactivity relate to clinical and psychological markers of disease? 156	
5.4	Discussion	157
5.4.1	Strengths	161
5.4.2	Limitations	161
5.5	Conclusion	162
Chapter 6 - Changes in CBF and CVR in CADASIL as measured by TCD and ASL over 1 year.		164
6.1	Introduction	164
6.2	Methods	165
6.2.1	Study cohort	165
6.2.2	Experimental procedures	165
6.2.3	TCD analysis	165
6.2.4	ASL analysis	165
6.2.5	Other radiological measures	169
6.2.6	Statistics	169
6.3	Results	169
6.3.1	Subjects	169
6.3.2	Cerebral blood flow - ASL	173
6.3.3	% Δ CBF and CVR - ASL	177
6.3.4	TCD - MFV and CVR	179
6.3.5	Correlation between TCD and ASL reactivity	180
6.4	Discussion	180
6.5	Conclusion	184
Chapter 7 - Progression of vascular, radiological and clinical markers in CADASIL over 1 year		185
7.1	Introduction	185
7.2	Methods	186
7.2.1	Study cohort	186
7.2.2	Experimental procedures	186

7.2.3	Neuropsychological assessment and analysis.....	186
7.2.4	MRI analysis	187
7.2.5	Baseline predictors.....	193
7.2.6	Statistics.....	193
7.3	Results.....	193
7.3.1	Patient characteristics	193
7.3.2	Radiological change over 1 year	194
7.3.3	Change in processing speed and executive function.	198
7.3.4	Predictors of change in MRI markers	200
7.3.5	Vascular predictors of neuropsychological decline.....	200
7.3.6	Radiological predictors of neuropsychological decline	200
7.4	Discussion	201
7.5	Conclusion	204
Chapter 8 - Does <i>ex vivo</i> myography correlate with <i>in vivo</i> vasoreactivity in CADASIL patients?		205
8.1	Introduction	205
8.2	Methods	207
8.2.1	Funding	207
8.2.2	Ethics.....	207
8.2.3	Patient recruitment.....	207
8.2.4	Study design.....	209
8.2.5	Vessel dissection	210
8.2.6	Myography	211
8.2.7	Data from longitudinal study	212
8.2.8	Imaging data	212
8.2.9	Control data.....	212
8.2.10	Statistics.....	213
8.3	Results.....	213
8.3.1	Concentration response curves.....	215
8.3.2	Effect of NAC	217
8.3.3	Relationship of vasoactive responses.....	217
8.3.4	Vasoactive responses to vessel diameter	218
8.3.5	Vasoactive responses and clinical outcomes	219
8.3.6	Vasoactive responses and radiological outcomes.....	220
8.3.7	<i>Ex vivo</i> vasoactive responses and <i>in vivo</i> vascular assessment	221
8.4	Discussion	222
8.4.1	Strengths	225
8.4.2	Limitations	226
8.5	Conclusion	227
Chapter 9 - Arterial branch order and lenticulostriate artery territory lacunes in CADASIL		228
9.1	Introduction	228
9.2	Methods	229
9.2.1	Sample	229
9.2.2	MRI analysis	229
9.2.3	Clinical rating.....	230
9.2.4	Statistical analysis	231
9.3	Results.....	233
9.3.1	Patient information	233
9.3.2	Lacune dimensions and vessel branching order.....	234
9.4	Discussion	236
9.4.1	Strengths	238
9.4.2	Limitations	238

9.5 Conclusion	239
Chapter 10 - Conclusions	241
10.1 Introduction	241
10.2 Summary of results	241
10.2.1 CADASIL is more common than previously thought.....	241
10.2.2 Age, impaired vasoreactivity and large vessel disease are related to MRI markers of disease	242
10.2.3 ASL MRI can be used effectively in CADASIL and shows that cerebral blood flow declines even over 1 year.	243
10.2.4 Vascular predictors of deterioration remain elusive but warrant further investigation.....	243
10.2.5 Systemic vessels are abnormal and a role for oxidative stress is suggested.....	244
10.3 Place in current literature	245
10.4 Future directions	246
10.5 Closing remarks	248
Appendix 1.....	249
Appendix 2.....	254
List of References	257

Author's declaration

All analyses are the work of the author unless otherwise stated.

Fiona C Moreton BSc (Hons), MBChB (Hons), MRCP (UK)
University of Glasgow, January 2016

Specific contributions are outlined below:

Contributor	Contribution	Chapter
Dr Breda Cullen	Performed and analysed all neuropsychological tests	Chapter 2, 5, 7
Dr Krishna Dani	Second opinion for presence or absence of microbleeds	Chapter 2, 5, 7
Dr Celestine Santosh	Clinical reporting of MRI scans including MR angiography	Chapter 2, 5, 6, 7
Dr Rosario Lopez Gonzalez	Generation of in house macro for cerebral blood flow maps	Chapter 5, 6, 7
Dr David Dickie	Created programme for automated segmentation of hyperintensities	Chapter 6, 7
Dr Paul Rocchiccioli	Gluteal biopsy procedure	Chapter 8
Dr Jane Cannon	Gluteal biopsy procedure	Chapter 8
Dr Aurelie Nguyen Dinh Cat	Myography	
Elisabeth Beattie	Vessel dissection	Chapter 8
Laura McPherson	Vessel dissection and myography	Chapter 8
Dr Thanh Phan	Arteriole branch scoring	Chapter 9
Dr Xuya Huang	Arteriole branch scoring	Chapter 9
Prof Srikanth Velandi	Arteriole branch scoring	Chapter 9
Prof Keith Muir	Arteriole branch scoring	Chapter 9
Dr Richard Beare	Provision of programme for overlaying of map onto scans	Chapter 9

Acknowledgement

I am eternally grateful to my supervisor, Professor Keith Muir, for his continued support throughout my time in Glasgow. Whilst his breadth of knowledge is incredible, the inspiration comes from the fact that patient care is always his primary focus. Professor Christian Delles, and his research team, have been a constant help throughout the four years.

I want to thank the other people who helped with this thesis. Dr Breda Cullen's work was essential for the completion of this thesis. Dr Celestine Santosh gave excellent image analysis support. Dr Maria Rosario Lopez Gonzalez and Dr John McLean were invaluable in my attempts to understand MR physics. Dr Krishna Dani and I enjoyed many useful discussions and Blue Peter style experimentation with gas challenge. Bharath Cheripelli and Salwa El Tawil were willing spare hands and heads when needed. Particular thanks to research nurses Nicola Day and Joanne Flynn, but also to Angela Welch, Wilma Smith and Sally Baird; and of course, Christine Atkin. Professor Rhian Touyz, Dr Augusto Montezano, Dr Aurelie Nguyen Dinh Cat, Elisabeth Beattie, and Adam Harvey were essential in the biopsy project. Dr Paul Rocchiccioli (along with Dr Jane Cannon) was an absolute hero for giving up so much of his time to biopsy buttocks.

I am thankful the University of Glasgow Clinical Research Fellowship committee who funded the initial two years of my post, and the Chief Scientist Office, The Stroke Association and the Neurosciences Foundation for grants.

The neuroradiographers at the INS are not only excellent at their job, but great fun and amazingly supportive. Xuya Huang, Dheeraj Kalladka, David Dickie and Adam Gilmour have kept my work on the straight and narrow in different ways, and I couldn't ask for better support or friends. I am grateful for the support of my Mum, Dad, Frances and Mary, and especially little Ettan for the final inspiration to get my thesis finished. Finally a huge thank you to all the patients and their families who have always made me feel that this research is worthwhile, and who have made the whole experience so enjoyable.

List of Tables

Table 1-1 Summary of differences between <i>Notch3</i> knock-out and <i>Notch3</i> mutant CADASIL mouse models	34
Table 1-2 Definitions relating to brain perfusion	54
Table 1-3 Summary of methods for examining cerebral blood flow	55
Table 2-1 Study schedule	66
Table 2-2 National Institute of Health Stroke Scale	68
Table 2-3 Modified Rankin Scale (mRS): An assessment of disability after stroke.	69
Table 2-4 Summary of cognitive tests used in this study	73
Table 2-5 Recommendations for standardization of subject conditions*	75
Table 2-6 MRI sequence parameters - Part 1	90
Table 2-7 MRI sequence parameters - Part 2	91
Table 2-8 Scheltens scale	96
Table 2-9 Recommended criteria for identification of cerebral microbleeds* ...	97
Table 2-10 EPVS Scale	98
Table 3-1 Mutations detected in the Scottish population	107
Table 3-2 The prevalence of neurological diseases	112
Table 4-1 Methods for delivery of gas	132
Table 4-2 Proposed recommendations for conducting respiratory challenge MRI	136
Table 5-1 Baseline characteristics of CADASIL cohort (n = 22)	149
Table 5-2 Study cohort vascular measurements	150
Table 5-3 Hypercapnia and cerebrovascular reactivity	151
Table 5-4 Brain and peripheral reactivity compared to age and blood pressure	152
Table 5-5 MRI outcomes variables compared to vascular measures	155
Table 5-6 Depression and disability compared with vascular measures	156
Table 5-7 Vascular and radiological markers compared to processing speed ...	157
Table 6-1 Subject characteristics at baseline and year 1	172
Table 6-2 CBF in brain regions measured by ASL and ROI	173
Table 6-3 Correlation and difference in CBF between baseline and year 1	175
Table 6-4 % Δ CBF at baseline and year 1	177
Table 6-5 CVR (%) at baseline and year 1	178
Table 7-1 Clinical and vascular measures at baseline and year 1	194
Table 7-2 MRI markers and prediction of neuropsychological decline	201
Table 8-1 Characteristics of gluteal biopsy cohort (n = 20)	214
Table 8-2 Relationship of vasoactive responses	218
Table 8-3 Vessel responsiveness compared to clinical parameters	220
Table 8-4 Vessel responsiveness compared to radiological measures	220
Table 8-5 <i>Ex vivo</i> vessel responsiveness compared to <i>in vivo</i> vessel reactivity	222
Table 9-1 Demographics and MRI variables of CADASIL patients with LSA lacunes (n = 10)	233
Table 9-2 Rating of each lacune and exclusions	234
Table 9-3 Dimensions of all LSA territory lacunes	235
Table 9-4 Dimensions in secondary and tertiary arterial branch lacunes	235

List of Figures

Figure 1-1 Theory of cognitive impairment in CADASIL	24
Figure 1-2 Natural history of the main clinical manifestations of CADASIL	26
Figure 1-3 The NOTCH3 receptor	28
Figure 1-4 3D Model of NOTCH3 first EGF-like repeat domain.....	30
Figure 1-5 Electron microscopy of a dermis arteriole in a patient with CADASIL	33
Figure 1-6 The NOTCH3ECD cascade hypothesis of CADASIL	37
Figure 1-7 Characteristic radiological findings in CADASIL - Subcortical hyperintensities.....	43
Figure 1-8 Characteristic radiological findings in CADASIL - Lacunes, microbleeds and perivascular spaces	44
Figure 1-9 Arterial spin labelling (ASL) technique	59
Figure 1-10 Summary of thesis aims	61
Figure 2-1 Hospital Anxiety and Depression Scale - Scoring Sheet	71
Figure 2-2 Pulse wave analysis	76
Figure 2-3 Carotid-femoral pulse wave velocity	78
Figure 2-4 Flow mediated dilatation of the brachial artery.....	80
Figure 2-5 Example of FMD result	81
Figure 2-6 Reactive hyperaemia index using Endo-PAT®.....	82
Figure 2-7 Carotid intima media thickness (CIMT).....	85
Figure 2-8 MRI room set up	89
Figure 2-9 MRI patient monitor interface	92
Figure 2-10 Gas administration set-up	93
Figure 2-11 Subcortical hyperintensity segmentation methods.....	100
Figure 2-12 Subcortical hyperintensity thresholding repeatability.....	101
Figure 2-13 Examples of subcortical hyperintensity segmentation	102
Figure 3-1 Cumulative number of CADASIL pedigrees diagnosed in Scotland....	106
Figure 3-2 Location of CADASIL probands.....	108
Figure 4-1 Physiology of gas transport	117
Figure 4-2 The effect of O ₂ and CO ₂ on cerebral blood flow.....	119
Figure 4-3 Fixed inspiratory challenge	127
Figure 4-4 Repeated challenges during continuous imaging	128
Figure 5-1 Calculation of intracranial cavity (ICC) volume.....	141
Figure 5-2 Perfusion and CBF maps created from ASL MRI	144
Figure 5-3 Creation of masks	145
Figure 5-4 Applying masks to CBF maps.....	146
Figure 5-5 Cerebral blood flow, mean flow velocity and age.....	151
Figure 5-6 Systolic blood pressure compared to cerebrovascular reactivity....	153
Figure 5-7 Factors associated with number of lacunes	154
Figure 6-1 Deep white matter mask	167
Figure 6-2 Repeatability of ASL region of interest measures in 5 individuals ...	168
Figure 6-3 Exclusions for ASL	170
Figure 6-4 Exclusions for TCD.....	171
Figure 6-5 Cerebral blood flow	174
Figure 6-6 CBF at baseline and year 1 in grey matter and deep white matter in centrum semiovale	176
Figure 6-7 Cerebral blood flow compared to age and change over 1 year.....	177
Figure 6-8 Cerebrovascular reactivity at baseline and year 1.	178
Figure 6-9 Transcranial Doppler ultrasound cerebrovascular reactivity baseline and year 1	179
Figure 6-10 Cerebrovascular reactivity at baseline and year 1.	180

Figure 7-1 Intracranial cavity volume at baseline and year 1.....	187
Figure 7-2 Creation of T1 difference maps for new lacune identification	189
Figure 7-3 Threshold SH volume compared to automated method.....	191
Figure 7-4 Automated subcortical hyperintensity segmentation of baseline and year 1 FLAIR images.....	192
Figure 7-5 Baseline versus Year 1 normalised subcortical hyperintensities.....	195
Figure 7-6 Subcortical hyperintensity probability maps	196
Figure 7-7 Percentage brain volume change (PBVC) over 1 year compared to age	197
Figure 7-8 T1 difference maps.....	198
Figure 7-9 Neuropsychological measures.....	199
Figure 7-10 Peripheral vasoreactivity and neuropsychological decline.....	200
Figure 8-1 Gluteal tissue sample in normal saline	210
Figure 8-2 Mulvany-Halpern myograph	211
Figure 8-3 Effect of acetylcholine (a) and sodium nitroprusside (b) on isolated resistance arteries from control subjects and patients with chronic heart failure	216
Figure 8-4 Concentration response curves in gluteal resistance arteries	216
Figure 8-5 Vessel responsiveness with and without N-acetylcysteine (NAC).....	217
Figure 8-6 Endothelium-dependent and independent relaxation at 10^{-5}	218
Figure 8-7 Vessel diameter and contraction to phenylephrine	219
Figure 8-8 Relaxation to sodium nitroprusside in comparison to number of lacunes	221
Figure 8-9 Flow mediated dilatation and contraction to phenylephrine	222
Figure 9-1 Lacune and brain on MNI template with overlaid microangiographic template	230
Figure 9-2 Worksheet for rating of lacunes and arterial branching order.....	232
Figure 9-3 Width and height in secondary and tertiary arterial branch lacunes	236
Figure 9-4 Lacune volume	236
Figure 10-1 Risk factors and potential biomarkers in CADASIL	246

Publications and Presentations

Papers

- Cerebral hyperperfusion on Arterial Spin Labelling MRI during CADASIL migrainous encephalopathy. Moreton FC, Santosh C, McArthur K, Muir KW. *Neurology* 2015, 85(24): 2177-2179
- Changing Clinical Patterns and increasing prevalence in CADASIL Moreton FC, Razvi SSM, Davidson R, Muir KW. *Acta Neurologica Scandinavica* 2014; 130(3): 197-203.
- Cerebral small vessel disease: Capillary pathways to stroke and cognitive decline. Østergaard L, Engedal TS, Moreton FC, Hansen MB, Wardlaw JM, Dalkara T, Markus HS, Muir KW. *JCBFM* 2016; 36(2): 302-325.
- Cysteine-sparing CADASIL mutations in NOTCH3 show pro-aggregatory properties in vitro. Wollenweber F, Hanecker P, Bayer-Karpinska A, Malik R, Bazner H, Moreton F, Muir K, Müller S, Giese A, Opherk X, Dichgans M, Haffner C, Duering M. *Stroke* 2015; 46(3):786-792
- Oxygen Challenge MR Imaging in Healthy Human Volunteers. Dani K, Moreton FC, Santosh C, Lopez-Gonzalez, MR, Brennan D, Schwarzbauer C, Goutcher C, O'Hare K, Macrae IM, Muir KW. *JCBFM* 2016 (online ahead of print).
- Resting state connectivity and cognitive performance in adults with cerebral autosomal dominant arteriopathy with subcortical infarcts and leukoencephalopathy (CADASIL). Cullen, B, Moreton, FC; Stringer, MS; Krishnadas, R, Kalladka, D; Lopez-Gonzalez, MR, Santosh, C; Schwarzbauer, C and Muir, KW. *JCBFM* (accepted 2016).
- Respiratory Challenge MRI - Practical Aspects. Moreton FC, Dani KA, Goutcher C, O'Hare K, Schwarzbauer C, Muir KW (submitted for review).
- Cerebral and peripheral vasoreactivity in CADASIL: comparison to structural MRI and neuropsychology. Moreton FC, Cullen B, Delles C, Santosh C, Lopez-Gonzalez R, Dani K, Schwarzbauer C, Muir KW. 2016 (in preparation).
- What size should a lacune be? A study in pure small vessel disease. Moreton FC, Phan T, Beare R, Huang X, Srikanth V, Muir KM . 2016 (in preparation)
- Capillary dysfunction in CADASIL. Engedal TS, Moreton FC, Cullen B, Boldsen JK, Eskildsen S, Dalby RB, Mikkelsen IK, Lopez-Gonzalez MR, Bo Hansen M, Mouridsen K, Muir KM, Østergaard, L. 2016 (in preparation).

Abstract publications

- Resting state connectivity and cognitive performance in adults with Cerebral Autosomal-Dominant Arteriopathy with Subcortical Infarcts and Leukoencephalopathy (CADASIL). Cullen B, Moreton F, Stringer M, Krishnadas R, Kalladka D, Lopez-Gonzalez, M.R, Santosh C, Schwarzbauer C, Muir KW. *INS/ASSBI 5th Pacific Rim Conference* 2015
- Arterial spin labelling MRI in CADASIL: Impaired cerebrovascular reactivity is associated with an increased number of lacunes. Moreton

- FC, Cullen B, Santosh C, Schwarzbauer C, Lopez Gonzalez MR, Muir KW. *International Journal of Stroke* (2015): 10(Suppl. S2): 369.
- **Dimensions of lacunar infarcts associated with the lenticular artery territory in CADASIL.** Moreton FC, Beare R, Huang X, Muir KW, Srikanth V, Phan T. *International Journal of Stroke* (2015): 10(Suppl. S2): 370.
 - **The role of microvascular dysfunction in CADASIL.** Engedal TS, Moreton F, Cullen B, Boldsen JK, Eskildsen SF, Mikkelsen IK, Hansen MB, Mouridsen K, Muir K, Østergaard L. *International Journal of Stroke* (2015): 10(Suppl. S2):329.
 - **Stability of SWI acute ischaemic signs during transient hyperoxia.** Dani K, Moreton F, Huang X, Kalladka D, Cheripelli B, Muir K. *International Journal of Stroke* (2015): 10 (Suppl. S2): 308.
 - **Increasing prevalence of CADASIL and delay to first vascular event.** Moreton FC, Razvi SSM, Davidson R, Muir KW. *International Journal of Stroke* 2012;7 (Suppl.2): 57.
 - **CADASIL phenotype associated with a cysteine-sparing NOTCH3 mutation.** Moreton FC, Bazner H, Davidson R, Muir KW. *Cerebrovascular Diseases* 2012; 33(Suppl. 2): 930-931.
 - **Peripheral vascular function in CADASIL: Endothelial dysfunction is associated with increased number of lacunes.** Moreton F, Delles C, Lopez-Gonzalez R, Santosh C, Muir K. *Scottish Cardiovascular Forum* 2/2014.
 - **Atypical ischaemia in CADASIL patients.** Moreton FC, Muir KW. *Cerebrovascular Diseases* 2013; 35 (Suppl. 3): 522.
 - **Compound heterozygosity for typical NOTCH3 mutations in CADASIL.** Moreton FC, Bradley T, Tyagi A, Muir KW. *Cerebrovascular Diseases* 2014; 37 (Suppl. 1): 639.
 - **Relationship between white matter hyperintensities and executive dysfunction in Cerebral Autosomal Dominant Arteriopathy with Subacute Infarcts and Leukoencephalopathy (CADASIL).** Cowan S, Moreton FC, Copstick S, Muir KW. *International Journal of Stroke* 2012;7 (Suppl.2): 43.
 - **Assessment of vascular phenotyping in patients at cardiovascular risk.** Brown C, Ghaus A, Currie G, Moreton F, Flynn J, Delles C. *Journal of Hypertension* 2014: 32(e-suppl. 1): e522.

Platform Presentations

- **CADASIL: Cerebral and peripheral perfusion and reactivity**
Invited speaker. Glasgow Neuroscience Day, Caledonia University 2015.
- **Impaired cerebrovascular and peripheral reactivity are associated with an increased number of lacunes in CADASIL**
Imaging Cerebral Physiology Symposium 2014; Leipzig, Germany.
- **CADASIL: a neurovascular perspective**
Invited speaker. Capillary transit time heterogeneity conference 2014; Aarhus, Denmark.
- **Impaired peripheral endothelial function is associated with number of lacunes in CADASIL.** Moreton FC, Delles C, Lopez-Gonzalez MR, Santosh C, Cullen B, Schwarzbauer C, Muir KW. ESC 2014. *Cerebrovascular Diseases* 2014; 37 (Suppl. 1):164

Definitions/Abbreviations

ACE	angiotensin-converting enzyme
ACh	acetylcholine
ADAS-Cog	Alzheimer's Disease Assessment Scale - cognitive subscale
Arg	arginine
ASL	arterial spin labelling
AI	augmentation index
AI@75	augmentation index at heart rate 75bpm
AP	anterior-posterior
BBB	blood brain barrier
BOLD	blood oxygenation level dependent imaging
BET	brain extraction tool
BHF GCRC	British Heart Foundation Glasgow Cardiovascular Research Centre
BP	blood pressure
CADASIL	cerebral autosomal dominant arteriopathy with subcortical infarcts and leukoencephalopathy
CBF	cerebral blood flow
CBV	cerebral blood volume
CMRO ₂	cerebral metabolic rate of oxygen
CMR _{gluc}	cerebral metabolic rate of glucose
CIMT	carotid intima-media thickness
cm	centimetres
CO ₂	carbon dioxide
CSF	cerebrospinal fluid
CSVD	cerebral small vessel disease
CT	computed tomography
CVR	cerebrovascular reactivity
CVR _{ASL}	cerebrovascular reactivity measured by arterial spin labelling
CVR _{TCD}	cerebrovascular reactivity measured by transcranial doppler
Cys	cysteine
DTI	diffusion tensor imaging
DWI	diffusion weighted imaging
ECD	extracellular domain
ECG	electrocardiography
EGF	epidermal growth factor
eGFR	estimated glomerular filtration rate
eNOS	endothelial nitric oxide synthase
ER	endoplasmic reticulum
EtCO ₂	fraction of end-tidal carbon dioxide concentration.
FiCO ₂	fraction of inspired carbon dioxide concentration
FLAIR	fluid Attenuated Inversion Recovery
fMRI	functional magnetic resonance imaging
FMD	flow mediated dilatation
FSL	FMRIB Software Library
GM	grey matter
GOM	granular osmiophilic material
GRE	gradient echo T2* weighted sequence
HADS	Hospital Anxiety and Depression Scale
HbA1c	glycated haemoglobin (A1c)
LSA	lenticulostriate arteries
MAP	mean arterial pressure

MARS	Microbleed anatomical rating scale
MDRS	Mattis dementia rating scale
MFV	mean flow velocity (in cm per second).
MIPAV	Medical Image Processing Analysis, and Visualisation
MMSE	Mini-mental state examination
MNI	Montreal Neurological Institute
MRA	magnetic resonance angiography
MRI	magnetic resonance imaging
mRS	Modified Rankin score
MTR	magnetisation transfer ratio
NAWM	normal appearing white matter
NIHSS	National Institutes of Health Stroke Scale
NO	nitric oxide
NOTCH3	human protein
<i>NOTCH3</i>	human gene
Notch3	non-human protein
<i>Notch3</i>	non-human gene
NBV	normalised brain volume
NLV	normalised lacune volume
NSH	normalised subcortical hyperintensity volume
OEF	oxygen extraction fraction
O ₂	oxygen
PaCO ₂	arterial tension of carbon dioxide
PET	positron emission tomography
Phe	phenylephrine
PWI	perfusion weighted imaging
PWA	pulse waveform analysis
PWV	pulse wave velocity
RBPJ-κ	Recombinant signal binding protein for immunoglobulin kappa J
RFA	Rankin focussed assessment.
RHI	reactive hyperaemia index
ROI	region of interest
SBP	systolic blood pressure
SD	standard deviation
SH	subcortical hyperintensities
SNR	signal-to-noise ratio
SNP	sodium nitroprusside
SPECT	single photon emission computed tomography
SRA	small resistance artery
SWI	susceptibility weighted imaging
TCD	transcranial Doppler
TE	echo time
TI	inversion time
TIA	transient ischaemic attack
TR	repetition time
TOF	time-of-flight
TOPF	test of premorbid function
T2	T2 weighted MR imaging
T2*-GRE	T2-weighted gradient-recalled echo
Tyr	tyrosine
VSMC	vascular smooth muscle cell
WM	white matter
Yrs	years

Chapter 1 - Introduction

1.1 Introduction

Cerebral autosomal dominant arteriopathy with subcortical infarcts and leukoencephalopathy, known by the acronym CADASIL, is a rare inherited small vessel vasculopathy (Joutel et al., 1996). It is caused by mutations in the *NOTCH3* gene, and inherited in an autosomal dominant pattern. The mutation is ubiquitous in small vessel smooth muscle cells throughout the body.

Symptomatology however is confined to the brain, with stroke, executive cognitive impairment, depression and apathy occurring, usually manifesting in young to mid-adulthood. The condition can have devastating effects, not only on the affected individual, but on their extended family, many of whom will also be at risk of developing the disease. This chapter will commence with a brief review of the clinical characteristics, and then focus on vascular pathophysiology and imaging methods for examining disease status *in vivo*.

1.2 Clinical characteristics of CADASIL patients

New diseases are identified by identifying a pattern of repeated clinical or pathological features. Otto Binswanger, a prominent German neuropathologist, described an insidious clinical condition characterised by weakness, disinhibition and cognitive impairment, which correlated with brain atrophy and blood vessel degeneration. “Binswanger’s disease” was proposed to be due to chronic hypertension resulting in small vessel disease and stroke (Caplan, 1995). The 1955 description of a similar disease in two sisters, but in the absence of hypertension, is thought to represent the earliest description of CADASIL in the medical literature (Van Bogaert, 1955). Several other families with an apparent autosomal dominant inherited condition resulting in stroke, neuropsychiatric disease and headache, in the absence of conventional cardiovascular risk factors, were identified across Europe over the next 40 years, and classified under a variety of eponyms (Sourander and Walinder, 1977, Sonninen and Savontaus, 1987, Salvi et al., 1992). In 1991, a large French pedigree was described where members experiencing stroke-like episodes demonstrated neuroimaging evidence of small infarcts and leukoencephalopathy (Tournier-

Lasserve et al., 1991). Shortly afterwards the affected gene was identified as *NOTCH3*, found on chromosome 19 (Joutel et al., 1996). The authors proposed the acronym CADASIL, to describe the genetic, radiological and histological features.

Whilst CADASIL has only been recently described, it has subsequently been proposed to be the cause of illness in both the philosopher Friedrich Nietzsche (1844 - 1900)(Hemelhoet et al., 2008), and the art critic and writer John Ruskin (1819 - 1900)(Kempster and Alty, 2008). Both wrote poetically about their thoughts and their illness, and their medical records were preserved.

Nietzsche, a philosopher with significant influence on 20th century politics, suffered severe headaches throughout his life time diagnosed as migraine, along with depression and periods of hypomania. An acute cognitive and psychiatric collapse prompted his admission under the care of Otto Binswanger in 1889. Diagnosed with tertiary syphilis, despite an absence of supportive physical symptoms, and evidence that Nietzsche was celibate (Sax, 2003), he lived another 11 years developing subcortical dementia (Butler, 2013). Several strokes prior to his death from pneumonia in 1900 left him bedbound and mute. His father, suffered headaches, depression, seizures and dementia, dying aged 36, and his paternal grandfather was also reported to have had similar symptoms (Hemelhoet et al., 2008). Butler et al, argued that Nietzsche's writing was influenced by his disease: his concise and distinctive style was necessitated by periods of inactivity brought about by severe migraines and depression (Butler, 2013).

John Ruskin was a prominent and well respected writer of the 19th century, whose writing was more verbose and evocative:

“Just before dinner, zigzag frameworks of iridescent light fluttered by in my eyes, and I could no longer read even large print” John Ruskin

Accompanying his migraines was a “relapsing encephalopathy” characterised by delusional thinking, hallucinations, agitation and confusion, associated with vomiting and pyrexia. Eventually his mental status declined, and he lost the ability to write. A history of mood disturbance and headache were also described in his father (Kempster and Alty, 2008).

Such cases, whilst remaining genetically unproven, give an idea of the symptoms that can be seen in CADASIL.

1.2.1 Subcortical ischaemic events

Stroke and transient ischaemic attacks (TIA) are a common manifestation of CADASIL, with a wide distribution in age of onset, but classically in early middle age (mean 46 years)(Chabriat et al., 2009). It may be the presenting feature. Recurrent ischaemic events occur in the absence of, or out of proportion to, conventional vascular risk factors, and may lead to progressive disability with impaired gait, pseudobulbar palsy and urinary incontinence (Opherk et al., 2004). Strokes are proposed to be due to small vessel disease affecting the white matter resulting in subcortical infarcts, although large territorial infarcts, and cortical microinfarcts have also been reported (Rubio et al., 1997). Intracerebral haemorrhage has been described (MacLean et al., 2005, Pradotto et al., 2012), associated with hypertension (Choi et al., 2006) and anticoagulant use (Werbrouck and De Bleecker, 2006).

1.2.2 Migraine

Migraine prevalence in CADASIL is significantly higher than in the general population at around 50% (Guey et al., 2015). This may vary according to the prevalence of migraine in the general population from which the patients originate as migraine has been found to be less common in Asian patients (Wang et al., 2011). The majority of patients with migraine have an associated aura, which is often atypical, characterised by prolonged or severe neurological disturbance (Liem et al., 2010). Migraine is often the first symptom a patient experiences. They may decrease in frequency or disappear entirely after the first ischaemic event (Dichgans et al., 1998).

A rare clinical event, termed “CADASIL coma” has been described in patients with a history of migraine (Schon et al., 2003). Patients experience a typical migraine, but then become confused with fever, behavioural change, hallucinations and seizures. Encephalitis may be suspected, but complete recovery is the norm, and stereotyped recurrences can occur (Schon et al., 2003).

1.2.3 Psychiatric disturbance

At least a quarter of CADASIL patients experience psychiatric or mood disturbance, depression being the most frequent complaint (Valenti et al., 2008). Depression is common in patients with stroke and theories for its aetiology include ischaemic interruption of frontal pathways, disruption of serotonin metabolism, or functional limitations and fear about the future (Spalletta et al., 2006). Depression in CADASIL can affect a patient's quality of life, and can contribute to apparent cognitive impairment (Peters et al., 2010). Adjustment disorders, substance dependence and suicide have all been reported, along with bipolar disorder (Valenti et al., 2011).

Psychotic presentations suggestive of schizophrenia have been described in CADASIL, including auditory hallucinations, grandiose delusions and catatonia (Harris and Christopher, 2001, Lagas and Juvonen, 2001). Given the prevalence of schizophrenia is around 0.5 - 1% (McGrath et al., 2008), co-existent diagnosis of the two diseases, rather than CADASIL being causative must be considered. Acute psychosis has been described, including post-partum (Pantoni et al., 2005), highlighting the manifest possible neuropsychiatric presentations.

Apathy, a reduction in goal-driven behaviour, is reported to be a major problem in CADASIL, present in 41% of patients (Reyes et al., 2009). Associated with older age, lack of education, and disability, it is often concurrent with depression.

1.2.4 Cognitive impairment

Cognitive impairment in CADASIL has been described as mainly affecting executive function, and is similar to the pattern seen in sporadic small vessel disease (Amberla et al., 2004, Buffon et al., 2006, Charlton et al., 2006). Progressive difficulties with decision-making, concentration, planning or judgement are seen. Patients may display inappropriate behaviour, such as aggression or personality change.

Deficits in working memory and processing speed may be found in asymptomatic patients (Amberla et al., 2004). Post-stroke, patients have been shown to develop further deficits in verbal fluency, error monitoring and visuospatial

skills, possibly caused by subcortical damage occurring at critical sites (Amberla et al., 2004). Deficits accrue slowly over time, and demented patients show impairments across multiple cognitive domains, but in contrast to Alzheimer's disease, episodic memory is well-preserved. One study suggested over 60% of patients over 60 years were demented, due to a progression of global cerebral damage, including atrophy (see Figure 1-1)(Buffon et al., 2006). Such figures need to be seen in the context of increasing diagnosis of CADASIL, which may result in the identification of milder disease phenotypes.

Many of the diagnostic criteria and standardised neuropsychological tests used for evaluation of cognition were developed for the detection of memory impairment characteristic of Alzheimer's disease, and may have less sensitivity for conditions like CADASIL. Testing for vascular cognitive impairment both clinically, and in trials, should therefore focus on tests of mental speed and executive function, in order to detect subtle early change, which may not be detectable in more global measurements of cognition such as the mini-mental state examination (Dichgans, 2009, Hachinski et al., 2006).

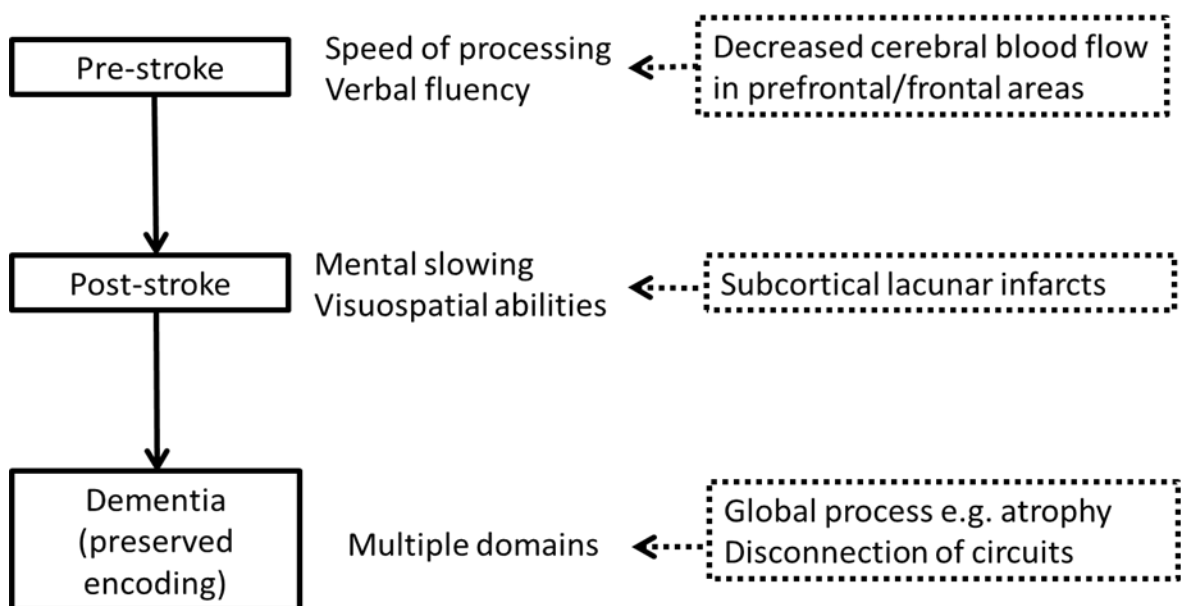


Figure 1-1 Theory of cognitive impairment in CADASIL

1.2.5 Other clinical manifestations

Seizures occur in approximately 10% of CADASIL patients probably as a consequence of subcortical damage (Dichgans et al., 1998). Status epilepticus has been described as the presenting feature of CADASIL in an 80 year old

female (Haddad et al., 2015). Auditory problems like sudden onset sensorineural hearing loss and tinnitus can occur, which may be related to pathology within the labyrinth artery (Phillips et al., 2005) or brainstem ischaemia.

Given that NOTCH3 is found throughout the body, it is surprising that clinical manifestations remain limited to the brain. Whilst case reports of systemic abnormalities occur, there has been no consistent evidence of clinically relevant end-organ damage, despite histological abnormalities. Retinal studies have demonstrated pathological abnormalities such as narrowed vessels and loss of vascular smooth muscle cells (Haritoglou et al., 2004), along with reduced retinal blood flow (Rufa, 2004). These changes may result in direct damage to the retinal nerve cells (Rufa et al., 2011), but functional complications of this have rarely been reported.

1.2.6 Natural history and phenotypic variability in CADASIL

Migraine is often the first presenting feature at around 30 years of age, with ischaemic stroke occurring in the 5th-6th decades, accompanied by psychiatric disturbance (see Figure 1-2). Cognitive deterioration follows these changes, and progresses over time (Chabriat et al., 2009).

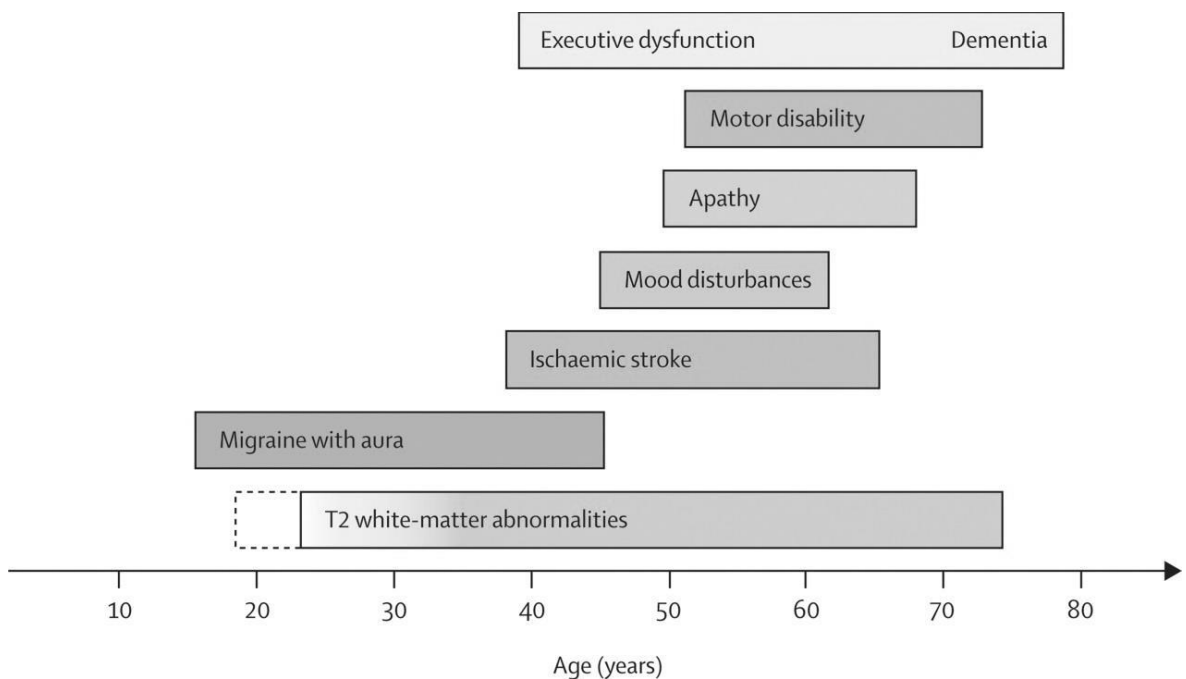


Figure 1-2 Natural history of the main clinical manifestations of CADASIL

The exact age at the earliest onset of first MRI abnormalities is uncertain (dotted line). The frequency of T2-white matter abnormalities increases progressively. Reprinted from *Lancet Neurology*; 8(7), Chabriat et al, CADASIL, 643-653, copyright (2009), with permission from Elsevier.

Despite well-described clinical features, there is a wide variation in severity and age of onset of clinical symptoms, even within families. Thus the natural history in CADASIL is unpredictable and longitudinal studies have demonstrated that patients can remain stable or even improve over significant periods of time (Opherk et al., 2004). As patients are so inherently variable, and definitive clinical events, such as stroke, are infrequent, demonstrating the effectiveness of any potential treatment would be difficult. Peters and colleagues calculated an average incidence rate of stroke of 10.4 per 100 person years in CADASIL patients. Power calculations demonstrated that for this endpoint and a minimum treatment effect of 20%, 2646 patients would need to be recruited, a prohibitively large number for a relatively uncommon disorder (Peters et al., 2004a).

1.2.7 Factors influencing disease progression in CADASIL

The natural history might be modified by conventional cardiovascular risk factors. Current smoking has been associated with an increased risk, and earlier onset of ischaemic events (Singhal et al., 2004). Hypertension may increase

stroke risk (Adib-Samii et al., 2010). Gender is relevant: migraine with aura is more frequent in women, and stroke more frequent in men before the age of 51 (as per the general population), but subjects become more similar after menopausal age (Gunda et al., 2011). Ovarian hormones may influence the natural history of CADASIL, although there is insufficient evidence for their therapeutic use (Gunda et al., 2011). Apolipoprotein E (*APOE*) genotype, a major risk factor for Alzheimer's disease and haemorrhages in amyloid, was thought not to be associated with structural MRI lesions in CADASIL (van den Boom et al., 2006). However a recent study of 448 CADASIL patients has suggested *APOE* ϵ 2 was associated with a higher volume of white matter disease (Gesierich et al., 2016).

Genetic factors have also been proposed to influence disease phenotype, but in a prospectively recruited study of 127 subjects from 65 families, no association between site of mutation and stroke, dementia, migraine or MRI lesion load was shown (Singhal et al., 2004). The study was hampered by only recruiting small numbers from each family. Genome-wide association studies have suggested multiple genes may have small effects on white matter disease burden (Opherk et al., 2014).

1.2.8 Health burden of CADASIL

Given the significant clinical manifestations secondary to CADASIL, patients can become severely disabled and may represent a significant health and social care burden. It is thought that CADASIL is rare (Razvi et al., 2005b), but as more is known about the disease, it is likely a wider spectrum of cases will be identified and the prevalence will increase. Dementia and disability are common, and indeed inevitable in CADASIL if a patient lives long enough. A better appreciation of the prevalence of CADASIL will be important in directing healthcare resources, and in planning the design of any therapeutic trials. The rare nature of the disease is however likely to necessitate any clinical trials being run internationally over multiple sites, and consortiums have already been developed to facilitate this (Gesierich et al., 2016)

1.2.9 The need for biomarkers in CADASIL

A biological marker, or biomarker, is defined as:

A characteristic that is objectively measured and evaluated as an indicator of normal biological processes, pathogenic processes, or pharmacologic response to a therapeutic intervention.

(Biomarkers Definitions Working Group, 2001)

The variable and infrequent nature of clinical endpoints such as stroke or death in CADASIL, make studies of factors which influence disease progression, and are thus potentially amenable to intervention more difficult. Therefore biomarkers which may represent pathogenic processes may be helpful in furthering understanding of this disease.

1.3 The molecular basis of CADASIL

1.3.1 The NOTCH3 receptor

CADASIL is caused by mutations of the *NOTCH3* gene on chromosome 19p13, which encodes a single pass heterodimeric transmembrane receptor, with a large extracellular domain comprised of 34 epidermal growth-factor (EGF) like repeats (Figure 1-3) (Joutel et al., 1996). NOTCH3 is a member of the highly conserved Notch signalling family, first identified in *Drosophila melanogaster*, where haploinsufficiency of Notch resulted in notched wing margins (Mohr, 1919). The Notch signalling pathway is essential for cell fate decision-making in the metazoan embryo via local cell-to-cell interactions (Artavanis-Tsakonas et al., 1999).



Figure 1-3 The NOTCH3 receptor

The extracellular domain is comprised of 34 epidermal growth factors (EGF) like repeats and 3 Notch-LIN12 repeats (LNR). The intracellular domain consists of a transmembrane zone (TM), 6 ankyrin repeats (ANK), and a PEST sequence (proline, glutamate, serine, threonine) degradation domain, which has a role in NOTCH receptor turnover (Rogers et al., 1986).

Produced by the endoplasmic reticulum (ER), the NOTCH3 receptor undergoes proteolysis in the Golgi apparatus, and is then expressed on the cell membrane. Here it interacts with transmembrane ligands such as Delta or Jagged, via its ligand-binding domain (EGF like repeats 10 and 11 in NOTCH3). This results in conformational change and cleavage of the receptor, with shedding of the extracellular domain (ECD), which subsequently undergoes transendocytosis (Parks et al., 2000). The remaining segment is a substrate for further proteolysis resulting in release of the NOTCH3 intracellular domain and its translocation to the nucleus (De Strooper et al., 1999). Interaction with the DNA transcription factor RBPJ- κ , results in activation of primary gene targets including the hairy and enhancer of split related (*HESR*) genes (Jarriault et al., 1995). Despite a relatively simple core pathway, Notch receptors have enormous context specific versatility. The pleiotropic effects of signalling is likely introduced through interactions with ancillary proteins, other signalling pathways and atypical ligands (Hofmann and Iruela-Arispe, 2007).

1.3.2 *NOTCH3* mutations causing CADASIL

The secondary structure of each EGF-like repeat in the NOTCH3 extracellular domain consists of a 2-stranded β -sheet stabilised by 3 disulphide bonds between 6 cysteine residues (Campbell and Bork, 1993). Mutations which result in an uneven number of cysteine residues in one of the EGF-like repeats cause CADASIL. Initially these were all thought to be missense mutations (Joutel et al., 1996), but splice-site (Joutel et al., 2000b), deletions (Dotti et al., 2004) and insertions (Mazzei et al., 2008) have subsequently also been identified (Federico et al., 2005). Alterations in disulphide bond formation is thought to result in aberrant protein folding and distorted secondary structures (Figure 1-4) (Dichgans et al., 2000).

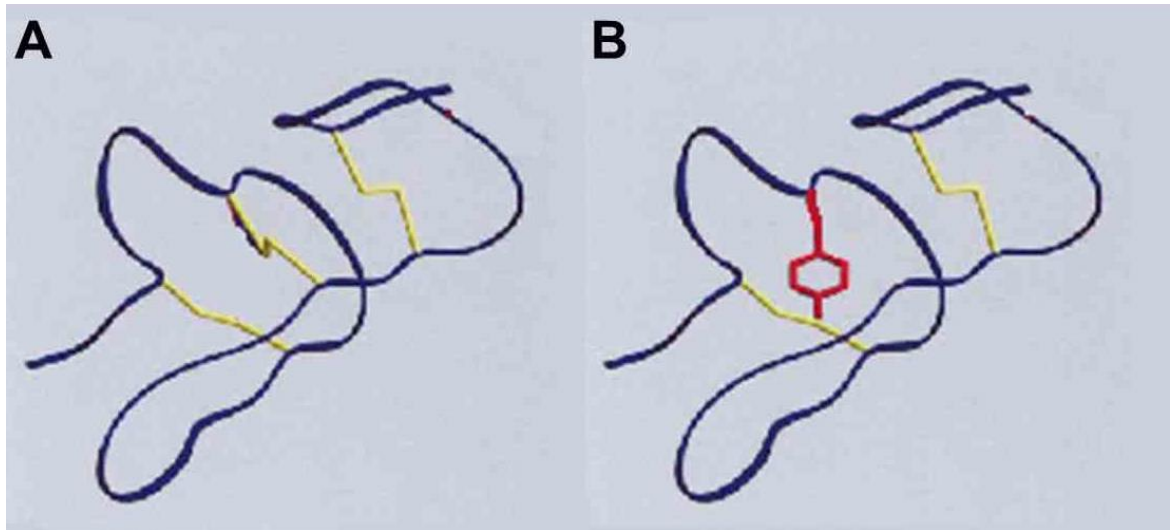


Figure 1-4 3D Model of NOTCH3 first EGF-like repeat domain

(A) A 2-stranded beta-sheet is followed by a double hairpin. The 6 cysteines form 3 disulphide bonds (yellow), which stabilise the beta-sheet and hairpin. (B) A mutated side chain at position 49 which represents the missense mutation Cys49Tyr. The stabilising disulphide bond is lost leading to loss of secondary protein structure. Modified with permission from Macmillan Publishers Ltd: [European Journal of Human Genetics, Dichgans et al, Small in-frame deletions and missense mutations in CADASIL: 3D models predict misfolding of Notch3 EGF-like repeat domains. European Journal of Human Genetics (2000); 8: 280-285.]

Mutations in *NOTCH3*, which do not involve cysteine residues, have been identified in families with similar clinical phenotypes, brain imaging and skin biopsy changes to CADASIL, which suggests the spectrum of mutations responsible for CADASIL may well be extended (Wollenweber et al., 2015).

Specific genotype-phenotype patterns have been proposed in CADASIL, particularly in those mutations which involve the ligand-binding domain. The Cys455Arg mutation in EGF-like repeat 11, was proposed to result in an earlier onset of stroke in patients (Arboleda-Velasquez et al., 2002). It is likely however, that due to the low prevalence of CADASIL and huge number of mutations, international databases of patients will be the only way to identify reliable genotype-phenotype correlations.

1.4 The vascular basis of CADASIL and disease biomarkers

1.4.1 The role of NOTCH3 in vascular development

The Notch signalling pathway has a key role in the development of the embryonic cardiovascular system, where endothelial cell precursors are remodelled into a complex system of arteries, veins and capillaries. As reviewed by Hofmann and Iruela-Arispe, loss of function mutations of key components of the Notch signalling pathway such as Notch1, Notch4, DLL4, JAG1 and Hey1/Hey2 genes results in embryonic lethality due to failure of vascular remodelling (Hofmann and Iruela-Arispe, 2007).

Notch3 null mice are viable and fertile suggesting that Notch3 is not essential for the development of the cardiovascular system in utero (Domenga et al., 2004). The blood vessels of new-born *Notch3* null mice are indistinguishable from wildtype littermates; both are immature, with a loose network of mural cells. If Notch3 has a role in the development of the embryonic vascular system, it appears to have functional overlap with other Notch receptors.

Postnatally the vascular system continues to develop based on genetic preprogramming, but also in response to environmental cues including flow and shear stress. The arterial vascular smooth muscle cells (VSMCs) of *Notch3* null mice at postnatal day 28, display abnormal orientation and morphology, with a disorganised VSMC layer and a venous pattern of maturation (Domenga et al., 2004). This suggests Notch3 is required to maintain the phenotypic specification of arterial VSMCs. Notch3 is proposed to act as part of a sensor, transducing changes in pressure and flow into rearrangements of the VSMC cytoskeleton, in order to maintain arterial phenotype whilst adapting to circulatory changes. Cyclic circumferential strain induced *in vitro* has been shown to downregulate Notch signalling *in vitro*, and hence reduce VSMC proliferation (Morrow et al., 2005). Examination of renal arterial tone in *Notch3* null mice, demonstrated a failure to adapt to changes in blood pressure (Boulos et al., 2011). Notch3 is therefore proposed to act as a signal transducer of biomechanical signals within vessels via regulation of VSMC differentiation, maturation and apoptosis

(Sweeney et al., 2004) potentially through the expression of key vascular components such as smooth muscle α -actin and platelet-derived growth factor (Nosedá et al., 2006, Jin et al., 2008). There is also evidence for *Notch3* being involved in blood vessel repair (Linder et al., 2001).

1.4.2 Histological abnormalities in CADASIL

The macroscopic appearance of the brain shows atrophy. White matter rarefaction is seen in the centrum semiovale and periventricular white matter, with lacunes and enlarged perivascular spaces (Ruchoux and Maura, 1997). Multiple lacunes are also seen in deep grey matter and brainstem.

Microscopic abnormalities affect the small penetrating arterioles and are characterised by a thickening of the arterial media with deposition of a granular, electron dense substance, termed granular osmiophilic material (GOM) (Baudrimont et al., 1993). Found within VSMC indentations (Figure 1-5), GOM is considered pathognomonic of CADASIL (Tikka et al., 2009) and the NOTCH3 extracellular domain is a key component (Joutel et al., 2001, Ishiko et al., 2006). VSMCs show significant abnormalities including swollen mitochondria, thin cells and multiple infoldings (Ruchoux et al., 1994). There is loss of tight junctions and VSMCs may be completely destroyed leaving ghost cells.

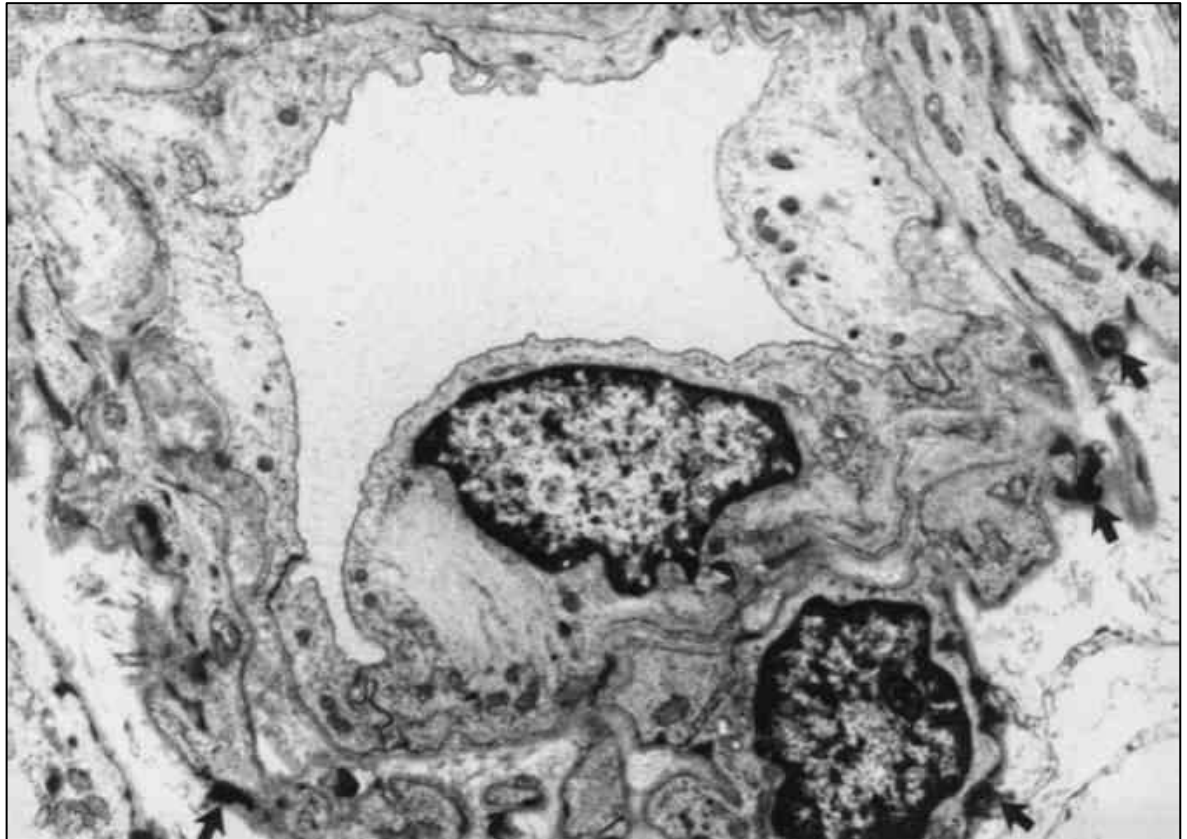


Figure 1-5 Electron microscopy of a dermis arteriole in a patient with CADASIL
Multiple accumulations of granular deposits in the broadened and reduplicated basal lamina (arrows). X 15800. Reproduced with permission from Springer Science and Business Media, *J Neurol* 246 (1999); 526-532, Mayer et al, Figure 4. Muscle and skin biopsies are a sensitive diagnostic tool in the diagnosis of CADASIL.

Endothelial cells display subtle abnormalities which may be secondary to VSMC dysfunction (Ruchoux and Maurage, 1998). Morphometric vessel analysis has been conflicting: Miao and colleagues suggested penetrating vessels have an increased wall thickness and narrowed lumen, which may lead to impaired cerebral blood flow (Miao et al., 2004), whereas Brulin and colleagues found vessel walls were not thickened but rather VSMC were destroyed and replaced by extracellular material (Brulin et al., 2002). This may lead to “earthen pipe” status where the vessel is devoid of autoregulation (Okeda et al., 2002).

Cortical grey matter was initially thought to be unaffected in CADASIL but vessel wall changes, GOM and cortical microinfarcts have now been demonstrated (Miao et al., 2004). Neuronal apoptosis, associated with subcortical white matter disease, has been demonstrated in cortical layers 3 and 5, subsequent to retrograde neuronal degeneration (Viswanathan et al., 2006a).

1.4.3 Putative mechanisms of vascular dysfunction

Typically genetic mutations which affect receptors result in haploinsufficiency or neomorphic gene function, and both have been proposed as the mechanism of CADASIL. The theories about the pathogenesis of CADASIL are outlined below.

1.4.3.1 Theory 1: Hypomorphic function

Mutation of a receptor may lead to loss of function of that receptor, and subsequent reduction in downstream signalling, called hypomorphic function. CADASIL mutant mice do not however, display the same vascular phenotype as mutant mice lacking *Notch3*. The differences are shown in Table 1-1.

Table 1-1 Summary of differences between *Notch3* knock-out and *Notch3* mutant CADASIL mouse models

	<i>Notch3</i> null model [*]	<i>Notch</i> mutant models [^]
Embryonic development & viability	Normal	Normal
Fertility	Normal	Normal
Histology	Thin & disorganised VSMC	Age dependent GOM deposits & Notch3 aggregation Reduced capillary density
Blood pressure	Normal	Normal
Resting CBF	Normal	Low
Vasoreactivity	Impaired vasoconstriction	Impaired vasodilatation
Parenchymal pathology	Nil	In some models

^{*}(Krebs et al., 2003, Domenga et al., 2004); [^](Ayata, 2010, Joutel et al., 2010)

Young CADASIL mutant mice are able to rescue a *Notch3* null mouse phenotype, arguing signalling and Notch3 function is preserved in mutant receptors (Monet et al., 2007). However, expression of another CADASIL mutant (Arg1031Cys) in older *Notch3* null mice, failed to rescue the stroke susceptibility phenotype, which may suggest this mutation displays a weak hypomorphic nature more evident with age (Arboleda-Velasquez et al., 2011). *In vitro* studies have

demonstrated that most mutations, show preserved ligand binding and retain their ability to activate normal signalling (Joutel et al., 2004, Low et al., 2007, Haritunians et al., 2002). The insidious onset of CADASIL also suggests that absence of normal signalling is unlikely to be responsible for the clinical picture.

However, mutations within the ligand-binding domain do result in reduced ligand binding and decreased downstream gene transcription (Joutel et al., 2004, Arboleda-Velasquez et al., 2011). They are unable to rescue a Notch3 null phenotype (Monet-Lepretre et al., 2009). GOM deposits still form with these mutations, suggesting ligand binding is not a prerequisite for its formation. Some authors have proposed that mutations within the ligand-binding domain are associated with different clinical phenotypes, but this is not consistently reported (Monet-Lepretre et al., 2009, Arboleda-Velasquez et al., 2002).

More recently families have been described with nonsense NOTCH3 mutations of exon 3, resulting in a truncated, non-functional protein (Rutten et al., 2013, Moccia et al., 2015). Whilst clinical and radiological features were similar to those seen in CADASIL and VSMC were abnormal, GOM was not detected, and the gene did not appear to be fully penetrant. Therefore whilst loss of NOTCH3 function is likely to have vascular significance, and may represent a different inherited cerebral small vessel disease, it is unlikely to be the driving force of CADASIL (Joutel, 2013).

1.4.3.2 Theory 2: Gain of function

Leu1515Pro is a gain of function mutation of exon 25, out with the EGFR, which results in over activation of the NOTCH3 receptor, and produces similar clinical effects to CADASIL (Fouillade et al., 2008). However it does not cause the accumulation of GOM, and therefore represents a novel small vessel disease rather than CADASIL.

1.4.3.3 Theory 3: Disordered receptor trafficking and recycling

The abnormal protein structure caused by mutations (Dichgans et al., 2000) is proposed to result in abnormal processing and trafficking of the receptor within the cell.

Once formed within the ER, NOTCH3 undergoes post-translational modifications, which modulates NOTCH ligand preference. *In vitro* models of several CADASIL mutations demonstrated a reduction in FRINGE glycosylation of the receptor, thought to affect receptor maturation and cleavage (Arboleda-Velasquez et al., 2005). Impaired S1 cleavage of Arg142Cys demonstrated in a mouse model, further suggested problems with receptor maturation, although experimental methods were criticised (Joutel et al., 2004, Karlstrom et al., 2002).

A human *in vitro* model of NOTCH3^{Cys542Tyr} suggested the mutation resulted in improper cell surface presentation and impaired signalling (Joutel et al., 2004), but most evidence suggested the amount of cleaved receptor presented at the cell surface is preserved (Arboleda-Velasquez et al., 2005). However this may reflect both impaired delivery and clearance. The NOTCH3 ECD accumulates at the plasma membrane suggesting impaired clearance (Joutel et al., 2000a) and the ratio of uncleaved:cleaved NOTCH3 is higher than normal (Peters et al., 2004b). Watanabe-Hosami and colleagues, found NOTCH3^{Cys185Arg} was degraded at the cell surface more slowly than wild-type NOTCH3, with impaired transendocytosis, and proposed this as the mechanism for ECD accumulation (Watanabe-Hosomi et al., 2012).

Proteome analysis of CADASIL human VSMC, demonstrated upregulation of proteins involved in ER quality control system and oxidative stress, suggesting the presence of misfolded proteins requiring recycling (Ihalainen et al., 2007). Saturation of protein degradation systems can result in the generation of reactive oxidative species and ER stress. Mitochondrial abnormalities have been described which may be due to the effect of oxidative free radicals (Annunen-Rasila et al., 2006). ER stress may be exacerbated by the formation of protein aggregates, and mutant receptors are known to show enhanced dimerization (Opherck et al., 2009). Expression of mutant CADASIL proteins in human embryonic kidney cells resulted in impaired protein degradation, and protein aggregation within the ER. This had a cytotoxic effect which resulted in reduced cellular proliferation (Takahashi et al., 2010).

Of note, impaired trafficking and accumulation of abnormal protein in the Golgi is a recognised pathogenic mechanism seen in Marfan's syndrome, where

mutations in the number of cysteine residues in EGF repeat of elastin, result in its accumulation in the ER (Aoyama et al., 1993).

Thus a hypothetical model is of impaired post-translational modification with abnormal secondary folding, impaired receptor cleavage and protein aggregation. Aggregation of abnormal protein both within and out with the cell, result in undetermined cytotoxic effects. The NOTCH3 ECD may act as a seed for formation of multiprotein aggregates (see Figure 1-6). However development of GOM alone is probably insufficient to explain vascular abnormalities seen as changes in VSMC are seen prior to the detection of GOM in murine models (Ruchoux et al., 2003).

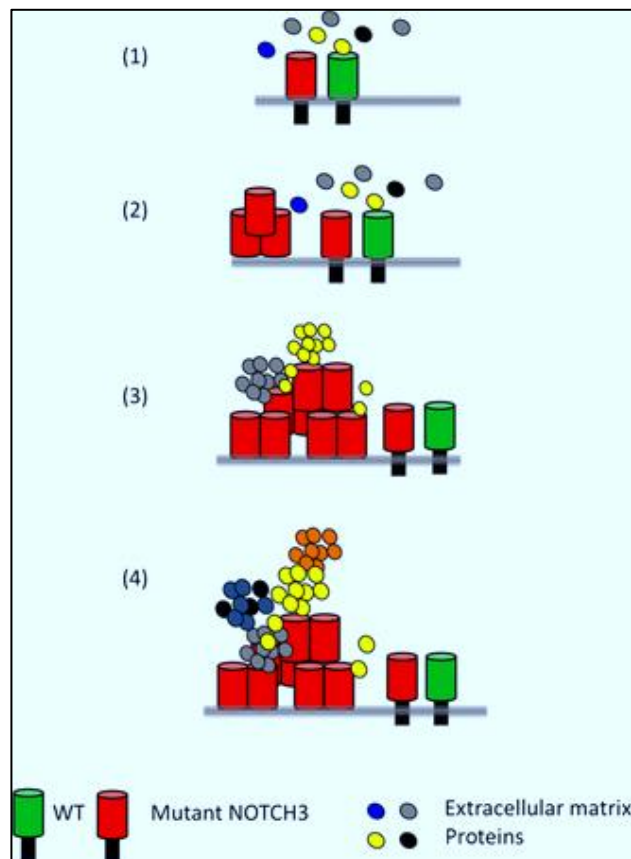


Figure 1-6 The NOTCH3ECD cascade hypothesis of CADASIL

A hypothetical model for extracellular domain of the NOTCH3 protein/granular osmiophilic material deposits formation. (a) Wild-type and mutant NOTCH3 receptors are expressed at the plasma membrane as heterodimers surrounded by proteins of the extracellular matrix. (b) The unpaired cysteine residue promotes the formation of multimers of the extracellular domain of the NOTCH3 protein. (c) When the extracellular domain of the NOTCH3 protein aggregates reach a given size or concentration, proteins of the extracellular matrix, such as TIMP3, are recruited, that in turn (d) can favour the recruitment of additional proteins, such as vitronectin. Reproduced with permission from Anne Joutel, The NOTCH3ECD cascade hypothesis of cerebral autosomal dominant arteriopathy with subcortical infarcts and leukoencephalopathy disease, *Neurology & Clinical Neuroscience* (2014); 3(1): 1-6, with permission from John Wiley and Sons

1.4.3.4 Theory 4: Interactions with other pathways

NOTCH3 does not work in isolation and has been shown to interact with other key pathways involved in the vascular system. NOTCH3 signalling influences expression of platelet-derived growth factor gene, and feedback between the two pathways may regulate VSMC expression (Jin et al., 2008). Interactions of the NOTCH3 with other signalling pathways remain to be explored.

1.4.3.5 Theory 5 – Protein elimination failure angiopathy

The brain does not have lymphatic vessels. Instead perivascular pathways surrounding cerebral capillaries and arterioles exist, which allow drainage of solutes and interstitial fluid out of the brain, including unwanted or toxic proteins (Iadecola, 2013). Failure of these drainage pathways to eliminate protein may be a feature of many neurodegenerative diseases including Alzheimer's disease, cerebral amyloid angiopathy and prion diseases. These are termed protein elimination failure angiopathies (PEFA) (Carare et al., 2013).

The mechanisms of failed elimination include abnormalities in the capillary basement membrane, resulting in trapping of proteins. The movement of fluid along the drainage pathways is thought to require normal blood flow pulsating through the vessels, and reduced blood flow, stiffened blood vessels or abnormal vascular smooth muscle cells may result in reduced motive force for drainage.

In CADASIL, GOM accumulates around capillaries and small arterioles, and is likely to create a physical barrier to drainage of solutes. Degenerating VSMCs will also lead to reduced force for drainage. The congestion of drainage pathways is likely reflected in the enlarged perivascular spaces seen in many CADASIL patients. These changes may also result in the disruption of the blood-brain barrier, and leakage of toxins or inflammatory cells.

It is likely that rather one of these theories being the explanation, a combination of different mechanisms leads to the pathophysiology, and the contribution of each may affect how the disease is expressed in individual patients.

1.4.4 The effect of CADASIL on the vascular system

1.4.4.1 Mouse models

A transgenic mouse model of CADASIL arteriopathy was created to express low levels of the mutant human *NOTCH3*, Arg90Cys. Its expression was driven by a *SM22a* promoter. Histological abnormalities were seen in this model. Tail arteries were particularly affected, showing age-dependent morphological abnormalities of VSMC and endothelial cells from 10 - 12 months. At around 14-16 months GOM and NOTCH3 deposits were detectable, suggesting these are not required for cell damage. Cerebral and systemic vessels also showed GOM and NOTCH3 deposits, but there was no evidence of parenchymal damage (Ruchoux et al., 2003). Tail vessels exhibited an increase in pressure-induced contraction and a decrease in flow-induced dilation and these changes were present before any evidence of histological abnormalities. In contrast, changes to chemical stimuli were not affected, suggesting they function through different pathways (Dubroca et al., 2005).

A more recent mouse model expressed high levels of Arg169Cys rat *Notch3* in arteries and capillaries, showed vascular deposits from an early age. From around 18 months old, mice developed extensive white matter disease, although no motor deficits were seen. Resting cerebral blood flow was reduced by 16% in white matter and 13% in grey matter. There was rarefaction of capillaries but the blood brain barrier remained intact and there were no overt changes in arterial structure. From age 5 - 6 months there was attenuated pressure-induced contraction with preserved responses to sodium nitroprusside and phenylephrine. This implied an impaired vasodilator reserve, which preceded the development of overt vasculopathy or parenchymal lesions (Joutel et al., 2010). It is proposed therefore that VSMC dysfunction leads to disordered autoregulation and chronic hypoperfusion. This results in ischaemic rarefaction of white matter and lacunes, with subsequent clinical effects. How the overexpression of NOTCH3, required for models to develop evidence of brain damage, affects the accuracy of the model for human disease is not known. Whilst mouse models provide useful observations, the lack of reproduction of clinical endpoints is problematic (Ayata, 2010).

Mouse models have some limitations including different brain architecture, shorter life span and gene overexpression. NOTCH3 knock-out mice are viable but postnatal vessel maturation suggesting a role for NOTCH3 in arterial specification. Different histological and functional changes are seen in transgenic mice expressing a NOTCH3 mutation, which demonstrates that CADASIL is not due to a loss of function of NOTCH3. Mouse models have therefore provided important information on the mechanisms of disease and continue to highlight possible therapeutic targets. Human studies

Human studies confirm that impaired vascular function and resulting chronic hypoperfusion is a fundamental problem. PET and SPECT studies of brain perfusion show that cerebral blood flow is globally reduced, particularly in white matter, and that this reduction precedes both symptoms, and in some cases development of overt white matter hyperintensities on brain MRI (Mellies et al., 1998, Tuominen et al., 2004).

Vascular reactivity is also impaired in peripheral vessels in CADASIL patients, including abnormal responsiveness of small gluteal resistance vessels to angiotensin II (Hussain et al., 2004). *In vivo* impairment of endothelial vasomotor function has been demonstrated with peripheral arterial tonometry (Campolo et al., 2011), and impaired peripheral vasoreactivity is correlated to cerebrovascular reactivity when measured with acetazolamide and SPECT in CADASIL patients (Fujiwara et al., 2012).

Carotid intima-media thickness (CIMT) is associated with atherosclerosis, and has been shown to predict the risk of future cardiovascular events (O'Leary and Bots, 2010). However it is also associated with a number of different diseases, and may also be associated with changes in blood pressure and endothelial function. Higher CIMT was shown to be independently associated with lower cognitive scales, with a non-significant trend towards an association with disability (Mawet et al., 2011). It is proposed that measures that examine the severity of atherosclerosis may also be related to clinical outcomes in CADASIL. Other studies have shown no difference between CIMT and measures of arterial stiffness such as augmentation index between CADASIL patients and controls (Stenborg et al., 2007)

1.4.5 Role of vascular abnormalities as biomarkers

Vascular dysfunction is a fundamental problem in the pathogenesis of CADASIL. It is thought to precede the development of histological abnormalities and brain lesions and therefore is potentially a target for both disease monitoring and therapeutic intervention. Much of the research has been performed in mouse models, but these often fail to fully recapitulate human disease. The vascular pathophysiology in human models needs to be explored if our understanding of the disease is to be furthered.

1.5 Imaging in CADASIL

Structural brain imaging in CADASIL typically identifies abnormalities some years in advance of clinical manifestations of cerebral ischaemia. Hyperintensities in white matter are seen from the third decade (sometimes younger), and are often confluent and dramatic in appearance even in asymptomatic individuals. However while the extent of these abnormalities correlates broadly with age (and therefore with scores of disability), the very wide variation among individuals (even within families) and slow rate of progression (Peters et al., 2004a) renders them of little value as a biomarker of disease progression over time scales that would be feasible for clinical trial use. Similarly lacunes generally appear later, and their clinical importance likely depends more upon location than load. Cerebral microbleeds occur later in the natural history of the disease, often in a different distribution to lacunes. Brain atrophy also occurs in CADASIL but is a common terminal pathway for many brain diseases, and has limited potential as a biomarker in presymptomatic CADASIL patients (Viswanathan et al., 2010).

1.5.1 Anatomical MRI markers

1.5.1.1 Subcortical hyperintensities

Abnormal hyperintensities on T2-weighted MRI imaging are a characteristic finding in CADASIL, although by no means diagnostic, as they are seen in a wide range of diseases, as well as being present in the asymptomatic elderly

population (Schmidt et al., 2003). Hyperintensities are usually present before the age of 35, and precede symptoms (Chabriat et al., 1998). Initially presenting as discrete lesions in periventricular regions, abnormalities increase and coalesce, to form confluent white matter hyperintensities (WMH). Lesions also form within the basal ganglia and brainstem, although the cerebellum is infrequently involved (van den Boom et al., 2003b)(Figure 1-7). Localisation to the anterior temporal pole and external capsule offers a high specificity for CADASIL in European populations (O'Sullivan et al., 2001), although this may be less common in other racial groups (Wang et al., 2011). The lesions may be due to chronic hypoperfusion of white matter secondary to dysfunction or destruction of perforating arteries or alternatively due to tissue oedema (De Guio et al., 2015). Collectively when including white matter, subcortical grey matter and brainstem lesions, they are termed subcortical hyperintensities (SH).

The radiological load of hyperintensities increases over time, and is correlated with age (Chabriat et al., 1998, van den Boom et al., 2003b). In a longitudinal study of 62 CADASIL patients over 2 years, a statistically significant increase in hyperintensities was demonstrated, and power studies demonstrated that if this measure was used in clinical trials as a surrogate marker, fewer patients would be needed that for clinical endpoints only (Holtmannspotter et al., 2005).

Early work in CADASIL imaging suggested that hyperintensity load was correlated with disability and cognitive dysfunction (Chabriat et al., 1998, Dichgans et al., 1999). These studies may have been limited by inclusion of patients without CADASIL (as they preceded full genetic screening) and an unclear distinction between hyperintensities and lacunes. More recent studies, adjusting for age and other radiological lesions, have failed to find a correlation between hyperintensity load and measures of disability or neuropsychological function (Liem et al., 2009b, Viswanathan et al., 2010). The likely reason hyperintensities fail to correlate with clinical measures is that it is purely visual measure of “brightness” and fails to give any information regarding the function of white matter tracts, but is rather a non-specific marker of “end-organ damage”.

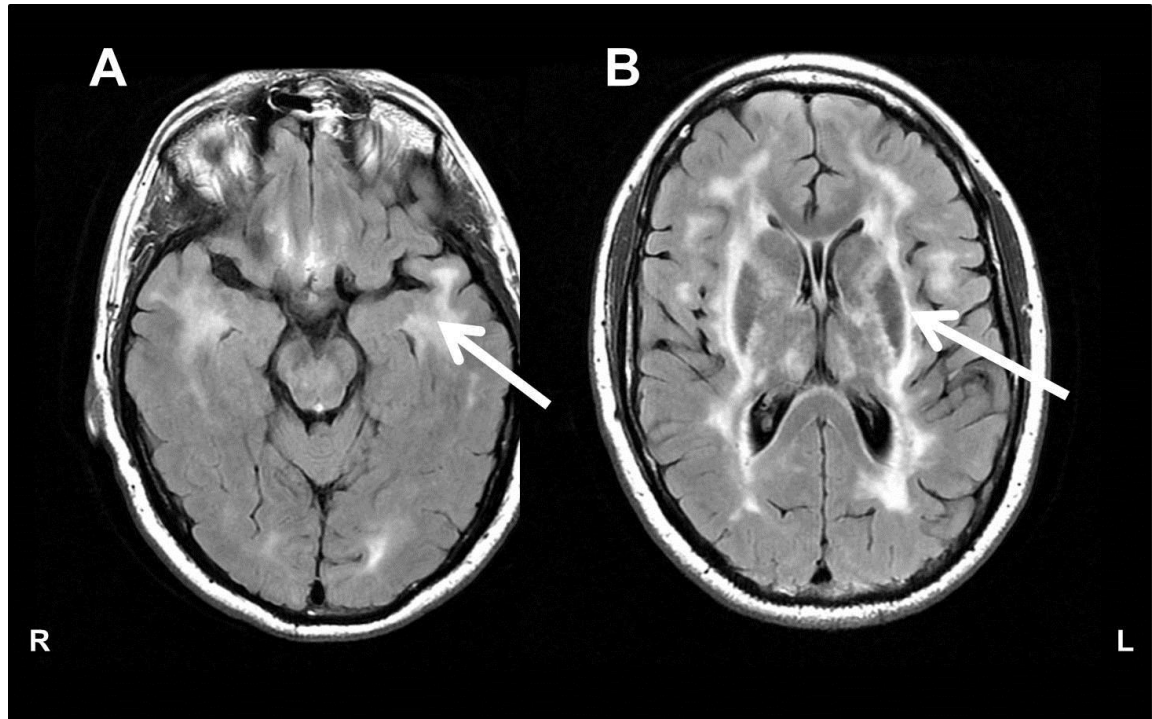


Figure 1-7 Characteristic radiological findings in CADASIL - Subcortical hyperintensities
 Subcortical hyperintensities visible on T2 FLAIR are usually the earliest radiological manifestation of CADASIL arteriopathy. (A) Involvement of the anterior temporal lobe and (B) external capsule are highly specific for CADASIL (arrowed).

Hyperintensities are therefore a sensitive radiological marker of CADASIL, but fail to correlate longitudinally with clinical measures thus negating their potential use as surrogate markers in clinical trials.

1.5.1.2 Lacunes and Subcortical infarcts

A lacune is a cavity within brain tissue filled with cerebrospinal fluid which is proposed to be due to subcortical infarct or haemorrhage in the territory of a single perforating artery (Wardlaw et al., 2013). There is no gradation of lacunes: it is a lacune or not (Filippi and Grossman, 2002), although size criteria of between 3 and 15mm in the axial plane have been suggested (Wardlaw et al., 2013). Supratentorial lacunes are usually visible in the 4th decade particularly within the centrum semiovale, basal ganglia and thalamus. Typically by the 5th decade, lacunes have increased in number and are found in infratentorial regions such as the pons (van den Boom et al., 2003b, Chabriat et al., 1999a) (see Figure 1.8). The cause of lacunes in CADASIL is not entirely clear, but theories include vasospasm or abnormal vascular tone resulting in localised ischaemia (Duering et al., 2013).

Subcortical infarcts refer to neuroimaging evidence of recent infarction in the territory of a single perforating artery, usually <20mm in the axial plane (Wardlaw et al., 2013). Subcortical infarcts can result in clinical stroke syndromes with resultant neurological and functional disability, and are visible on diffusion weighted imaging (DWI). Over time these will usually transform into lacunes, but may alternatively become hyperintensities or disappear entirely (Wardlaw et al., 2013). Silent subcortical infarcts also occur. In a small study, 2 out of 19 CADASIL patients undergoing DWI-MRI demonstrated changes consistent with recent silent infarction (O'Sullivan et al., 2003). The proposition that the detection of silent infarcts on DWI could be used as surrogate markers for trials in CADASIL may have been premature due to lack of longitudinal or clinical correlation.

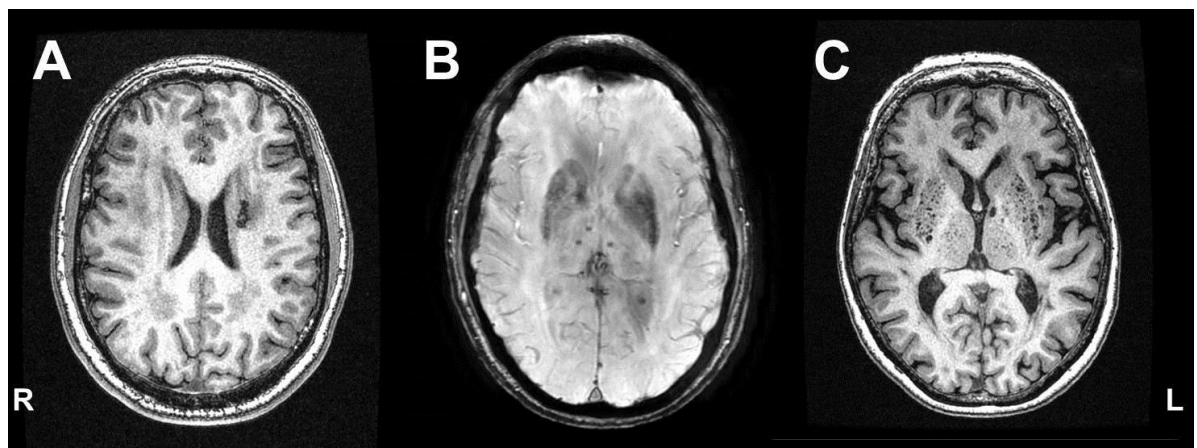


Figure 1-8 Characteristic radiological findings in CADASIL – Lacunes, microbleeds and perivascular spaces
 (A) Lacunes occur in the basal ganglia, centrum semiovale and brainstem (lacune in left centrum semiovale shown). (B) Cerebral microbleeds, visible on T2* weighted sequences may be demonstrated (bilateral thalamic microbleeds shown), and (C) multiple perivascular spaces occur which are marked in the basal ganglia (demonstrated) or in the subcortical-cortical junction, where they are termed subcortical lacunar lesions.

Lacunes have more promise as a marker of disease severity and progression. Liem and colleagues undertook a cross-sectional study of 40 CADASIL patients and 22 controls performing MRI and a battery of neuropsychological tests. They demonstrated in a regression model that lacune load was correlated to dysfunction in most cognitive tests, whereas white matter hyperintensities, age, and microbleeds were not. They postulated that lacunes may account for the stepwise decline in cognition proposed in CADASIL. A further cross-sectional study of 138 patients using MMSE and MDRS as measures of cognitive dysfunction,

suggested that normalised lacune volume and age were independently related to both disability and cognition (Viswanathan et al., 2007).

A small longitudinal study demonstrated that lacune load was one of the factors (along with atrophy and microbleeds) that contributed to cognitive decline, whereas white matter hyperintensities did not (Liem et al., 2009b). This study was affected by multiple statistical testing. A cross-sectional multimodal analysis proposed lacune load accounted for 13% of disability and 7% of cognitive dysfunction, as measured by the modified Rankin Scale. It is also suggested lacune load is more important earlier in the disease, with brain atrophy becoming the key determinant of function later on (Viswanathan et al., 2010).

Recently MRI scans from 215 patients have undergone voxel-based lesion-symptom mapping in a study examining the importance of lesion location (both lacunes and hyperintensities) in predicting cognition (Duering et al., 2011). Significant clusters for cognitive performances were found in the anterior thalamic radiation and forceps minor, and in multivariate testing regional ischaemic load in these locations predicted cognitive performance whereas global volume did not. Severely disabled patients were less able to complete cognitive testing, and registration of MRI scans was more difficult, which biased these results. This detailed study supports the argument however, that ischaemic lesion location is more important than load.

Lacune load therefore changes with time, and likely correlates with clinical outcomes, although any correlation remains small. In order for lacunes to be used as a surrogate marker the method for measuring load needs to be quantitative and reliable. Lacunes present early in the disease, often before symptoms, and therefore their prevention may be possible with therapeutic interventions. However the biological relationship between lacunes and the pathophysiology of CADASIL remains incompletely understood.

1.5.1.3 Cerebral microbleeds

The rupture of small perforating blood vessels supplying white matter can result in cerebral microbleeds. Usually clinically asymptomatic, they can be visualised on T2* gradient echo MRI or susceptibility-weighted imaging (SWI) which detects

paramagnetic haemosiderin. Haemosiderin is released from lysed erythrocytes and stored within macrophages. Microbleeds appear larger on gradient echo/SWI due to a “blooming effect” meaning comparison of microbleed volume is difficult as it is influenced by MRI extrinsic parameters.

Microbleeds are seen in a variety of diseases and detected in asymptomatic patients in population studies (Roob et al., 1999). They are more common with age, hypertension, concomitant aspirin use, and lobar microbleeds are a key diagnostic marker of cerebral amyloid angiopathy (Greenberg et al., 2009).

First described in CADASIL by Lesnik Oberstein and colleagues, the detection of microbleeds in CADASIL has ranged from 25 - 69% (Lesnik Oberstein et al., 2001, Dichgans et al., 2002). They represent a later stage of the radiological natural history of CADASIL, tending to appear in the 5th decade (van den Boom et al., 2003b). They are associated with older age, higher blood pressure and elevated HbA1c (Viswanathan et al., 2006b). Their distribution is different to lacunes and subcortical hyperintensities, tending to be concentrated in the thalamus, cortico-subcortical junction and occurring within the cerebellum (Figure 1.8). Dichgans et al proposed that this differential distribution was evidence that microbleeds represent an independent complication of vasculopathy. This may be due to a different pathological processes, or differences in local cytoarchitecture (Dichgans et al., 2002). Microbleeds may also be associated with risk of intracerebral haemorrhage (Choi et al., 2006). Cases with massive and confluent microbleeds have also been described (Oh et al., 2014)

Cross-sectional studies have demonstrated that number of microbleeds is an independent predictor of neurological disability (Viswanathan et al., 2006b). Liem and colleagues demonstrated in a small longitudinal study that microbleed load could be correlated with executive and global cognitive function (Liem et al., 2009b). It is postulated that focal damage caused by a microbleed in a strategic area leads to disruption of cortico-subcortical circuitry which may result in disability.

However microbleeds may also be a proxy indicator of the severity of other pathologies, or of the age of the patient. The presence of microbleeds in CADASIL is in itself associated with a higher load of hyperintensities and lacunes.

In multivariate analysis microbleeds show an independent but small contribution to disability (Viswanathan et al., 2010). They seem to represent a later stage in the natural history of CADASIL and may therefore not be an ideal marker for therapeutic trials for the prevention of CADASIL complications in younger patients. It is also difficult to account for the volume of microbleeds due to the “blooming effect”. As a successful clinical trial in CADASIL would need to be multi-centre, there may be differences in scanners and sequence parameters which affect comparability between centres. If lacunes and microbleeds represent different consequences of the same vascular pathology, then both may need to be taken into account in clinical trials.

1.5.1.4 Perivascular spaces and subcortical lacunar lesions

A perivascular space is filled with interstitial fluid and surrounds a blood vessel in the brain. With normal aging they can dilate to become visible on brain imaging (Zhu et al., 2011), where they may be mistaken for lacunes. They may be due to shrinkage of perivascular cerebral tissue, or an abnormality of the blood brain barrier of perforating vessels, resulting in leakage of plasma proteins and expansion of the extracellular space. Perivascular spaces were seen in 78% of 50 patients with CADASIL, concentrated in the lentiform nucleus and temporal white matter (Cumurciuc et al., 2006) (Figure 1.8). Dilated perivascular spaces were more common with increased age but did not correlate to disability measures or risk factors. They were not related to other ischaemic manifestations.

Van den Boom and colleagues detected subcortical lacunar lesions (SLLs) in 20 out of 34 patients with CADASIL and in none of 4 control groups giving a specificity for CADASIL of 100% (van den Boom et al., 2002). They described this apparently novel radiological finding as

“linearly arranged groups of rounded, circumscribed lesions just below the cortex at the junction of grey and white matter with a signal intensity identical to CSF”

Neuropathological correlation suggested they represent dilation of perivascular spaces around perforating vessels, with atrophy of the surrounding parenchyma. They increase in number with age. The authors suggested that the distinct

anatomical distribution of these lesions implied they were not perivascular spaces, however other authors disagree (Cumurciuc et al., 2006).

It can be concluded from limited cross-sectional data that dilated perivascular spaces are common in both normal aging and CADASIL, thus lacking disease specificity. Whether SLLs are a novel marker for CADASIL, or a perivascular variant, there is currently insufficient longitudinal data to consider them an appropriate MRI marker. Neither has yet been shown to correlate with clinical outcome measures.

1.5.1.5 Brain atrophy

The brain atrophies with age but the speed at which this occurs is influenced by a variety of factors including gender, drugs, diet, alcohol and the presence of brain disease (Enzinger et al., 2005). In CADASIL, age and male gender were independent predictors of normalised brain volume, but age and systolic blood pressure predicted rate of brain volume loss (Peters et al., 2006). Lacune load and white matter tract damage were also related to brain volume (Jouvent et al., 2007). More recently it has been suggested that large volumes of hyperintensities may actually increase brain volume, due to fluid accumulation (Yao et al., 2012).

The annual rate of brain volume in loss in CADASIL patients has been reported as 0.56%, twice that of healthy people of a similar age (Peters et al., 2006). However others have reported slower rates. Over a 7 year period brain volume reduced from 82.6% to 81.8%, with a similar volume in controls (80.8% to 80%) (Liem et al., 2008). This slow decline may limit its use in shorter clinical trials, although it has been suggested to reduce the numbers needed in a trial compared to clinical outcomes (Peters et al., 2004a, Peters et al., 2006)

A large (n = 147) cross-sectional study demonstrated that brain volume correlated with clinical outcome measures (Jouvent et al., 2007). Viswanathan et al calculated brain volume explained 35% of the variance in cognitive scores and 38% of the variance in disability scores (modified Rankin score), which was the largest contributor to variance (Viswanathan et al., 2010).

Increase in ventricular volume may have more relevance than brain volume per se, as it represents central brain atrophy which may have more functional relevance (Liem et al., 2008). In a 7 year study, ventricular volume increased in CADASIL patients from 2.5% to 2.9% (controls 1.9% to 2.1%).

1.5.2 Imaging brain function *in vivo*

One of the limitations of using measures of abnormal appearing tissue is that it does not really tell us what is happening within the tissue. Subcortical hyperintensities represent a spectrum of neuronal dysfunction, from minor structural change to neuronal loss, and this variation in function likely explains the minimal correlation with clinical markers, as well as the clinical picture in individual patients. Therefore there is increased interest in techniques which study tissue function or integrity.

1.5.2.1 Diffusion weighted imaging (DWI) and Diffusion tensor imaging (DTI)

Diffusion describes the movement of water molecules, which in solution, will diffuse randomly in any direction (isotropic). In brain tissue, structural features such as cell membranes and large molecules restrict the movement of water. Diffusion is partially restricted within white matter tracts, where ordered arrangement of axons encourages the water to diffuse in a direction parallel to the axon. White matter tissue is thus termed anisotropic tissue.

Diffusion weighted imaging (DWI) allows the visualisation of diffusion within brain tissue, and is derived from the apparent diffusion coefficient (ADC) - a measure of the movement of molecules across an area of tissue per second. A low ADC indicates an area of restricted diffusion, such as may be seen after an acute stroke, where swelling of ischaemic cells results in reduced extracellular space for water diffusion.

Diffusion tensor imaging (DTI) allows the quantitative analysis of white matter tract integrity by visualising the 3-D movement of water molecules. The technique uses at least 6 co-linear directions to derive two key parameters. Mean diffusivity is a measure of the amount of diffusion occurring in a region, and fractional anisotropy is a measure of water direction, taking any value from

0 (no preferred direction) to 1 (diffusion in one direction only). These quantitative measures are reproducible and can be used to produce global or localised readings.

Chabriat and colleagues used DTI in 16 CADASIL patients to demonstrate diffusivity changes in WMH compared to normal appearing white matter in age-matched healthy controls (Chabriat et al., 1999b). Diffusion measures correlated with changes in disability (modified Rankin scale, mRS) and cognition (mini mental state examination, MMSE). Abnormal diffusion was proposed to be due to loss of axons and myelin, with disorganisation of white matter and expansion of extracellular space. Diffusion was also higher in “normal appearing white matter” (NAWM) indicating that the functional abnormalities were not restricted to areas that appear abnormal on T2. This study did not adjust for other measures such as lacune load or brain atrophy, but created interest as a potential surrogate marker.

Using DTI and regions of interest, cross sectional studies demonstrated that increased diffusion in frontal white matter networks (O'Sullivan et al., 2005), grey matter (Molko et al., 2001) and the thalamus (O'Sullivan et al., 2004), could all be correlated to cognitive and executive dysfunction. The authors suggested that damage within cortico-subcortical circuits leads to executive dysfunction with several papers suggesting a key role of the cingulum bundle in relaying connections (O'Sullivan et al., 2005).

Whole brain histograms derived from diffusion imaging give a measure of global microstructural damage and are both quantitative and reproducible. Molko and colleagues demonstrated that the shape of the diffusion histogram was different in CADASIL patients (n = 22) compared to controls (n = 12) with a greater mean diffusivity and a wider distribution of the diffusivity curve (Molko et al., 2002). This suggested widespread white matter damage. 14 patients went on to complete a second MRI study, offering longitudinal information. Mean diffusion increased in patients but not controls. At baseline and subsequent scanning mean diffusion correlated to mRS and negatively correlated with MMSE. There was no significant change in the clinical measures between the examinations however, highlighting their short-term insensitivity. The study had several flaws: there was no adjustment for other MRI parameters and the time between MRI

scans was variable (21 months \pm 6 months). Control patients were slightly younger (mean 51 years \pm 11 years) compared to patients (54 years \pm 11 years).

Holtmannspotter and colleagues extended this work in a longitudinal study of 62 CADASIL patients (Holtmannspotter et al., 2005). Changes in mean diffusivity (but not white matter hyperintensity load) correlated with clinical outcome measures including mRS and Barthel index longitudinally, and power studies indicated the use of diffusion histograms would require fewer patients in clinical trials. Brain atrophy was not controlled for, and relatively crude neuropsychological measures were used, but the technique undoubtedly demonstrated potential as a surrogate marker by showing both longitudinal changes and clinical correlation.

Despite its potential there are some limitations to DTI. It is not specific to a particular pathological process and changes may represent a variety of causes of white matter dysfunction. It required coupling with conventional MRI in order to measure diffusivity in particular regions of interest (e.g. NAWM). It has a limited spatial resolution and thus we cannot easily identify where white matter tracts actually are. This may be aided by the use of more complex DTI imaging techniques such as tractography, which allows the visualisation of individual tracts. Finally standardisation of DTI acquisition parameters over the multiple sites required for a clinical trial would be difficult. However, the correlation of DTI with cognitive and disability measures over time does suggest it has a potential role. Interestingly, multi-modal analysis by Viswanathan of 147 CADASIL patients suggested however that whilst mean diffusivity correlated to cognitive measures (MDRS) it did not explain variance in disability measures (mRS) (Viswanathan et al., 2010).

1.5.2.2 Magnetisation transfer ratio (MTR)

In tissues there are protons that are bound (e.g. to myelin or macromolecules) and those that are free (e.g. in tissue water). The bound pool protons have a very short T2 and are usually invisible to direct imaging. If a saturation pulse is applied which saturates the bound protons, the magnetisation is quickly transferred to the free protons, and the observed MR signal is reduced. This is

referred to as magnetisation transfer and is thought to indicate the structural integrity of tissue. The amount of signal loss can be characterised by the magnetisation transfer ratio (MTR) (McRobbie et al., 2007).

A low MTR represents a state in which macromolecules are less able to exchange magnetisation due to tissue damage. Studies in multiple sclerosis have suggested the technique produces data which are not only quantitative and reproducible but sensitive to change over a short period. It also has some clinical correlates (Filippi et al., 2000).

One study has used MTR in patients with CADASIL. A cross-sectional study of 33 CADASIL patients and 12 healthy unmatched controls (8 years younger on average) measured MTR metrics both globally and in lesions. CADASIL patients had lower MTR values in most areas compared to controls, suggesting tissue damage both within lesions and normally appearing tissue. Multivariate analysis demonstrated that average lesion MTR was associated with disability (mRS) once corrected for age (Iannucci et al., 2001).

MTR requires a reasonably long acquisition time, and is scanner characteristic dependent, meaning its multi-centre use may be limited by standardisation requirements. The 2-proton model may be over simplistic. DTI is thought to correlate better with clinical outcome measures than MTR in other neurological conditions (Schiavone et al., 2009).

1.5.2.3 MR spectroscopy

MR spectroscopy is a technique which uses MRI to investigate the chemical composition of tissues and characterise metabolic abnormalities. Some research in CADASIL has used MR spectroscopy to demonstrate widespread metabolic abnormalities in both WMH and NAWM suggestive of axonal injury and myelin loss (Auer et al., 2001). Changes may be seen in pre-symptomatic patients (Stromillo et al., 2009), and levels of N-acetylaspartate, which suggests demyelination and axonal injury, correlated with disability (measured by mRS) (Auer et al., 2001).

MR spectroscopy is time-consuming and methodologically complex with problems in quantification and result reproducibility. As such, at present it is unlikely to represent a viable option as a biomarker in longitudinal studies.

1.5.3 Imaging perfusion, haemodynamics and metabolism

The normal functioning of the brain is dependent on its perfusion (a measure of the vascular supply to a tissue) and its ability to alter perfusion in response to various insults or demands (cerebrovascular reactivity). Measures such as cerebral blood flow, cerebral blood volume, transit time and cerebrovascular reactivity may potentially be investigated with brain imaging techniques, sometimes in combination with a vasoreactivity challenge (see Table 1-2).

CADASIL is characterised by damage to VSMC and this is postulated to result in functional impairment with failure of autoregulation, therefore there has been much interest in using measures of perfusion and reactivity to investigate disease pathophysiology and predict disease progress. Imaging techniques may measure perfusion, reactivity and metabolism. Their advantages and disadvantages are in Table 1.3.

Table 1-2 Definitions relating to brain perfusion

Cerebral blood flow	CBF	The volume of blood passing through brain tissue in a defined time i.e. rate. This is usually defined in units of millilitres per 100 grams per minute.
Cerebral blood volume	CBV	The fraction of tissue volume occupied by blood.
Cerebral metabolic rate for oxygen	CMRO ₂	The amount of oxygen consumed by 100g of brain in one minute.
Oxygen Extraction Fraction	OEF	The difference between the partial pressure of oxygen leaving a tissue and the partial pressure of oxygen entering the tissue.
Cerebrovascular reactivity	CVR	Cerebral blood flow (CBF) changes in response to stimuli (usually measured as a percentage).
Mean transit time	MTT	Represents the time taken for blood to pass through a tissue. The ratio of cerebral blood volume to cerebral blood flow. $MTT = CBV/CBF$.
Cerebrovascular resistance		The resistance to the passage of blood created by arterioles and capillaries.
Autoregulation		Cerebral vascular bed alters vascular resistance to maintain blood flow in the face of changes in systemic blood pressure to match metabolic needs.
Vascular steal		A stimulus results in the redistribution of blood flow from regions of exhausted cerebrovascular reactivity (maximally dilated vessels) to areas with preserved vasodilatory capacity.

Table 1-3 Summary of methods for examining cerebral blood flow

Technique	Principal	Advantages	Disadvantages
Positron emission tomography (PET)	Radiolabelled tracer injected or inhaled, and tracers detected with tomographic scans.	<ul style="list-style-type: none"> Measures multiple haemodynamic parameters May be quantifiable Reproducible 	<ul style="list-style-type: none"> Expensive Specialised centres only Technically demanding
Single photon emission computed tomography (SPECT)	Injection of a radioactive tracer, which travels to brain and emits gamma-rays, which are then detected to create a 3D image of flow.	<ul style="list-style-type: none"> Whole brain coverage Fairly reproducible 	<ul style="list-style-type: none"> Radioactivity required Specialist equipment Can have poor spatial resolution
Arterial spin labelling (ASL)	Radiofrequency pulse applied to blood passing into brain tissue, where it causes a reduction in magnetization proportional to flow. Compared to a non-labelled image.	<ul style="list-style-type: none"> Good spatial resolution No contrast or radiation Repeatable Quantifiable Flexible 	<ul style="list-style-type: none"> Poor SNR Less accurate at low flow rates Sensitive to motion artefact
Transcranial Doppler ultrasound (TCD)	Measurement of blood flow velocity via Doppler ultrasound.	<ul style="list-style-type: none"> Safe No contrast or radiation required 	<ul style="list-style-type: none"> Very limited spatial resolution Operator dependent
Dynamic susceptibility contrast MRI (DSC-MRI)	Non-ionizing contrast (gadolinium) causes magnetic field inhomogeneities and T2 signal attenuation which is dependent on flow.	<ul style="list-style-type: none"> Measures of relative CBF, CBV and MTT available High spatial resolution Whole brain coverage 	<ul style="list-style-type: none"> IV contrast Nephrogenic systemic fibrosis Lack of standardization in interpretation/quantification
Phase contrast MRI (PC-MRI)	Measures moving fluid and hence total CBF entering the brain, using vessels as regions of interest.	<ul style="list-style-type: none"> No contrast No radiation Images of blood vessels 	<ul style="list-style-type: none"> No assessment of smaller vessels (i.e. those affected in CADASIL).
Perfusion CT	Injection of iodinated contrast with continuous CT scan, and identification of first pass of contrast into tissue.	<ul style="list-style-type: none"> Widely available Quantifiable 	<ul style="list-style-type: none"> Use of radiation and contrast. Less additional sequences can be obtained

1.5.4 Positron Emission Tomography (PET) and Single Photon Emission Computed Tomography (SPECT)

Positron Emission Tomography (PET) provides quantitative information on brain haemodynamics and metabolism by imaging the distribution of a radioactive tracer. Useful studies have been performed in CADASIL patients. A 58 year old asymptomatic patient with white matter changes but no infarcts demonstrated a 40% diffuse decrease in cerebral blood flow (CBF) within the cortex and white matter, with a preserved oxygen consumption rate ($CMRO_2$) and increased oxygen extraction fraction (OEF). A demented patient, with numerous infarcts, had a 65% decrease in CBF and $CMRO_2$ in white matter. These results suggested low CBF preceded metabolic depression, and that infarcts may result in metabolic depression responsible for dementia (Chabriat et al., 1995). Tuominen and colleagues performed ^{15}O -PET in 14 CADASIL patients and 25 controls (Tuominen et al., 2004). Reduced CBF was demonstrated in white matter after age 30 years, and the amount was inversely proportional to WMH load. Cortical perfusion was however preserved and in some cases hyperaemic. No clinical correlation was performed, and the patients were young (mean age 32.8yrs, $SD \pm 6.7$). Tatsch performed PET with ^{18}F -FDG to examine glucose metabolism (Tatsch et al., 2003). 11 patients had reduced CMR_{Gluc} globally compared to controls.

Single Photon Emission Computed Tomography (SPECT) is a method requiring the introduction of a radioactive compound, usually Technetium-99m when measuring CBF. A SPECT study in CADASIL patients demonstrated global hypoperfusion in 6 subjects which appeared worse in the older and more severely affected patients. This was particularly within the frontal and temporal regions (Mellies et al., 1998). The relationship between CBF, radiological measures and clinical outcome is not straightforward: a study using SPECT showed the demented patient had the highest CBF and fewest radiological lesions, whereas the functionally independent patient had the lowest CBF and was cognitively normal (Scheid et al., 2006).

1.5.4.1 Contrast-enhanced MRI

MRI uses a different mathematical model to calculate haemodynamics based on the dynamic imaging of “tagged” arterial blood as it passes through the brain. Specific sequences are used to maximise the effect of the contrast on the microvasculature and a signal decay curve is generated, from which relevant perfusion parameters are calculated. In dynamic-susceptibility contrast (DSC) MRI, an agent such as gadolinium is injected into the patient and passes through the capillary bed of the brain. The agent causes a decrease in T2 or T2* signal and images are obtained before, during and after contrast injection. Relative measures of brain haemodynamics (rCBV, rCBF, rMTT) can be obtained. Two studies have used DSC-MRI in CADASIL to examine brain haemodynamics. Bruening and colleagues used a susceptibility-weighted imaging sequence to image 24 CADASIL patients (Bruening et al., 2001). Relative CBV (rCBV) in NAWM was $4.4 \pm 1.3\text{mL}/100\text{g}$ (mean \pm SD) and $2.7 \pm 0.8/100\text{g}$ in WMH. Lacunes had an rCBV of 0ml/100g. There was a trend towards reduced rCBV in patients with higher disability scores and in patients dichotomised on the basis of their cognitive results (MMSE), patients with dementia had significantly lower rCBV. No evidence was found of blood-brain-barrier abnormality. The correlation of rCBV with even crude disability measures is encouraging for DSC-MRI use in prospective studies. Chabriat and colleagues used spin-echo planar imaging (EPI) to track a gadolinium bolus, before and after the administration of acetazolamide (Chabriat et al., 2000). Both mean relative and absolute values were calculated and rCBV and rCBF were reduced in CADASIL patients in the centrum semiovale, WMH and occipital cortex (compared to 10 healthy controls). Cortical perfusion was preserved, but there was a reduced response to acetazolamide in WMH.

DSC-MRI has confirmed flow abnormalities in CADASIL and some correlation with clinical measures. However perfusion MRI has not been used to measure brain haemodynamics longitudinally; which in part may be due to lack of standardisation of results. For the indicator-dilution theory to be applied the blood-brain-barrier must be intact, but recent work using contrast-enhanced MRI in CSVD has suggested this is associated with increased BBB permeability in lesions and NAWM (Topakian et al., 2010). If this is the case in CADASIL, the

model of indicator-dilution would need modification, further complicating quantification of perfusion.

1.5.4.2 Phase-contrast MRI

An alternative method to calculate total CBF is by measurement of flow entering the brain by delineating the internal carotids and basilar artery as a region of interest. This method is a global measure of total CBF based on extraparenchymal vessels and does not require injection of contrast. Van den Boom and colleagues found a reduction in total CBF in CADASIL patients compared to non-age matched controls, but no difference in CVR as measured by response to acetazolamide (van den Boom et al., 2003a). This finding was replicated in a study of 14 CADASIL patients and 9 controls, with CADASIL patients having a lower total CBF but similar CVR (Liem et al., 2009a). Patients with a lower CVR were found to have a faster rate of WMH lesion progression than those with preserved CVR, which suggested a role for CVR as a predictor of disease progression.

This method offers a global measurement of CBF and suggests global hypoperfusion but does not replicate changes suggested by SPECT studies in CVR. This may be as the method uses larger intracranial blood vessels not affected by CADASIL.

1.5.4.3 Arterial spin labelling ASL

An alternative method of imaging perfusion using MRI is termed arterial spin labelling (ASL). Here water molecules in arterial blood act as the contrast material and are “tagged” by an inversion or saturation pulse when entering the brain (see Figure 1.9).

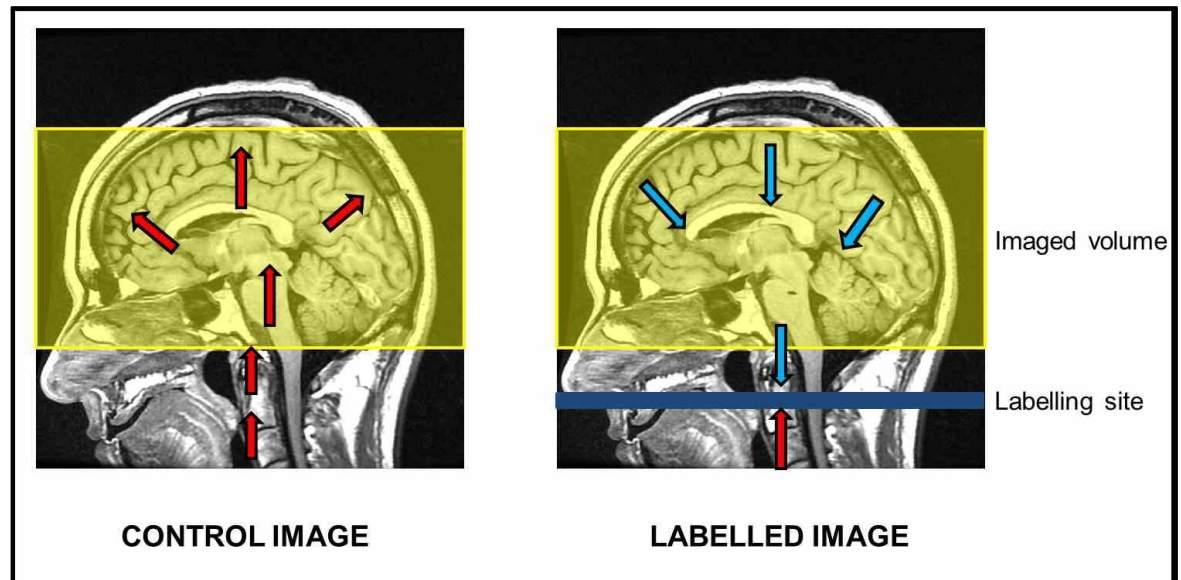


Figure 1-9 Arterial spin labelling (ASL) technique

Arterial blood flows into the tissues being imaged and contains water molecules with positive nuclear spins (red arrows). In the labelled image, an inversion pulse applied below the area to be imaged alters the spins of the water molecules. These spins then enter the tissue and cause an attenuation of brain signal proportional to the flow. A control image, without an inversion pulse, is also obtained. The control image can be subtracted from the labelled image producing an image which reflects brain perfusion. Further quantification is required to obtain absolute values from this image.

There are various methods to undertake ASL which has several advantages (see Table 1.3). No studies using ASL have been used in CADASIL but it has been used in several other neurodegenerative diseases. Bastos-Leite demonstrated a reduction in global CBF in patients with confluent compared to punctiform WMH (Bastos-Leite et al., 2008). Murphy and colleagues used ASL in healthy volunteers to establish its reliability and potential use in clinical trials. Using power calculations they suggested that to detect a 15% decrease in CBF between two groups 20-40 people would be needed per group, and confirmed that ASL had acceptable reliability (Murphy et al., 2011). The use of ASL in CADASIL in both cross-sectional and longitudinal studies warrants further investigation.

1.5.5 Transcranial Doppler ultrasound (TCD)

An alternative method used in CADASIL to examine haemodynamics is transcranial Doppler (TCD) ultrasound. It is non-invasive, inexpensive, and easily performed even in more disabled individuals. It has established value in detection of vasospasm after subarachnoid haemorrhage, monitoring carotid endarterectomy and reactivity testing using either CO₂ or acetazolamide (Sloan et al., 2004, Markus and Harrison, 1992). However it is highly operator

dependent. It also measures flow velocity, and indirect marker of altered CBF in downstream vessels.

TCD has been used to study CADASIL patients. In a study of 29 CADASIL patients and controls, MFV declined with age and CVR, tested with CO₂ challenge, was impaired in patients (Pfefferkorn et al., 2000). However Singhal et al studied CVR and autoregulation in 24 non-demented CADASIL patients and 20 controls. Whilst resting MFV was lower in CADASIL patients, there was no impairment of CVR or autoregulation (Singhal and Markus, 2005). These differences may be caused by technical differences, or different patient characteristics in the recruited cohorts.

TCD has been used as a biomarker however in therapeutic drug trials in CADASIL (Peters et al., 2007).

1.6 Summary and aims of thesis

CADASIL is well-defined genetically, radiologically and phenotypically, but patients still show a wide variation in natural history which cannot currently be predicted by examining genotypes or cardiovascular risk factors. For investigation of any possible therapeutic agent in these patients, more accurate measures of disease progression are needed.

A number of different MRI based methods have been proposed to function as biomarkers of disease progression in CADASIL. Some authors have demonstrated that measures such as T2 hyperintensity load, atrophy and DTI diffusion parameters, may allow smaller numbers of patients to be included in clinical trials than those required when using clinical measures alone. However these still exceed a realistic number of patients for a disease with low prevalence. Vascular dysfunction is thought to represent an earlier stage of pathophysiology, and may precede clinical features and anatomical radiological abnormalities. Better understanding of vascular pathophysiology in human CADASIL patients, may highlight which measures have potential as biomarkers.

This thesis aims to improve understanding of vascular pathophysiology in CADASIL, particularly with reference to using vascular measures as markers of

disease progression (see Figure 1-10). In order to facilitate this, investigations into how common CADASIL is and how vascular function can be measured non-invasively were performed.

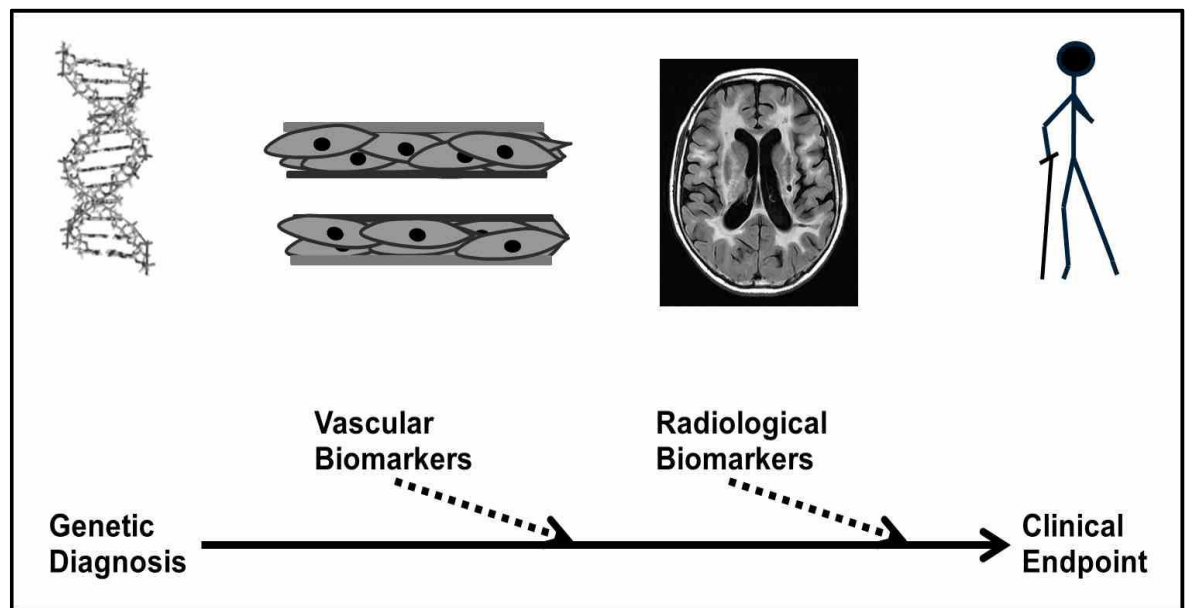


Figure 1-10 Summary of thesis aims

Whilst the genetic diagnosis and clinical endpoints are well defined, understanding of vascular and radiological biomarkers remains incompletely understood and are a target for research.

The aims of the thesis are:

- 1) investigate how best to measure vascular reactivity using MRI and non-invasive techniques which would be most useful in longitudinal clinical trials;
- 2) determine how common CADASIL is in the west of Scotland, and how this compares to other neurological diseases;
- 3) establish how vascular reactivity relates to traditional measures of disease status including MRI anatomical markers and neuropsychological measures;
- 4) assess the change in cerebral blood flow and reactivity in CADASIL patients over 1 year;
- 5) determine if vascular function predicts changes in radiological or disease status over time;

- 5) investigate if *in vivo* vascular function and reactivity measures relate to *ex vivo* studies of arterial function;
- 6) establish if non-invasive MRI can be used to determine which the vessels responsible for lacunes in CADASIL.

Chapter 2 – Materials and Methods

This chapter provides a description of the materials and methods used for the study, “Cerebral and peripheral perfusion and reactivity in CADASIL: A longitudinal pilot study”, which comprises the bulk of this thesis.

2.1 Funding

This study was funded by:

- Project Grant ETM/244, Chief Scientist Office, Scotland.

2.2 Ethics

Ethical approval was obtained from the West of Scotland Research Ethics Service; project reference WS/12/0295. The study was sponsored by NHS Greater Glasgow and Clyde Research and Development Service (reference GN12NE144). The study is registered on the UK Clinical Research Network (ID 13794). Written informed consent was obtained for all study participants in accordance with the Declaration of Helsinki.

2.3 Patient recruitment

Recruitment of subjects was performed between May and November 2013. Patients who attended the Neurovascular Genetics Clinic at the Southern General Hospital, and fulfilled the inclusion criteria, were considered. Potential participants were contacted by letter with a follow up telephone call.

2.3.1 Inclusion criteria

Inclusion criteria were as follows:

- Diagnosis of CADASIL confirmed with a characteristic mutation in exons 2 - 24 of the *NOTCH3* gene on chromosome 19.
- Over 18 years of age.

- Capacity to give informed consent.
- Able to participate in the study, and willing to comply with all procedures, either alone or with the aid of a responsible care giver.

2.3.2 Exclusion criteria

Exclusion criteria were as follows:

- Any condition contraindicating an MRI scan including recent surgery with metallic implants, intracranial metallic implants, metallic fragments in the eyes or body, pregnancy.
- A history of co-existent disease that may interfere with participation in the study e.g. chronic alcohol or drug abuse; untreated major depression; any medical condition with an expected life expectancy of less than 12 months; a diagnosis of another progressive neurodegenerative condition (such as Alzheimer's disease or Parkinson's disease).
- Any medical condition contraindicating the administration of carbon dioxide: respiratory illness; heart failure; haemodynamic instability; uncontrolled hypertension; history of subarachnoid haemorrhage, intracranial aneurysm or arteriovenous malformation.
- Conditions/medications that may affect the results of peripheral vascular tests: Raynaud's disease; peripheral arterial disease; current use of calcium antagonists or ACE-inhibitors.

2.3.3 Withdrawal of participants

Participants could be withdrawn from the study for the following reasons

- withdrawal of consent;
- intolerance of carbon dioxide administration;
- deemed necessary for clinical reasons.

2.4 Management of participants

All study participants were allocated a unique study number, which served as an individual identifier for all clinical data and biological samples. Clinical research files were kept in a secure location in the Southern General Hospital. Biological samples were kept securely at the British Heart Foundation Glasgow Clinical Research Centre (BHF GCRC). Transport was provided for the participants for all visits if required.

2.4.1 Study Protocol

Study participants were reviewed at baseline, year 1 and year 2. The study schedule is shown in Table 2-1. Visit 1 was also the first visit. Visits 2, 3, 4 and (6, 7, 8 and 10, 11, 12) could occur in any order. It was planned that visits at baseline, year 1 and year 2 should occur within a 2 month period.

Table 2-1 Study schedule

Month	Baseline (0 + 2 mth)				6 mth	Year 1 (12 \pm 1 mth)			18 mth	Year 2 (24 \pm 1 mth)		
VISIT	1	2	3	4	5	6	7	8	9	10	11	12
Eligibility	X											
Consent	X											
Medical history	X				X	X			X	X		
Demographics	X				X	X			X	X		
Medication	X				X	X			X	X		
NIHSS	X					X				X		
mRS	X				X	X			X	X		
Bloods/ urine		X								X		
Height/ weight		X				X				X		
HADS		X				X				X		
Vascular studies		X				X				X		
Neuro psychology			X				X				X	
TCD	X							X				X
MRI				X				X				X
End of study												X

Abbreviations: NIHSS - National Institute of Health Stroke Scale; mRS - modified Rankin score; HADS - Hospital Anxiety and Depression Scale; TCD - transcranial Doppler ultrasound; MRI - magnetic resonance imaging. X represents a visit where an activity occurred.

2.5 Clinical assessment

For each subject, information on demographics and medical history, including past and current diagnoses, living circumstances and concomitant medication were collected on their first visit using a data collection form.

2.5.1 Clinical definitions

Hypercholesterolaemia was recorded if there was documentation of a cholesterol ≥ 5.2 mmol/L in previous medical records. Hypertension was defined as a systolic BP >140 mmHg or a diastolic BP >90 mmHg on more than 2 occasions, or use of antihypertensive medication together with a past diagnosis of hypertension. Patients on hypertensive medication for migraine prophylaxis were not given a diagnosis of hypertension solely based on medication use.

Stroke was defined as a neurological deficit of sudden onset with focal dysfunction and symptoms lasting more than 24 hours presumed to be vascular in origin. Transient ischaemic attacks (TIA) was defined as above but lasting less than 24 hours and without symptoms typical for migraine with aura.

Cognitive disturbance was recorded if it was self-reported by the patient, or recorded in clinical history, as was psychiatric disturbance. History of migraine was recorded if patients description matched that of the International Headache Society (IHS) of migraine with or without aura (Headache Classification Committee of the International Headache Society, 2013).

2.6 Clinical Scales

2.6.1 National Institute of Health Stroke Scale (NIHSS)

The National Institute of Health Stroke Scale (NIHSS) is a standardised measurement of neurological deficit (Table 2-2). This 0 - 42 point non-linear scale was designed as a research tool for acute stroke trials, but now has widespread clinical use in many stroke units (Brott et al., 1989). It can be used to predict survival and functional recovery in patients in the first week following an acute ischaemic stroke (Weimar et al., 2004).

Whilst not designed specifically for longitudinal assessment, the NIHSS offers a structured and rapid neurological assessment of patients which identifies potentially disabling deficits.

Investigators performing the NIHSS had completed online video training in administration of the scale and received certification of competency.

Table 2-2 National Institute of Health Stroke Scale

Region		Definition
Level of consciousness	0	Alert
	1	Aroused by minor stimulation
	2	Not alert; required repeated stimulation to attend
	3	Responds only with reflex effects or unresponsive
Level of consciousness questions	0	Answers both correctly
	1	Answers one correctly
	2	Answers neither correctly
Level of consciousness commands	0	Performs both correctly
	1	Performs one correctly
	2	Performs neither correctly
Gaze palsy	0	Normal
	1	Partial gaze palsy
	2	Forced deviation
Vision	0	No visual loss
	1	Partial hemianopia
	2	Complete hemianopia
	3	Bilateral hemianopia
Facial palsy	0	Normal movements of face
	1	Minor paralysis of face
	2	Partial paralysis of face
	3	Complete paralysis of one or both sides
Motor Arm Score for individually left and right arm	0	No drift to bed in 10 seconds
	1	Drifts during 10 seconds but does not hit bed
	2	Some effort against gravity but drifts to bed
	3	No effort against gravity
	4	No movement
	UN	Amputation or joint fusion
Motor Leg Score individually left and right leg	0	No drift to bed in 5 seconds
	1	Drifts during 5 seconds but does not hit bed
	2	Some effort against gravity but drifts to bed
	3	No effort against gravity
	4	No movement
	UN	Amputation or joint fusion
Limb ataxia	0	Absent
	1	Present in one limb
	2	Present in two limbs
	UN	Amputation or joint fusion
Sensory	0	Normal
	1	Mild-to-moderate sensory loss
	2	Severe or total sensory loss
Language	0	No aphasia
	1	Mild-to-moderate aphasia
	2	Severe aphasia
	3	Mute
Dysarthria	0	Normal
	1	Mild-to-moderate dysarthria
	2	Severe dysarthria or mute/anarthria
	UN	Intubated or other physical barrier
Extinction and inattention	0	No abnormality
	1	Inattention or extinction to one sensory modality
	2	Hemi-inattention or extinction to >1 sensory modality

2.6.2 Modified Rankin Scale (mRS)

The modified Rankin Scale (mRS) is a global measure of disability and handicap, designed for use in trials as a clinician-reported measure of functional outcome after stroke (Rankin, 1957, van Swieten et al., 1988). It is a 7 point scale ranging from 0 (total independence), to 6 (death) which assesses the ability of an individual to perform tasks such as walking, dressing and managing finances (Table 2-3).

Table 2-3 Modified Rankin Scale (mRS): An assessment of disability after stroke.

Score	Definition
0	No symptoms at all
1	No significant disability despite symptoms, able to carry out all usual duties and activities.
2	Slight disability; unable to carry out all previous activities, but able to look after their own affairs without assistance.
3	Moderate disability; requires some help for more complex tasks (e.g. finances) but able to walk without assistance. Able to manage at home for at least 1 week.
4	Moderate severe disability: unable to walk without assistance and unable to attend to own bodily needs without assistance. Able to be left alone for a few hours during the day.
5	Severe disability: bedridden, incontinent, requiring constant nursing care and attention.
6	Dead

2.6.2.1 Rankin Focussed Assessment Tool (RFA)

The Rankin Focussed Assessment (RFA) tool (UCLA Stroke Center, Los Angeles, California) was developed to provide a clear and practical assessment of the mRS (Saver et al., 2010). It was required as there is subjectivity between several mRS grades and limited inter-observer agreement, with improvement shown with the use of structured interview approaches (Wilson et al., 2002). It has been demonstrated to have a high interrater reliability in comparison to other methods (Quinn et al., 2009). Ratings of disability for Rankin levels 2,3,4 and 5 were based on all the patient's medical conditions, not just prior strokes;

whereas Rankin level 1 was based on symptoms caused only by prior strokes (Saver et al., 2010).

The pre-stroke RFA was used in all cases with reference to guidance available from the authors. Investigators performing mRS assessments had undertaken online training in the administration of mRS.

2.6.3 Hospital Anxiety and Depression Scale (HADS)

The Hospital Anxiety and Depression Scale (HADS) was developed by Zigmond and Snaith to provide a practical and simple screening tool to detect anxiety and depression in medical patients (Zigmond and Snaith, 1983). The aim was to distinguish psychiatric disorders from symptoms of sadness and tension in people suffering from a physical illness. Physical indicators associated with depression such as weight loss or pain, are avoided as they are likely to be symptoms of the illness itself rather than psychological distress. The scale is designed to be sensitive to mild symptoms, withstand situational influences, and be representative of a prolonged rather than a transient state.

It is a self-rating 14 item scale which takes less than 5 minutes to complete. It has an excellent response rate and reliability (Herrmann, 1997) and is widely used in hospitals across the UK (Figure 2-1).

The HADS has clear cut off scores which can distinguish depression and anxiety. The depression subset (D-scale) comprises 7 items expressed both positively and negatively, giving a maximum score of 21. The anxiety subset (A-scale) also comprises 7 items with a maximum of 21. For both subsets, scores of 0-7 are regarded as normal, scores of 8-10 indicate a 'possible' case and scores of 11 and more indicate a 'probable' case.

The HADS scoring sheet (GL Assessment Limited, London) was given to the subject with a brief reinforcement of the instructions stated at the top of the sheet. Subjects were asked to underline the answer that best reflected their feelings over the past few days (Snaith and Zigmond, 1994).

A	D			A	D
		I feel tense or 'wound up'	I feel as if I am slowed down		
3		Most of the time	Nearly all the time	3	
2		A lot of the time	Very often	2	
1		From time to time, occasionally	Sometimes	1	
0		Not at all	Not at all	0	
		I still enjoy the things I used to enjoy	I get a sort of frightened feeling like 'butterflies' in the stomach		
	0	Definitely as much	Not at all	0	
	1	Not quite so much	Occasionally	1	
	2	Only a little	Quite often	2	
	3	Hardly at all	Very often	3	
		I get a sort of frightened feeling as if something awful is about to happen	I have lost interest in my appearance		
3		Very definitely and quite badly	Definitely	3	
2		Yes, but not too badly	I don't take as much care as I should	2	
1		A little, but it doesn't worry me	I may not take quite as much care	1	
0		Not at all	I take just as much care as ever	0	
		I can laugh and see the funny side of things	I feel restless as if I have to be on the move		
	0	As much as I always could	Very much indeed	3	
	1	Not quite so much now	Quite a lot	2	
	2	Definitely not so much now	Not very much	1	
	3	Not at all	Not at all	0	
		Worrying thoughts go through my mind	I look forward with enjoyment to things		
3		A great deal of the time	As much as I ever did	0	
2		A lot of the time	Rather less than I used to	1	
1		Not too often	Definitely less than I used to	2	
0		Very little	Hardly at all	3	
		I feel cheerful	I get sudden feelings of panic		
	3	Never	Very often indeed	3	
	2	Not often	Quite often	2	
	1	Sometimes	Not very often	1	
	0	Most of the time	Not at all	0	
		I can sit at ease and feel relaxed	I can enjoy a good book or radio or television programme		
0		Definitely	Often	0	
1		Usually	Sometimes	1	
2		Not often	Not often	2	
3		Not at all	Very seldom	3	
TOTAL				A	D

Figure 2-1 Hospital Anxiety and Depression Scale - Scoring Sheet
(GL Assessment Limited, London)

2.7 Neuropsychological Testing

2.7.1 General Testing Conditions

Neuropsychological testing was performed at the Southern General Hospital, by Dr Breda Cullen, a trained clinical neuropsychologist.

Testing took place in a quiet room and lasted approximately 2 hours including time for a break.

A summary of results was provided to the participant's General Practitioner after testing and filed in their case notes. If it was felt further clinical assessment or input by a clinical neuropsychologist was required this was discussed with the participant's health care provider.

Testing aimed to establish baseline premorbid intellectual ability and global cognitive ability, but was directed at eliciting subtle deficits in executive function. Table 2-4 summarises the tests used.

Table 2-4 Summary of cognitive tests used in this study

Test name	Ability assessed	Test details
TOPF	Estimated premorbid intellectual ability	An initial estimate of premorbid intellect and memory using 70 words.
ADAS-Cog	Global cognitive function	Global assessment covering memory, orientation, language and praxis.
Symbol digit modalities test (SDMT)	Processing speed	Pairing of geometric figures with specific numbers.
Digit Span forwards Digit Span backwards	Verbal working memory	Examiner reads a sequence of numbers; subject recalls numbers in same order. Examiner reads a sequence of numbers; subject recalls numbers in reverse order.
WMS-IV Symbol Span	Visual working memory	Subjects recall sequences of symbols, increasing in size with each correct completion.
Category fluency Letter fluency	Word generation / executive function	Subject generates the maximum numbers of words from a specific category or with a specific letter in a set time.
Trailmaking Test	Executive function	Subjects connect numbers (part A) and numbers and letters (part B) in a specific order as quickly as possible.
Stroop Test	Executive function	Subject must say either the written word, or name the ink colour the word is written in.
WAIS-IV Similarities	Verbal reasoning	Subject presented with two words that represent common objects or concepts, and must describe how they are similar.
WAIS -IV Block Design	Visuospatial ability	Subject views a model and a picture, or a picture only, and uses blocks to recreate the design.
WMS -IV Verbal Paired Associates	Verbal memory	Subjects must recall or recognize a word when prompted by an unrelated word that was paired with it during the presentation of word pairs.
BMIPB Design Learning	Visual memory	Subject uses visual memory to recall abstract shapes.

TOPF = test of premorbid function; BMIPB = Birt Memory and Information Processing Battery; ADAS-Cog = Alzheimer's Disease Assessment Scale - Cognitive; WMS = Wechsler Memory Scale; WAIS = Wechsler Adult Intelligence Scale

2.8 Vascular Studies

2.8.1 Training of the Investigators

All vascular tests included in this thesis were performed by the author, who had undergone training over 3 months in the principles and techniques of all the tests. The author examined patients with the same methodology as part of another study “Target organ damage in predicting cardiovascular risk” prior to this study commencing.

Vascular tests were performed as per a standard operating procedure and data collected in a vascular case report form.

2.8.2 General testing conditions

All vascular tests took place at the BHF GCRC in temperature controlled rooms (between 22 and 24°C). A trained staff nurse was available at all times. Equipment used in the study was maintained by staff at the BHF GCRC.

Participants attending for vascular studies were asked to refrain from taking alcohol or caffeine for 4 hours prior to the study visit. Vascular studies were performed with reference to published guidelines (Van Bortel et al., 2002) (see Table 2-5). Height and weight were recorded at the start of the study, and a questionnaire administered to identify any issues that may affect or prevent testing (e.g. previous mastectomy, menstrual cycle). Supine blood pressure and heart rate were measured following 10 minutes of rest (OMRON 705IT, Omron corporation, Kyoto, Japan). Blood pressure was measured 3 times, and the mean of the last 2 results taken.

Table 2-5 Recommendations for standardization of subject conditions*

Confounding Factor	In practice
Room temperature	Temperature controlled room (24 degrees Celsius) and temperature documented in case report form.
Time of day	Similar time of day for repeated measurements.
Smoking, eating	Patients asked to refrain from drinking caffeine or smoking for 4 hours prior to measurements. Food intake was recorded.
Alcohol	Patients asked to refrain from drinking alcohol for 10 hours prior to measurements.
Speaking	Patients were asked not to speak during studies.
Position	Supine ideally; position recorded.
Cardiac arrhythmia	Any disturbance recorded as may affect results and have clinical relevance.
Menstrual cycle (for women)	Stage in menstrual cycle recorded; similar stage in cycle for repeat measurements.

*adapted from (Van Bortel et al., 2002).

2.8.3 Pulse Wave Analysis

2.8.3.1 Background

Arterial stiffness partly depends on smooth muscle tone, and can be assessed non-invasively with pulse wave analysis (PWA). The arterial pressure waveform is a summation of the forward pressure wave created by ventricular contraction, and a reflected wave. The waveform is modified along the arterial tree, as the degree of reflection varies. In elastic vessels, the speed of the reflected wave is slow, and thus the wave arrives during diastole and augments diastolic flow to the heart. In stiff vessels, reflection is quick, and the wave arrives prematurely during systole. This augments the systolic pressure and increases the demand on the heart (O'Rourke and Gallagher, 1996).

If a measure of the peripheral radial waveform is obtained, a mathematical model can be used to generate a measure of the aortic waveform. The augmentation phenomenon can then be quantified by the augmentation index: the difference between the second and first systolic peaks ($P2 - P1$) expressed as a percentage of the pulse pressure (Skinner et al.). The augmentation index is influenced by heart rate, age, aortic PWV, diastolic blood pressure, and height.

Augmentation index has been demonstrated to be related to cardiovascular risk and mortality (Mancia et al., 2009).

2.8.3.2 Method and Analysis

Pulse wave analysis was performed with a SphygmoCor® system (AtCor Medical Pty Ltd, Sydney, Australia). A micromanometer-tipped probe (Millar®) was placed on the surface of the skin overlying the radial artery. For accurate readings, this was applied with a light pressure so that the transmural forces within the vessel were perpendicular to the arterial surface. The peripheral radial pulse wave was continuously recorded and 10 pulse waves were analysed. The right radial was chosen unless there was a contraindication.

Integral SphygmoCor® software used a validated transfer function and radial artery waveform to calculate the aortic pulse waveform and aortic systolic and diastolic blood pressure (Chen et al., 1997). The augmentation index was normalised to a standardised heart rate of 75 beats per minute (AI@75; Figure 2-2). The mean of 2 pulse wave readings with an operator index of >80% was taken.

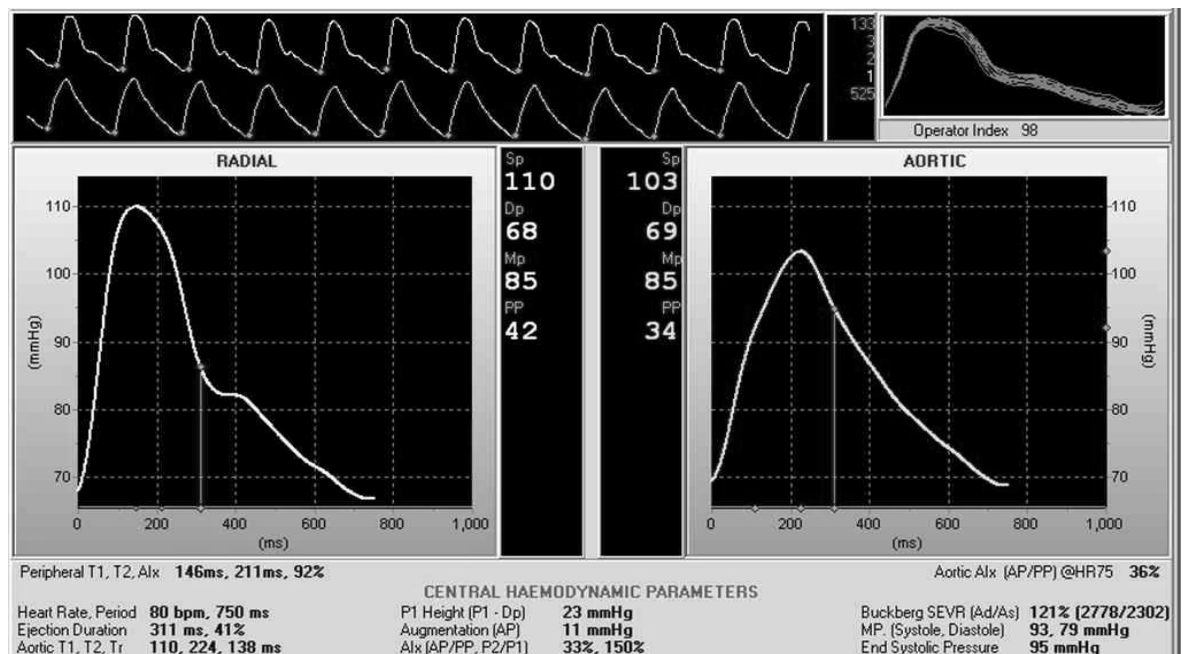


Figure 2-2 Pulse wave analysis

Screenshot of Clinical Report Screen showing Quality Control area (top right) and radial and derived aortic pulse wave forms. Aortic augmentation index at 75bpm was 36%.

2.8.4 Pulse Wave Velocity

2.8.4.1 Background

Arterial stiffness reflects the pressure on the heart, and has clinical relevance in epidemiological studies of cardiovascular risk (Laurent et al., 2001). The gold-standard measurement is carotid-femoral pulse wave velocity (PWV) which is measured along the aorto-iliac pathways (Laurent et al., 2006). PWV is measured in metres/second and derived as follows:

$$\text{PWV} = \frac{\text{distance between carotid and femoral measurement site (metres)}}{\text{transit time (seconds)}}$$

Usual values are between 6 and 10 m/s. A 1.0 m/s increase in carotid-femoral PWV is associated with a 7% increase in vascular events (Ben-Shlomo et al., 2014).

2.8.4.2 Method and Analysis

3 ECG stickers were placed on the chest. An applanation tonometer (Millar®) was used to identify the pressure wave by sequentially placing over the femoral artery (distal site), and then the common carotid artery (proximal site). The surface distance between the 2 recording sites was determined with a measuring tape.

The systolic upstroke, or foot, of the pressure wave was identified by an integral algorithm within the SphygomoCor® software and used as the reference point. The time between the R wave of the ECG and the proximal carotid pulse was subtracted from the time between the R wave and the distal femoral pulse to obtain a pulse wave transit time, Δt . PWV was then automatically calculated (Figure 2-3).

The mean of 2 readings with a standard deviation of <10% was taken. If only one reading with <10% standard deviation was available, it was used alone.

At year 1 the distance measurements from baseline were used, as the error introduced by user repetition was felt to likely exceed the potential difference in placement of the tonometer.



Figure 2-3 Carotid-femoral pulse wave velocity
Screenshot from Clinical Screen. Femoral and radial pulse waveforms are shown with ECG readings below. The pulse wave velocity, with a standard deviation of <10% is shown.

2.8.5 Flow-mediated dilatation of the brachial artery (FMD)

2.8.5.1 Background

Shear stress is a major regulator of vascular tone. Increased blood flow leads to shear stress which opens potassium channels and hyperpolarises the cell (Olesen et al., 1988). Calcium enters and nitric oxide is generated. Nitric oxide causes smooth muscle cells to vasodilate to accommodate the increased blood flow (Pohl et al., 1986).

Increased blood flow can be generated in response to ischaemia. A BP cuff is placed which results in forearm ischaemia and dilatation of downstream resistance vessels in the hand. When the cuff is deflated, blood rapidly flows into the low resistance dilated downstream vessels. This creates shear stress, nitric oxide release, and dilatation of the brachial artery. This dilatation can be measured by ultrasound, and the process termed flow mediated dilatation of the brachial artery (FMD).

Measurement of this response is the gold-standard technique for non-invasive measurement of endothelial function (Celermajer et al., 1992). FMD is inversely related to age, blood pressure, body mass index, lipid lowering medication and smoking (Benjamin et al., 2004). However it adds little additional information when attempting to stratify cardiovascular risk, so its clinical utility remains undetermined (Yeboah et al., 2009). Due to its non-invasive nature it is repeatable but is highly technician dependent, and guidelines for its assessment should be followed (Corretti et al., 2002). Baseline responses in healthy populations are generally 5 - 8% depending on the baseline brachial artery diameter (Anderson and Phillips, 2015).

2.8.5.2 Method

The subject was supine with their right arm extended in a comfortable position. A blood pressure cuff was placed on the right forearm (Hokanson SC12, DE Hokanson, Inc, Bellevue, WA, USA). ECG leads were attached. The brachial artery was identified 5-15cm above the antecubital fossa in a 2-D longitudinal plane using a 7MHz linear array transducer (Acuson, Sequoia). A segment with clear lumen-intima boundaries on both near and far wall was required for imaging. The probe was then held in position with a stereotactic clamp (Figure 2-4A). At baseline this was an in-house clamp. At year 1 and 2 a clamp produced by Rose & Krieger (RKC 80/189, Rose & Krieger, Potsdamer, Germany) was used. After a rest period, a baseline image was obtained including a mid-artery flow velocity. A 3 minute baseline clip of brachial artery diameter triggered by the R wave of the ECG was then obtained (Figure 2-4B). In 1 patient, the left arm was used due to previous breast surgery.

Arterial occlusion was created by cuff inflation to 50mmHg above systolic pressure or at least 200mmHg, maintained with a constant pressure regulator. After a 5 minute period the cuff was released. A further mid-artery pulsed signal was obtained on cuff release to assess hyperaemia velocity. A 5 minute clip of the brachial artery was obtained.

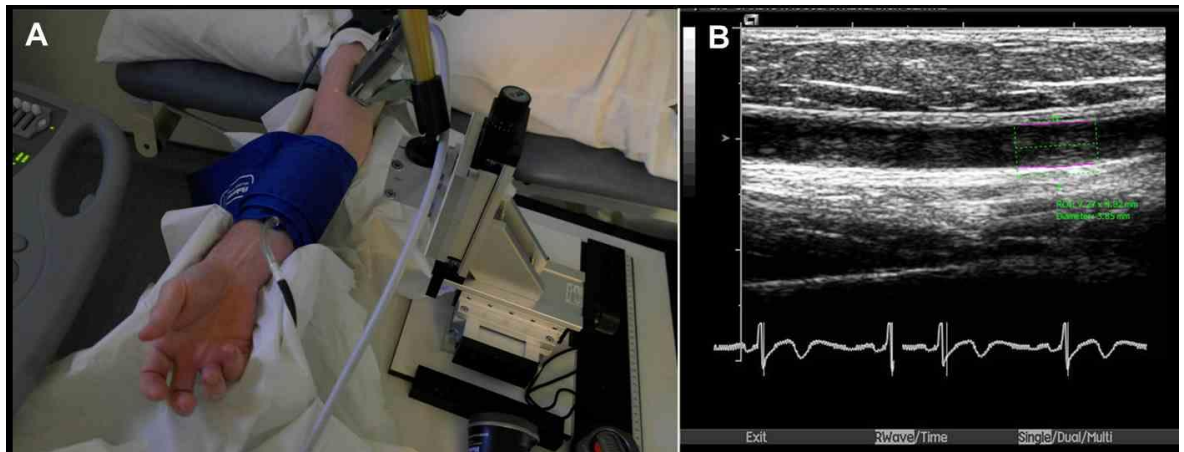


Figure 2-4 Flow mediated dilatation of the brachial artery
(A) FMD set up. (B) Brachial artery identified with ultrasound. The ROI is visible with the pink lines outlining the vessel borders.

2.8.5.3 Analysis

Flow-mediated dilatation offline analysis was performed with specialist software (Brachial Analyzer, MIA LLC, Coralville, IA, USA). The principle measurement is flow mediated dilatation (FMD) calculated as the percentage maximum change in diameter from baseline:

$$\text{FMD} = \frac{\text{Brachial diameter}_{\text{Peak post occlusion}} - \text{Brachial diameter}_{\text{Baseline}}}{\text{Brachial diameter}_{\text{Baseline}}} \times 100$$

All measurements were performed by a single reader (FM). Ultrasounds were graded as poor, average or good based on the ability to visualise the vessel walls and the degree of vessel movement. Poor ultrasounds were not included in the results. An ROI was placed in a region where the near and far brachial artery borders were clearly visualised. Automated optimal graph search-based segmentation was used to determine the vessel wall borders then the analysis was run for each clip. Analysed images were reviewed and edited where required to ensure image did outline the intima-lumen interface (Medical Imaging Applications, 2006). Images where the diameter measurement confidence was less than 70% or those which were on the incorrect interface were rejected. The baseline diameter was determined as the mean of 30 baseline images. The highest diameter (within the first 3 minutes post dilatation) was determined and the mean of the 3 readings around this was taken as the “peak” diameter (see Figure 2-5 for an example of FMD). Analysis was repeated twice, more than 1 month apart, and the average used.

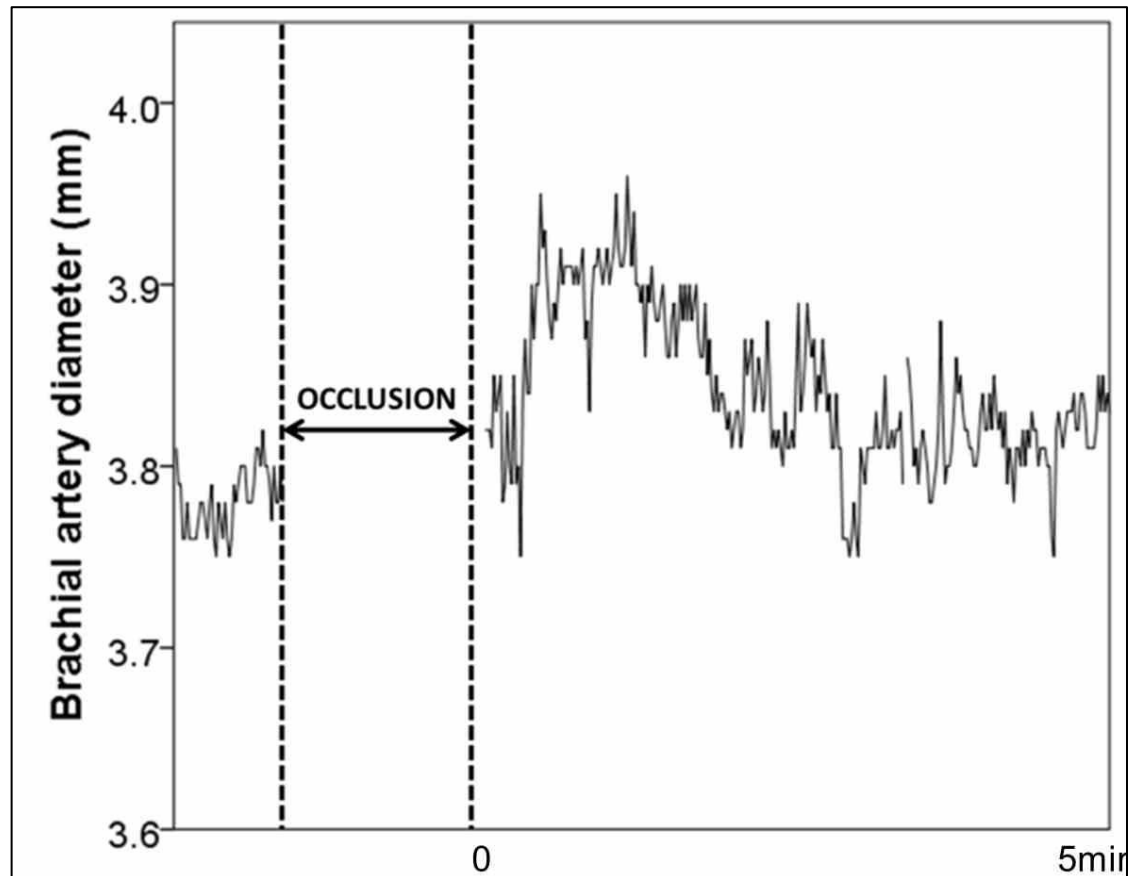


Figure 2-5 Example of FMD result

A 5 minute period of occlusion (not shown in real time) preceded and followed by, measurements of brachial artery diameter.

2.8.6 Peripheral artery tonometry

2.8.6.1 Background

An alternative method of assessing endothelial function is peripheral arterial tonometry (PAT). This requires the use of a finger plethysmograph to sense changes in the volume of blood in a finger with each pulse. Following a period of arterial occlusion, a hyperaemic response should occur. This is due to release of nitric oxide from endothelium subsequent to an increase in shear stress within the microcirculation of the finger. This hyperaemic response has been shown to correlate with brachial FMD measurements and with the presence of cardiovascular risk factors and coronary artery disease (Kuvin et al., 2003).

2.8.6.2 Method and Analysis

Endothelium-mediated vasodilatation elicited by a downstream hyperaemic response, was measured with a non-invasive plethysmographic method (Endo-

PAT2000, Itamer Medical Ltd, Caesarea, Israel). The device records changes in the digital pulse waveform, known as the PAT signal.

A blood pressure cuff (Hokanson SC12, DE Hokanson, Inc, Bellevue, WA, USA) was placed on 1 upper arm (study arm) while the contralateral arm served as a control (control arm). The forearms were supported with arm supports. The index fingers of both hands were placed in probes, which were inflated (see Figure 2-6A)

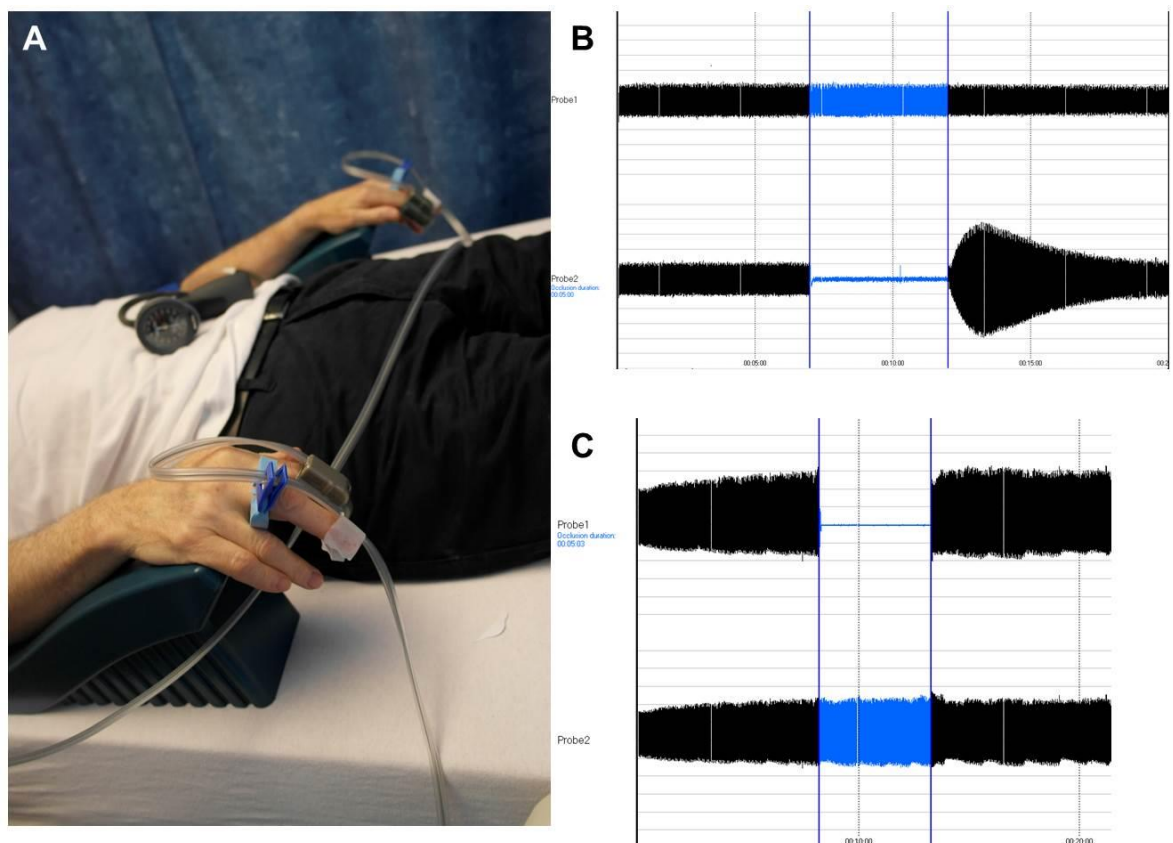


Figure 2-6 Reactive hyperaemia index using Endo-PAT®
(A) Endo-PAT set up shown. **(B)** An example output with normal reactive hyperaemia following blood pressure occlusion. **(C)** A subject with impaired reactive hyperaemia.

After a 10 minute equilibrium period, signal recording started. Changes in pulsatile volume were sensed by a pressure transducer in the probe, which relayed the signal to a personal computer for analysis and display. After 5 minutes, the blood pressure cuff on the study arm was inflated to 50mmHg above systolic pressure for 5 minutes (minimum 200mmHg). The cuff was then deflated to induce reactive hyperaemia. Signal was recorded for a further 5 minutes.

The PAT score output known as the reactive hyperaemia index (RHI), was automatically calculated as the ratio of the PAT signal averaged post and pre-occlusion. The value was normalised to measurements in the contralateral arm which serves as a control for non-endothelium dependent systemic effects (for example increased sympathetic nerve outflow due to pain from hyperaemia). An RHI of <1.67 is thought to represent impaired endothelial function (Itamer, 2015). Normal values are thought to be about 2.0 (Anderson and Phillips, 2015) (Figure 2-6). Patients were excluded if there was incomplete occlusion or excessive movement artefact.

2.8.7 Carotid intima-media thickness (CIMT)

2.8.7.1 Background

Clinical carotid ultrasound is used in the assessment of patients with stroke or TIA to evaluate for the presence of occlusive carotid plaques, and to assess blood flow. However visualisation of 2 echogenic lines, representing the interfaces between the lumen and adventitia, allows measurement of the intima-media thickness of the carotid wall (CIMT). Increased CIMT in the common carotid represents an adaptive hypertrophy to shear stress and changes in blood flow, and is a marker of generalised atherosclerosis. It signifies an increased risk of cardiovascular and cerebrovascular disease (Bots et al., 1997, O'Leary and Bots, 2010).

CIMT increases with age but is also associated with sex, blood pressure, BMI, cholesterol, and diabetes (O'Leary and Bots, 2010). A measurement of $>0.9\text{mm}$ is regarded as definitely abnormal, although the relationship between thickness and cardiovascular risk is thought to be a continuous one (Mancia et al., 2007, Lorenz et al., 2007).

Change in CIMT in individual patients over time is very small (0.0147 mm/year) and for individual patients the error in measurement, likely exceeds the change (O'Leary and Bots, 2010). However, changes can be used in clinical trials with larger numbers of patients to assess the effect of therapeutic interventions.

The widespread application of CIMT has been limited by the requirement for comprehensive training, and technical variations across protocols. The development of a consensus document aims to standardise CIMT readings (Stein et al., 2008)

2.8.7.2 Method

B-mode ultrasonography of the right common carotid artery was performed with a 7-MHz linear array transducer (Acuson, Sequoia). Depth was set at 40mm and frequency 8MHz. 3 ECG leads were attached to the patient to allow R-wave synchronisation.

The patient was positioned supine with their head extended and positioned slightly towards the left. A Meijer Carotid Arc© (Meijer Medical Ultrasound, Netherlands) and head rest was used to position the patient. The participant's nose was at 240°.

A longitudinal image of the carotid was displayed, with the anterior (near) and posterior) far walls of the carotid artery evident as bright lines separated by a hypoechogenic space. The carotid bulb and the distal 1cm of the common carotid artery were visualised (see Figure 2-7).

2 static images (synced to the R wave of the ECG) and a loop image with 3 heart beats were recorded with the ultrasound probe at 90° and 135°.

Finally an assessment of internal carotid velocity was made. If this is >1.25 m/s this may indicate significant upstream carotid stenosis and therefore the magnetic resonance angiography image was reviewed. In 1 patient at baseline (aged 36) velocities over 1.25m/s were recorded, but no carotid lesion was seen on MR angiography.

The above process was then repeated on the left carotid.

2.8.7.3 Analysis

CIMT was calculated by off-line analysis with dedicated software (Siemens Syngo® Arterial Health Package). This uses automatic border detection. The

distal 1cm of common carotid was selected, and the borders automatically detected with manual correction if required. Readings were taken from R-wave synchronised images at 90° and 135° where available. All readings were repeated twice. The mean of both studies at 90° and 135° on both sides was calculated to give a single overall CIMT.

Single measures intraclass correlation coefficient for average CIMT at baseline was 0.96 (0.90 - 0.98) and 0.98 (0.95 - 0.99) at year 1. In 3 patients, only the right carotid was imaged at baseline. These were included as there was no significant difference between right and left carotids at baseline or year 1.

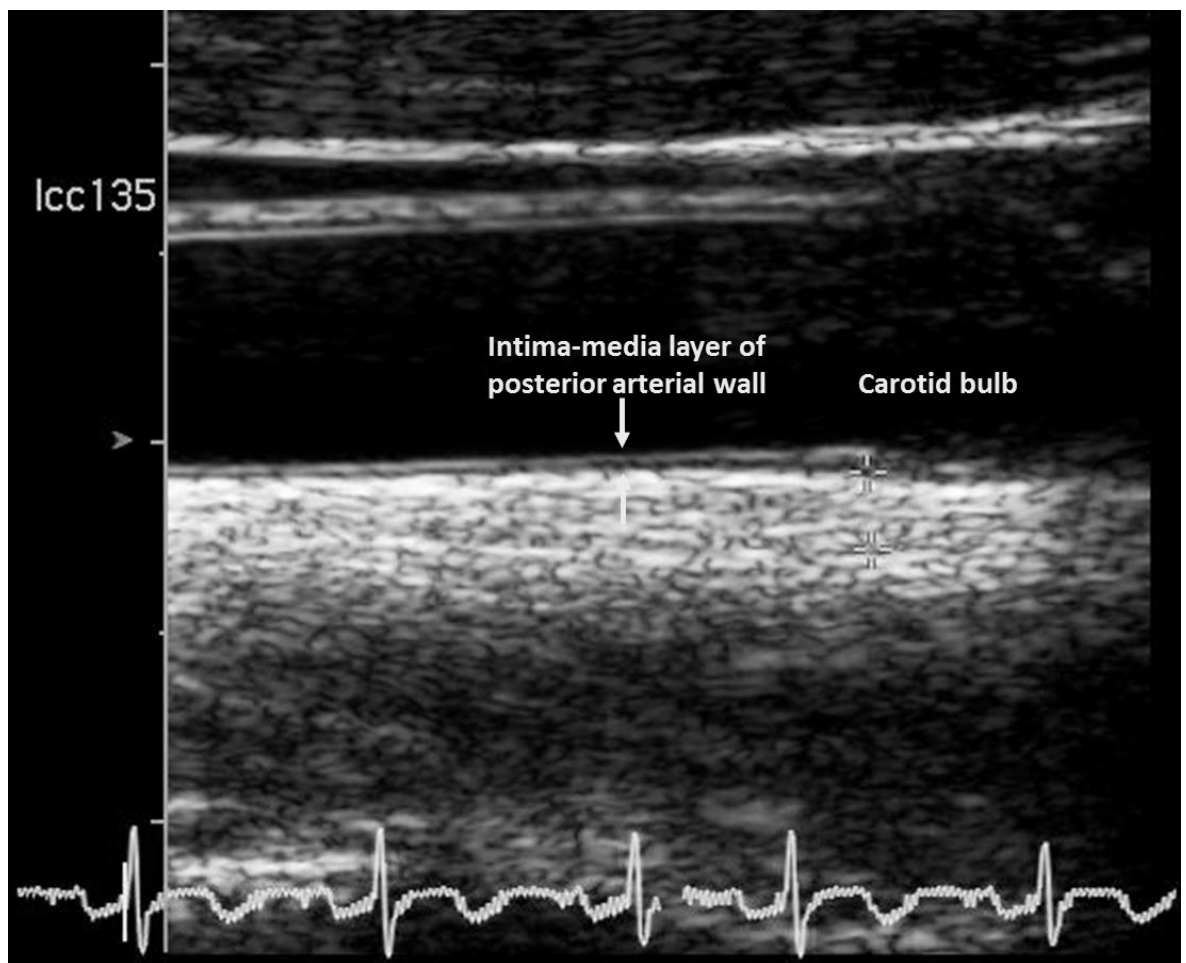


Figure 2-7 Carotid intima media thickness (CIMT)

The left carotid has been identified at angle 135 degrees. The intima-media layers of the posterior arterial wall are clearly seen and are shown with white arrows. The start of the carotid bulb is marked with +.

2.9 Transcranial Doppler Ultrasound

2.9.1 General Testing Conditions

Transcranial Doppler ultrasound was performed at the Southern General Hospital by the author. Recommendations for vascular studies were followed where possible (Van Bortel et al., 2002). Patients were asked to avoid caffeine and cigarettes for 4 hours prior to the procedure. The test was performed in a quiet room with the patient semi-supine.

2.9.2 Procedure

The procedure was performed as per a standard operating procedure (Appendix 2). Transcranial Doppler studies were performed with a ST3/Model PMD 150 (Spencer Technologies, Seattle, WA). PMD provides 33 gates of continuous Doppler information over a 6mm wide and 66mm deep volume, which allows for rapid vessel location and image acquisition.

Blood pressure was recorded after a 5 minute rest period whilst supine. A pulse oximeter was attached and pulse rate, oxygen saturation and respiratory rate were measured continuously during the course of the study (IntelliVue MP30, Philips Medical Systems, Netherlands). Data every 12 seconds were recorded. Inspired and end expiratory gases were also measured. If this monitor was not available ETCO_2 was recorded with a capnograph (Handheld Capnograph, Nellcor, Tyco Healthcare Group).

The middle cerebral artery (MCA) was identified in the transtemporal ultrasound window, by placing a lubricated 2Hz ultrasound probe over the zygomatic arch and angling towards the contralateral ear. Depth was set at 50mm and modified to get maximum spectrogram signal. Once identified, the ultrasound probe was secured to a probe fixation head frame (Marc Series, Spencer Technologies, Seattle, WA). The left middle cerebral artery was then identified with the same procedure. The vessels were labelled with RMCA (right middle cerebral artery) or LMCA (left middle cerebral artery). Once an adequate spectrogram trace was obtained an envelope trace was activated which tracked the maximum blood flow velocity in the spectrogram.

Once a signal was obtained the patient was allowed to rest for several minutes whilst other equipment was set up. An anaesthetic mask (QuadraLite Mask, Ref 7193, Intersurgical Ltd, Wokingham, Berkshire, UK) and filter (Clear-Therm 3 HMEF, Luer Lock Port, Ref 1541, Intersurgical) were attached to the patient with a latex-free harness (Ref 2224, Intersurgical Ltd).

A catheter mount (Ref 3514, Intersurgical Ltd), filter (Clear-Therm 3 HMEF, Luer Lock Port, Ref 1541, Intersurgical Ltd) and unidirectional breathing circuit (Ref 2013014, Intersurgical Ltd) were attached with oxygen tubing to a cylinder containing 6% CO₂/air mixture (BOC Medical, Manchester, UK, Medical Special's Licence Number ML/0735/01).

The subject breathed normal air for 3 minutes and then the anaesthetic mask was connected to the hypercapnia circuit and 6% CO₂/air mixture was administered for 3 minutes. The patient was then administered normal air for a further 3 minutes.

TCD data was continuously monitored by the Data Stream Output function and digitally recorded for off-line analysis. The data included

- Data time stamps
- Doppler settings: Vessel label, Depth, Power, Sample
- Spectrogram envelope derived peak, diastolic, and mean velocities each second for each channel.

2.9.3 Analysis

If both MCAs were successfully recorded, the mean of the 2 sides was used for analysis; otherwise a single MCA was used. Traces were excluded if end-tidal carbon dioxide was not maintained during the hypercapnia challenge suggesting a circuit leak. EtCO₂ readings that were clearly outliers (>1kPa from average) were excluded from calculation of mean EtCO₂.

Peak systolic velocity (PSV), diastolic flow velocity (DFV) and mean flow velocity (MFV) were automatically calculated by integral software.

Cerebrovascular reactivity (CVR_{TCD}) was calculated as percentage change in mean flow velocity in hypercapnia compared to normocapnia per kPa:

$$CVR_{TCD} = \frac{MFV_{hypercapnia} - MFV_{normocapnia}}{MFV_{normocapnia}} \times \frac{100}{EtCO_2 \text{ hypercapnia} - EtCO_2 \text{ normocapnia}}$$

2.10 Magnetic Resonance Imaging

2.10.1 General Testing Conditions

Magnetic Resonance Imaging (MRI) took place in the Neuroradiology Department of the Southern General Hospital. Recommendations for vascular studies were followed where possible (Van Bortel et al., 2002). The participant was asked to remove any metal objects and make up. Medical staff supervising the MRI scans had undergone training in MRI safety from a Clinical Physicist.

2.10.2 MRI screening

A brief MRI screening assessment was performed on the participant's first study visit in order to identify any possible contraindications to MRI scanning. Allergies to contrast and recent eGFR were also recorded, and this record was passed on to the MRI radiographers in advance. On the day of each MRI scan a full screening was performed by a trained neuroradiographer.

2.10.3 MRI procedure

The participant was asked to lie on the MRI scanner. A standard 8-channel head coil (GE Medical Systems, Milwaukee, Wisconsin) was placed around their head. The participant was given earplugs and a hand-held alarm which they could press if they were distressed or unwell. The patient was continually under observation and could be communicated with via the intercom. The set-up of the MRI room is shown in Figure 2-8.

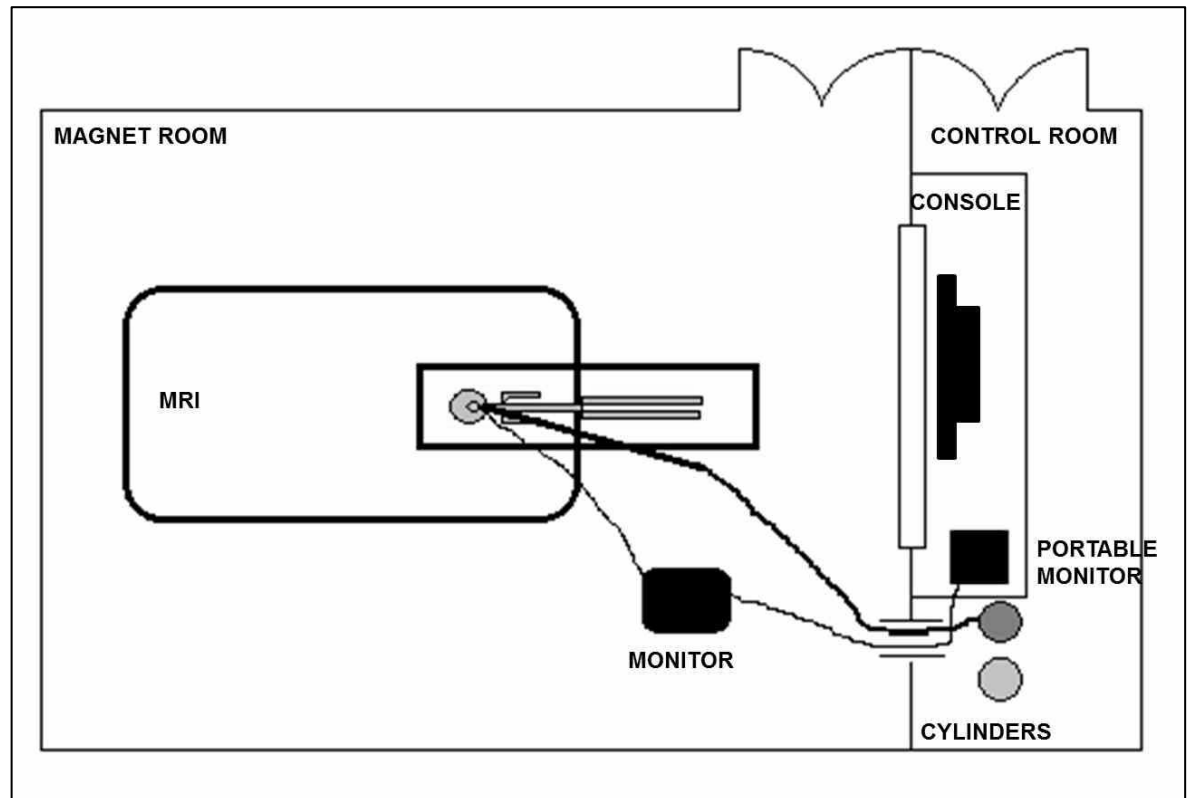


Figure 2-8 MRI room set up

The patient and monitor were in the magnet room. Medical staff and neuroradiographers could observe the patient. Gas tubing was passed through the wave guide from gas cylinders kept in the MRI control room.

The MRI scanning protocol was divided into 2 sessions lasting approximately 30 minutes each. This was to improve patient comfort and reduce movement artefact that might occur with one hour of MRI scanning.

After the first scanning session the participant was allowed a short break. MRI scans which required patient monitoring and gas administration were then performed (further details below). On the first MRI visit a venflon was then inserted into the antecubital fossa for the administration of gadolinium.

2.10.4 Imaging protocol

Tables 2-6 and 2-7 give details of the MRI sequences which were performed on a 3.0 Tesla (3T) scanner (General Electric Signa® Excite). At 1 year and 2 year follow up scans, MRA and gadolinium perfusion was not performed. Not all sequences have been analysed as part of this thesis.

Table 2-6 MRI sequence parameters – Part 1

Seq.	Localiser	T1 sagittal	T2 FLAIR	3D T1	ASSET	SWAN	DTI	fMRI	MRA
TR	5	2500	10000	9	150	Min full	9000	2000	8.6
TE	1.2	Min full	140	3.6	2.1	25	Min full	30	3.5
TI	-	920	2250	450	-	-	-	-	-
Flip angle	30	90	90	12	50	15	90	78	8
NEX	1	1	1	1	1	1	1	1	0.629
No slices	15	30	27	156	36	84	37	40	329
Slice thickness	10	3	5	1	7	3.6	3.5	3.5	1.2
Space between slices	15	5	6.5	1	7	1.8	4.5	4.5	0.6
Matrix	256 x 128	320 x 224	384 x 256	320 x 320	64 x 64	320 x 224	64 x 64	64 x 64	320 x 224
Φ FOV	1	1	1	0.8	1	1	1	1	0.9
FOV	240 x 240	240 x 240	240 x 240	240 x 240	300 x 300	240 x 240	224 x 224	224 x 224	260 x 260
Orientation	3 plane	AC-PC	AC-PC	AC-PC	Axial	Axial	AC-PC	AC-PC	Sagittal
Time	0:12	1:31	3:20	4:28	0:06	02:15	05:15	10:12	3:11

TR = repetition time, TE = echo time, TI = inversion time, NEX = number of excitations, FOV = field of view, DTI = diffusion tensor imaging, fMRI = functional MRI, MRA = magnetic resonance angiography, SWAN = susceptibility weighted angiography.

Table 2-7 MRI sequence parameters – Part 2

Seq.	Localiser	T1 sagittal	3D ASL (air)	3D ASL (CO ₂)	PWI (air)	PWI (CO ₂)
TR	5	2500	4864	4864	2000	2000
TE	1.2	Min full	10.1	10.1	25.9	25.9
TI	-	920	-	-	-	-
Flip angle	30	90	155	155	78	78
NEX	1	1	3	3	1	1
No slices	15	30	40	40	?22	?22
Slice thickness	10	3	3.5	3.5	3.5	3.5
Space between slices	15	5	3.5	3.5	5.5	5.5
Matrix	256 x 128	320 x 224	512 x 8	512 x 8	128 x 128	128 x 128
Φ FOV	1	1	1	1	1	1
FOV	240 x 240	240 x 240	240 x 240	240 x 240	240 x 240	240 x 240
Orientation	3 plane	AC-PC	Axial	Axial	Axial	Axial
Details			pCASL	pCASL	Half dose gadolinium	Half dose gadolinium
Post Label Delay	-	-	2025	2025	-	-
Gas			Air	6% CO ₂	Air	6% CO ₂
Time	0:12	1:31	04:42	04:42	03:00	03:00

TR = repetition time, TE = echo time, TI = inversion time, NEX = number of excitations, FOV = field of view, ASL = arterial spin labelling, PWI = perfusion weighted imaging, pCASL = pseudo continuous ASL.

2.10.5 Gas administration and equipment

Subjects were monitored with an MRI compatible anaesthesia patient monitor (Veris® Vital Signs Monitor, MEDRAD, Indianola, PA) (Figure 2-9).

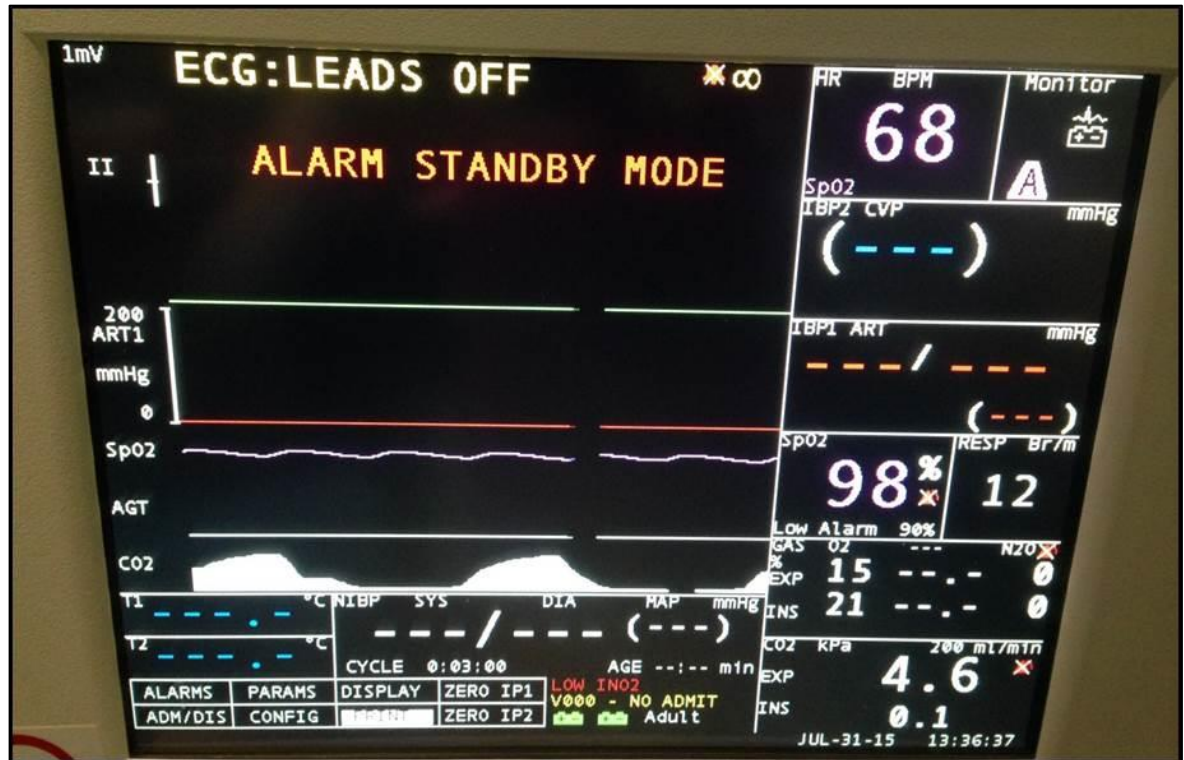


Figure 2-9 MRI patient monitor interface

Heart rate, respiratory rate, oxygen saturation and inspiratory and expiratory O₂ and CO₂ could all be measured. Blood pressure and ECG was not monitored during these experiments.

A face mask (Ref 1141, Intersurgical Ltd) was placed on the subject's face. The expiratory ports were closed with tape, and the mask secured to the patients face with tape to improve seal. The mask was then connected to a specially designed unidirectional breathing circuit (Ref 2013014, Intersurgical Ltd) via a catheter mount (Ref 3514, Intersurgical Ltd) and filter (Clear-Therm 3 HMEF, Luer Lock Port, Ref 1541, Intersurgical). Bubble tubing (ID 3mm, Ref 032-10-067, Flexicare Medical Ltd, UK) was attached to the circuit with a 22M connector (Ref 1968, Intersurgical Ltd), and then fed through the waveguide into the MRI control room (Figure 2-10). Here it was attached to a cylinder containing medical air or 6% CO₂/air mix (BOC Medical, Manchester, UK, Medical Special's Licence Number ML/0735/01). Both gases were administered by a common tubing system to avoid change of mask or tubing during the scan.

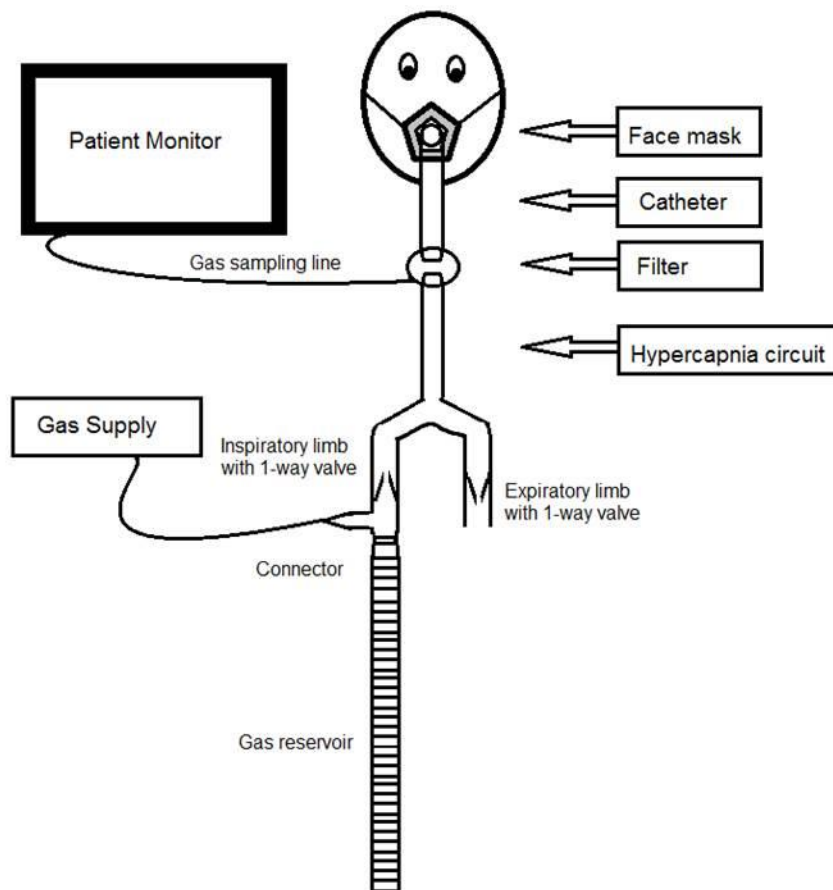


Figure 2-10 Gas administration set-up

If the face mask was not tolerated (1 patient) a single use dual nare nasal cannula with gas monitoring was used (Ref 032-10-127, Flexicare Medical Ltd, UK) and attached to the bubble tubing via a connector. The first 3 patients at baseline had gas delivered via a Quadralite anaesthetic face mask (Ref 7193, Intersurgical Ltd) attached with a CPAP harness (Ref 2224, Intersurgical Ltd) as per TCD testing. These patients underwent perfusion imaging with the Neurovascular head coil. After 3 patients this was switched to the head coil for improved signal-to-noise ratio.

2.11 MRI image processing

MRI scans were anonymised and then transferred to University of Glasgow XNAT (open source imaging informatics platform). Scans were then downloaded in DICOM format and transformed to NIFTI using dcm2nii from MRICron (Rorden et al., 2007). Image analysis took place on either a Dell PC with “WindowsTM” 7 platform, with an Intel Core i7 processor; or a Linux based platform on a Dell PC.

2.11.1 Lesion definitions

White matter hyperintensities were defined as signal abnormality of white matter showing hyperintensity on fluid-attenuated inversion recovery images (Wardlaw et al., 2013). Where lesions in the subcortical grey matter or brainstem were included the term subcortical hyperintensities (SH) was used (Wardlaw et al., 2013).

Lacunes were defined as: round or ovoid, subcortical, fluid-filled cavities (signal similar to CSF) of between 3-15mm in diameter, consistent with a previous acute small subcortical infarct or haemorrhage in the territory of 1 perforating arteriole (Wardlaw et al., 2013).

Subcortical lacunar lesions were defined as groups of rounded, circumscribed lesions just below the cortex at the junction of grey and white matter with a signal intensity identical to CSF (van den Boom et al., 2002).

Cerebral microbleeds were defined as small (usually 2-5mm in diameter but up to 10mm) areas of signal void with associated blooming seen on susceptibility weighted imaging (Wardlaw et al., 2013).

Perivascular spaces were defined as fluid-filled spaces (similar signal intensity to CSF) which follow the course of a vessel as it passes through brain tissue. They appear linear when imaged parallel to the course of a vessel, and round when imaged perpendicular to the vessel course. They do not have a hyperintense rim (unless passing through white matter hyperintensity) (Wardlaw et al., 2013). They were defined as <3mm in diameter, unless they were in region of the anterior commissure where giant perivascular spaces can be seen (Saeki et al., 2005).

2.11.2 Visual examination of scans

Visual examination of scans took place on a Dell workstation using the PACS system. Scans were reviewed twice, at least one month apart, without reference to previous results. Scans were inspected for hyperintensities, lacunes, subcortical lacunar lesions and enlarged perivascular spaces.

2.11.2.1 Scheltens score

This semi-quantitative scale examines anatomical regions, taking into account both lesion size and number (Scheltens et al., 1993). It scores 3 periventricular regions, 4 white matter lobar regions, 5 basal ganglia structures and 5 infratentorial regions (Table 2-8). The scale was also modified for CADASIL patients by including assessment of the following areas: external-capsule-insula and corpus callosum. Involvement of the temporal lobe was also categorised by location: anterior, posterior or anterior-posterior. The posterior margin of the amygdala was taken as the boundary between anterior and posterior portions (O'Sullivan et al., 2001). Scans were scored 3 times by the same reader and the median of the last 2 runs taken at baseline. At year 1, scans were scored twice, and the median taken.

Table 2-8 Scheltens scale

Periventricular Hyperintensities (PVH 0 - 6)	
Caps - Occipital	0 = absent
Caps - Frontal	1 = <5 mm
Bands - Lateral ventricles	2 = >5 mm and <10 mm
White matter hyperintensities (WMH 0 - 24)	
Frontal	0 = absent
Parietal	1 = <3mm, $n \leq 5$
Occipital	2 = <3mm, $n > 6$;
Temporal	3 = 4 - 10mm, $n \leq 5$
	4 = 4mm - 10mm, $n \geq 6$;
	5 = >11mm, $n > 1$
	6 = confluent
Basal Ganglia Hyperintensities (BG 0 - 30)	
Caudate nucleus	0 = absent
Putamen	1 = <3mm, $n \leq 5$
Globus pallidus	2 = <3mm, $n > 6$;
Thalamus	3 = 4 - 10mm, $n \leq 5$
Internal capsule	4 = 4mm - 10mm, $n \geq 6$;
	5 = >11mm, $n > 1$
	6 = confluent
Infra-tentorial foci of hyperintensity (ITF 0 - 24)	
Cerebellum	0 = absent
Mesencephalon	1 = <3mm, $n \leq 5$
Pons	2 = <3mm, $n > 6$;
Medulla	3 = 4 - 10mm, $n \leq 5$
	4 = 4mm - 10mm, $n \geq 6$;
	5 = >11mm, $n > 1$
	6 = confluent
CADASIL modified (0 - 12)	
External capsule-insula	0 = absent
Corpus callosum	1 = <3mm, $n \leq 5$
	2 = <3mm, $n > 6$;
	3 = 4 - 10mm, $n \leq 5$
Temporal lobe location (anterior, posterior, ant/post)	4 = 4mm - 10mm, $n \geq 6$;
	5 = >11mm, $n > 1$
	6 = confluent

2.11.3 Lacune number and volume

3D T1 image was loaded into Analyze® with equalisation of voxels. Lacunes were identified visually and a seed placed within the lacune. If present lacunes were counted in the following areas on both sides of the brain: brainstem, cerebellum, caudate, globus pallidus, putamen, thalamus, internal capsule, external capsule, corpus callosum, deep and periventricular white matter, and frontal, parietal, temporal and occipital lobes. Lacunes were subdivided into two size categories: 3-<10mm and 10-15mm. 3D seed-based thresholding tools were then used to outline the lacune (Analyze v 11.0, Analyze Direct Inc.,

United States). This was repeated for each lacune creating an object map. The volume of lacunes was calculated. Lacune volume was normalised to intracranial cavity volume (NLV, %).

This was performed twice on scans at baseline. Single measures intraclass correlation was 0.935 (0.845 - 0.973). However as lacunes are binary, i.e. present or not present, only the second score was taken for analysis.

2.11.4 Subcortical lacunar lesions

Presence or absence of these lesions was recorded in the following areas: anterior temporal, posterior temporal, frontal, parietal, and occipital lobe.

2.11.5 Cerebral microbleeds

Identification of cerebral microbleeds was assisted by the current recommended criteria detailed in Table 2-9 (Greenberg et al., 2009).

Table 2-9 Recommended criteria for identification of cerebral microbleeds*

Black lesions on T2*-weighted MRI (or susceptibility weighted imaging)
Round or ovoid lesions (rather than linear)
Blooming effect
Devoid of signal hyperintensity on T1-weighted or T2-weighted sequences.
At least half of lesion surrounded by brain parenchyma
Distinct from other potential mimics such as iron, calcium, bone or vessel flow voids.
Clinical history excluding traumatic diffuse axonal injury

*(adapted from Greenberg, 2009)

SWI scans were inspected for assessment of microbleeds, with reference to anatomical scans (T1 and FLAIR) to exclude mimics. The Microbleed Anatomical Rating Scale (MARS), a validated rating scale for cerebral microbleeds, which has shown good intra-rater agreement over time, was used to classify microbleeds on the basis of certain/uncertain, location, size and number (Gregoire et al., 2009). As recommended for research studies, only definite microbleeds were

included in the final count, but uncertain microbleeds were recorded for longitudinal comparison (Charidimou et al., 2012).

The rater (FM) received training in microbleed detection from a senior neuroradiologist, Dr C Santosh. At baseline, microbleeds were counted on scans 3 times. If there was disagreement between the 2nd and 3rd review, a second reviewer (Dr Dani) was asked to decide if a microbleed was present or not. At year one, scans were scored twice and the same process followed.

2.11.5.1 Perivascular spaces

The number of perivascular spaces was assessed on T2 FLAIR and T1 sequences using the Enlarged Perivascular Spaces (EPVS) scale (Potter et al., 2014). This was designed for use on T2 weighted images although these were not available. This rates EPVS in 3 areas: basal ganglia (including the insular cortex but excluding the anterior perforated substance), midbrain and centrum semiovale. Both sides of the brain were reviewed and the side with the higher number of EPVS was counted. The rating categories are shown in Table 2-10.

Table 2-10 EPVS Scale

	Rating	Description
Basal ganglia and centrum semiovale	0	No EPVS
	1	1-10 EPVS (mild)
	2	11-20 EPVS (moderate)
	3	21-40 EPVS (frequent)
	4	>40 EPVS (severe)
Midbrain	0	No EPVS visible
	1	EPVS visible

The scans were scored 3 times and the median taken. The weighted kappas between the second and third runs were: good for basal ganglia, 0.63 (0.39 - 0.88); moderate for centrum semiovale 0.54 (0.14 - 0.94); and good for midbrain, 0.77 (0.34 - 1).

2.11.6 Subcortical hyperintensity segmentation

There are a variety of techniques used to outline or segment subcortical hyperintensities (including grey matter and brainstem hyperintensities). Several were investigated in this project. 5 randomly selected scans were used as practice scans to validate method reliability.

2.11.6.1 Method1: Manual segmentation

Manual maps were drawn by hand using the paint tool in FSL on the original FLAIR image. This was entirely manual and not based on thresholds.

2.11.6.2 Method 2: Manual maps with thresholding

The FLAIR image was loaded into the software package “Medical Image Processing, Analysis and Visualisation” (MIPAV, National Institutes of Health, Bethesda, MD, USA). Hyperintensities were identified and a seed placed within the region. The “lasso” feature was then used to vary the threshold of the seed to best outline the hyperintensity. This was repeated in all areas of hyperintensity.

2.11.6.3 Methods 3 and 4: Thresholding

T1 3D scans were co-registered to FLAIR using optimized automatic 3D registration in MIPAV (affine 12, trilinear interpolation, cost function - correlation ratio, search algorithm: Powell’s calling Brent’s, no weight). The transformed T1 image was then skull-stripped in FSL using BET (-“B” f 0.1) (Smith, 2002, Smith et al., 2004). Manual modification of brain mask was used if required. The skull stripped scans were then segmented using FAST in FSL (Zhang et al., 2001). Mixed type partial volume effect map was binarised; manually modified if required and then was used to mask the FLAIR to create a brain parenchyma image. This was edited if required.

Two options were then investigated. In method 3, the mode of the masked FLAIR image was multiplied by 1.3 and this number used to threshold the image. Once maps were created, manual modification to remove single or cortical voxels was

used. In method 4, two areas of normal appearing white matter (NAWM) were identified and a region of interest drawn. The mode of these two regions was multiplied by 1.45 and used to threshold the image. These techniques were based on the segmentation method described by Smart et al (Smart et al., 2011), but the mode was different to ensure optimal thresholding in a different cohort of patients.

The different methods and two example patients can be seen in Figure 2-11.

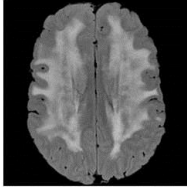




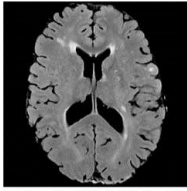




		Method 1	Method 2	Method 3	Method 4
09					
20					
		Draw round SH using FSL paint tool	Identify SH manually	Register T1 to FLAIR	Register T1 to FLAIR
			Use lasso tool in MIPAV to outline SH	Segment T1 to create brain mask using FSL	Segment T1 to create brain mask using FSL
				Determine modal intensity of masked FLAIR	Determine modal intensity NAWM
				Segment FLAIR with threshold = 1.3 X modal intensity	Segment FLAIR with threshold = 1.45 X modal intensity NAWM

Figure 2-11 Subcortical hyperintensity segmentation methods
 Method 1 is a manual method, Method 2 manual with lasso tool to outline SH and methods 3 and 4 based on thresholding. Examples of patients 09 and 20 can be seen. NAWM= normal appearing white matter, SH = subcortical hyperintensity, FLAIR = fluid attenuated inversion recovery.

2.11.6.4 Choice of method

Entirely manual segmentation (method 1) was very labour intensive and was felt likely to introduce excessive user dependent error in longitudinal analysis. Method 2 was used as gold standard as was manually derived, to compare to methods 3 and 4, and when masks were overlapped the median percentage of shared voxels was 71% for both methods 3 and 4. Method 3 was chosen as it could be difficult to identify NAWM on some patients (for example 09 in Figure 2-11) and also this was felt to introduce more individual user variability. This method was repeated in 5 patients and it showed a high level of repeatability as this method was mainly automated (Figure 2-12). SH maps were therefore created with method 3 at baseline (Figure 2-13).

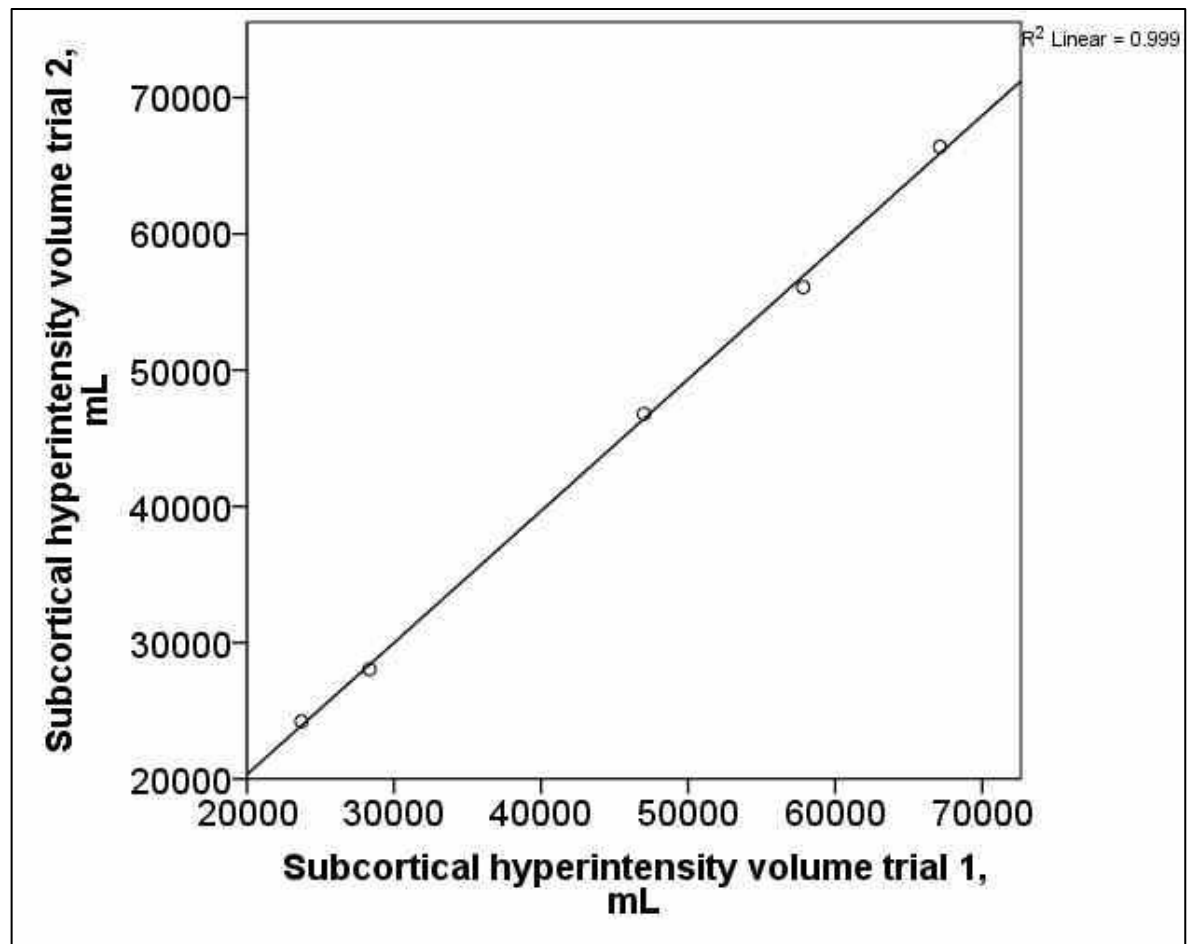


Figure 2-12 Subcortical hyperintensity thresholding repeatability

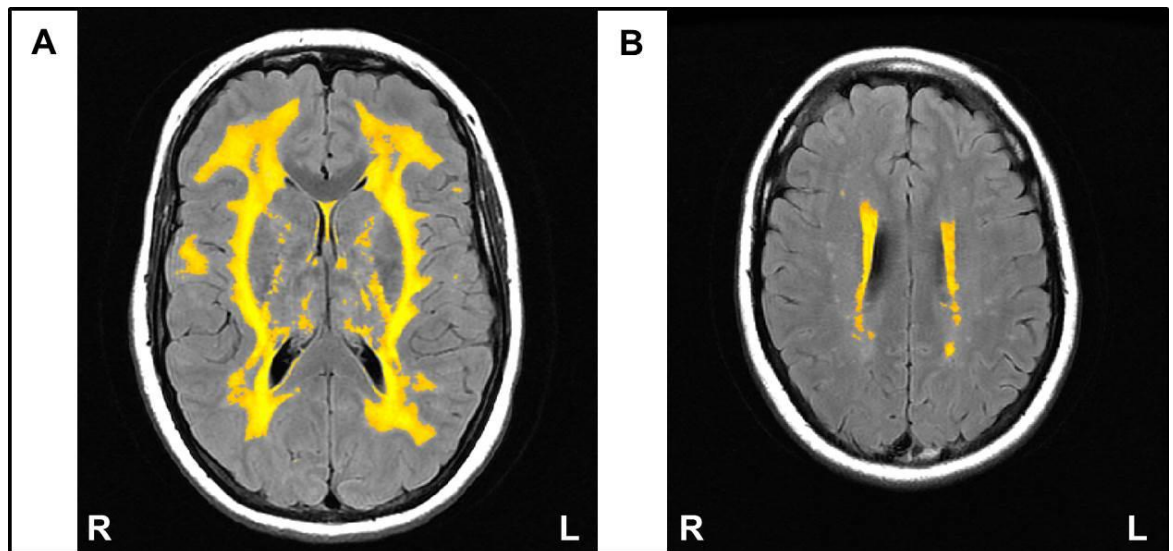


Figure 2-13 Examples of subcortical hyperintensity segmentation

2.11.7 Other imaging processing

Details of other image processing methods are contained in individual chapter methods sections.

Chapter 3 – Epidemiology of CADASIL in the West of Scotland

3.1 Introduction

Whilst CADASIL is proposed to be the most common cause of inherited stroke and exist in all ethnic groups, accurate epidemiological data remain limited. In 2004, the prevalence of confirmed CADASIL in adults in the west of Scotland, was estimated at 1.98 per 100,000 with an estimated mutation prevalence of 4.15 per 100,000 population (Razvi et al., 2005b). The study was hampered by incomplete genetic screening, and the prevalence data were felt to be an underestimate of the true disease prevalence. Contributing factors identified as likely to lead to an under diagnosis of CADASIL included a high local burden of confounding differential diagnoses including multiple sclerosis and conventional cerebrovascular disease, and recognition of the disease only in large pedigrees with typical imaging findings (Razvi et al., 2005a). The first two pedigrees diagnosed with hereditary vascular dementia (subsequently confirmed as CADASIL) in our unit in 1986, had over 100 members at the time of formal diagnosis (St Clair et al., 1995).

Recent changes have led to the proposition that a higher prevalence of CADASIL may now be identifiable. These include the capacity for full genetic screening for typical cysteine involving mutations in exons 2 to 23 of the NOTCH3 gene, available locally since 2007. Atypical mutations have also now been proposed to cause CADASIL, including those which do not involve a cysteine residue (Wollenweber et al., 2015). The development of a specialist clinical service based at a single centre in the west of Scotland, allows the opportunity for near complete capture of cases. Improved awareness amongst clinicians of the manifestations of the disease, along with wider use of brain MRI aiding identification of specific radiological features such as external capsule hyperintensity (O'Sullivan et al., 2001) may lead to increasing numbers of diagnosed cases over time.

Given that knowledge of the epidemiology of a disease is vital for planning of clinical services, as well as social care cost planning, I aimed to investigate the epidemiology of CADASIL in the west of Scotland. The aims of this chapter are:

- 1) to calculate the disease prevalence of CADASIL in 3 health boards in the West of Scotland;
- 2) to estimate the disease prevalence (heterozygote frequency) within the Glasgow area.

3.2 Methods

3.2.1 Identification of cases

A neurovascular genetics clinic was established in 2002 in association with local clinical genetics services, to facilitate the diagnosis and management of patients with CADASIL. Referrals are accepted from stroke physicians, neurologists, general practitioners and family members across Scotland. Subjects were included if their diagnosis of CADASIL was prior to 31st December 2012.

Individuals were classified as having confirmed CADASIL if they had a pathogenic mutation on analysis of exons 2-23 of the NOTCH3 gene. First, second and third degree relatives (symptomatic or asymptomatic) of confirmed CADASIL cases in whom genetic testing had not been undertaken were defined as having a 50%, 25% or 12.5% a priori risk of CADASIL.

Clinical records from the neurovascular clinic and genetic records from the West of Scotland Clinical Genetics Service were reviewed. Pedigrees were constructed and drawn using Progeny CLINICAL Version 8 (Progeny Software LLC, Delray Beach, FL, www.progenygenetics.com).

3.2.2 Population and Geographical area

Although clinic attendees came from a wide geographical area, the majority of patients were from west and central Scotland (represented by Greater Glasgow and Clyde [GGC], Lanarkshire and Forth Valley Health boards). This population is predominantly of Scottish and Irish origin. The 2011 mid-year population estimates of total residents (all ages) for GGC, Lanarkshire and Forth Valley health boards were 1,210,254, 563,185 and 295,541 respectively. The combined total population in GGC and Lanarkshire was 1,773,439. The adult age (18 and above) populations were 974,040, 443,821 and 234,237 respectively (National

Records of Scotland, 2012). The total and adult population for Scotland was 5,254,800 and 4,218,391. To estimate mutation prevalence I recorded the location and status of all known living family members from pedigrees from the GGC and Lanarkshire health boards, and excluded those known to be living out with this area. The number of people 'at risk' was then multiplied by the percentage risk to give an estimate of affected people:

Mutation prevalence

$$= \text{No of known CADASIL cases} + (\text{No of 1}^{\text{st}} \text{ degree at risk relatives} \times 0.5) + (\text{No of 2}^{\text{nd}} \text{ degree at risk relatives} \times 0.25) + \text{No of 3}^{\text{rd}} \text{ degree at risk relatives} \times 0.125)$$

3.2.3 Statistics

For prevalence estimates where the number of subjects was less than 100, 95% confidence intervals were derived from the Poisson distribution. If the number of subjects was over 100 the normal approximation was used:

$$\frac{\text{Number of cases}}{\text{Population}} \pm Z_{\alpha/2} \left(\frac{\sqrt{\text{Number of cases}}}{\text{Population}} \right)$$

where $Z_{\alpha/2}$ is the $\alpha/2$ -level for the normal deviate (e.g. 1.96 for 95% confidence intervals) (Washington State Department of Health, 2002).

3.3 Results

3.3.1 Disease prevalence

49 families with CADASIL were identified. 105 subjects (52 male, 52 female) were identified to have had CADASIL, of whom 15 were deceased. Status was unknown in 3 patients. All were of White ethnicity. The cumulative number of pedigrees diagnosed over time is shown in Figure 3-1. 21 different mutations were identified in 49 pedigrees with 61% of mutations occurring in exon 4 (Table 3.1). The spread of mutations was similar to that previously reported in UK populations (Markus et al., 2002).

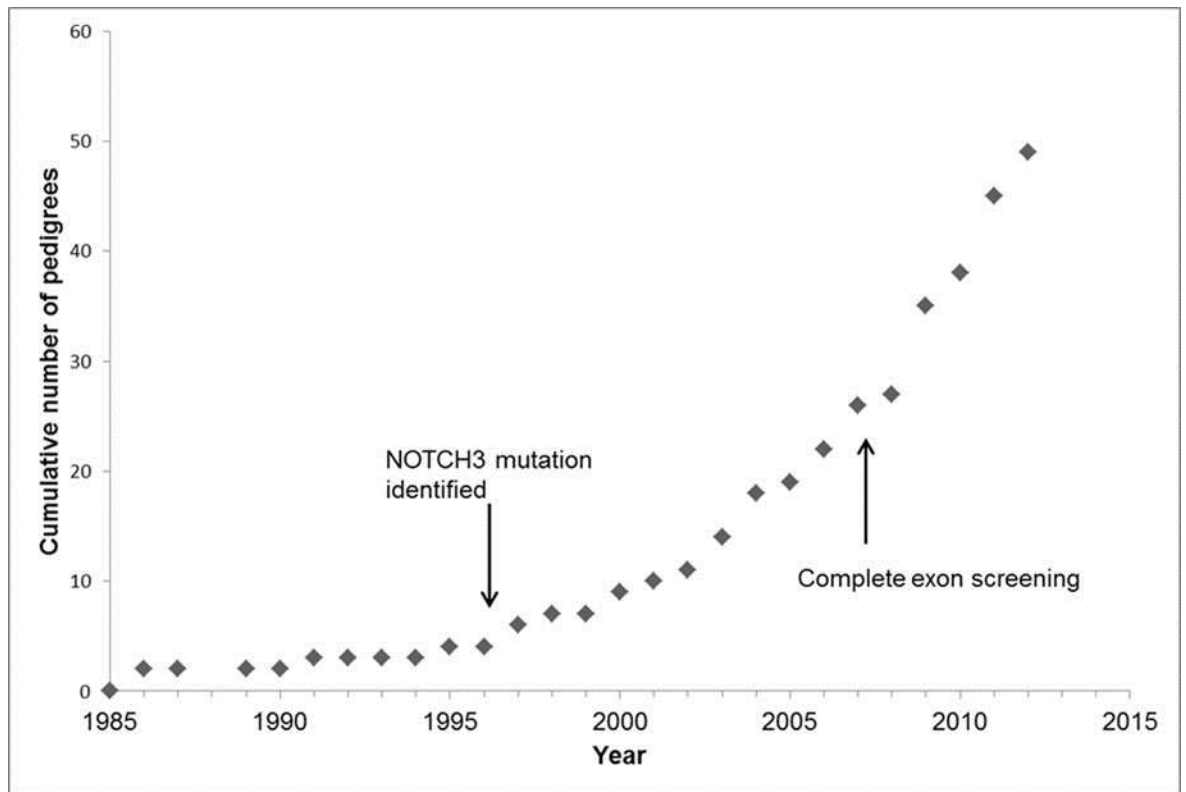


Figure 3-1 Cumulative number of CADASIL pedigrees diagnosed in Scotland

Table 3-1 Mutations detected in the Scottish population

Exon	Mutation Site*	Amino acid change	Number of pedigrees
2	c.160 C>T	Arg54Cys	3
3	c.239 A>G^	Asp80Gly	1
3	c.328 C>T	Arg110Cys	2
4	c.397 C>T	Arg133Cys	4
4	c.421 C>T	Arg141Cys	9
4	c.457 C>T	Arg153Cys	3
4	c.505 C>T	Arg169Cys	5
4	c.544 C>T	Arg182Cys	2
4	c.547 T>C	Cys183Arg	2
4	c.580 T>A	Cys194Ser	2
4	c.619 C>T	Arg207Cys	2
4	c.664 T>C^	Cys222Arg	1
5	c.683 T>G^	Phe228Cys	1
5	c.733 T>A	Cys245Ser	2
5	c.778 T>C	Cys260Arg	1
5	c.779 G>A	Cys260Tyr	1
6	c.994 C>T	Arg332Cys	3
6	c.931 T>A	Cys311Ser	1
8	c.1336T>G	Cys446Gly	1
18	c.2956 T>C^	Cys986Arg	1
22	c.3664 T>G^	Cys1222Gly	2

*Mutation description at the DNA level in coding sequence of NOTCH3. Nucleotide number starting from as of the AGT translation initiating methionine(Dunnen and Antonarakis, 2000). ^Previously unreported mutations

87 people with CADASIL were confirmed as alive and resident in Scotland across a number of health boards (Figure 3-2). For the 3 relevant health boards, the number of living adults with confirmed CADASIL was 45 (GGC), 15 (Lanarkshire), and 8 (Forth Valley), giving a prevalence of 4.6 (95% confidence intervals 3.4 - 6.2), 3.4 (1.9 - 5.6) and 3.4 (1.4 - 6.7) per 100,000 adults respectively. Average disease prevalence across the 3 regions was 4.1 per 100,000 adults (3.2 - 5.2).

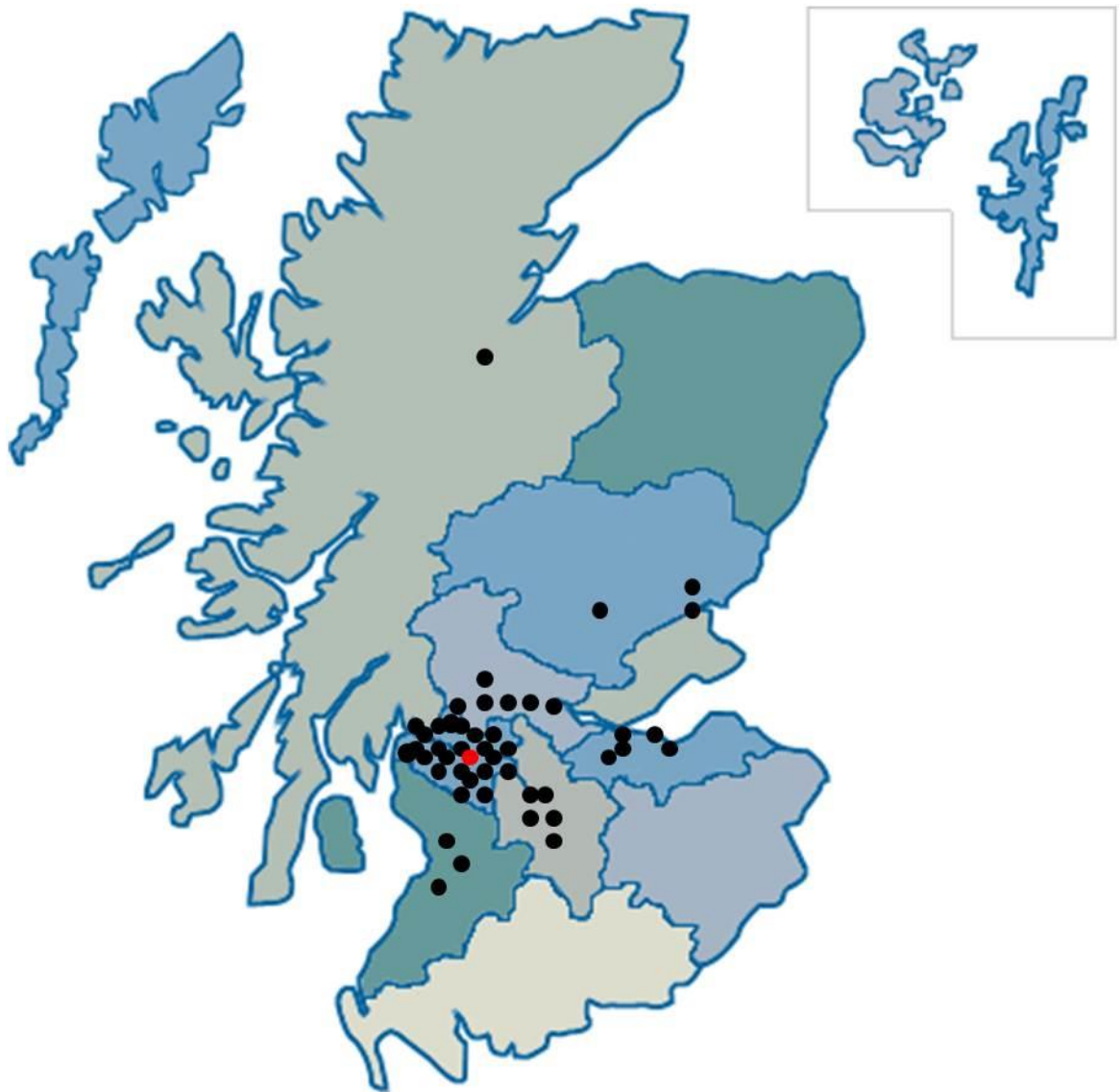


Figure 3-2 Location of CADASIL probands

Location of probands for 47 pedigrees across health boards in Scotland (black dots). The position of the Southern General Neurovascular Clinic is shown (red dot).

3.3.2 Mutation prevalence

Previous estimates of mutation prevalence in the west of Scotland were based on establishing the location of “at risk relatives” (Razvi et al., 2005b). Due to the large number of living relatives establishing exact location of all individuals was problematic. 27 pedigrees were mainly resident in GGC and Lanarkshire health boards, with 637 living family members. 51 were definitely not resident within GGC or Lanarkshire health boards. For the remaining family members there were 141 at 50% risk, 191 at 25% risk and 93 at 12.5% risk, with the remainder at less than 12.5% risk. Estimated gene prevalence was 190 (130

estimated + 60 confirmed) NOTCH3 mutation carriers, with a predicted mutation prevalence of 10.7 per 100,000 population (9.2 - 12.2).

3.3.3 Projected affected cases in Scotland

If the prevalence of CADASIL in the west of Scotland (4.1/100,000 adults) is extrapolated to Scotland in general (4,213,391 adults) it can be estimated that there are 173 (135 - 219) adults with CADASIL in Scotland.

3.4 Discussion

The minimum disease prevalence in CADASIL in Glasgow is 4.6 per 100,000 adult residents, a figure more than twice that calculated in 2005. Estimated mutation prevalence is approximately 1 per 10,000 people. This figure exceeds recent estimates in the North East of England of an “at-risk” population that included only first degree relatives of 6.11 per 100,000, although this study lacked complete exon screening and only included a small number of pedigrees (Narayan et al., 2012).

Out with the screening for genetic diseases in the newborn, estimation of the prevalence of rare diseases is difficult. Levy and Feingold discussed a number of rules necessary for study design when determining prevalence including a well-defined geographical area (GGC Health board), homogenous diagnostic criteria (NOTCH 3 mutation), accurate denominator details based on official statistics (2011 population estimates) and careful evaluation of family members (Levy and Feingold, 2000). In fully penetrant autosomal dominant diseases, such as CADASIL and Huntington’s disease, where homozygotes are negligible in frequency, the disease frequency and heterozygote frequency should be the same. However, many heterozygotes will be symptomless for most of their life, and thus not all are recognised as affected (Harper, 2002). Systematic screening of asymptomatic family members in order to calculate mutation prevalence is neither ethical nor cost-effective, and uptake of presymptomatic screening in other genetic neurodegenerative diseases has been shown to be low (Harper et al., 2000).

Some support for this figure for mutation prevalence may be gained from examining the experience in Huntington's disease. Estimates of the heterozygote frequency in Huntington's disease (using those with CAG frequencies in the definite range) suggested the frequency was between around 2.5 times the prevalence estimate (Conneally, 1984). Whilst the two diseases are not entirely equivalent, both are adult onset autosomal dominant diseases with high penetrance. If applied to this CADASIL population in GGC and Lanarkshire, the heterozygote frequency (mutation prevalence), would be estimated at 10.3 per 100,000 population, very close to my estimate.

There are some limitations to this study. The large number of relatives of the 27 pedigrees in GGC and Lanarkshire meant determining the exact location of all was unfeasible. Pedigree information was often recorded when the index patient was first seen, and only updated periodically. Thus I cannot be sure that all relatives included in mutation estimation remain in the defined geographical areas.

A further criticism is the use of crude risk percentages which are based upon knowledge of the rules of autosomal dominant inheritance. This method is believed to overestimate prevalence, and whilst methods have been suggested to correct for this, they require a defined age- related risk (Harper, 2002). Given the variable natural history of CADASIL, this is difficult to establish.

Overestimation is possible, but under ascertainment of CADASIL cases may also have occurred. Neurological services at this hospital cover GGC and Lanarkshire, and cases of CADASIL in Forth Valley are also routinely referred. Therefore, I am unlikely to have missed any known CADASIL cases in these health boards. However in other Scottish health boards, patients may be managed within their local neurological services or by their General Practitioner. There is also likely to be a larger pool of cases of CADASIL that are undiagnosed or misdiagnosed, particularly in older patients presenting with symptoms who do not undergo an MRI. Some patients, particularly those with conventional cardiovascular risk factors will also be assumed to have conventional small vessel disease. Accurate family histories are also not always available (Razvi et al., 2005a), and in particular the importance of psychiatric disease may not be appreciated.

This is implied by extrapolation of the GGC prevalence to Scotland, which suggests only around half of the cases of CADASIL are actually diagnosed.

Why does the prevalence of a disease matter? CADASIL remains, by the European Union definition of less than 50/100,000 population, a rare disease (European Commission, 2008). However 1 in 17 of the population will suffer a “rare disease” at some point in their life (www.raredisease.org.uk). Knowing how common a disease is will undoubtedly influence health and research resource allocation.

2% of the UK population is disabled by a neurological condition (The Neurological Alliance, 2003). The burden of neurological disease is underestimated by epidemiological statistics based solely on mortality rates. The Global Burden of Disease study (Murray et al., 1996) measured both premature mortality and disability (disability-adjusted life years), and highlighted that neurological diseases posed a significant burden on health care, which will increase with an ageing population (World Health Organisation, 2006). Disability not only incurs the direct costs required by provision of services by health and social care, but often leads to the loss of a person from the work force. CADASIL causes stroke and disability in patients of working age, with minimal effect on life expectancy (Opherk et al., 2004) and thus incurs a significant burden on resources. The National Service Framework for Long-term conditions, developed with input from patients with neurological diseases, aims to improve services for these patients and address the unmet need in the UK (Department of Health, 2007). However CADASIL remains a disease that is poorly understood by many of the providers of such services and thus patients suffering from this disease have a further barrier to their care. Furthermore the cognitive changes associated with the disease, including apathy and poor organisation, means patients may not be the most effective advocates of their own care.

Providing accurate estimates of disease prevalence, particularly in comparison to other neurological diseases (Table 3.2), as well as increasing awareness of the disease, may lead to increased provision of services for patients with CADASIL and similar disorders.

Table 3-2 The prevalence of neurological diseases
(modified from a table from the Neurological Alliance (The Neurological Alliance, 2003) and
The National Service Framework for long-term conditions (Department of Health, 2007).

Neurological conditions	Prevalence (cases per 100,000 population)	Approximate total numbers in the UK
Alzheimer's disease	1000	700,000
Epilepsy	430 - 1000	182,750 - 425,000
Stroke	500	300,000
Parkinson's disease	200	120,000
Charcot-Marie-Tooth disease	40	23,600
Huntington's disease	13.5	6000 - 10,000
<i>CADASIL (estimated)</i>	<i>10.7</i>	<i>6750</i>
Motor neurone disease	7	4000
Progressive supranuclear palsy	6	3600
Multiple system atrophy	1	600
Ataxia-telangiectasia	0.3	200
Variant Creutzfeldt Jacob disease	127 cases since 1995	NA

However, evidence of need does not always result in provision, and allocation of resources can be driven by a variety of pressures including those from high-profile patient advocacy groups (for example International Huntington Association, Motor Neurone Disease Association), which CADASIL currently lacks.

3.5 Conclusion

CADASIL is more common than originally supposed, and should no longer be regarded as a footnote in Neurovascular textbooks. The prevalence is likely to rise, but what is important for patients is that awareness of the disease, amongst neurologists, clinicians and resource allocators, matches this increase.

Chapter 4 - Respiratory Challenge MRI: Practical Aspects

4.1 Introduction

Changes in cerebral blood flow can be caused by alterations in the concentration of oxygen (O_2) and carbon dioxide (CO_2) in the bloodstream (Kety and Schmidt, 1948a). When used in combination with imaging techniques, this response can be used to investigate brain physiology (Aaslid et al., 1989, Battisti-Charbonney et al., 2011, Novack et al., 1953). Magnetic resonance imaging (MRI) is a non-invasive, repeatable technique which allows detailed structural and functional information about the brain to be obtained. “Respiratory challenge MRI” can be defined as the modification of the concentration of arterial oxygen (PaO_2) and/or carbon dioxide ($PaCO_2$) to induce a change in cerebral function or metabolism which is then measured by MRI. Investigation of brain pathophysiology including cerebral blood flow, oxygenation, metabolic rate and microvascular function in diseases such as stroke (Dani et al., 2010), dementia (Cantin et al., 2011), epilepsy (Kalamangalam et al., 2012) and brain tumour (Yetkin and Mendelsohn, 2002, Hsu et al., 2010) has been undertaken.

A number of respiratory challenge approaches have been attempted. These can range from modification of respiratory rate, including breath hold (Hsu et al., 2010) and hyperventilation, to complex modelling of both respiratory parameters and brain signal change (Shen et al., 2011, Mutch et al., 2012). There are significant practical challenges to undertaking this technique however.

The aims of this chapter are to:

- 1) review the rationale for respiratory challenge MRI in brain disease;
- 2) discuss techniques, equipment, monitoring and planning such experiments;
- 3) propose some recommendations for optimization of these studies;
- 4) discuss the potential use of this in cerebrovascular disease.

4.2 Rationale

The human brain employs an elegant system of regulation of cerebral blood flow (CBF) to ensure adequate delivery of O₂ and nutrients to brain tissue, according to need and regardless of changes in blood pressure, oxygenation or other factors. CBF is determined by the following equation:

$$\text{CBF} = \frac{\text{cerebral perfusion pressure}}{\text{cerebrovascular resistance}}$$

Normal global CBF is around 50mL/100g/min (Kety and Schmidt, 1948b) with higher values found in grey matter than white matter (Leenders et al., 1990). CBF varies according to age, time of day, anatomical area and neuronal activity in order to maintain adequate nutrient delivery. The principle mechanism by which CBF is adjusted according to demand is by changing cerebrovascular resistance. This is governed by small cerebral vessels, particularly pre-capillary arterioles (<100µm)(Wei et al., 1980), which are able to change calibre in response to a number of stimuli, a process known as cerebrovascular reactivity (CVR). Capillaries may also have an important role through the action of pericytes. Dilation of pericytes may account for the majority of CBF augmentation in response to neuronal activation (Hall et al., 2014). If CVR is impaired, then autoregulation of CBF may fail.

Whilst a variety of methods exist for measuring CBF, there are difficulties in obtaining accurate, quantifiable CBF measurements, including inter-individual variability (Leenders et al., 1990), external factors(to be discussed further below)(Laurent et al., 2006), and inaccuracies in modelling methods (Eskey and Sanelli, 2005). Large patient cohorts may be required to detect differences in CBF in disease states.

Measuring cerebrovascular reactivity (CVR) is an alternative technique. CVR may be measured by applying a “challenge” such as the vasodilator acetazolamide (Vagal et al., 2009) or modification of arterial gas concentration. The use of a challenge uses the individual as their own control and negates some of the problems of direct measurement (Eskey and Sanelli, 2005). CBF, and hence CVR,

can be measured by MRI sequences including arterial spin labelling (ASL) or dynamic susceptibility contrast perfusion MRI (Wintermark et al., 2005).

Changes in vessel calibre in response to a challenge can lead to changes in other parameters. This includes oxygenation and cerebral blood volume (CBV) which are then measurable by other MRI techniques. Therefore the change in signal is defined as:

$$\% \text{ change} = \frac{\text{MRI parameter}_{\text{postchallenge}} - \text{MRI parameter}_{\text{baseline}}}{\text{MRI parameter}_{\text{baseline}}} \times 100$$

For standardization of signal change, it should be corrected for the change in gas concentration delivered to, or expired by, the subject. Therefore the general formula for defining CVR in respiratory challenge MRI is:

$$\text{CVR} = \frac{\text{MRI parameter}_{\text{postchallenge}} - \text{MRI parameter}_{\text{baseline}}}{\text{MRI parameter}_{\text{baseline}}} \times \frac{100}{[\text{Gas}]_{\text{postchallenge}} - [\text{Gas}]_{\text{baseline}}}$$

4.2.1 Gases

O₂ and CO₂ have well described effects on cerebral vessel calibre and blood flow in health (Kety and Schmidt, 1948a). These effects are rapid and reversible, with minimal side effects. Rapid initiation and cessation of a gas challenge allows repeated measurements during MRI.

4.2.1.1 The physiology of gas transport

Air, comprising 21% O₂ and 0.04% CO₂, is inhaled through the mouth and nose, and conducted to the lungs by the trachea and bronchi, which form anatomic dead space (i.e. they do not take part in gas exchange). Inspired air mixes with expired gas in the conducting airways and the concentration of O₂ falls, and CO₂ rises. In the alveoli, O₂ diffuses into capillaries and is transported to the heart. The majority of O₂ (>98%) is carried bound to haemoglobin within red blood cells, as oxyhaemoglobin, but the remaining amount is transported in arterial blood as a dissolved gas (referred to as the PaO₂). The total amount of O₂ delivered to the tissues is a combination of dissolved and bound O₂ and is the O₂ content (CaO₂).

The CaO_2 can be calculated as follows:

$$\text{CaO}_2 = (1.34 \times \text{Hb} \times \frac{\text{SaO}_2}{100}) + (0.023 \times \text{PaO}_2)$$

Where:

SaO_2 = arterial oxygen saturation (%)

PaO_2 = arterial partial pressure of oxygen (kPa)

CaO_2 = arterial oxygen content (mL/dL)

Hb = Haemoglobin (g/dL)

Once arterial blood is delivered to tissues, the more acidic and hypercarbic environment causes O_2 to be released from oxyhaemoglobin for use in tissues. Metabolising tissues release CO_2 which diffuses from tissue capillaries into the venous circulation. It is transported as dissolved gas, bicarbonate, and bound to blood proteins. In the lungs, CO_2 diffuses along its concentration gradient into the alveoli, and is expired where it can be measured as end-tidal CO_2 (EtCO_2 ; Figure 4-1). Normal EtCO_2 is 4.0-5.7kPa, and is 0.3-0.7kPa lower than PaCO_2 due to the mixture of gas in alveolar dead space. In normal healthy individuals, the difference is negligible but this becomes more marked in cardiac and pulmonary disease due to increased dead space. This is also the case for differences in EtO_2 and PaO_2 (Bengtsson et al., 2001).

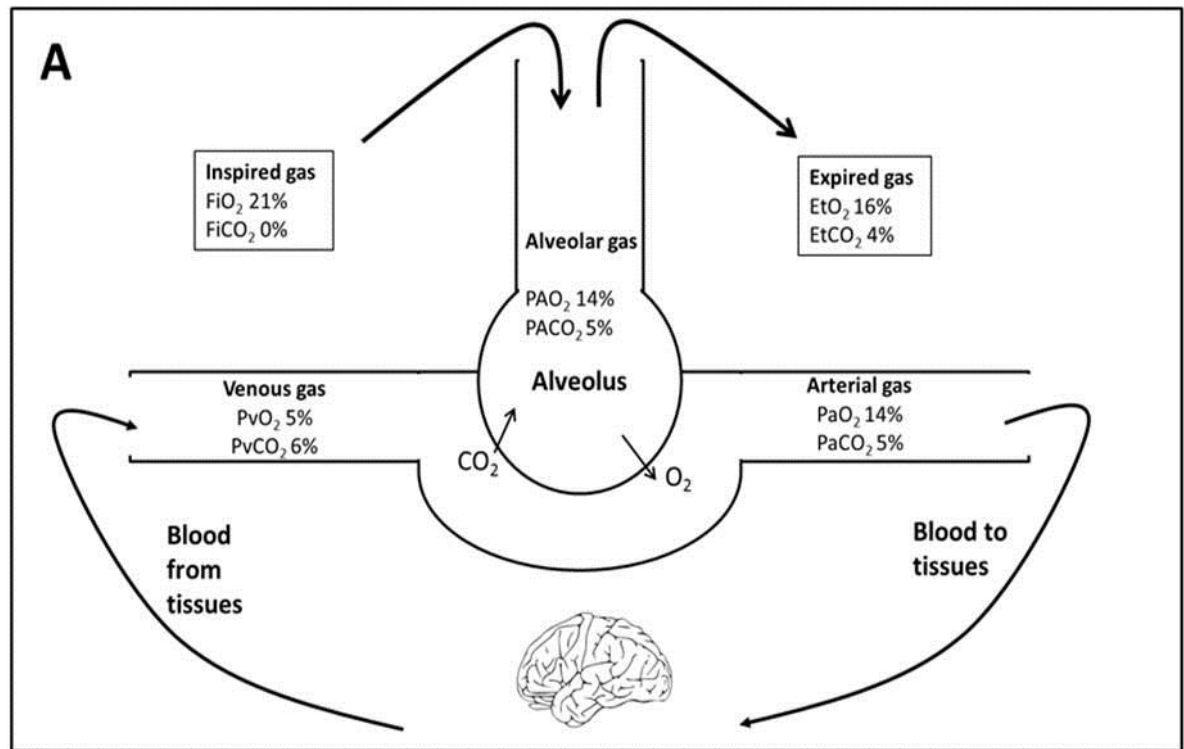


Figure 4-1 Physiology of gas transport

Oxygen (O_2) is inspired into the alveoli and passes into the arterial blood for delivery to tissues. Carbon dioxide (CO_2) produced by metabolizing cells is carried in the venous system and expired through the lung. PvO_2 and PvCO_2 is the partial pressure of oxygen and carbon dioxide in venous blood. For other abbreviations see Table 1-3.

4.2.2 Carbon dioxide

CO_2 is one of the most important modulators of vascular tone, with increased CO_2 (hypercapnia) leading to a relaxation of vascular smooth muscle and increased CBF. For each 1mmHg increase in PaCO_2 , CBF increases by 1-2ml/100g/min (Brian, 1998, Kety and Schmidt, 1948a). This relationship is characterized by a sigmoidal curve, with attenuated responses at the extremes (Reivich, 1964) (See Figure 4-2). Resistance arterioles (40-100 μm) are more responsive to hypercapnia than larger arterioles (up to 400 μm), but responses to hypocapnia are independent of vessel size. Recent evidence has suggested that even major vessels, such as the middle cerebral artery, demonstrate diameter change in response to altered CO_2 concentration (Coverdale et al., 2014). CBF has a similar sigmoidal relationship to changes in PaCO_2 (Grubb et al., 1974).

CO_2 is proposed to exert its effects after dissociating into the vasoactive agents H^+ and HCO_3^- . Increased H^+ concentrations lead to activation of potassium channels and endothelial hyperpolarization (Ainslie and Duffin, 2009) which is relayed to vascular smooth muscle cells. Intracellular calcium concentration

reduces and vasorelaxation occurs (Edvinsson and Krause, 2002). Alterations in CO₂ were originally thought not to affect metabolic O₂ consumption (Kety and Schmidt, 1948a) but more recent evidence suggests hypercapnia may lead to altered neuronal activity (Hall et al., 2011).

Rapid CO₂ diffusion across alveoli allows CBF change within 6 seconds of a rise in CO₂ with a CBF plateau being obtained within 45 seconds (Poulin et al., 1996). However, the fall in CBF following restoration of normocapnia occurs within seconds (Poulin et al., 1996). Adaptation to sustained hypercapnia does occur, with gradual restoration of normal CBF despite sustained hypercapnia. This is thought to occur within hours, although others have argued this can occur within 10 minutes (Ellingsen et al., 1987).

Side effects such as nausea, flushing, hyperventilation, and transient neurological symptoms (Spano et al., 2013) may occur with hypercapnia along with anxiety, sensory stimulation and a panic-like disorder (Colasanti et al., 2012). Hyperventilation induced by hypercapnia may increase motion artefacts (Taylor et al., 2001). Ainslie and Duffin (Ainslie and Duffin, 2009) recommended limiting delivery of FiCO₂ to 8% for both subject safety and comfort. Despite side effects most subjects tolerate hypercapnia experiments. A review of 434 CVR MRI examinations using a rebreathing circuit and targeted EtCO₂ of 50mmHg (6.7kPa), reported transient symptoms in 11.1% of studies, no major complications and successful CVR map generation in 83.9% of studies (Spano et al., 2013). Examined patients had a variety of diagnoses including atherosclerosis, Moyamoya vasculopathy, arteriovenous malformation, vasculitis and dissection.

Hypercapnia is a potent stimulator of minute ventilation and can increase systemic blood pressure (BP) (Kety and Schmidt, 1948a), due to activation of the sympathetic nervous system, which may affect CVR measurements (Hetzl et al., 1999, Ainslie and Duffin, 2009). The vascular response to hypercapnia is lost when vessels are maximally dilated in response to low systemic BP (e.g. hypovolaemia), in an effort to maintain CBF (Grubb et al., 1974). There is therefore a limit on the capacity to autoregulate. CVR to breath-hold and 6% CO₂ breathing showed improved correlation when changes in blood flow velocity (measured by transcranial Doppler ultrasound) were corrected for changes in

blood pressure, and therefore monitoring BP during MRI experiments should be considered (Prakash et al., 2014).

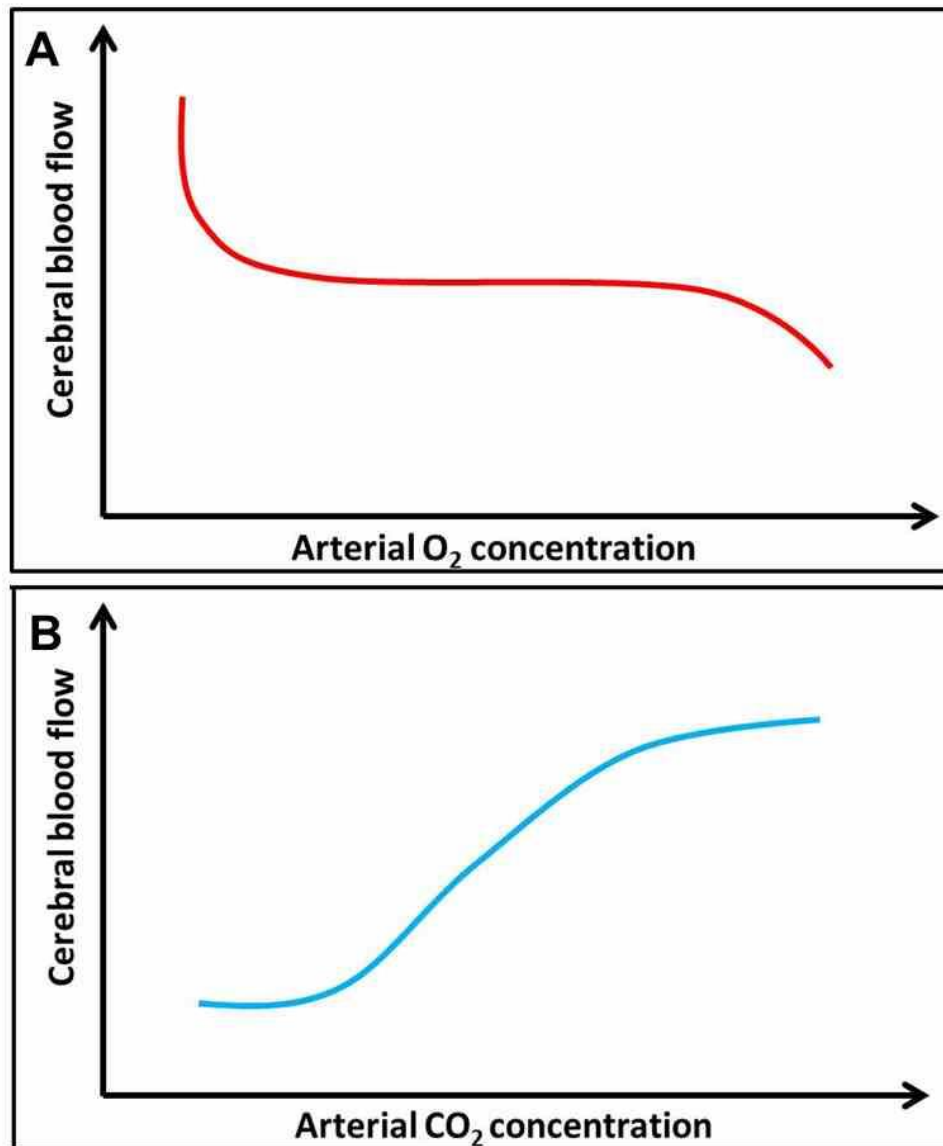


Figure 4-2 The effect of O₂ and CO₂ on cerebral blood flow

Graphs A and B represent the principle of the effect of O₂ and CO₂ on CBF. Cerebral blood flow (CBF) in the normal physiological range of O₂ (red line) is stable, but CBF increases in response to hypoxia and decreases in response to hyperoxia. Rising CO₂ causes a linear increase in CBF (blue line) except at the extremes, producing a sigmoid curve, as vasoactive properties of the vessels are exhausted. The graphs represent the theoretical effect of altered gas on CBF rather than representing numerical values.

4.2.3 Oxygen

Within normal physiological values, changes in PaO₂ have little effect on vessel calibre or CBF (see Figure 4-2)(Watson et al., 2000). Once PaO₂ drops below 6.7kPa, metabolic signals such as adenosine, along with the direct action of hypoxia on vascular smooth muscle, results in vasodilation and increased CBF,

allowing O_2 delivery to remain constant (Golanov and Reis, 1997). MRI experiments using hypoxia have been performed, usually in young healthy individuals (Noth et al., 2008, Xu et al., 2012). Hypoxic experiments require well controlled experimental conditions and may be inappropriate in patients with cerebrovascular disease.

The effects of hyperoxia are slightly less clear but most studies have suggested that it causes a reduction in CBF. In young healthy subjects, blood flow measured using phase-contrast MR angiography, decreased by up to 25% when an FiO_2 100% challenge was administered (Watson et al., 2000). Bulte and colleagues using ASL proposed that CBF decreased even with mild levels of hyperoxia, and continued to decline with higher FiO_2 (Bulte et al., 2006). The “on” and “off” response times to changes in PaO_2 are longer than those of $PaCO_2$ (Ellingsen et al., 1987). Hyperoxia is proposed to have a direct vasoconstrictive effect on vessels partly by attenuation of the effects of nitric oxide (Demchenko et al., 2000). This is more marked with hyperbaric O_2 (Omae et al., 1998). However the effect of hyperoxia is complicated by two major factors. Firstly hyperoxia leads to a small but significant reduction in $EtCO_2$ probably due to increased tidal volume. Reduced $EtCO_2$ leads to vasoconstriction, and this may be responsible for the change in CBF. When changes in $EtCO_2$ were corrected for in a phase-contrast MRI experiment, changes in FiO_2 did not have a significant effect on CBF, suggesting the $EtCO_2$ decrease is the predominant modulator of CBF change (Xu et al., 2012). The second factor is that hyperoxia also changes the MR properties of tissue, specifically reducing the T_1 of arterial blood and tissue, which may have profound effects on CBF measurements. Adjustment for this may be required for the accurate quantification of CBF (Pilkinton et al., 2012).

Studies using hyperoxia may therefore need to consider the role and measurement of $EtCO_2$, and correct for changes in T_1 , which adds to the complexity of the experimental paradigm. Hyperoxia can be used alone, or in combination with CO_2 (carbogen), in respiratory challenge experiments. Carbogen increases both CBF and PaO_2 availability.

As well as affecting CBF, O_2 has important effects on the BOLD signal in fMRI. With a FiO_2 of 21% and normal atmospheric pressure, arterial haemoglobin (Hb)

is almost saturated with O_2 (creating diamagnetic oxyhaemoglobin). Elevated FiO_2 increases the amount of gas dissolved in plasma in linear proportion to the partial pressure (Kalamangalam et al., 2012). This dissolved paramagnetic O_2 alters the susceptibility between blood and tissue. It also has an effect via the oxygen-haemoglobin dissociation curve. Due to increased PaO_2 in capillaries, there is a reduction in the dissociation of O_2 from haemoglobin as the PaO_2 does not fall sufficiently to allow its release. In conditions of hyperoxia therefore, the amount of deoxyhaemoglobin is nearly constant during capillary transit. This results in an increased $T2^*$ signal and hyperoxic BOLD contrast (Schwarzbauer and Deichmann, 2012).

Hyperoxia is associated with the release of oxygen free radicals, which may overwhelm endogenous antioxidant mechanisms, and lead to lipid peroxidation and plasma membrane breakdown particularly in the lungs (Jamieson et al., 1986). Human glioblastoma cells exposed to graded hyperoxia demonstrated membrane blebbing which was reduced by co-application of antioxidants (D'Agostino et al., 2009). Reversible alveolar changes after 17 hours of $>95\%$ oxygen suggested changes in alveolar-capillary barriers (Davis et al., 1983). Subjects may develop substernal pain, tracheobronchial irritation and tissue destruction and pulmonary oedema. This is thought to occur only if $FiO_2 >50\%$ is used, but “safety thresholds” for oxygen administration remain unclear (Jackson, 1985, Martin and Grocott, 2013). Hyperoxia may also lead to nitrogen washout and airway collapse (Duggan and Kavanagh, 2005). These effects occur only after several hours to days of hyperoxia, although they are enhanced by elevated atmospheric pressure (Jackson, 1985). The duration of hyperoxia given within the context of an MR experiment are not thought to have any detrimental effects.

4.2.4 Acetazolamide

Acetazolamide is often used as an alternative “challenge” to assess cerebrovascular reactivity. It is thought to work by causing inhibition of erythrocyte carbonic anhydrase resulting in impaired clearance of CO_2 and acidosis which causes vascular smooth muscle relaxation. This causes an increase in CBF, without affecting $CMRO_2$ (Vorstrup et al., 1984). Usually administered

with a standard dose of 1000mg, it is safe and usually well tolerated, without changes in systemic parameters (Vagal et al., 2009). A 30-60% increase in CBF is achieved in healthy volunteers, but there is variability in response among individuals (Fierstra et al., 2013)

There are a number of disadvantages however. Reported side effects include paraesthesia and headaches, and once the drug has been given these are not reversible until the drug has been excreted. It has a number of drug interactions and must also be used with caution in subjects with hepatic or renal dysfunction or electrolyte disturbances, limiting its use in some patient groups (Eskey and Sanelli, 2005). It requires IV access and can only be repeated once in the experimental period which makes it less useful for applying recurrent challenges in a single MRI session. Reports of reversible neurological deficits thought secondary to ischaemia have been reported in response to acetazolamide (Komiya et al., 1997), but it has been used in a large number of patients with chronic cerebrovascular disease without clinical ischaemic consequences (Vagal et al., 2009, Choksi et al., 2005).

4.3 Technique

4.3.1 Preparation

Subjects with cerebrovascular disease may have difficulties with informed consent and comprehension of protocols. Well-planned exclusion criteria accompanied by thorough and early screening for any contraindications to MRI, may prevent subject drop out, avoid scanning delays and enhance data quality.

4.3.1.1 Exclusions

Normal MRI exclusion criteria should be followed (Kanal et al., 2013). Subjects with claustrophobia or anxiety may struggle with MR scanning, and use of a face mask within the confines of the scanner bore may exacerbate this. Panic disorder patients may be hypersensitive to the anxiety inducing effects of CO₂ (Colasanti et al., 2012). Patients with significant pulmonary or cardiac disease may need to be excluded from studies due to difficulties tolerating abnormal gas concentrations, issues with monitoring (see Monitoring below), and altered

cerebral haemodynamics, such as in atrial fibrillation (Lavy et al., 1980, Petersen et al., 1989).

4.3.1.2 Oxygen

Patients requiring continuous O₂ such as those with pneumonia (relevant in acute research such as stroke) may not tolerate periods of normoxia. Due to the potential risk of pulmonary atelectasis from hyperoxia, patients with bronchiectasis should be excluded. Subjects with type II respiratory failure have inadequate ventilation, causing a rise in resting PaCO₂; hence the respiratory centre becomes driven by hypoxaemia. Hyperoxia can reduce ventilation leading to rises in PaCO₂. Therefore patients with certain types of chronic obstructive pulmonary disease or respiratory muscle weakness (e.g. uncontrolled myasthenia gravis) should be excluded.

4.3.1.3 Carbon dioxide

Subjects with known type II respiratory failure should not be subjected to hypercapnia in order to avoid further increase in PaCO₂. Hyperventilation (to induce hypocapnia) should be avoided in those with a history of epilepsy as it may induce seizures (Guaranha et al., 2005). In subjects with unruptured intracranial aneurysms, conditions that cause alterations in the aneurysm's transmural pressure gradient, such as hypertension or sudden alterations in intracranial pressure secondary to hyperventilation, are proposed to increase the risk of rupture during aneurysm surgery (Chowdhury et al., 2014), and therefore these patients should be excluded if respiratory MRI challenge designs are likely to cause this.

4.3.2 Standardisation of testing conditions

Factors that may influence CBF and CVR include time of day (Strohm et al., 2014), nicotine (Shinohara et al., 2006), food (Tsai et al., 2004), alcohol (Gundersen et al., 2013), body mass (Selim et al., 2008), haematocrit (Hudak et al., 1986) and hormonal cycles (Bartelink et al., 1990). Visual stimulation and speaking will result in increased CBF to active brain regions (Ito et al., 2001), but sleep can reduce the cerebrovascular response to CO₂ (Ainslie and Duffin,

2009), so studies may be best performed on awake, silent subjects with closed eyes. Numerous medications may influence cerebral haemodynamics including statins (Murakami et al., 2008), angiotensin-receptor enzyme inhibitors (Walters et al., 2004), calcium channel blockers (Kuridze et al., 2000) and hormone replacement therapy (Ohkura et al., 1995), and patients may need to be excluded or medication withheld.

Caffeine reduces CBF (Lunt et al., 2004) and thus abstinence for a short period prior to a study may be advisable. However chronic caffeine use may lead to upregulation of vascular adenosine receptors to preserve CBF, and abstinence prior to a study could lead to a “withdrawal” rebound increase in CBF (Addicott et al., 2009). As this is only likely to occur in patients with very high caffeine use (>600mg/day or 4 - 7 cups of coffee) it has been suggested that these subjects should be excluded from perfusion studies (Addicott et al., 2009) but the exact dosage of caffeine intake can be difficult to ascertain due to the variety of sources including tea, coffee, energy drinks and other soft drinks.

Temperature is known to alter cerebral blood flow (Kuluz et al., 1993). The temperature within the bore of a magnet may increase as scanning progresses due to radiofrequency energy (Westbrook et al., 2011). For studies using repeat imaging or prolonged scanning sessions, an increase in temperature could therefore potentially influence perfusion characteristics of the subject in the bore as there may be an increase in CMRO₂ (Edvinsson and Krause, 2002).

Standardised testing conditions designed for peripheral vascular function tests are similarly applicable to cerebral perfusion studies, although potentially harder to implement (Table 2-5) (Van Bortel et al., 2002, Laurent et al., 2006).

4.3.3 A trial run

A trial run of the challenge outside the MRI with close monitoring of the patient and inspired and expired gases allows priming of the subject to the experience of the respiratory challenge in a less claustrophobic environment. This allows the subject to ask questions and notify the clinician of side effects. Safety concerns such as alterations in heart rate or blood pressure may also be

identified. Compliance and experimental success is likely to be increased (Taylor et al., 2001).

4.3.4 The respiratory challenge

For highly accurate monitoring and modulation of PaO_2 and PaCO_2 a completely closed circuit between patient, monitor and gas delivery system is required, i.e. an intubated and ventilated patient, which is clearly inappropriate for the majority of these studies. Therefore exact accuracy of gas measurement has to be sacrificed in order to undertake a respiratory challenge that is practical and tolerable to patients, whilst still giving reliable gas concentrations.

4.3.4.1 Ventilatory techniques

Ventilatory techniques, in their simplest form, do not require additional equipment, but do require patient compliance, limiting their use in cognitive impairment or confusion. Breath-holding causes hypercapnia and increased CBF, comparable to that achieved with 5% CO_2 (Kastrup et al., 1999, Ratnatunga and Adiseshiah, 1990). Breath hold may occur at the end of inspiration or expiration. End-expiration breath hold leads to an immediate rise in EtCO_2 , but the tolerable duration is shorter (due to hypoxia) and it may be more unpleasant for the patient thus increasing motion artefacts (Ratnatunga and Adiseshiah, 1990). In comparison, end-inspiration breath hold is longer and more comfortable but changes in intrathoracic pressure result in a biphasic change in BOLD signal (Thomason et al., 2007, Thomason and Glover, 2008). Both techniques are simple and practical for use in MRI. There are concerns about experimental repeatability due to variations in breath-hold duration (Thomason et al., 2007). However if EtCO_2 is measured breath hold duration need not be the same for accurate and repeatable measurements (Bright and Murphy, 2013). Additions to the technique include visual cueing, measurement of compliance with an abdominal pneumatic belt and paced breathing (Thomason et al., 2005, Scouten and Schwarzbauer, 2008), all of which add complexity and may reduce subject acceptability.

Voluntary hyperventilation causes hypocapnia and reduced CBF (Raichle and Plum, 1972). A period of more than 60 seconds can induce a fall of around 25%

(Rostrup et al., 2005). Subjects are asked to modify their breathing rate and depth via visual cues, for a certain period or to a target EtCO_2 , which require training outside MRI (Vogt et al., 2011). Hyperventilation may increase motion artefacts (Naganawa et al., 2002) .

4.3.4.2 Fixed inspiratory challenge

Delivery of a fixed gas concentration via a non-rebreathing mask is passive, repeatable and straightforward. It requires a constant gas supply and a delivery method. Premixed gas cylinders can be used to deliver fixed gas mixtures, or gas blenders may allow more variation in gas concentrations. 5% CO_2 is proposed to raise CBF by 50% (Kety and Schmidt, 1948a) and 100% O_2 reduce CBF by up to 25% (Watson et al., 2000). Fixed inspiratory challenge is effective for steady-state measures, including arterial spin labelling MRI (Figure 4.3), or those with a block design, where a stimulus is given for set periods on several occasions in order to allow summation of results, usually with a continuous imaging method (Kalamangalam et al., 2012) (Figure 4.4).

Gas delivery systems must be of a high enough flow rates to support increased tidal volume seen with hypercapnia. The flow rate may depend on circuit design, and whether or not reservoir bags are used. An undershoot in EtCO_2 , may be seen in hypercapnia experiments as patients hyperventilate to expel excess CO_2 (Wise et al., 2007). A fixed FiO_2 or FiCO_2 does not necessarily equate to a specific arterial concentration as this depends on ventilation, metabolic rate, and the adequacy of the delivery circuit (Fierstra et al., 2013). End-tidal gas concentrations should therefore be monitored to allow accurate signal quantification.

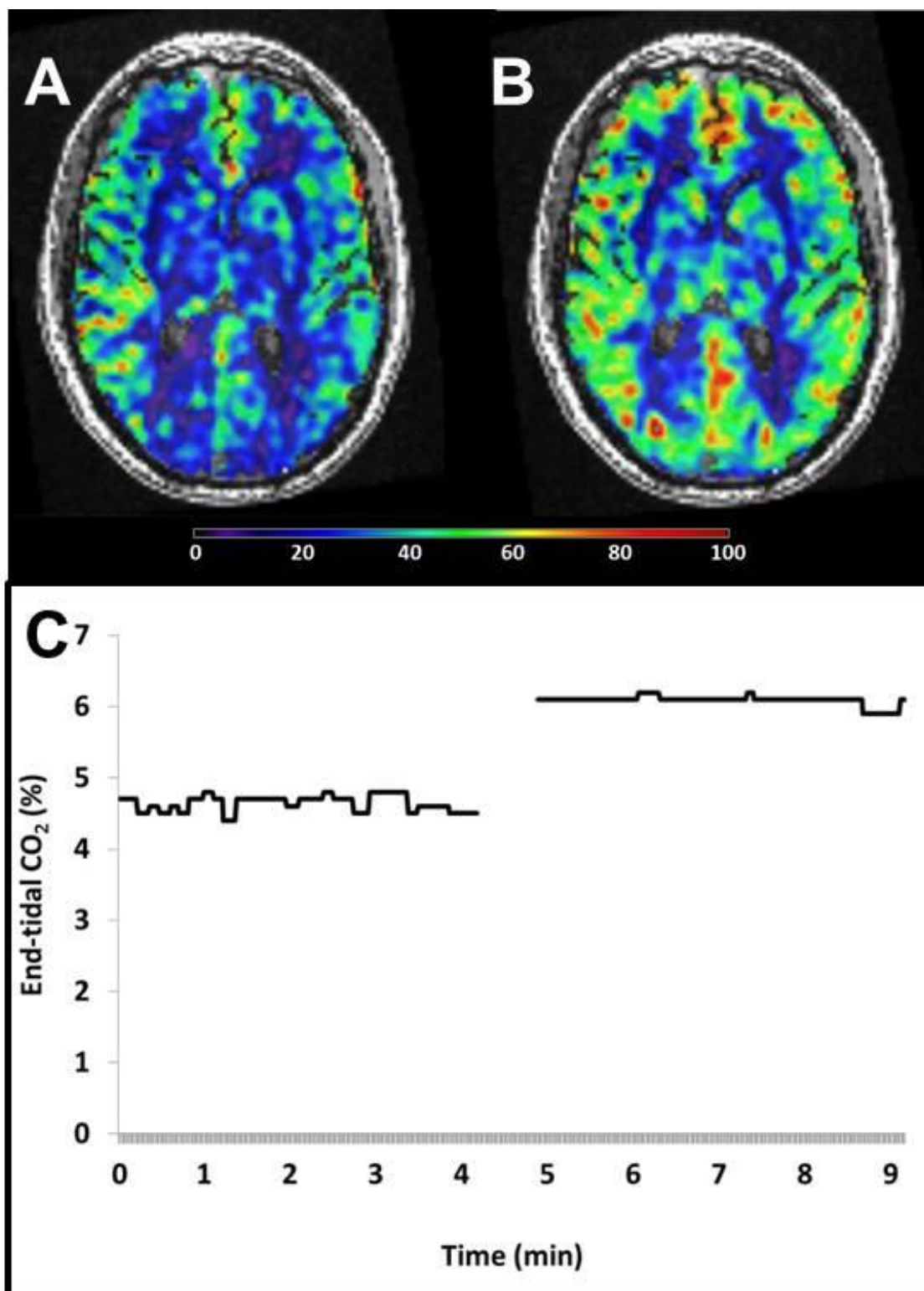


Figure 4-3 Fixed inspiratory challenge

Arterial spin labelling (ASL) MRI performed whilst receiving air (A) and 6% CO₂/air mixture (B) in a patient with CADASIL, demonstrating an increased CBF in response to hypercapnia. Delivery of 6% CO₂ caused a change in end-tidal CO₂ (C).

Ventilatory responses to a fixed challenge may result in change in gas concentration despite an unchanged inspired concentration e.g. increased ventilation in response to hypercapnia may lead to elevated EtO₂, which may influence MRI signal (Wise et al., 2007).

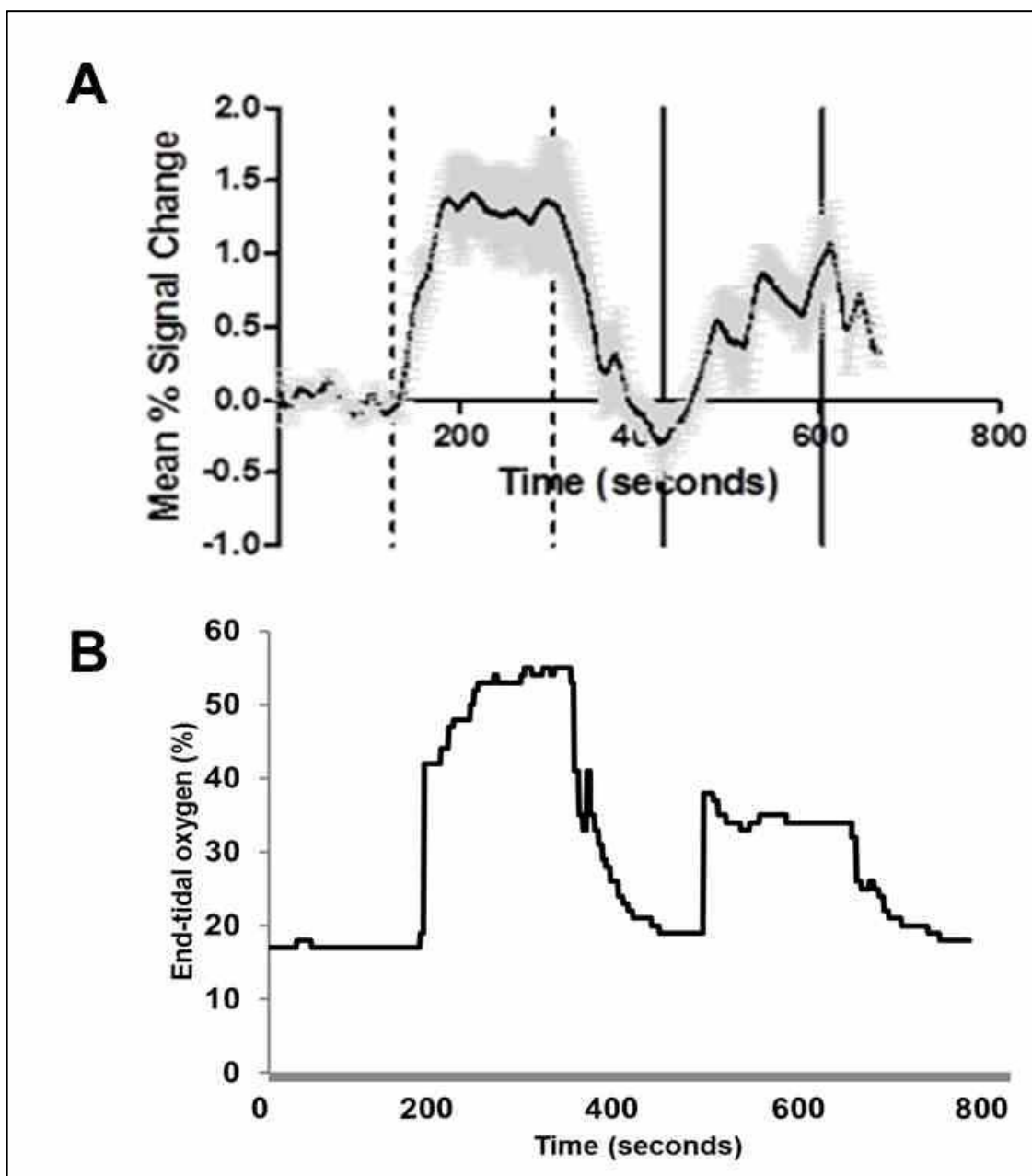


Figure 4-4 Repeated challenges during continuous imaging

(A) BOLD signal change is measured throughout an 11 minute MRI sequence, during which changes in inspired oxygen are reflected by the end-tidal oxygen concentration (B). Figure A courtesy of Dr K Dani.

4.3.4.3 Rebreathing

Rebreathing of exhaled gas will result in equilibration of alveolar and arterial gases and a gradual increase in PaCO_2 . It is performed with a simple breathing circuit, with or without additional gases, and is generally well tolerated (Saunders, 1980). However the speed and values of PaCO_2 are not predictable and a plateau is difficult to achieve. Partial rebreathing circuits with fixed inspiratory challenges are proposed to achieve more stable EtCO_2 , but require significant patient cooperation (Vesely et al., 2001). Rebreathing techniques

allow the measurement of dynamic changes to a range of EtCO_2 (Ainslie and Duffin, 2009).

Rebreathing in a closed circuit will lead to a fall in delivered FiO_2 . Isooxia should be maintained for CVR measurement and to prevent the patient receiving a hypoxic gas mixture. Rebreathing methods where isooxia is achieved and EtCO_2 is representative of PaCO_2 have been described (for a recent review see Fierstra and colleagues (Fierstra et al., 2013)).

4.3.4.4 Dynamic end-tidal forcing

More precise control of EtCO_2 and EtO_2 has been advocated to permit more accurate adjustment of changes in MRI signal responses. Dynamic end-tidal forcing uses breath-by-breath computer control of inspired gas to achieve target EtCO_2 and EtO_2 . This may increase repeatability both between subjects and sessions, and allows more complex variations of respiratory challenges to be performed (Wise et al., 2007). It is more expensive and complex to run than fixed inspiratory challenges, and breath-by-breath analysis can be hampered by the need for long gas sampling lines in MRI. It requires a high flow rate and there is the potential for the delivery of an anoxic mixture although this is avoided with use of the correct circuit (Wise et al., 2007). Even with this technique, issues with the accuracy of using EtCO_2 to predict PaCO_2 remain (Fierstra et al., 2013).

4.3.4.5 Prospective end-tidal targeting.

Prospective end-tidal targeting has been developed as a method to permit more accurate correlation of changes in EtCO_2 with MRI signal responses (Ito et al., 2008). A tight-fitting mask is attached to a 3-valve circuit with inspiratory and expiratory reservoirs. Gas flow to the mask moves through a computer-controlled gas blender (Respiract; Thornhill Research, Toronto, Canada) which supplies O_2 , CO_2 and nitrogen to achieve target EtCO_2 and EtO_2 independent of breathing pattern. Its advantages are that it allows rapid changes in gas concentration and that the end-tidal gases are equivalent to that of alveolar ventilation, and thus more accurately reflect tissue concentrations (Fierstra et al., 2013). A more detailed explanation of the method is available in Fierstra et

al (Fierstra et al., 2013). It has been used to study cerebral physiology in a number of different disease states (Heyn et al., 2010, Mikulis et al., 2005, Fierstra et al., 2011). This method in theory could allow the inclusion of patients with pulmonary disease as the EtCO₂ will continue to accurately reflect PaCO₂ (Ito et al., 2008), although the danger of exposure to hypercarbia or hyperoxia in these patients remains.

4.3.5 The Environment and equipment

Use of respiratory challenge adds complexities to the already difficult MR environment. As subject safety is paramount, all staff should undergo MRI safety induction training as per local guidelines (Farling et al., 2002).

4.3.5.1 Monitoring

Monitoring of gas concentrations is important for calculation of CVR, but is also required for subject safety. Access to subjects is limited as the head is placed in a tight-fitting receiver coil (to enhance signal), padded and secured to limit movement. This complicates the delivery of gas, monitoring of subjects and verbal communication. Additional equipment must be MR safe or MR conditional and effective, and close liaison with anaesthetists is recommended. Standard monitoring equipment must be correctly positioned to avoid the formation of inductive loops which may cause burns (Dempsey and Condon, 2001). ECG leads are prone to interference (Farling et al., 2002) and fiberoptic MR connections preferred. Anaesthetic guidelines recommend that remote MR monitoring in the control room is available to reduce occupational exposure to magnetic fields and hearing damage (Farling et al., 2002, Farling et al., 2010).

Whilst respiratory challenge MRI aims to modify cerebral tissue O₂ and CO₂, this is difficult to measure directly, and whilst arterial concentrations are representative they also require invasive monitoring. Non-invasive measurement of end-tidal gases is a more straightforward, if indirect, measurement. Sampling, which allow the measurement of delivered and end-tidal gases, should be as close to the subject's expired air flow as possible. The long sample lines necessitated by MRI will increase the time delay between sampling and recording (up to 20 seconds) (Farling et al., 2002). Secretions may block lines, and water

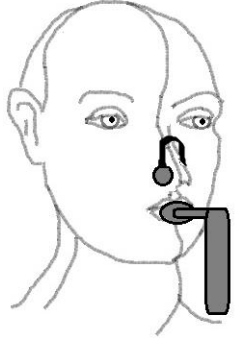
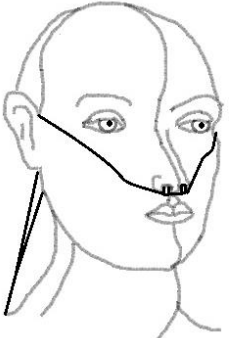
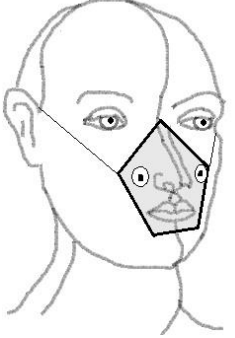
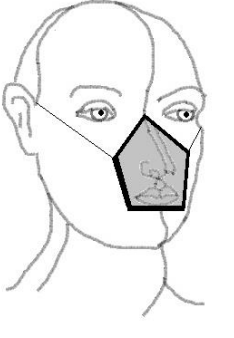
traps dry out the sampled air, giving a dry value for expired gas. In normal atmospheric pressure a wet gas correction value of 0.94 can be applied to dry gas measurements (Bengtsson et al., 2001). Capnography involves both the measurement and display of the EtCO₂ value and waveform. It offers the advantage of assessment of circuit integrity (i.e. a reasonable seal) and allows identification of leaks or unplanned build-up of CO₂.

There does however remain some question as to the accuracy of end-tidal measurements. Use of EtCO₂ may only be appropriate with use of regression equations to adjust for changes in tidal volume, as ventilation will increase with a rise in delivered carbon dioxide (Ainslie and Duffin, 2009). Use of prospective end-tidal targeting may offer advantages over unadjusted end-tidal gas readings (Slessarev et al., 2007, Ito et al., 2008).

4.3.5.2 Gas delivery

The simplest form of respiratory challenge e.g. hyperventilation or breath hold does not require a gas delivery method. For other types options include nasal cannula, mouth piece and nasal clip and face masks. The choice will depend on tolerability versus the need for accurate delivery and monitoring. The options are summarised in Table 4-1.

Table 4-1 Methods for delivery of gas

	Mouth piece and nasal clip	Nasal cannula	Standard face mask	Non-vented face mask
				
Use	Variable FiO_2 (will be affected by entrained air) Fixed concentrations of CO_2 mixture	FiO_2 24-44%(1 - 6L/min) Fixed concentrations of CO_2 mixture	FiO_2 up to 60% Fixed concentrations of CO_2 mixture	FiO_2 up to 100% Fixed concentrations of CO_2 mixture
Pros	Simple Cheap Well tolerated	Simple Cheap Well tolerated Unimpeded communication	Fit most subjects Higher O_2 concentrations Generally well tolerated	Improved seal Reduced mask volume Controlled gas delivery and sampling May improve test reliability
Cons	Communication hampered Entrain air around mouth piece	Drying of nasal mucosa Can still mouth breath	May not fit/be tolerated in tight head coil Room air entrained through vents diluting the delivered gas	Less malleable and tighter so less tolerated Harder to fit in MRI coil Risk of rebreathing so must be used with appropriate breathing circuit

4.4 MRI sequences and examples of use in cerebrovascular disease

4.4.1 BOLD signal

Functional MRI using gradient-echo echoplanar imaging with strong T2*-weighted imaging measures the blood-oxygenation level dependent (BOLD) signal.

Oxyhaemoglobin is diamagnetic and has limited effect on T2*-weighted signal.

Deoxyhaemoglobin is paramagnetic and leads to a reduction in T2*-weighted signal. The BOLD signal depends on CBF, CBV, CMRO₂, haematocrit and PaO₂ although in healthy subjects the signal is dominated by CBF (Shiino et al., 2003).

Hypercapnia-induced rises in CBF, “washes out” deoxyhaemoglobin causing an increase in T2*-weighted signal (Shiino et al., 2003). The signal difference between normocapnia and hypercapnia can be used to measure CVR. In 25 patients with arterial steno-occlusive disease there was a strong correlation between hemispheric CVR using BOLD MRI and ASL MRI (Mandell et al., 2008). In Moyamoya disease, CVR correlated with disease severity and the presence of collaterals (Heyn et al., 2010). CVR mapping performed pre and post-operatively showed that areas of vascular steal which correlated with severe stenosis, resolved following successful revascularization. This suggested CVR mapping could be used for pre-operative planning (Mikulis et al., 2005) (Han et al., 2011).

In hyperoxic states, the O₂ remains bound to haemoglobin in tissues, reducing the concentration of deoxyhaemoglobin, and thereby increasing T2* signal. Dani and colleagues investigated respiratory O₂ challenge T2*-weighted MRI in subjects with stroke within 24h of onset. The putative infarct core showed diminished T2*-weighted signal increase compared to normal tissue, signifying this technique may be able to tease out changes in metabolic activity (Dani et al., 2010).

BOLD imaging allows the use of continuous measurements and assessment of dynamic responses to altered gas concentrations. In patients with Alzheimer's disease, where vascular function is thought to be abnormal, maximal BOLD signal

took longer to achieve than in normal controls implying some vasomotor impairment (Cantin et al., 2011).

BOLD imaging with respiratory challenge has therefore been used to: demonstrate physiological impairments such as reduced vascular reserve and vascular steal phenomenon; correlate with clinical outcome measures; and to plan and predict outcomes of surgical revascularization.

4.4.2 Cerebral blood flow

ASL involves magnetically labelling protons in the arterial blood supply. As this blood passes into the brain, it causes a small signal loss in brain tissue compared to non-labelled images, which allows measurement of CBF (see Chapter 1). When used with a challenge, paired blood flow measurements, i.e. a baseline and then a stimulus, can be obtained allowing calculation of CVR. ASL offers the advantages of being non-invasive, repeatable, and quantifiable, but has the disadvantage of low signal-to-noise ratio in comparison to dynamic susceptibility weighted contrast methods for investigating perfusion (Wintermark et al., 2005).

Brain perfusion in dementia has been investigated using ASL and a 5% CO₂ challenge in 49 patients. Regional CBF (rCBF) was lower and CVR impaired in frontal cortices of Alzheimer's disease patients, compared to lower white matter rCBF in vascular dementia (Gao et al., 2013). Transcranial Doppler ultrasound (TCD) failed to demonstrate any difference in blood velocity or CVR in these patients however. If regional patterns distinguish different types of dementia, this may offer an advantage over global measures of flow such as TCD. A rebreathing challenge was used to demonstrate an association between high cardiovascular risk profile and impaired hippocampal vasoreactivity in mild cognitive impairment (Glodzik et al., 2011), which was more sensitive than baseline CBF or brain volume. ASL performed with hypocapnic hyperventilation and CO₂ rebreathing (95% O₂, 5% CO₂) challenge in 39 chronic large territory stroke patients, demonstrated reduced ipsilateral CBF but widespread impaired vasodilatory capacity beyond the infarcted region. The continuous ASL technique used has been shown to be quantifiable, although the long transit times seen in stroke may lead to underestimation of blood flow in stroke patients (Zhao et al.,

2009). This is because the flow is so slow, that the signal decays by the time it has reached the tissue being imaged.

Perfusion imaging with gadolinium bolus tracking is less commonly used in respiratory challenge experiments due to it being less easily repeated, requiring IV access, and gadolinium contrast having safety concerns in the face of extravasation or impaired renal function. MRI bolus tracking and acetazolamide challenge was used in 15 patients with CADASIL (cerebral autosomal dominant arteriopathy with subcortical infarcts and leukoencephalopathy) to show impaired perfusion and reactivity in white matter hyperintensities (Chabriat et al., 2000). DSC accompanied by BOLD imaging has also been proposed as a technique for calculating $CMRO_2$ (Shiino et al., 2012).

4.4.3 Dual echo imaging (BOLD and perfusion)

BOLD and ASL can be used in sequence to provide information about the cerebrovascular system. Using both methods can permit the assessment of multiple measures of cerebral haemodynamics including CBF, CVR, BOLD CVR, oxygen extraction fraction (OEF) and cerebral metabolic rate of oxygen ($CMRO_2$). In a study of patients with internal artery occlusion, BOLD CVR signal was lower in the affected middle cerebral artery territory (De Vis et al., 2015).

Vessel-specific labelling of blood, known as vessel encoded ASL (VE-ASL) has also been used in combination with BOLD in patients with cerebrovascular disease. BOLD signal change and CBF reactivity correlated significantly in response to carbogen, and was able to identify disease lateralisation in steno-occlusive carotid disease, although its application remains complex (Faraco et al., 2015)

4.4.4 Cerebral blood volume

Cerebral blood volume (CBV) has a linear relationship to changes in $PaCO_2$ but a non-linear relationship to changes in CBF (Grubb et al., 1974). The vascular space occupancy (VASO) technique is a CBV-weighted imaging technique where blood water signal is nulled and extravascular tissue recorded. Decrease in tissue signal represents an increase in blood volume seen with neuronal activity (Donahue et al., 2012). It has better spatial resolution than BOLD, but a poor

signal to noise ratio. It has been used to demonstrate signal decreases (suggesting increased intravascular blood volume) in grey matter in response to short periods of breath-hold in normal individuals (Hsu et al., 2010). More negative response to VASO reactivity in response to breath-hold challenge was seen in patients with internal carotid artery stenosis compared to controls, proposed to represent haemodynamic impairment (Donahue et al., 2009). Using VASO with BOLD techniques may help extract the influence of CBV on the BOLD signal in disease states.

4.5 Recommendations

Despite the variety of techniques available, application of respiratory challenge MRI may benefit from some standardization. Subject withdrawal may be reduced by ensuring the recruitment of subjects without MR or gas exclusions and undertaking a trial run of the procedure outside the MR scanner (Taylor et al., 2001). Whilst centres will vary in the availability of equipment or expertise to use certain challenges or MR sequences, recording subject parameters and standardizing testing conditions may reduce testing variability and allow studies to be compared more readily. Some proposed recommendations for the conduct of respiratory challenge MRI studies are outlined in Table 4-2.

Table 4-2 Proposed recommendations for conducting respiratory challenge MRI

Recommendations
Perform a trial run of gas delivery with the subject outside the scanner to assess tolerability and optimize compliance.
Standardize testing conditions by following published guidelines for performing vascular tests such as those outlined in Table 2-5.
Record delivered and end-tidal gases, along with respiratory rate and heart rate to ensure patient safety and to allow correlation with signal change. These values can then be used to for quantification of the change in MR parameter.
Liaise with anaesthetists and MR physics department to ensure breathing apparatus and monitoring equipment is safe and MR appropriate
Exclude patients with significant cardiac or pulmonary disease.
Ensure the gas supply is sufficient to support increases in minute ventilation.
For fixed inspiratory challenges use a maximum FiCO_2 of 8% to avoid subject discomfort (Ainslie and Duffin, 2009) or target to a specific change in EtCO_2 .

4.6 Conclusion

Respiratory challenge MRI has the potential to be used widely in the assessment of cerebrovascular disease due to its safety, tolerability and repeatability. Whilst problems remain with reliable gas administration, it has been used to provide valuable insights into brain pathophysiology. For such techniques to function as biomarkers to assess disease progression or treatment response, standardisation of testing is important but must still be realistic for clinical situations.

Chapter 5 – Impaired cerebral and peripheral vasoreactivity are associated with higher numbers of lacunes in CADASIL.

5.1 Introduction

Both animal and human studies have demonstrated that impaired vasoreactivity may have a role in the pathophysiology of CADASIL. In animal models, impaired vascular function is thought to precede both histological and clinical evidence of disease (Ayata, 2010). Impaired cerebrovascular reactivity has been demonstrated to be related to increased progression of WMH in a 7 year study, but the clinical relevance of WMH remains unknown (Liem et al., 2009a). More conventional markers of vascular dysfunction, such as CIMT and blood pressure are also postulated to have a role in disease severity (Mawet et al., 2011, Viswanathan et al., 2006b).

Much of the research in CADASIL has focussed on the role of structural brain abnormalities including hyperintensities, lacunes, microbleeds and atrophy. These have limited use as biomarkers of disease progression in clinical trials, due to their wide inter-individual variation and slow progression (Peters et al., 2004a). They may also represent a late stage of the disease process, and vascular dysfunction may be an earlier manifestation of the disease. The long asymptomatic or preclinical phase in CADASIL (Oberstein et al., 2003), along with the ability to identify affected individuals with genetic testing, offers the potential for early intervention to delay ischaemia or disability. Given the need for biomarkers in an uncommon disease with a varied natural history, clear characterisation of peripheral and cerebral vascular function and reactivity in CADASIL patients is needed. Associating these markers with relevant clinical and neuropsychological measures may allow us to identify correlations which may direct us to which factors could prove useful in monitoring disease progression and the effect of therapeutic intervention. Initially cross-sectional associations should be investigated.

Using a variety of techniques to characterise peripheral and cerebral vasoreactivity the aims of this chapter are:

- 1) characterise cerebral and peripheral vascular function measures in adult patients with CADASIL;
- 2) investigate how vascular measures relate to conventional MRI markers;
- 3) investigate how vascular measures relate to clinical and neuropsychological markers of disease.

The main hypothesis of this study is that there is a relationship between cerebral vasoreactivity and the neuropsychological markers of disease.

5.2 Methods

5.2.1 Study cohort

Patients were recruited as stated in Chapter 2. Patients attended for 4 baseline study visits: (1) transcranial Doppler ultrasound (TCD) and clinical assessment, (2) peripheral vascular tests, (3) MRI, and (4) neuropsychology. Visit 1 took place first but otherwise the visits were in any order.

5.2.2 Study procedures

5.2.2.1 TCD

Mean flow velocity (MFV) in the middle cerebral artery and cerebrovascular reactivity CVR_{TCD} were calculated as Chapter 2.

5.2.2.2 Peripheral vascular tests

Peripheral vascular tests were performed as stated in Chapter 2. Measures included systolic blood pressure (SBP), augmentation index at 75bpm (AI@75), pulse wave velocity (PWV), carotid intima media thickness (CIMT), flow mediated dilatation of the brachial artery (FMD), and reactive hyperaemia index (RHI). History of smoking was dichotomised into: (1) never smoker or <20 pack years; and (2) current smoker or >20 pack years.

5.2.2.3 MRI

In this chapter data from the following scans obtained at baseline were used: axial T2 FLAIR, axial 3D T1 BRAVO, axial SWAN, sagittal Inhance 3D velocity MR angiography (carotid and vertebral arteries), 3D ASL air and 3D ASL hypercapnia. Sequence parameters can be found in Chapter 2.

5.2.2.4 Neuropsychological assessment

Assessment in this study focussed on processing speed and executive function as the primary cognitive domains affected in CADASIL. Composite scores were calculated as the mean of the domain-specific individual tests after conversion of raw scores to standardised scores (z-scores, corrected for age or age and education, with reference to published normative tables). These calculations were undertaken by Dr Breda Cullen (neuropsychologist). Subjects included in the analysis had no known visual disabilities that would impair performance but one subject was unable to complete some tests due to dysarthria and inability to hold a pen.

5.2.3 MRI analysis

5.2.3.1 Visual inspection

MR angiograms were inspected by a Consultant Neuroradiologist (Dr Celestine Santosh) for evidence of carotid or vertebral stenosis. Scans were scored for hyperintensities, perivascular spaces, subcortical lacunar lesions (SLLs), microbleeds and lacunes as detailed in Chapter 2. The total perivascular space score was calculated.

5.2.3.2 Brain tissue volume and intracranial cavity volume

Brain tissue volume, normalised for subject head size, was estimated with SIENAX (Jenkinson and Smith, 2001, Smith, 2002) part of FSL (Smith et al., 2004). SIENAX started by extracting brain and skull images from T1 3D image, using a brain extraction tool (BET) with an f 0.1 value. This was chosen after multiple f values were trialled with visual inspection of results. The brain image

was then affine-registered to MNI152 space (Jenkinson and Smith, 2001) to permit normalisation for head size. Tissue-type segmentation with partial volume estimation was carried out in order to calculate the total volume of brain tissue (this includes estimates of grey matter, white matter and ventricular CSF volume) (Zhang et al., 2001). The normalised brain volume was used in analysis (NBV, L).

Intracranial cavity (ICC) volume was calculated using the brain extraction tool (BET; f 0.5) on the SWI image (see Figure 5-1). A binary ICC mask was created and the voxels counted.

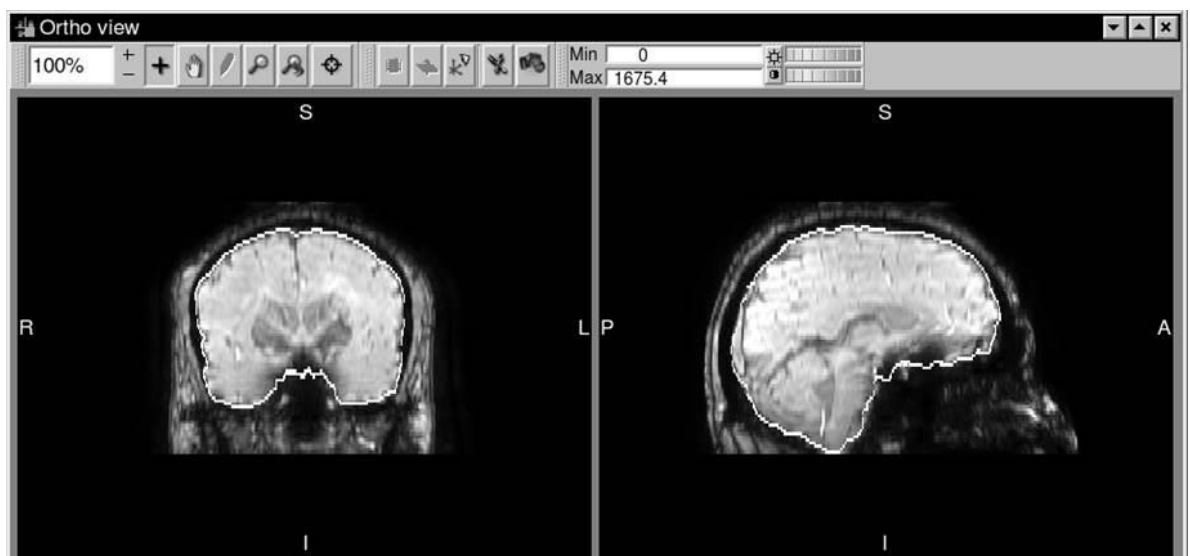


Figure 5-1 Calculation of intracranial cavity (ICC) volume

The SWI image was skull stripped using brain extraction tool. The brain region is shown outlined on the original image displayed in FSLview.

5.2.3.3 Lacune count and segmentation

Lacune number and volume were calculated as described in Chapter 2. Volume of lacunes was then normalised to ICC to give normalised lacune volume (NLV, %).

5.2.3.4 Subcortical hyperintensity segmentation

Subcortical hyperintensity (SH) maps were created by a thresholding the FLAIR image as detailed in Chapter 2. After the volume of the SH map was calculated, this was normalised to ICC to give normalised subcortical hyperintensity (NSH, %).

5.2.3.5 MRI marker stratification

MRI markers were stratified according to their baseline median value (or their presence or absence) to give categorical outcome variables.

5.2.3.6 ASL – creation of CBF maps

Anatomical MRI and ASL images were co-registered (Analyze version 11). Quantitative CBF maps were then generated using an in-house ‘macro’ for Image J (Rasband, W.S., ImageJ, U.S. National Institutes of Health, Bethesda, Maryland, USA, <http://imagej.nih.gov.ij/>, 1997-2014) with the following equation (operator manual for optima edition 23 based software, GE Healthcare):

$$CBF = 6000 * \lambda \frac{\left(1 - \exp\left(-\frac{ST}{T_{1t}}\right)\right) \exp\left(\frac{PLD}{T_{1b}}\right)}{2T_{1b} \left(1 - \exp\left(-\frac{LT}{T_{1b}}\right)\right) \varepsilon * NEX_{PW}} \left(\frac{PW}{SF_{pw} PD}\right)$$

Where:

CBF = Cerebral blood flow, ml/100g/min.

T_{1b} = T1 of blood, assumed to be 1.6 seconds at 3T.

T_{1t} = T1 value obtained on grey matter, set at 1200ms.

ST = Saturation time, set at 2 seconds.

λ = Partition coefficient, set at 0.9.

ε = Efficiency: a combination of both inversion efficiency (0.8) and background suppression efficiency (0.75), resulting in an overall efficiency of 0.6.

PLD = Post labelling delay of 2025ms.

LT - Labelling duration (1.5 seconds)

SFPW = Scaling factor of the PW sequence

NEXPW = the number of excitations for the PW images (3).

Examples of CBF maps are shown in Figure 5-2.

5.2.3.7 ASL – brain masks

The T1 image that had been transformed into ASL space was masked with a skull-stripped SWI and then segmented to create parenchyma, grey matter and white matter images using FSL (Zhang et al., 2001). SH maps were transformed into ASL space to create an SH mask. SH pixels were then removed from grey matter and white matter images, creating grey matter (GM) and white matter (WM) masks (see Figure 5-2). All masks were applied to normocapnia and hypercapnia CBF scans for measurement of CBF (see Figure 5-3).

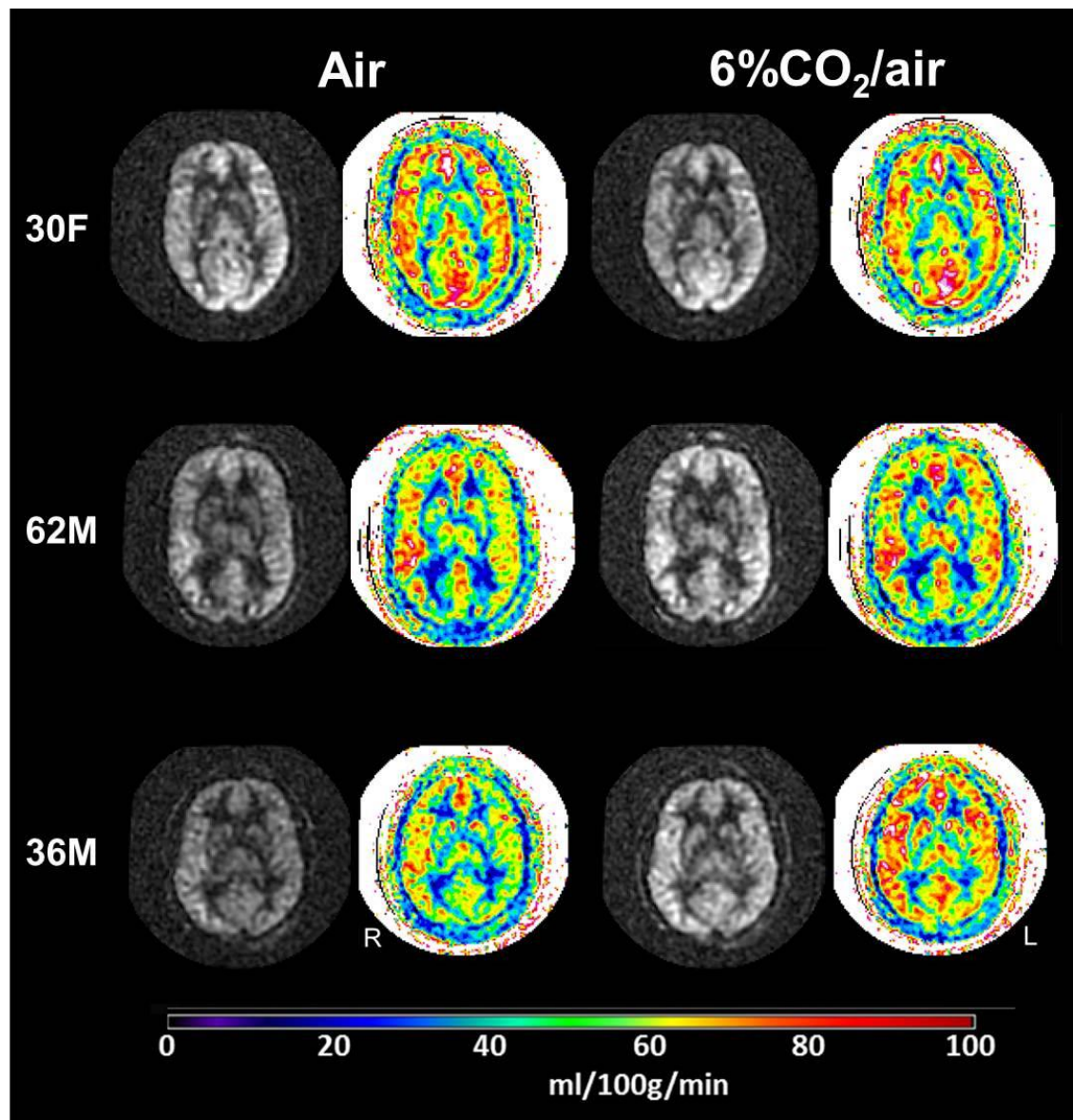


Figure 5-2 Perfusion and CBF maps created from ASL MRI
Raw perfusion maps (greyscale) and CBF maps (quantitative maps in colour) of three patients. Scans whilst breathing air and 6%CO₂/air mixture are shown. The age and gender of each patient is shown.

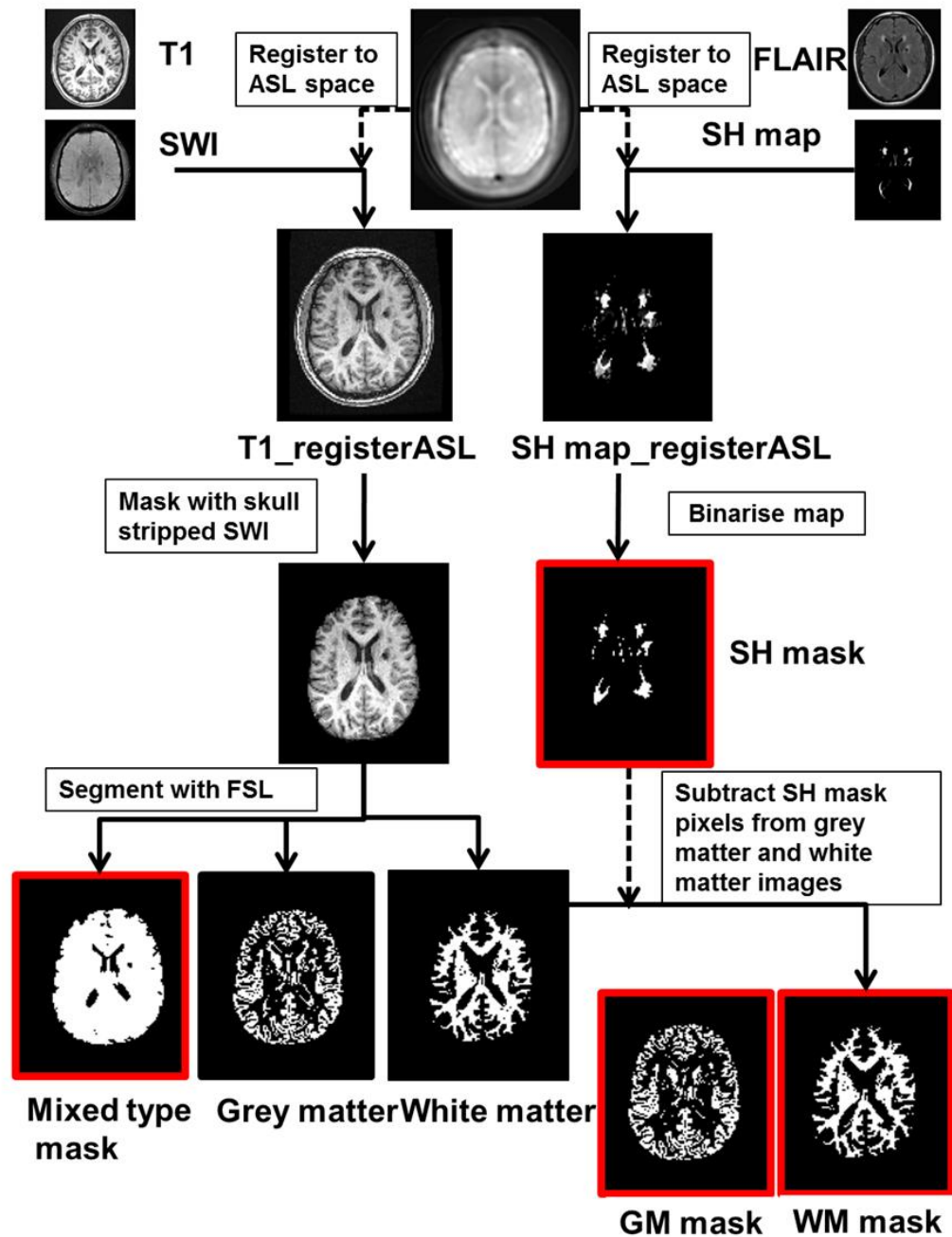


Figure 5-3 Creation of masks

SWI, T1, FLAIR, ASL hypercapnia and SH masks were all registered to ASL proton density normocapnia space using Analyze 3D voxel registration. The T1 image was then masked by a BET skull stripped SWI image. The stripped T1 image was then segmented into grey matter, white matter, and mixed type binary images. SH mask pixels were removed from grey and white matter masks to produce grey matter and white matter masks. All masks that were applied to ASL are shown surrounded by a red box.

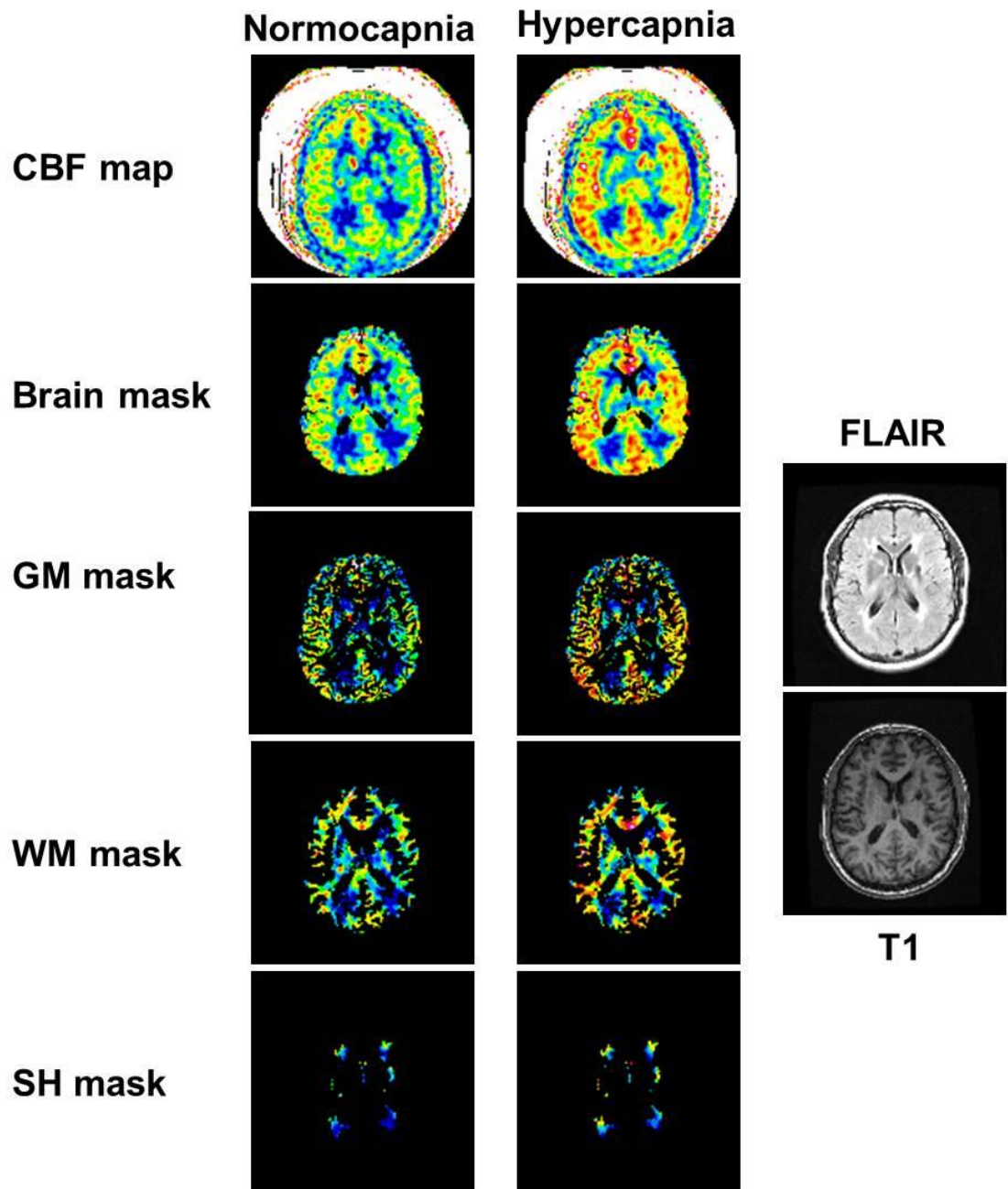


Figure 5-4 Applying masks to CBF maps

Generated CBF maps were then masked with brain, GM, WM and SH masks. The average CBF in these masks was recorded.

5.2.3.8 ASL –calculation of % Δ CBF and CVR

For each mask percentage change in CBF (% Δ CBF) was calculated in Microsoft Excel:

$$\% \Delta \text{CBF} = \frac{\text{CBF}_{\text{hypercapnia}} - \text{CBF}_{\text{normocapnia}}}{\text{CBF}_{\text{normocapnia}}} \times 100$$

Expiratory gas data was used if EtCO₂ whilst breathing air was between 3.5 and 6.5%, suggesting reasonable mask seal. Where expiratory gas data was available, % Δ CBF was corrected for change in end tidal CO₂ to calculate cerebrovascular reactivity (CVR_{ASL})

$$\text{CVR}_{\text{ASL}} = \frac{\% \Delta \text{CBF}}{\Delta \text{EtCO}_2}$$

As brain masks were created in an automated manner, repeatability was not assessed.

5.2.4 Statistical analysis

Statistical analysis was performed with IBM SPSS Version 21 (IBM Corp, Armonk, NY, USA). CBF or CVR in different brain regions in individual patients were compared with paired t-tests. Continuous variables were compared to Spearman's rank correlation. Radiological variables were dichotomised by their median. For categorical outcome variables, normally distributed continuous variables were tested with independent t-tests, and non-normally distributed continuous variables with independent samples Mann-Whitney U tests. Normality was tested with Shapiro-Wilk. Results are expressed as mean (standard deviation, SD) unless otherwise stated.

Although multiple comparisons were used as this is an exploratory study significance was set at $p < 0.05$.

5.3 Results

22 patients (11 female) from 19 pedigrees were recruited. There were 9 different mutations in this cohort, in 5 exons, with Arg169Cys the most common mutation (7 patients). Patient demographics, vascular risk factors, clinical measures and imaging characteristics are reported in Table 5-1. All patients attended all study visits over a mean of 79 days (standard deviation 26 days). There was no evidence of extracranial vessel disease on MRA in 20/22 (one patient age 30 did not undergo MRA and one patient had artefact at the carotids, but no carotid abnormalities on ultrasound).

Table 5-1 Baseline characteristics of CADASIL cohort (n = 22)

Characteristics	Cohort (n =22)
Demographic characteristics	
Age, mean (SD) (years)	49.6 (11.2)
Female, n (%)	11 (50)
Body mass index, median (IQR) (kg/m ²)	28 (5.7)
Clinical scores	
NIH stroke scale, median (range)	0 (0 - 3)
Modified Rankin Score, median (range)	0 (0 - 3)
Anxiety score, median (range)	6 (2 - 16)
Depression score, median (range)	4 (0 - 18)
Clinical Features, n (%)	
Stroke or TIA	11 (50)
Migraine	21 (95)
Depression	10 (45)
Urinary incontinence	4 (18)
Seizures	0 (0)
Vascular Risk Factors, n (%)	
Current or ex-smoker	11 (50)
Hypertension	0 (0)
Hypercholesterolaemia	13 (59)
Diabetes mellitus	0 (0)
Medication, n (%)	
Statin	16 (73)
Antiplatelet	18 (82)
Antidepressant	8 (36)
Beta-blocker [§]	2 (9)
Imaging characteristics, mean \pm SD, range, median*	
No. of lacunes	9 \pm 1, 0 - 34, 5
No. of microbleeds	2 \pm 3, 0 - 10, 0
NLV, %	0.04 \pm 0.04, 0 - 0.15, 0.02
NSH, %	6.0 \pm 3.8, 1.0 - 15.5, 5.2
NBV, L	1.55 \pm 0.09, 1.40 - 1.75, 1.55
Total EPVS score	4 \pm 1, 1 - 6, 3
Presence of SLLL, n (%)	7 (35)

[§]Not prescribed for hypertension. *n = 21 for all imaging characteristics except microbleeds where n =20.

5.3.1 MRI markers at baseline

MRI markers are shown at baseline. CADASIL modified Scheltens score correlated with NSH ($n = 21$, $r_s = 0.826$, $p < 0.001$).

5.3.2 Blood flow and reactivity

Resting CBF measured by ASL was available in 19 subjects. In one subject ASL was not performed due to body habitus and 2 were excluded due to movement artefact. $\% \Delta \text{CBF}$ was available in 18 subjects (1 patient could not fit a face mask), and CVR_{ASL} in 13. 5 patients did not have reliable CO_2 readings due to poor mask fit or issues with the monitor.

21 patients underwent TCD (in one patient neither middle cerebral artery could be detected). Study cohort vascular measurements are shown in Table 5-2.

Table 5-2 Study cohort vascular measurements

Measurement	Mean (SD)	Number
SBP, mmHg	120 (11)	22
AI@75, bpm	17 (13)	22
PWV, m/s	7.5 (1.1)	21
RHI, %	2.1 (0.7)	20
CIMT, mm	0.64 (0.1)	21
FMD, %	4.1 (1.9)	18
MFV, cm/s	40 (9.5)	21
Brain parenchyma CBF, ml/100g/min	46 (8.6)	19
GM CBF, ml/100g/min	51 (9.4)	19
WM CBF, ml/100g/min	43 (7.6)	19
SH CBF, ml/100g/min	30 (5.6)	19

CBF was highest in the GM mask. CBF and MFV were not significantly related to age (GM CBF, $n=19$, $r_s = -0.383$, $p = 0.106$; MFV, $n = 21$, $r_s = -0.370$, $p = 0.099$) (Figure 5-4).

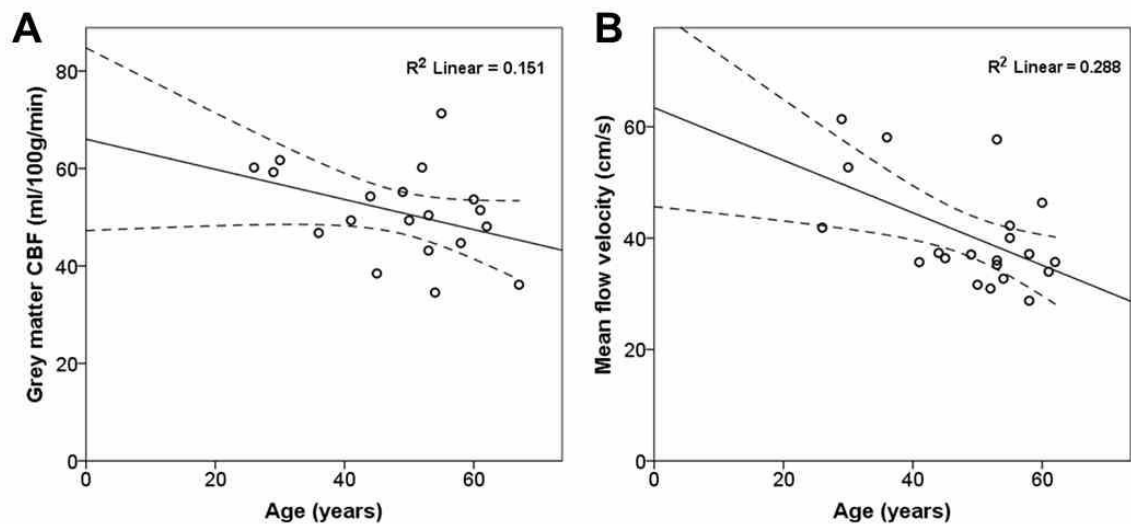


Figure 5-5 Cerebral blood flow, mean flow velocity and age

(A) Grey matter CBF and (B) MFV compared to age. The solid line represents the line of best fit, and the dashed lines the 95% confidence intervals of the mean.

CVR_{ASL} and CVR_{TCD} varied widely among patients but intra-subject measures in individual brain regions were highly correlated with each other (see Table 5-3).

Table 5-3 Hypercapnia and cerebrovascular reactivity

	n	CVR, %, median (range)	Paired correlation to brain parenchyma CVR	Paired sample t-test to parenchyma CVR, p value
TCD	21	6.3 (2 to 18)		
Brain parenchyma	13	6.2 (-3 to 22)		
GM mask	13	6.2 (-4 to 28)	0.965, 0.000	0.303
WM mask	13	5.9 (-3 to 26)	0.972, 0.000	0.277
SH mask	13	5.7 (0 to 23)	0.961, 0.000	0.606

CVR_{TCD} was not associated with MFV ($n = 21$, $r_s = -0.371$, $p = 0.099$). $\% \Delta CBF$ (GM, $n = 18$, $r_s = -0.094$, $p = 0.711$) and CVR were not associated with CBF in any of the brain masks (GM, $n = 13$, $r_s = 0.121$, $p = 0.694$).

AI@75, PWV and CIMT were associated with increasing age. Reactivity measures (CVR_{TCD} , CVR_{ASL} , RHI, FMD) were not. Brain reactivity was better in patients with higher systolic blood pressure (SBP) (Table 5-4; Figure 5-5).

Table 5-4 Brain and peripheral reactivity compared to age and blood pressure

		Age (years)	Systolic blood pressure (mmHg)
AI@75	r_s	0.529	-0.087
	p	0.011	0.702
	n	22	22
PWV	r_s	0.561	-0.165
	p	0.008	0.475
	n	21	21
CIMT	r_s	0.584	-0.27
	p	0.005	0.236
	n	21	21
RHI	r_s	0.091	0.013
	p	0.704	0.956
	n	20	20
FMD	r_s	-0.203	0.33
	p	0.42	0.181
	n	18	18
GM CBF	r_s	-0.389	-0.400
	p	0.100	0.09
	n	19	19
TCD CVR	r_s	-0.038	0.462
	p	0.869	0.035
	n	21	21
GM %ΔCBF	r_s	-0.080	0.521
	p	0.754	0.026
	n	18	18
GM CVR	r_s	-0.305	0.567
	p	0.31	0.043
	n	13	13
SH CVR	r_s	-0.395	0.671
	p	0.181	0.012
	n	13	13

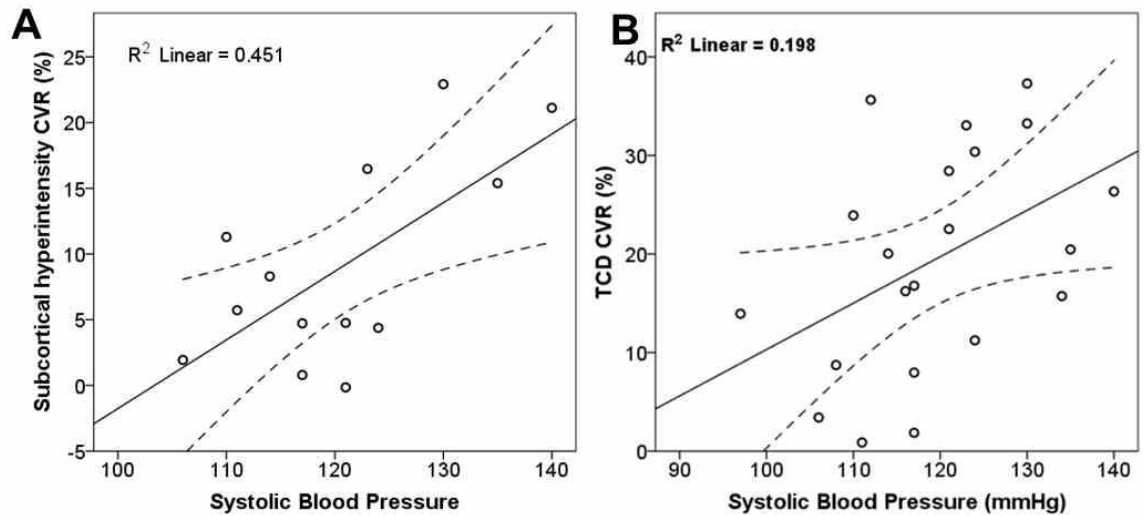


Figure 5-6 Systolic blood pressure compared to cerebrovascular reactivity
(A) Subcortical hyperintensity CVR and (B) TCD CVR were positively correlated to systolic blood pressure. (Solid line represents line of best fit and dashed lines the 95% confidence interval of the mean).

CVR_{ASL} was positively correlated with FMD (parenchyma, $n = 13$, $r_s = 0.615$, $p = 0.033$; GM, $n = 13$, $r_s = 0.566$, $p = 0.055$; SH, $n = 13$, $r_s = 0.455$, $p = 0.138$) but not RHI (GM, $n = 12$, $r_s = -0.231$, $p = 0.471$). CVR_{TCD} was not correlated with either FMD ($n = 17$, $r_s = 0.121$, $p = 0.643$) or RHI ($n = 19$, $r_s = 0.076$, $p = 0.756$).

FMD was negatively correlated to the diameter of the brachial artery ($n = 18$, $r_s = -0.472$, $p = 0.048$) and was higher in females than males (female, $n = 7$, 5.3% (1.4) v male, $n = 11$, 3.3 (1.7); $p = 0.02$). Measures of peripheral endothelium dependent vasoreactivity (brachial FMD and RHI) did not correlate with each other ($n = 17$, $r_s = 0.184$, $p = 0.479$).

Current smokers or those with a greater than 20 year pack history, had higher RHI than those who had never smoked (1.9% (0.5) v 2.6 (0.8); $p = 0.032$). Subjects not on statins tended to be younger (42yrs (13) v 52 (9); $p = 0.049$) but other vascular measures did not vary.

5.3.3 Is peripheral and cerebral vessel function associated with conventional MRI markers?

A lower NBV was associated with increased PWV and CIMT, and lower CVR. It showed non-significant trends towards association with lower CBF. The presence of many lacunes (≥ 5) was associated with higher age, increased CIMT, lower

FMD and lower CVR (Figure 5-6). Higher NLV was also associated with older age and lower FMD, but also higher RHI (Table 5-5). The number of microbleeds and NSH was not significantly correlated with age or any measures of peripheral or cerebral vessel function. SLLs were more found in older people (no SLLs, $n = 14$, 46yrs (13) v SLLL, $n = 7$, 55yrs (4); $p = 0.03$). Gender and smoking history had no effect on MRI markers.

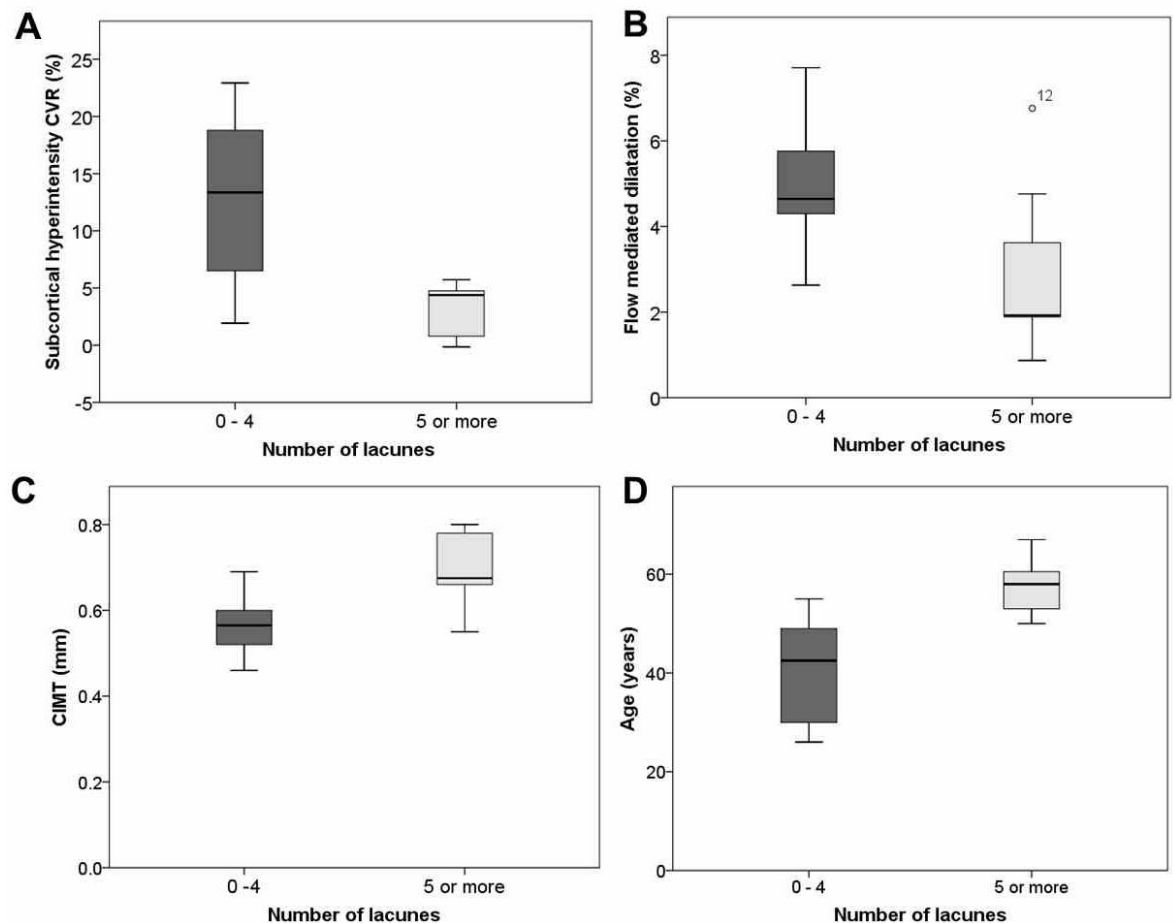


Figure 5-7 Factors associated with number of lacunes
 (A) SH CVR was lower in patients with more lacunes, as was FMD (B). Conversely, CIMT (C) and age (D) were higher in those with more lacunes.

Table 5-5 MRI outcomes variables compared to vascular measures

		No of Lacunes		No of Microbleeds		NBV (L)		NSH (%)		NLV (%)	
		0-4	>5	Absent	Present	<1.548	≥1.548	<5.23	≥ 5.23	<0.024	≥0.024
Age	n	10	11	11	9	11	10	10	11	10	11
	mean (SD)	41 (10)	57 (5)	46 (11)	53 (11)	46 (11)	53 (12)	46 (14)	53 (7)	44 (11)	55 (10)
	p value		<0.001		0.080*		0.191		0.165		0.016*
PWV	n	10	10	11	8	11	9	10	10	10	11
	mean (SD)	7.2 (0.9)	7.9 (1.1)	7.4 (1.2)	7.8 (1.1)	7 (0.9)	8 (0.8)	7.4 (1.0)	7.7 (1.1)	7.2 (1.0)	7.9 (1.1)
	p value		0.109		0.513		0.01		0.540		0.197
CIMT	n	10	10	11	9	10	9	9	11	10	10
	mean (SD)	0.57 (0.07)	0.70 (0.81)	0.63 (0.11)	0.65 (0.10)	0.59 (0.09)	0.69 (0.09)	0.61 (0.11)	0.66 (0.08)	0.60 (0.09)	0.67 (0.10)
	p value		0.001		0.547		0.025		0.260		0.170
RHI	n	10	9	10	9	10	9	8	11	10	9
	mean (SD)	1.9 (0.5)	2.4 (0.7)	2.2 (0.7)	2.3 (0.6)	2.0 (0.6)	2.3 (0.8)	2.3 (0.7)	2.1 (0.7)	1.9 (0.5)	2.5 (0.7)
	p value		0.080		0.739		0.549*		0.476		0.035
FMD	n	10	7	11	6	11	6	9	8	9	8
	mean (SD)	4.9 (1.4)	2.9 (2.1)	4.1 (1.4)	3.4 (2.1)	4.5 (1.7)	3.3 (2.2)	4.1 (1.8)	4.1 (2.2)	4.9 (1.4)	3.1 (2.0)
	p value		0.034		0.396		0.218		0.991		0.044
GM CBF	n	10	9	10	7	10	9	10	9	10	9
	mean (SD)	55 (9)	47 (8)	52 (8)	47 (9)	55 (9)	47 (8)	53 (8)	49 (10)	53 (9)	39 (10)
	p value		0.065		0.235		0.076		0.418		0.334
GM %ΔCBF	N	9	9	10	6	10	8	9	9	9	9
	mean (SD)	16 (15)	5 (8)	12 (15)	12 (10)	15 (15)	6 (8)	14 (15)	8 (11)	15 (13)	7 (12)
	p value		0.074		0.941		0.181		0.388		0.225
GM CVR	n	8	5	7	4	8	5	7	6	7	6
	mean (SD)	14 (9)	2 (4)	11 (10)	8 (7)	13 (8)	3 (3)	11 (11)	8 (7)	12 (7)	6 (6)
	p value		0.013		0.609		0.021		0.644		0.181
SH CVR	n	8	5	7	4	8	5	7	6	7	6
	mean (SD)	13 (8)	3 (3)	11 (9)	8 (5)	13 (8)	3 (3)	11 (9)	7 (5)	11 (7)	6 (8)
	p value		0.008		0.528		0.009		0.372		0.280

*Non-parametric test used. SBP, AI@75 and TCD CVR not shown as all p values over >0.1. P values <0.05 shown in bold typeface.

5.3.4 Does vasoreactivity relate to clinical and psychological markers of disease?

Subjects with depressive symptoms (HADS ≥ 8) had reduced % Δ CBF but changes in CVR_{ASL} did not reach significance (see Table 5-6). Disabled patients showed similar results but group numbers were very small (see Table 5-6). All patients with a mRS ≥ 2 had HADS depression scores of 8 or more. Vascular measures did not vary with neurological impairment (NIHSS) or HADS anxiety score.

Table 5-6 Depression and disability compared with vascular measures

		Depression (HADS)		mRS	
		<8	≥ 8	0-1	≥ 2
Age	n	12	9	15	7
	mean (SD)	49 (11)	49 (13)	49 (12)	52 (10)
	p value		0.949		0.583
A@I75	n	12	9	15	7
	mean (SD)	18 (14)	15 (13)	16 (13)	18 (14)
	p value		0.657		0.806
PWV	n	12	8	15	6
	mean (SD)	8 (1)	8 (1)	8 (8)	8 (2)
	p value		0.956		0.918
CIMT	n	12	8	15	6
	mean (SD)	0.6 (0.1)	0.7 (0.1)	0.6 (0.1)	0.7 (0.1)
	p value		0.230		0.161
RHI	n	12	7	15	5
	mean (SD)	2.1 (0.7)	2.2 (0.8)	2.2 (0.7)	2.0 (0.5)
	p value		0.732		0.583
FMD	n	12	6	14	4
	mean (SD)	4.2 (2.1)	3.7 (1.2)	4.1 (2.1)	3.9 (1.1)
	p value		0.543		0.831
GM CBF	n	12	6	15	4
	mean (SD)	51 (9)	51 (11)	50 (10)	54 (8)
	p value		0.961		0.554
TCD CVR	n	11	9	14	7
	mean (SD)	20 (12)	17 (10)	22 (12)	14 (8)
	p value		0.573		0.094
GM % Δ CBF	N	12	5	14	4
	mean (SD)	14 (14)	2 (4)	14 (13)	0.1 (3)
	p value		0.01		0.054
GM CVR	n	10	3	11	2
	mean (SD)	12 (9)	1 (5)	11 (9)	-0.9 (4)
	p value		0.086		0.083
SH CVR	n	10	3	11	2
	mean (SD)	11 (8)	2 (2)	11 (7)	1 (1)
	p value		0.076		0.105

Processing speed declined with high NLV and lower NBV (see Table 5-7).

Processing speed was associated with lower CIMT and higher % Δ CBF and non-significantly with CVR_{ASL} . Executive function was non-significantly associated with NBV ($n = 19$, $r_s = 0.441$, $p = 0.059$) but no other radiological or reactivity measures.

Table 5-7 Vascular and radiological markers compared to processing speed

Processing speed		
Age	r_s	-0.253
	Sig (2 tail)	0.268
	N	21
CIMT	r_s	-0.463
	Sig (2 tail)	0.04
	N	20
GM % Δ CBF	r_s	0.507
	Sig (2 tail)	0.038
	N	17
GM CVR	r_s	0.500
	Sig (2 tail)	0.082
	N	13
SH CVR	r_s	0.429
	Sig (2 tail)	0.144
	N	13
NLV	r_s	0.667
	Sig (2 tail)	0.001
	N	20
NBV	r_s	0.512
	Sig (2 tail)	0.021
	N	20

*SBP, AI@75, PWV, RHI, FMD, Grey matter CBF and TCD, NSH, microbleeds not shown as all p values >0.1 .

5.4 Discussion

In this cross-sectional study, it was identified that indices of cerebral and peripheral vascular function correlate with key radiological and clinical features of CADASIL. Impaired peripheral and cerebral vasoreactivity was significantly associated with a higher number of lacunes, a feature known to relate to poorer clinical status (Liem et al., 2007). Patients with greater disability, higher depressive symptoms and poorer processing speed, showed a tendency to worse cerebral vasoreactivity but group numbers were very small. Lacunes and normalised brain volume also showed associations with CIMT, vessel stiffness

(PWV), and age. Clearly there are complex interactions between these factors which require larger group numbers to unravel than are included in this study. However the observation that impaired vasoreactivity is associated with lacunes suggests it may have potential as a therapeutic target.

Reduced CBF, attenuated cerebrovascular responses to hypercapnia and acetazolamide, and abnormal cerebral autoregulation have been demonstrated to precede the development of vascular and brain lesions in transgenic mouse models (Lacombe et al., 2005, Joutel et al., 2010). Whilst mouse models fail to recapitulate human CADASIL entirely, as they do not develop lacunes, the models suggest that functional impairment of VSMC and hence cerebral vascular pathophysiology, leads to the development of brain lesions in CADASIL (Joutel and Faraci, 2014). Increasingly there is evidence that capillary dysfunction, secondary to loss of pericytes, may also have a key role, due to their role in cerebral autoregulation (Hall et al., 2014). Impaired blood-brain barrier integrity may also contribute (Henshall et al., 2015). A number of human studies have suggested impairment of cerebral vascular function (Chabriat et al., 2000, Pfefferkorn et al., 2001, Peters et al., 2008). Reductions in CBV and CBF have been associated with worse clinical or radiological outcomes (Chabriat et al., 2000, van den Boom et al., 2003a), and impaired TCD CVR with CO₂ has been associated with disability (Pfefferkorn et al., 2001). Over a 7 year follow up, a lower CVR in response to acetazolamide was associated with a larger increase in WMH, but not microbleeds or lacunes (Liem et al., 2009a).

The trend towards association of vasoreactivity markers with disability, depression and delays in processing speed is interesting and warrants further assessment in longitudinal studies. Whether this is a state preceding or following the development of lacunes and atrophy is unclear.

Cerebral and peripheral reactivity were associated in this study as has previously been shown in other studies in CADASIL (Fujiwara et al., 2012). Peripheral vascular function has previously been demonstrated to be impaired, particularly in resistance vessels (Gobron et al., 2006, Stenborg et al., 2007, Campolo et al., 2011). Peripheral vascular tests may offer some advantages by being less expensive, and generally easier to undertake, particularly in disabled individuals, and with a demonstrated role as disease biomarkers in

cardiovascular studies (Mancia et al., 2007, Laurent et al., 2001, Celermajer et al., 1992). FMD is known to be lower in patients with lacunes compared to healthy controls, although this likely reflects their cardiovascular risk factors (Pretnar-Oblak et al., 2006). Previous studies have not demonstrated differences in FMD between CADASIL patients and controls (Gobron et al., 2006, Stenborg et al., 2007) whereas this study found it to be associated with lacunes. Non-continuous measurement of FMD diameter (Gobron et al., 2006) and limited time for measurement (Stenborg et al., 2007) may have hampered the ability of these previous studies to detect peak diameters, particularly as there is evidence that post-occlusion hyperaemia profiles in CADASIL patients may have a delayed time to peak (Gobron et al., 2006). In this study, brachial artery diameter was measured on every R wave from around 20 seconds post cuff deflation to 5 minutes, enhancing my ability to detect peak diameter. FMD does vary with gender and size of vessel, and this would need to be factored into larger studies. Interestingly, the RHI, an alternative measure of endothelial function, was higher in those with a current or significant history of smoking, and those with higher NLV. The reason for this is unclear and FMD and RHI did not correlate.

In this study no participants had co-existent hypertension, diabetes or carotid stenosis, but 11 (50%) patients were current or ex-smokers, and a similar number had a history of hypercholesterolaemia (59%). Exclusion of those on treatment with calcium channel blockers or angiotensin converting enzyme inhibitors restricted the recruitment of hypertensive patients. PWV, a reflection of large artery stiffness (Laurent et al., 2001) and CIMT, a surrogate marker of generalised atherosclerosis load (O'Leary and Bots, 2010), were also associated with number of lacunes. Increased CIMT has been associated with an increased risk of stroke and coronary disease (Lorenz et al., 2007). This indicates that in CADASIL a combination of large vessel disease presumably resulting from smoking and hyperlipidaemia, and small vessel dysfunction, caused by CADASIL, is particularly damaging to patients. This study highlights the importance of encouraging a healthy lifestyle in order to potentially delay complications of CADASIL.

This is, as far as I am aware, the first study using arterial spin labelling MRI in CADASIL to investigate CBF and CVR, and has demonstrated its feasibility and potential utility. Global CBF of 46ml/100g/min is compatible with the literature

(Kety and Schmidt, 1948b). CBF within specific brain regions can be studied: CBF was lowest within subcortical hyperintensities which suggests either that CBF falls as a consequence of the pathology underlying hyperintensities, or that hyperintensities tend to occur in arterial end zones initially, where CBF is likely to be lowest (Duering et al., 2013). However it may also be due to difficulties accurately measuring white matter CBF (van Gelderen et al., 2008).

One unanticipated finding was that patients with lower resting SBP had lower CVR. The resting SBP was obtained in a temperature-controlled environment, on a different day to both the TCD and MRI. Alterations in BP dynamics have been described in CADASIL. In transgenic mouse models, the lower limit of CBF autoregulation is shifted to a higher mean arterial blood pressure (MABP), although BP does not rise to compensate for this (Joutel et al., 2010). A lower BP profile is seen in CADASIL compared to normal controls, due to reduced daytime values (Rufa et al., 2005). Daytime MABP has been positively correlated to cognitive impairment as measured by the MMSE, suggesting either that low blood pressure is harmful or that it reflects more severe disease (Rufa et al., 2005). Low BP profiles are also associated with dementia in elderly non-CADASIL populations (Guo et al., 1996). Alterations in BP may be explained by impairments in autonomic function, due to central damage to autonomic or circadian control centres (Rufa et al., 2007).

An alternative hypothesis is that tissue in CADASIL patients has worsened capillary transit time heterogeneity (CTTH) and CBF (and perhaps BP) is reduced as a protective mechanism to minimise heterogeneity and preserve oxygen extraction (Jespersen and Østergaard, 2012). In this study, however baseline CBF was not related to CVR, unlike SBP. CTTH in CADASIL is currently the source of ongoing research (Engedal et al., 2015). The role of BP remains complex as hypertension appears to have deleterious effects in CADASIL being associated with both a higher risk of stroke (Adib-Samii et al., 2010), and more microbleeds (Viswanathan and Chabriat, 2006).

Patients with more lacunes were older but otherwise age did not correlate to other measures of MRI damage such as microbleeds or SH, unlike other studies (van den Boom et al., 2003b). Whilst the age range was 26 to 67 years, half the

patients were between the age of 50 and 60. This study may be underpowered to detect the effect of age.

5.4.1 Strengths

Strengths of this study include a CADASIL population with a wide age range, and a number of affected exons, who lacked conventional risk factors for stroke such as hypertension, diabetes or carotid disease, meaning any cerebral pathology is likely to predominantly reflect CADASIL alone. All tests were performed by a single, trained rater and attendance at 100% of visits was achieved. High quality MRI scans were available, with hypercapnic challenge undertaken with monitoring of inspired and expired gases allowing accurate calculation of CVR.

5.4.2 Limitations

There are limitations to this study which must be noted. First, the number of subjects is small, largely due to the comprehensive assessment and multiple visits required. Whilst patients were asked to refrain from nicotine, caffeine and alcohol for 4 hours prior to study visits, they were not fasted and medications were not stopped. Testing also took place at multiple visits over a maximum of 3 months, although participants experienced no new strokes or hospital admissions between visits. Ideally tests would have taken place over a shorter time period. All MRI vasoreactivity testing occurred between 10am and 2pm, and 18/21 TCD tests between 10am and 12pm. There was more variation in the time of peripheral vascular assessment. Time of testing is known to affect vasoreactivity measurements, and I cannot exclude that this is relevant in my results.

One important limitation of this study is the lack of a control group. The study was designed as a longitudinal study examining for disease biomarkers in this specific patient group, relating vascular markers to clinical progress. It has been demonstrated that CADASIL patients are different from healthy controls in a number of other studies. The number of visits required for this study, time-consuming image analysis requirements, and financial constraints, necessitated the decision not to include control subjects. This limits the interpretation of CBF and CVR in these patients. It is therefore not known if these findings are specific to CADASIL. This is a major limitation of this study, and is also relevant in

Chapters 6 and 7. It may be that control patients could be obtained as part of different studies performed by researchers at the University of Glasgow, which may allow more direct comparison.

Dichotomising radiological measures is arbitrary but given the number of statistical tests it was felt sensible to simplify the outcomes measures. Indeed it is unlikely any damage caused by impaired reactivity would occur in a linear relationship; instead there may be a threshold at which impaired vasoreactivity has a deleterious effect.

A large number of statistical tests and multiple comparisons were used in this study without correction for this. This raises the possibility that any significant results were purely by chance. Whilst the results are consistent with what we would expect knowing about the pathophysiology of the disease, a more defined primary hypothesis would have improved the robustness of the results.

Additionally it would have been beneficial for a number of the tests for examples FMD analysis or lacune volume counting to include a second, or an entirely independent rater, particularly as these are the results which have shown some significant relationships. A rater blind to study hypothesis and all clinical information is more scientifically rigorous although the amount of analysis required for this to be done is significant. Whilst the author made every attempt to avoid any reference to previously obtained results, when repeating analysis, bias may have been introduced during analysis. A blind rater may also have been more stringent in applying quality control to scans. In a small study there is a desire to maximise inclusion of results but quality must also be paramount.

5.5 Conclusion

Impairment of cerebral and peripheral vasoreactivity is associated with number of lacunes, an important established correlate of clinical severity. Ageing, cardiovascular risk factors and large vessel disease may also play a crucial role. To establish if vasoreactivity could function as a potential biomarker in CADASIL, further longitudinal analysis is required. The finding of lower BP being associated

with impaired vasoreactivity may warrant the further investigation of the changes in BP of CADASIL patients over time.

Chapter 6 – Changes in CBF and CVR in CADASIL as measured by TCD and ASL over 1 year.

6.1 Introduction

In order to develop a feasible imaging biomarker, techniques need to be reliable and repeatable over the time period used in clinical studies i.e. months to years. ASL MRI has proved attractive for longitudinal studies of changes in CBF, as it is quantifiable, and does not require the use of radiation or intravenous contrast, making it safe.

Inter-subject variability in CBF is very high. Intra-subject measures are more consistent. In 34 subjects continuous ASL (CASL) was used to make repeated measurements of CBF, in controlled conditions, and CBF was stable (Parkes et al., 2004). Using 3D pseudo-continuous ASL (pCASL) with a post-labelling delay of 2.5 seconds, high repeatability was shown even using different scanners in 8 healthy patients (Wu et al., 2014). Intra-class correlation for global CBF has shown to be >0.90 for elderly subjects at risk of Alzheimer's disease using pCASL (Xu et al., 2010).

The advantages and disadvantages of both ASL and TCD have been reviewed in Chapter 2. No studies have used ASL to study CBF or CVR in CADASIL patients, either in cross-sectional or longitudinal studies. TCD has been used to study CADASIL patients but with conflicting results (see Chapter 2). As discussed in Chapter 3 administering a CVR respiratory challenge has difficulties, and establishing if the techniques used can give reliable and repeatable results is important before deciding whether the technique has promise as a biomarker.

Changes in CBF and CVR in CADASIL may well have relevant clinical implications, but as inter-subject variability of CBF is so high, this may well be more identifiable by change in CBF over time. The main hypothesis of this chapter is that cerebral blood flow and cerebrovascular reactivity will decline in CADASIL patients over one year.

Therefore the aims of this chapter are:

- 1) confirm CBF is variable in different brain regions;
- 2) establish if CBF, velocity or CVR changes in 1 year in a cohort of CADASIL patients;
- 3) assess the repeatability of ASL and TCD measurements of CBF, velocity and CVR.

6.2 Methods

6.2.1 Study cohort

Subjects recruited in this study were recruited as described in Chapter 2. Data include baseline and year 1 measurements.

6.2.2 Experimental procedures

Procedures including TCD and MRI were undertaken as described in Chapter 2.

6.2.3 TCD analysis

TCD were analysed as described in Chapter 2 and 5.

6.2.4 ASL analysis

CBF maps were generated and percentage change in CBF ($\% \Delta \text{CBF}$) and CVR were calculated as detailed in Chapter 5.

Year 1 ASL, T1 and FLAIR maps were co-registered with baseline ASL normoxia maps. Where this was not available or had been excluded, Year 1 T1 and FLAIR was registered to the ASL year 1 image.

Three methods were used to analyse the ASL: (1) whole brain masks; (2) single slice masks through centrum semiovale, (3) regions of interest.

6.2.4.1 (1) Whole brain masks

3D-T1 images were skull-stripped and segmented as described in Chapter 5. SH maps were created using an automated method which used the original SH maps (see Chapter 2) as a reference. More detail on this method is provided in Chapter 7. This method was used to create masks at baseline and year 1.

SH masks were then transformed into ASL space using the FLAIR matrix. The FLAIR was 27 slices and the ASL map 40 slices, and this led to some distortion of the SH mask. The SH mask was a probability map with values of 0 -1, and was thresholded at 0.5 and binarised, to ensure only definite hyperintensities were included.

SH mask pixels were removed from grey and white matter images, to create GM, WM and SH masks. Baseline ASL data were reanalysed using these new masks.

6.2.4.2 (2) Single slice centrum semiovale masks

As whole brain masks include brain regions such as the cerebellum and pons, a more localised measure of CBF was also created. CBF and CVR were measured from a single segmented slice above the centrum semiovale (CS). These are referred to as brain_CS, GM_CS, NAWM_CS and SH_CS.

Due to the problems identified with GM pixel leakage into WM voxels, a deep WM mask was created for analysis at this stage. A brain slice just above the ventricles was identified on the WM mask (as above). Holes in the WM mask were filled and then the mask underwent two erosions (Image J, Rasband, W.S., U.S. National Institutes of Health, Bethesda, Maryland, USA, <http://imagej.nih.gov/ij/>, 1997-2014). This mask of deep WM included both normal appearing and abnormal WM, and was applied to CBF maps (Figure 6-1).

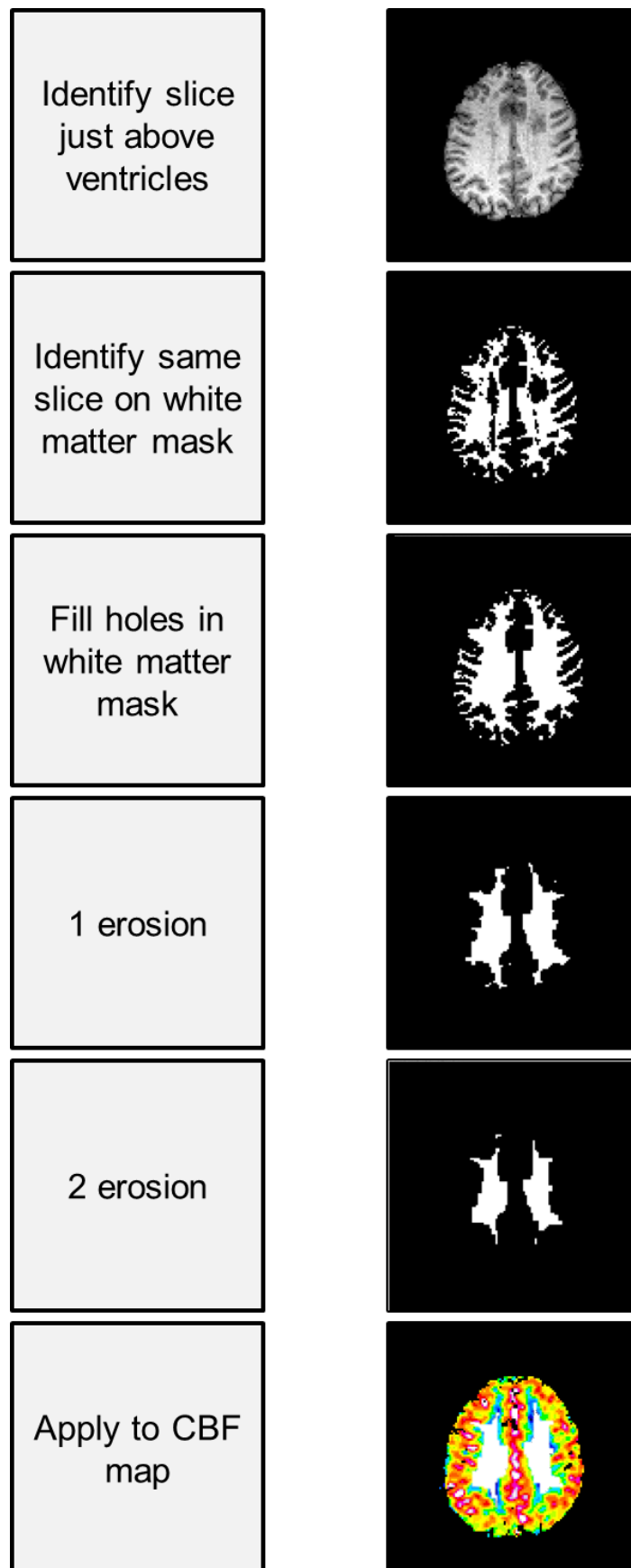


Figure 6-1 Deep white matter mask

6.2.4.3 (3) Regions of interest

The following 10 regions of interest (ROI) were identified with reference to the anatomical images: cortical grey matter, putamen, caudate, corpus callosum, internal capsule, anterior temporal lobe, cerebellum, pons, normal appearing white matter (NAWM) and centrum semiovale white matter hyperintensity (WMH) (Figure 6-5). ROI manager in Image J was used. The ROIs were then applied to the CBF maps, and average of right and left used.

Within each ROI percentage change in CBF (% Δ CBF) was calculated in Microsoft Excel:

$$\% \Delta \text{CBF} = \frac{\text{CBF}_{\text{hypercapnia}} - \text{CBF}_{\text{normocapnia}}}{\text{CBF}_{\text{normocapnia}}} \times 100$$

To investigate repeatability, ROIs were drawn for a second time in 5 randomly selected individuals without reference to the original ROIs. The single measures intraclass correlation for normocapnic CBF was 0.720 (95% confidence intervals 0.61 - 0.80) and for % Δ CBF 0.11(-0.09 - 0.30; Figure 6-2). % Δ CBF (and CVR) within individual ROI was therefore not further investigated due to poor repeatability.

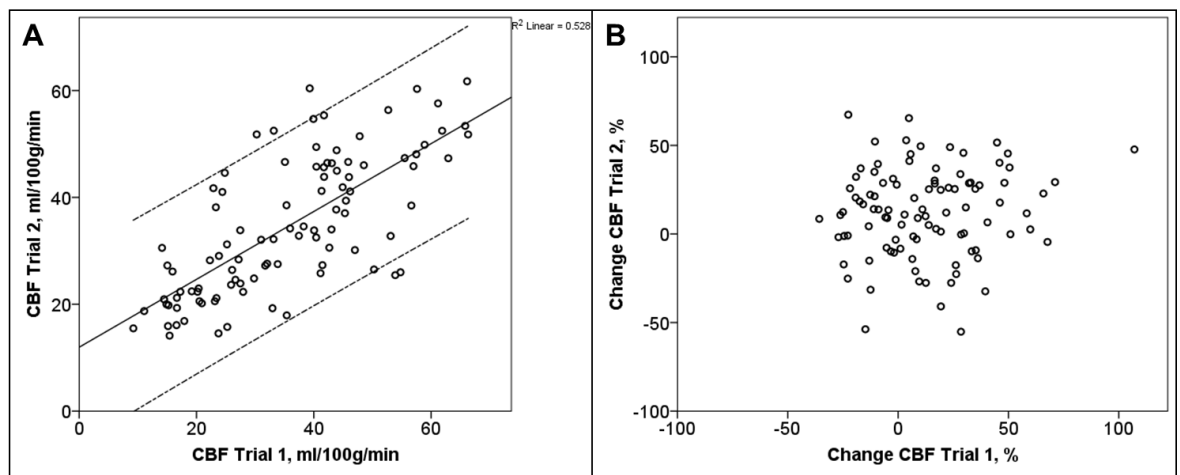


Figure 6-2 Repeatability of ASL region of interest measures in 5 individuals
(A) Cerebral blood flow. Line represents best fit line, dashed lines the individual 95% confidence intervals. **(B) Percentage change in CBF.**

The ROIs were also applied to the year 1 CBF maps. The average of right and left was again used. If baseline NAWM was now a WMH, this ROI was repositioned into a NAWM area for year 1 analysis.

6.2.5 Other radiological measures

6.2.5.1 Percentage brain volume change (PBVC)

Percentage brain volume change (PBVC) between baseline and year 1 was estimated on T1 3D images using SIENA (Smith, 2002), part of FSL (Smith et al., 2004). This was compared to change in CBF.

6.2.6 Statistics

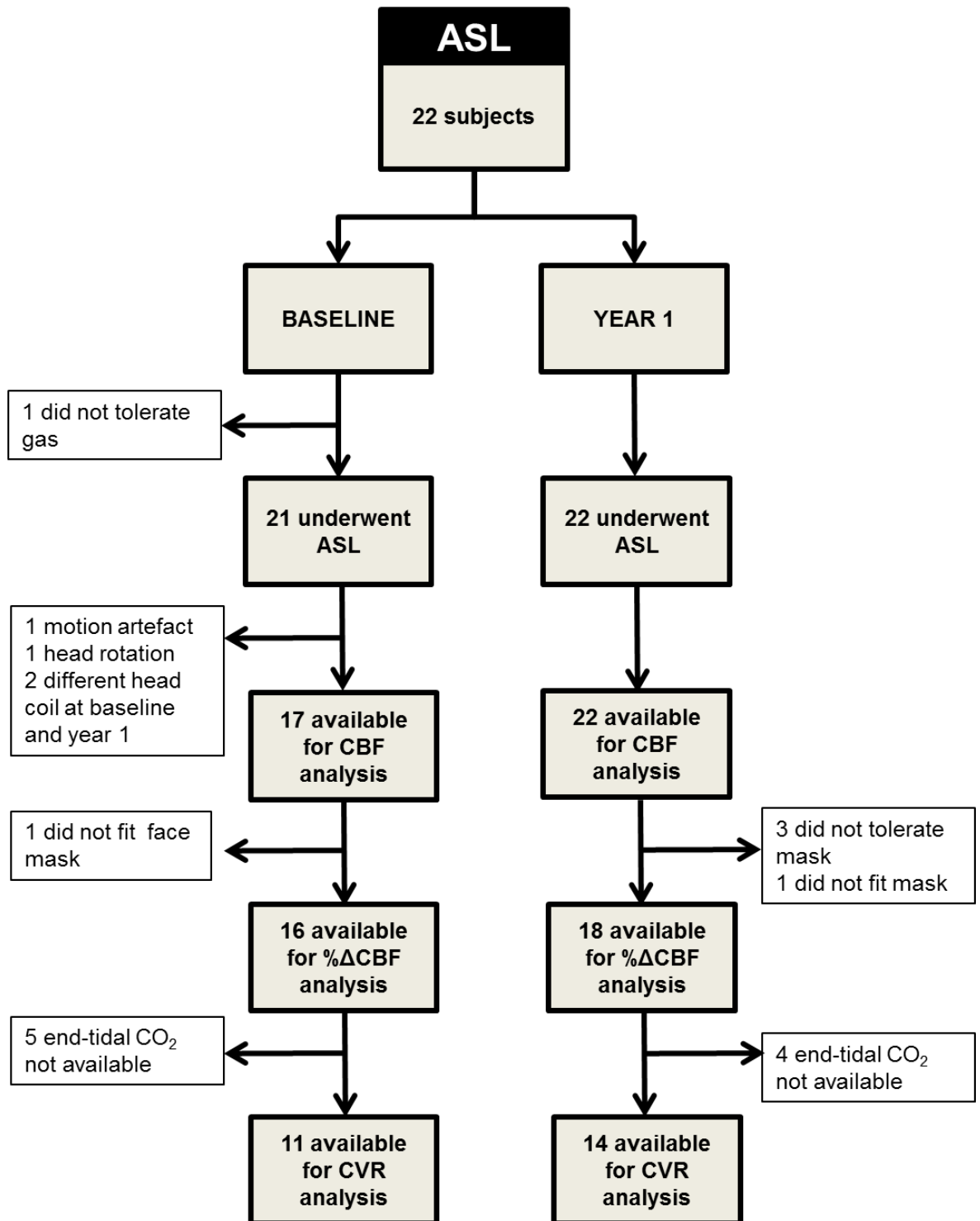
Statistical analysis was performed with IBM SPSS Version 21 (IBM Corp, Armonk, NY, USA). Normality for continuous variables was tested with Shapiro-Wilks test. Difference in CBF or CVR between baseline and year 1 in individuals was tested with a paired t-test for normally distributed data, with Related Samples Wilcoxon Signed Rank Test. Correlations between paired samples were tested with paired samples correlations. For the effect of gender and smoking, Chi-squared test was used. Significance was set at $p < 0.05$. Data is expressed as mean (SD) unless otherwise stated.

6.3 Results

6.3.1 Subjects

21 subjects underwent TCD at baseline, and 20 at year 1. 21 subjects underwent ASL MRI at baseline and 22 at year 1. There were 345 (25) days between baseline and year 1 scans. The exclusions for analysis are shown in Figure 6-3 and 6-4.

At baseline MRI and TCD took place on a different day, while at year 1, they generally took place on the same day. Time of day, caffeine use, smoking, and pre-test blood pressure are shown in Table 6-1. The median difference in time of scan between baseline and year 1 was 53min (0 - 90min), and for TCD 105min (0 - 330min).

**Figure 6-3 Exclusions for ASL**

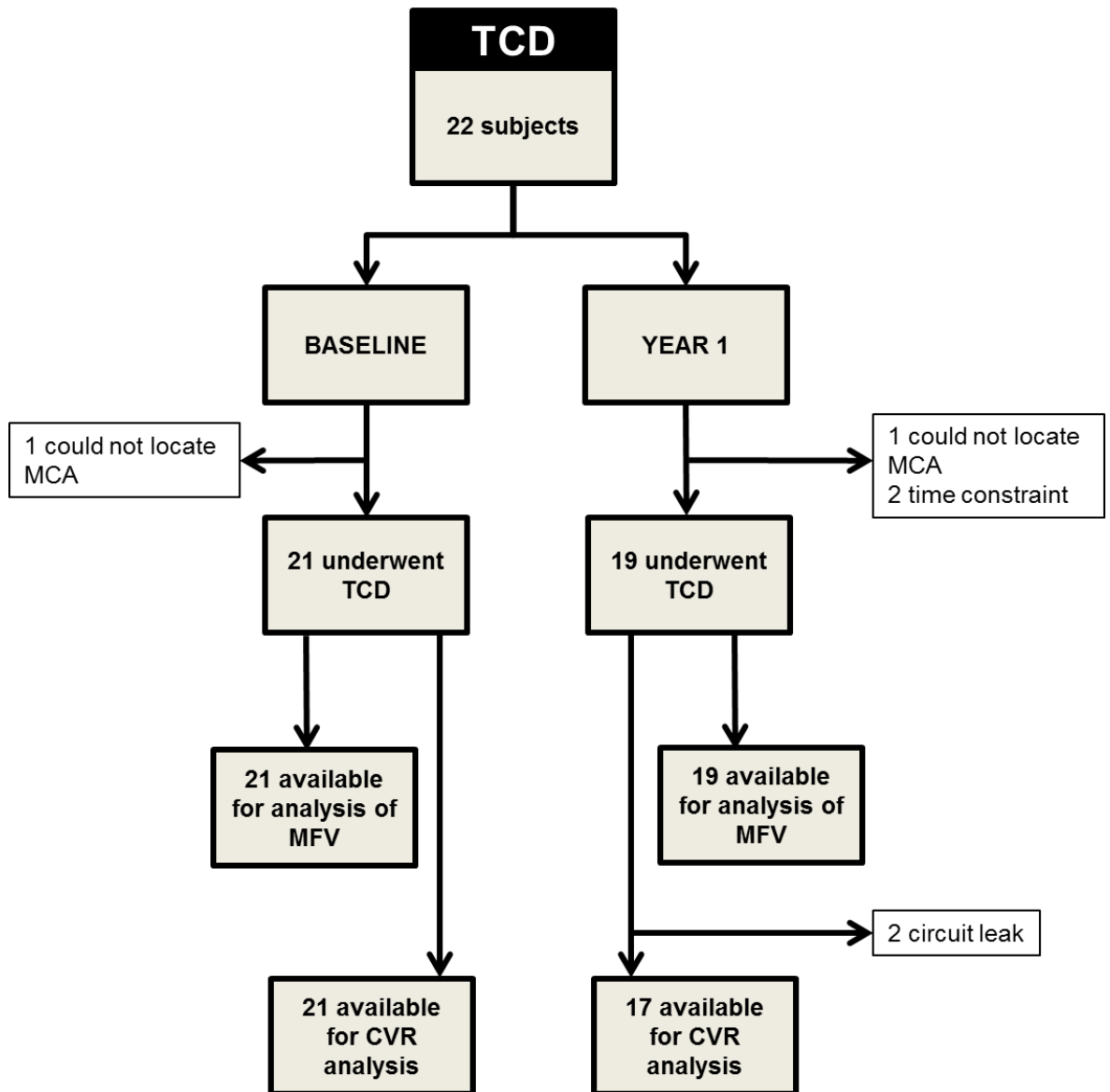


Figure 6-4 Exclusions for TCD

TCD = transcranial Doppler ultrasound; MFV = mean flow velocity; MCA = middle cerebral artery

Table 6-1 Subject characteristics at baseline and year 1

	ASL MRI								TCD							
	Time of day*		Caffeine		Smoking		Blood pressure		Time of day*		Caffeine		Smoking		Blood pressure	
	Base	Yr1	Base	Yr1	Base	Yr1	Base	Yr1	Base	Yr1	Base	Yr1	Base	Yr1	Base	Yr1
1	9:30	10:30	0	0	0	0	NA	107/70	09:00	10:00	0	0	0	0	130/84	120/76
2	13:15	13:30	0	0	0	0	NA	NA	10:30	13:00	1	0	0	0	112/71	109/67
3	12:15	12:15	0	1	0	0	NA	107/72	10:00	11:45	0	1	0	0	125/85	107/72
4	13:30	14:00	0	0	0	0	124/79	135/70	11:45	14:00	1	0	0	0	127/72	117/71
5	11:00	12:30	0	0	0	0	133/64	107/59	10:00	12:45	0	0	0	0	120/71	107/59
6	13:45	13:00	0	0	0	0	134/78	106/63	11:45	12:30	0	1	0	0	135/77	104/63
7	12:30	11:15	0	1	0	0	117/87	137/61	15:00	11:45	1	1	1	0	116/69	137/61
8	13:30	12:00	0	0	0	0	110/67	NA	12:45	NA	0	NA	0	NA	119/74	NA
9	11:45	10:45	0	0	0	0	116/68	125/70	15:45	10:15	0	0	0	0	102/53	125/70
10	NA	13:30	NA	1	NA	0	NA	126/69	12:00	11:15	1	1	0	0	110/61	126/69
11	13:45	13:30	0	0	0	0	124/82	129/77	10:55	13:00	0	0	0	0	120/75	129/77
12	12:30	13:30	0	1	1	0	132/69	129/77	11:30	NA	0	NA	1	NA	116/69	N/A
13	12:30	12:45	0	1	0	1	116/67	107/58	12:00	11:30	1	1	1	0	96/58	107/58
14	11:30	10:45	0	1	0	0	134/81	125/70	10:30	10:00	0	1	0	0	131/76	125/70
15	13:30	13:30	0	0	1	1	124/69	110/62	12:15	13:00	0	0	0	0	99/57	110/62
16	12:30	13:15	0	0	0	0	119/54	122/74	16:30	14:00	0	0	1	0	112/74	122/74
17	13:30	14:30	0	1	1	1	96/68	89/59	11:45	14:00	0	0	1	0	109/62	89/59
18	13:15	13:30	0	1	0	0	127/82	NA	11:30	11:30	1	0	0	0	127/71	118/76
19	13:30	14:30	0	0	0	0	120/68	137/83	11:45	14:00	0	0	0	0	116/62	137/83
20	12:45	11:45	0	0	0	0	143/71	115/68	10:15	11:00	0	0	0	0	125/72	115/68
21	12:30	14:00	1	1	0	0	133/88	122/63	11:45	12:30	1	1	0	0	128/82	122/63
22	10:45	11:15	0	0	0	0	140/96	145/77	11:45	10:45	0	0	0	0	133/77	145/77

*Stated to the nearest 15minutes. Base = Baseline; Yr1 = year 1

6.3.2 Cerebral blood flow – ASL

6.3.2.1 CBF in different brain regions

As all 22 patients had CBF data at year 1, this is displayed in Table 6.2. CBF was highest in cortical GM at 55 (10) ml/100g/min and lower in NAWM and WMH (see Figure 6-5). All ROI had significantly lower CBF than the cortical GM ROI (all p values <0.003). There was no significant difference between striatum and thalamus ($p = 0.215$) or NAWM and corpus callosum ($p = 0.179$) or internal capsule ($p = 0.067$).

Table 6-2 CBF in brain regions measured by ASL and ROI

Region of interest	n	CBF (ml/100g/min)
		Mean (SD)
Cortical GM	22	55 (10)
NAWM*	20	25 (4)
WMH	22	19 (4)
Striatum	22	48 (11)
Thalamus	22	46 (10)
Internal capsule	22	38 (27)
Corpus callosum	22	39 (27)
Anterior temporal lobe	22	36 (9)
Cerebellum	22	46 (11)
Pons	22	39 (8)

*2 patients had no NAWM.

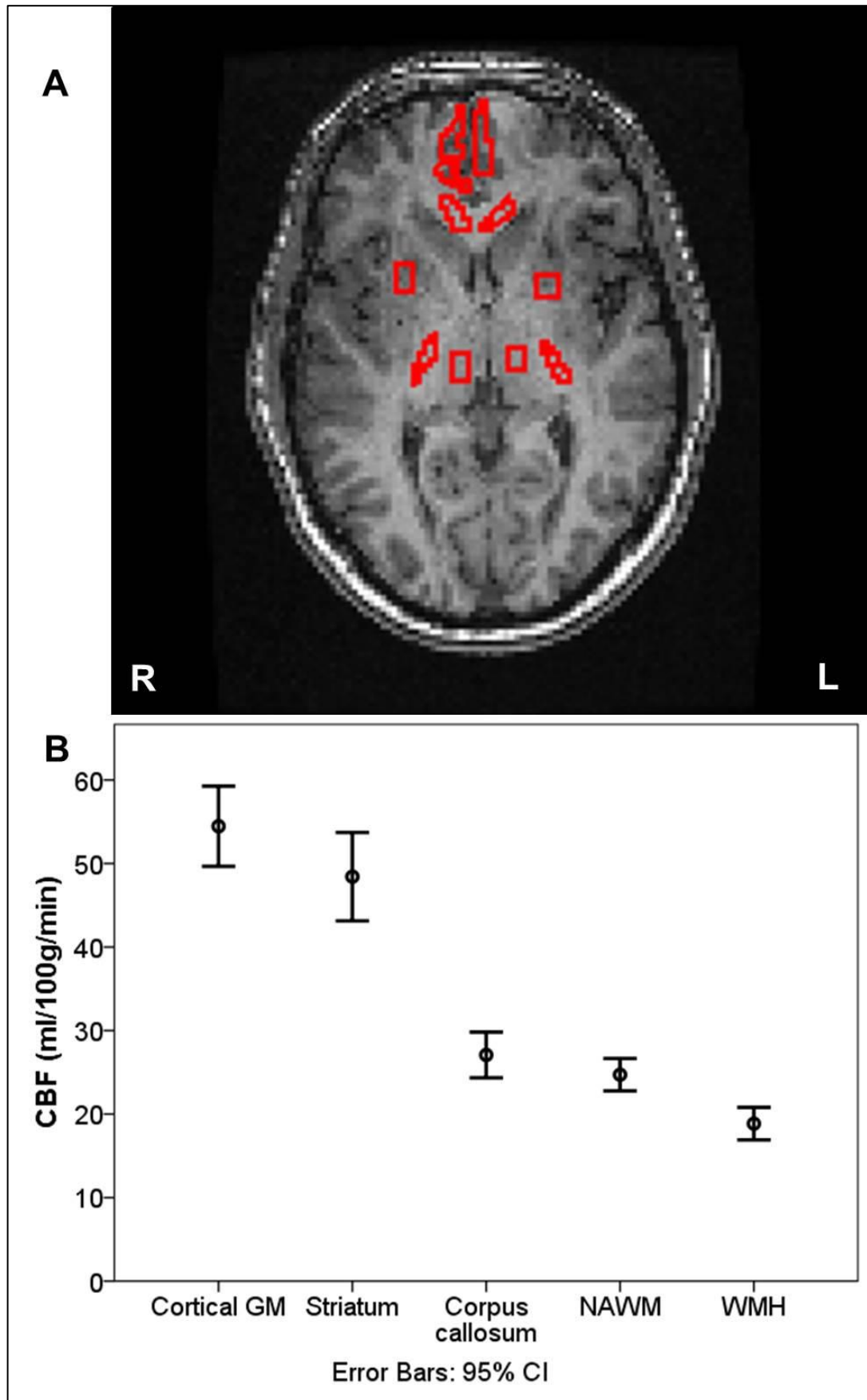


Figure 6-5 Cerebral blood flow

(A) Regions of interest were identified on anatomical images. In this slice cortical grey matter, corpus callosum, striatum, thalamus and internal capsule on right and left are seen. (B) CBF within grey matter was the highest, followed by white matter and then white matter hyperintensities (WMH) NAWM = normal appearing white matter.

6.3.2.2 CBF at baseline and year 1

The correlations and differences between blood flow at baseline and year 1 can be seen in Table 6-3; Figure 6-6. There was correlation between baseline and year 1 CBF except in some ROI (NAWM, pons, internal capsule). Parenchymal CBF was lower at year 1 compared to baseline ($n = 17$, mean reduction of $6\% \pm \text{SD } 11\%$).

CBF was lower at year 1 in both cortical and central GM (striatum). CBF was also lower in the deep WM at year 1 (year 1 $25 \pm 4 \text{ ml/100g/min}$ v baseline $27 \pm 5 \text{ ml/100g/min}$; $p = 0.036$). There was no relationship between change in CBF between the two time points and age (GM change $n = 17$, $r_s = -0.032$, $p = 0.903$) or brain volume change ($n = 17$, $r_s = -0.221$, $p = 0.395$).

Table 6-3 Correlation and difference in CBF between baseline and year 1

		CBF (ml/100g/min)		Paired T-test p value	Paired samples correlation	P value
		Baseline	Year 1			
Whole brain masks	Brain	46 (9)	43 (7)	0.015	0.817	<0.001
	GM	50 (10)	46 (8)	0.007	0.845	<0.001
	NAWM	42 (8)	40 (6)	0.078	0.759	<0.001
	SH	23 (5)	21 (3)	0.074	0.740	0.001
Centrum semiovale mask	Brain	45 (9)	42 (7)	0.028	0.788	<0.001
	GM	52 (11)	47 (9)	0.015	0.838	<0.001
	NAWM	40 (7)	38 (6)	0.218	0.676	0.003
	SH	21 (4)	20 (3)	0.172	0.643	0.005
	Deep WM	27 (5)	25 (4)	0.036	0.745	0.001
ROI	Cortical GM	60 (12)	55 (11)	0.026	0.749	0.001
	NAWM	26 (5)	25 (5)	0.334*	0.287	0.299
	WMH	20 (4)	19 (4)	0.361	0.665	0.004
	Cerebellum	51 (14)	47 (11)	0.122	0.780	<0.001
	Pons	41 (8)	40 (7)	0.926	0.186	0.474
	Anterior temporal	38 (9)	36 (10)	0.252	0.895	<0.001
	Striatum	54 (10)	48 (9)	0.005	0.692	0.002
	Thalamus	49 (13)	45 (10)	0.191	0.568	0.017
	Internal capsule	27 (5)	27 (5)	0.619*	0.218	0.402
	Corpus callosum	30 (8)	27 (5)	0.038	0.737	0.002

*Non-normally distributed - tested with Related Samples Wilcoxon Signed Rank Test

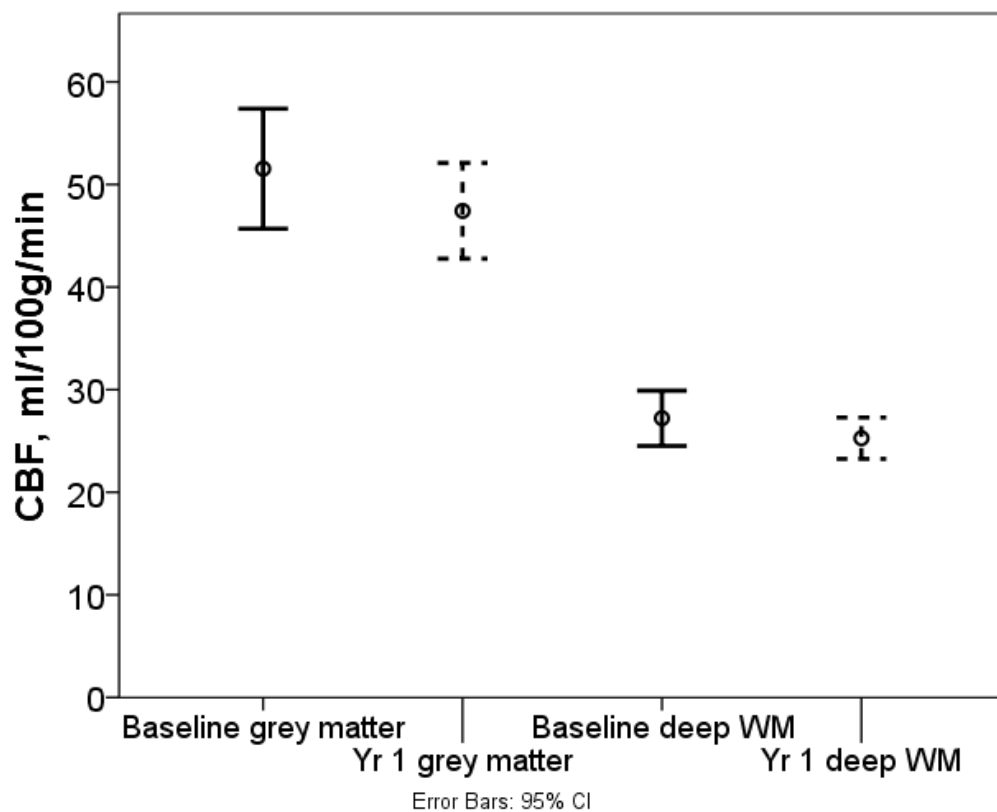


Figure 6-6 CBF at baseline and year 1 in grey matter and deep white matter in centrum semiovale

CBF declined between baseline and year 1 in whole brain, grey matter and deep white matter masks in the centrum semiovale. Baseline is shown with complete line, year 1 with dashed line. 95% error bars shown.

Age correlated with year 1 GM_CS CBF ($n = 22$, $r_s = -0.492$, $p = 0.020$; Figure 6-7A) but no other region (GM, $r_s = -0.390$, $p = 0.073$). Gender did not affect CBF in any brain region at either time point (women GM CBF, 47 (8) v male GM CBF 45 (7); $p = 0.614$).

There was a significant relationship between baseline CBF and change in CBF over 1 year, with patients with higher baseline CBF showing higher rates of CBF decline over one year ($n = 17$, $r_s = -0.556$, $p = 0.020$; Figure 6-7B). Percentage decline in CBF was not related to CVR_{ASL} (GM, $n = 11$, $r_s = 0.173$, $p = 0.612$) or CVR_{TCD} (GM, $n = 16$, $r_s = -0.044$, $p = 0.871$).

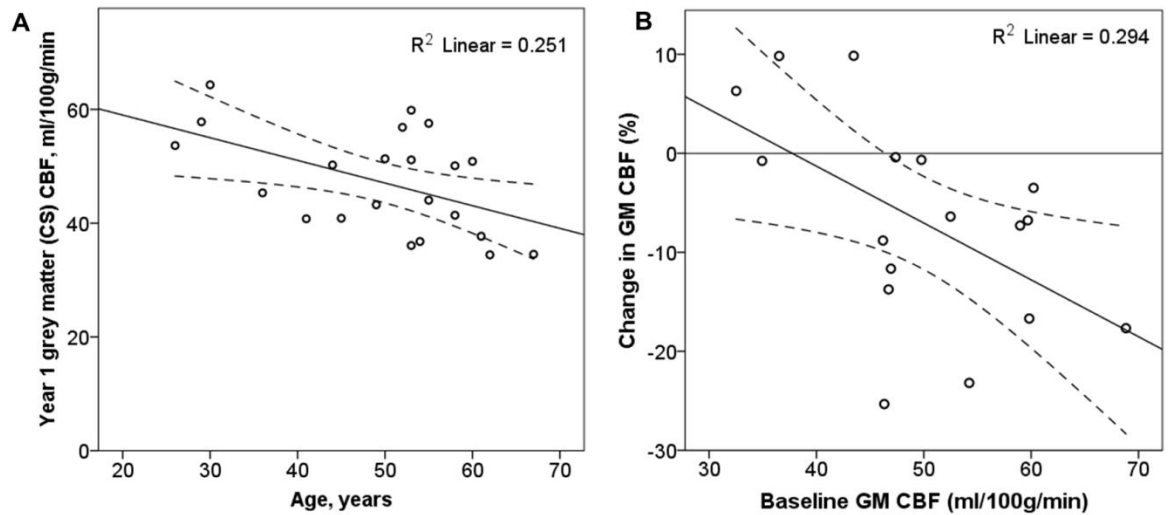


Figure 6-7 Cerebral blood flow compared to age and change over 1 year. (A) Year 1 GM CBF was correlated to age in the centrum semiovale slice. (B) GM CBF decreased more in patients with a higher baseline CBF. The solid line represents the line of best fit and the dashed lines the 95% confidence interval of the mean.

6.3.3 % Δ CBF and CVR – ASL

% Δ CBF did not demonstrate significant paired samples correlations between baseline and year 1 in any mask. There was no significant difference between the two time points (Table 6-4).

Table 6-4 % Δ CBF at baseline and year 1

		% Δ CBF		Paired T-test p value	Paired Samples correlations	P value
		Baseline	Year 1			
Whole brain mask	Brain	13 (12)	18 (14)	0.320	0.452	0.105
	GM	13 (12)	17 (14)	0.320	0.393	0.164
	WM	14 (13)	18 (15)	0.192	0.494	0.073
	WMH	16 (9)	18 (14)	0.580	0.399	0.157
Centrum semiovale mask	Brain	13 (12)	18 (15)	0.305	0.410	0.146
	Grey matter	13 (13)	17 (14)	0.312	0.373	0.189
	WM	14 (13)	19 (17)	0.307	0.455	0.102
	WMH	13 (7)	18 (15)	0.234	0.233	0.422
	Deep WM	13 (10)	18 (15)	0.285	0.337	0.238

There was a paired samples correlation in CVR_{ASL} in NAWM mask. The other masks did not show significant correlations but they were closer to significance than $\% \Delta CBF$ had been. There was no significant change in CVR_{ASL} between baseline and year 1 (Table 6-5; Figure 6-8).

Table 6-5 CVR (%) at baseline and year 1

		CVR_{ASL} (%)		T-test p value	Paired samples correlations	P value
		Baseline	Year 1			
Whole brain masks	Brain	13 (10)	12 (11)	0.770	0.596	0.052
	GM	13 (10)	12 (10)	0.767	0.560	0.073
	NAWM	13 (10)	13 (11)	0.794	0.637	0.035
	SH	14 (8)	11 (10)	0.409	0.543	0.084
Centrum semiovale masks	Brain	13 (9)	12 (10)	0.772	0.569	0.068
	GM	13 (10)	12 (10)	0.798	0.542	0.085
	NAWM	13 (10)	12 (11)	0.768	0.596	0.053
	SH	11 (5)	12 (12)	0.751	0.508	0.110
	Deep WM	12 (7)	11 (11)	0.875	0.573	0.065

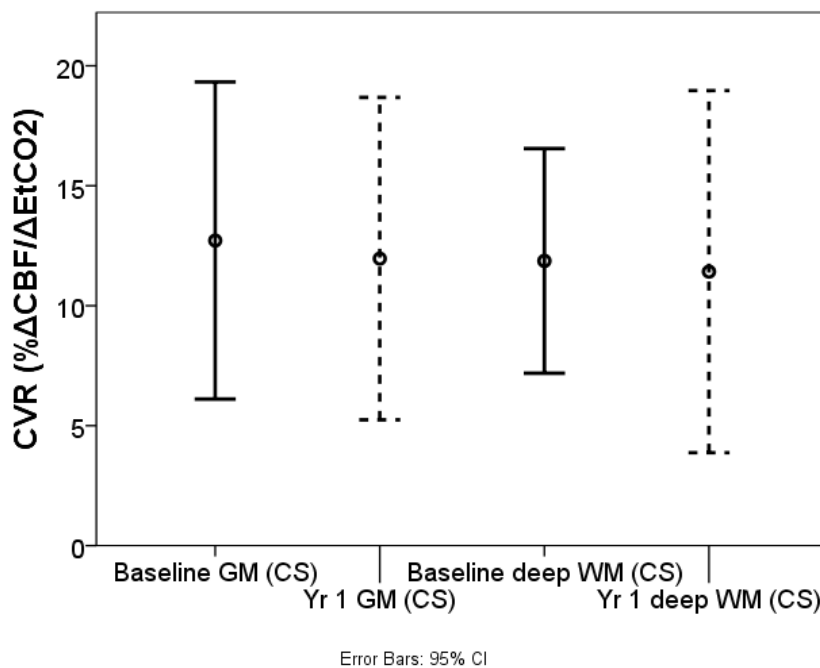


Figure 6-8 Cerebrovascular reactivity at baseline and year 1.

6.3.4 TCD – MFV and CVR

2 patients had one probable ACA insonated instead of MCA so these vessels were not included in mean MFV at year 1. Mean MFV showed a statistically significant paired sample correlation ($n = 19$, correlation = 0.620, $p = 0.005$). There was no difference in average MFV between baseline and year 1 (baseline 42 (10) v year 1 43 (12); $p = 0.536$, Related Samples Wilcoxon Signed Rank test).

Baseline and year 1 TCD_{CVR} were correlated (0.474, $p = 0.047$; Figure 6-9). There was no difference between TCD_{CVR} at baseline and year 1 (baseline 17 (10), year 1 17 (11); $p = 0.889$). Age correlated with year 1 MFV ($n = 19$; $r_s = -0.457$, $p = 0.049$).

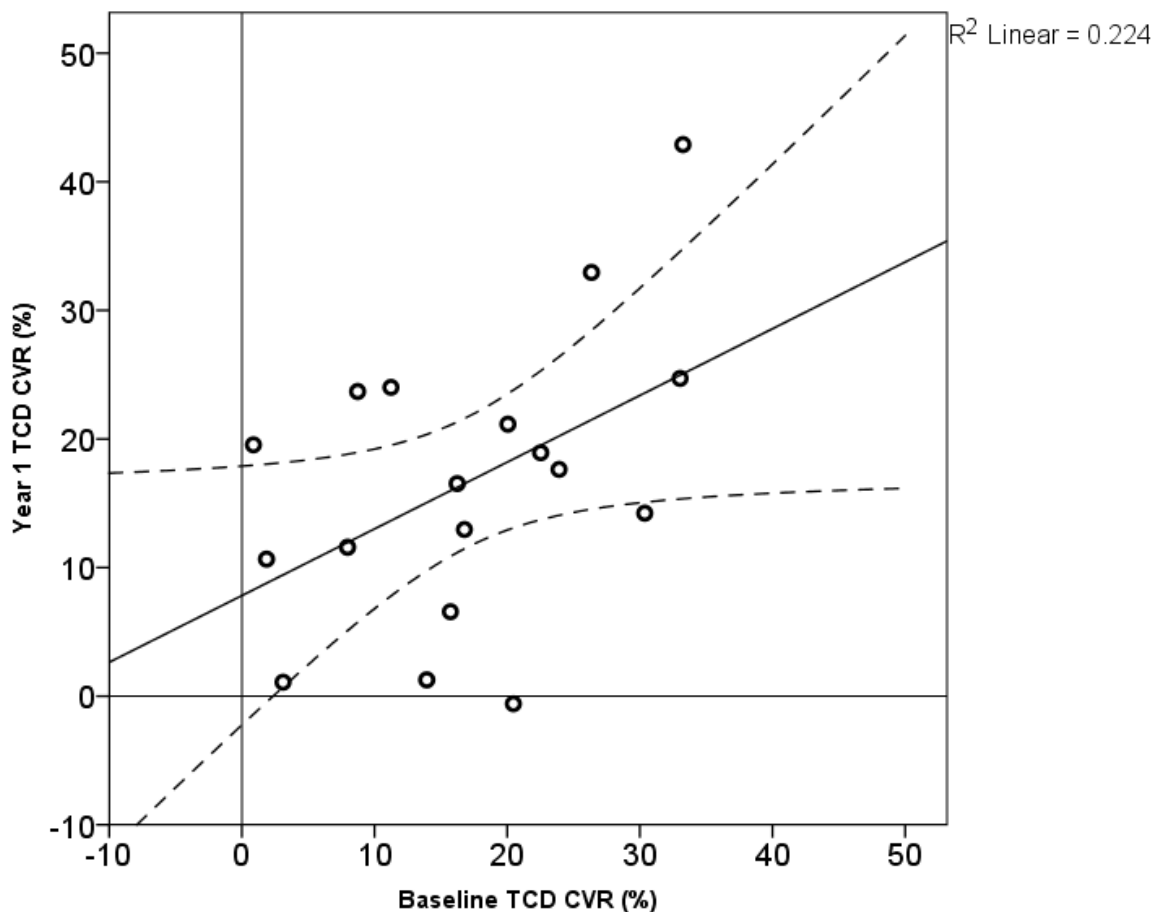


Figure 6-9 Transcranial Doppler ultrasound cerebrovascular reactivity baseline and year 1
Solid line represents line of best fit, and dashed lines 95% confidence interval of the mean.

6.3.5 Correlation between TCD and ASL reactivity

At baseline CVR_{TCD} correlated with CVR_{ASL} in grey matter ($n = 11$, $r_s = 0.682$, $p = 0.021$) and to $\% \Delta CBF$ ($n = 16$, $r_s = 0.979$, $p < 0.001$). However at year 1, this relationship was not seen with either CVR_{ASL} ($n = 12$, $r_s = -0.091$, $p = 0.779$) or $\% \Delta CBF$ ($n = 15$, $r_s = -0.118$, $p = 0.676$) (Figure 6 -10).

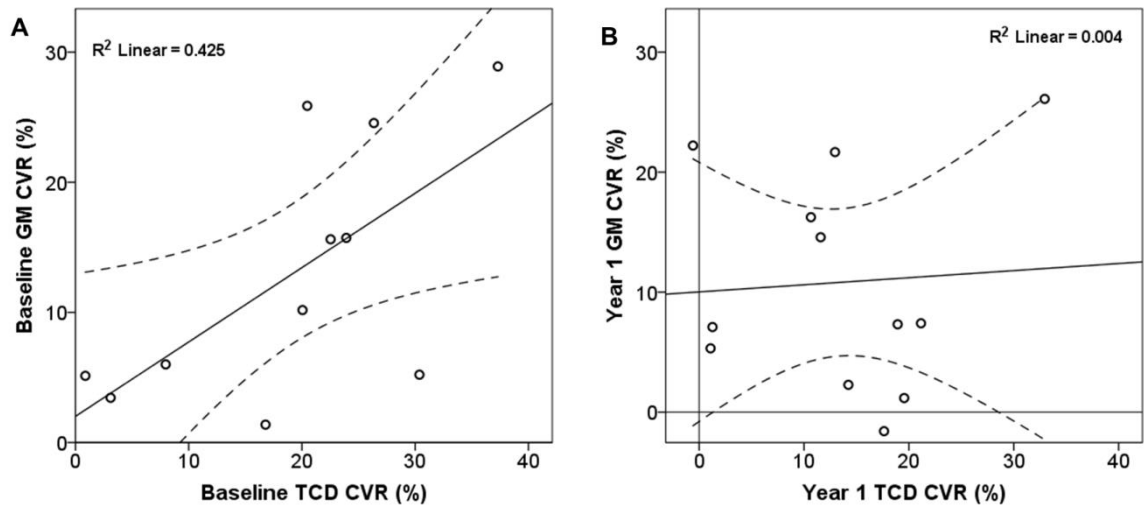


Figure 6-10 Cerebrovascular reactivity at baseline and year 1.

Whilst at baseline (A) ASL and TCD CVR was correlated, this relationship was not seen at year 1 (B). Solid line is line of best fit; dashed lines are 95% confidence interval of the mean.

6.4 Discussion

This study examined CBF, MFV and CVR with two methods at two time points in a cohort of CADASIL patients. Grey matter CBF declined by 6% over 12 months which was not explained by age, brain atrophy or CVR. Faster rates of decline were seen in patients with higher baseline CBF. CBF between baseline and year 1 was correlated despite the overall decline. MFV and CVR_{TCD} correlated at baseline and year 1, but did not change over a one year period.

Decline in CBF of 6% over 12 months in CADASIL patients far exceeds the values stated for normal aging of 0.45% per annum (Leenders et al., 1990). In some respects this value seems high, and further longitudinal assessment will be needed. Decline in CBF seen with normal aging is partly explained by thinning of the brain cortex, as CSF voxels contaminate the grey matter (Firbank et al., 2011). As individual masks were created at baseline and year 1, this is unlikely

to have had an effect in this experiment. Whilst brain atrophy in CADASIL exceeds that of healthy individuals (Peters et al., 2006), it did not correlate to change in CBF, so does not explain the change alone. Decline in individual patients with CADASIL has not previously been demonstrated, although hypoperfusion with worsening disease severity has been described (Chabriat et al., 1995).

No gender difference was seen in CBF values at either time point. In healthy individuals CBF is higher in women than men by around 10ml/100g/min in grey matter (Parkes et al., 2004). In this cohort this lack of a difference may be explained partly by the fact women were slightly older than the men (52 years ± 10 v 48 years ± 12).

One finding of interest is that rates of decline in GM were higher in those with higher baseline CBF. This may reflect the theory that presymptomatic patients may have higher than normal cortical GM blood flow (Tuominen et al., 2004), which may reflect an attempt to compensate for abnormal small vessel function with increased flow rates (Østergaard et al., 2015). At some point this compensation may fail and lead to more dramatic drops in CBF. Indeed 3 out of the 4 patients with the lowest CBF actually showed an increase in CBF between baseline and year 1 of up to 10%, which may reflect a degree of inter-individual variability.

In order to enhance repeatability patients were asked to refrain from smoking or drinking caffeine prior to testing. This request was generally, although not always followed, which may reflect the cognitive problems some of these patients have. However both TCD and ASL MRI took place at least 60 minutes after the visit began, so no patient had taken caffeine or a cigarette immediately before testing. I aimed to undertake testing at the same time of day at baseline and year 1. Exact timing of experiments was not always possible, usually due to patients work or childcare commitments.

ASL can be used to identify regional differences in CBF in CADASIL patients. However ASL has disadvantages. Poor spatial resolution means alignment is difficult, and small errors in alignment may produce changes in CBF values, particularly in ROI analysis as the ROI is much smaller than in masks. Given the

lack of CVR_{ASL} repeatability in individual ROI at one time point, use of small ROI may have limited utility for CVR measurements.

White matter is the area which is thought to be most abnormal in CADASIL, but is also the most difficult to measure with ASL (van Gelderen et al., 2008). White matter signal is only just above background signal because arterial transit time is longer and CBF is lower. This can make it difficult to detect hypoperfusion in white matter (van Gelderen et al., 2008). Further division into NAWM and WMH may be problematic as WMH tend to be deeper and therefore have lower flow and less GM contamination than NAWM. This could lead to the potentially false conclusion that WMH have reduced flow due to being hyperintense, rather than it being the most “at risk” tissue. Some authors have however suggested the use of white matter as a reference value, and use of grey matter/white matter ratios. Mutsaerts and colleagues suggested using eroded white matter masks avoided grey matter contamination, and as the signal in these maps was different to that outside the brain, it suggested the presence of white matter signal (Mutsaerts et al., 2014). In this study using an eroded “deep white matter” mask, which included both normal appearing and hyperintense white matter, allowed us to demonstrate a decline in CBF over 1 year of 8% (SD 13%). Dynamic contrast MRI has shown basal perfusion is reduced in white matter hyperintensities (van den Boom et al., 2003a, Chabriat et al., 2000).

Transcranial Doppler ultrasound also showed significant correlation between baseline and year 1. The difficulties of ensuring repeatability of baseline MFV are that different parts of the vessel (e.g. M1 or M2) may have been selected at baseline and year 1. Keeping a more standard depth could have enhanced the chance of identifying the same vessel each year. Average MFV was around 42m/s, which is lower than values stated as normal in the literature: for healthy individuals between 50 and 59, average MFV was 51 ± 9.7 m/s (Ringelstein et al., 1990). This finding, along with the negative correlation with age, is in keeping with previous studies in CADASIL using TCD (Pfefferkorn et al., 2001).

CVR correlation at baseline and year 1 was better with TCD. This may reflect that more data was available for TCD repeatability ($n = 17$) compared to ASL ($n = 11$) probably due to better facemask fit (use of an anaesthetic mask), with higher CO_2 delivery and more accurate gas monitoring. This results in more

accurate adjustment of CVR. In the MRI scanner, a standard gas mask with sealed ports and with fit enhanced with swabs and tape was used, as the anaesthetic mask was too rigid to fit in the confines of the head coil. Some MRI scanners with more open head coils will be more amenable to improved mask fit but may allow more patient movement. Alternatively a respiratory challenge method like Respiract®, which relies less on mask fit and more on breath-by-breath analysis, could be used (Mandell et al., 2011). This equipment is not widely available however. There is a concern that unless the reliability of CVR measurements can be improved, it is not currently useful as a biomarker for this disease. This is particularly the case when any trials are likely to still be reliant on small numbers, and therefore data dropout is concerning.

At baseline, CVR using ASL and TCD correlated but this relationship could not be demonstrated at year 1. This may reflect the effect of outliers on small study numbers or the loss of ASL data due to smaller subject numbers.

This study demonstrates the problem of using change in CBF without correcting for change in EtCO₂. %ΔCBF actually non-significantly increased between baseline and year 1. This is probably due to the fact investigators were more skilled in fitting the mask, which may have led to either more accurate gas recording, or better delivery of gas. Failing to correct %ΔCBF by ΔEtCO₂ therefore leads to inaccuracies between time points.

Healthy age matched controls using the same scanner and same CVR technique is not available. However as ASL is quantifiable, these values should be comparable to those in the literature obtained in other ASL experiments.

As mentioned in Chapter 5, this study did not include control subjects for these experiments using either the same scanner or the same CVR technique. This is a limitation to this study as it does not allow us to directly compare the changes to those seen with healthy individuals. Scanner drift, which is change occurring over time in the superconducting magnets field, can cause differences in the acquired signal over time, and thus potentially the recorded CBF. Including healthy controls, or using specific quality control procedures on the scanner, limits our ability to adjust for this.

Also images were not assessed for quality by an independent assessor, and no additional corrections for movement artefact were made (out with that made by the MRI scanner programme itself). Asymmetric coil sensitivity due to poor head positioning was inspected for by examining the images but again by the author alone. To improve the robustness of these results, independent analysis of all scans by a researcher blinded to all other clinical information and study hypothesis, would be best practice.

Whilst CBF measured by ASL is thought to have reasonable repeatability between sessions in individuals, this is not known for CVR. It would have been useful to re-test several individuals. This could either be done by doing ASL at the beginning of the session and the end, or repeating all scans the following week. This would have allowed assessment of the test-retest reliability of a number of scans, but most importantly ASL and CBF, which may well be very variable. We do not know if CADASIL patients show more variability in resting CBF than healthy individuals for example. Repeating all sequences after a short time, would allow assessment of whether measures such as atrophy and SH volume are also stable when using this combination of MRI scanner, sequence and analysis techniques.

The study also uses a number of statistical tests and multiple comparisons. Use of Bonferroni correction may have been appropriate. Adjustment for age and gender for example were considered, but small numbers of subjects prohibited these adjustments.

6.5 Conclusion

ASL can be used in CADASIL patients to identify a significant decline in CBF over one year. This appears to be higher than normal rates of decline in the literature. CVR measured with ASL poorly correlates between baseline and year 1 suggesting problems with methodology. TCD CVR however shows correlation over 1 year, suggesting a role in CVR monitoring. However, this may be due to more effective gas delivery and monitoring allowing the inclusion of higher numbers of patients.

Chapter 7 – Progression of vascular, radiological and clinical markers in CADASIL over 1 year

7.1 Introduction

CADASIL is a disease that can result in disability in young adults, or be detected radiologically in asymptomatic elderly patients. This variability makes prognostication for patients difficult, and exacerbates problems in using clinical endpoints in any potential therapeutic intervention. Chapter 5 identified vascular and radiological correlates of disease severity in CADASIL, but for these to function as a biomarker, they must correlate over time.

The ideal characteristics of biomarkers in central nervous system disease have been stated as (Jain, 2013):

- non-invasively (or minimally invasively) detectable in living subjects;
- reproducible;
- positively correlated to the cause or progression of the disease.

Over a short time period, in small numbers of patients, change in disability measures or number of incident strokes, are unlikely to give sufficient change to allow comparison to potential biomarkers. Cognitive impairment however can be detected early in CADASIL, even prior to ischaemic manifestations (Buffon et al., 2006). Standardised tests are available for its assessment, and impairment of cognition is a major factor, along with depression, in the patient's quality of life. It also represents cumulative damage to the brain.

In other neurodegenerative conditions, such as cerebral amyloid angiopathy, altered vascular reactivity to visual stimulation has been demonstrated and shown to be partly reversible. This suggesting its possible role as a potential biomarker, with the advantage of having a mechanistic role in disease development (Greenberg et al., 2014).

The association of peripheral and cerebral vasoreactivity, along with CIMT and PWV with radiological measures of disease, may suggest a role for these as biomarkers. This was assessed over one year in the cohort of CADASIL patients.

The main hypothesis is that vasoreactivity at baseline will predict changes in neuropsychological markers of disease.

Therefore the aims of this chapter are to:

- 1) examine which baseline measures predict changes in radiological markers of disease;
- 2) examine which baseline measures predict changes in neuropsychological markers of disease.

7.2 Methods

7.2.1 Study cohort

Subjects recruited in this study were recruited as described in Chapter 2. Data include baseline and year 1 measurements.

7.2.2 Experimental procedures

Procedures including TCD, MRI, vascular studies and neuropsychology were undertaken as described in Chapters 2 and 5.

7.2.3 Neuropsychological assessment and analysis

Methods for calculation of cognitive measures are detailed in Chapter 5. Processing speed and executive function was again used as the key outcome variables.

Differences in baseline and year 1 in these variables were dichotomised by whether they improved or declined over one year.

7.2.4 MRI analysis

7.2.4.1 Intracranial cavity volume

Intracranial cavity (ICC) volume was calculated using brain extraction tool (f 0.5) on the SWI image at baseline and year 1. A binary ICC mask was created and the voxels counted. ICC volume between baseline and year 1 was highly correlated ($n = 22$, Pearson = 0.993, $p < 0.001$). 3 scans had different slice thickness at baseline from year 1. When these patients were excluded correlation improved ($n = 19$, Pearson = 0.996, $p = < 0.001$; Figure 7-1). ICC measurements were therefore robust. Year 1 ICC volume was used to normalise baseline and year 1 lacune and SH volumes. In one patient, with a large head size, there was a small amount of missing cerebellum at year 1, so his baseline ICC volume was used.

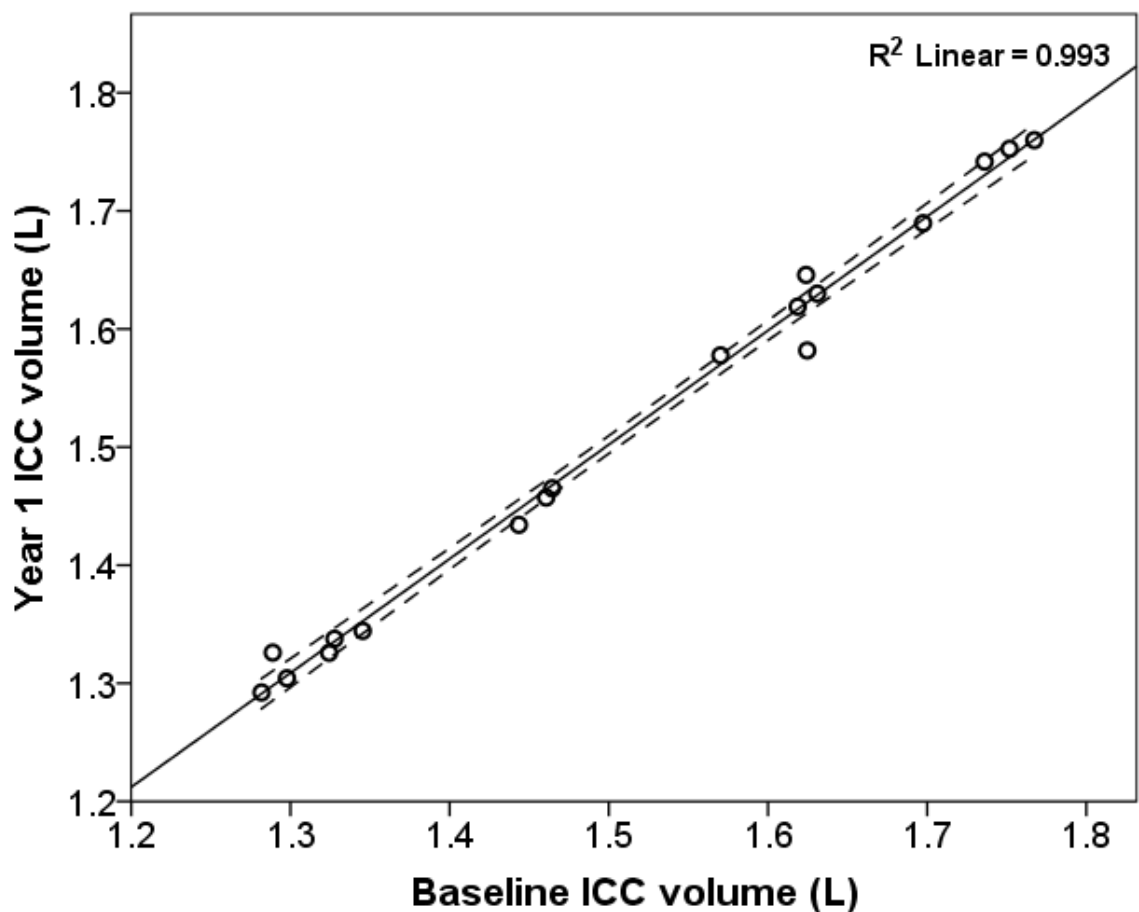


Figure 7-1 Intracranial cavity volume at baseline and year 1

7.2.4.2 Percentage brain volume change (PBVC)

Percentage brain volume change (PBVC) between baseline and year 1 was estimated on T1 3D images using SIENA (Smith, 2002), part of FSL (Smith et al., 2004).

7.2.4.3 New lacunes

Number of lacunes and lacune volume were calculated at baseline, and normalised to the new ICC (NLV, %). In order to avoid human error in recounting lacunes that were already present, a method was designed to identify new lacunes. SWI images were registered to T1, skull stripped, and then used to mask the T1 image to create a brain image (using FSL tools). This was done at baseline and year 1. The baseline brain image was registered to Montreal Neurological Institute 1mm brain template with 6 degrees of freedom. The brain year 1 image was then registered to this image with 12 degrees of freedom. The images were then bias corrected. The MNI registered maps were subtracted from each other to create a T1 difference map (see Figure 7-2).

This image was reviewed at intensities -500 to 500 and -1000 to 1000 to identify new areas of abnormality. Reference was then made to original scans to ensure the new abnormality was a lacune and not a new perivascular space or hyperintensity. Images were reviewed twice. Once lacunes were identified on the intensity map, the equivalent new lacune on the original T1 image was identified and outlined with seed-based thresholding as per baseline to calculate the volume. This was added to baseline lacune volume, and normalised to the ICC (NLV, %).

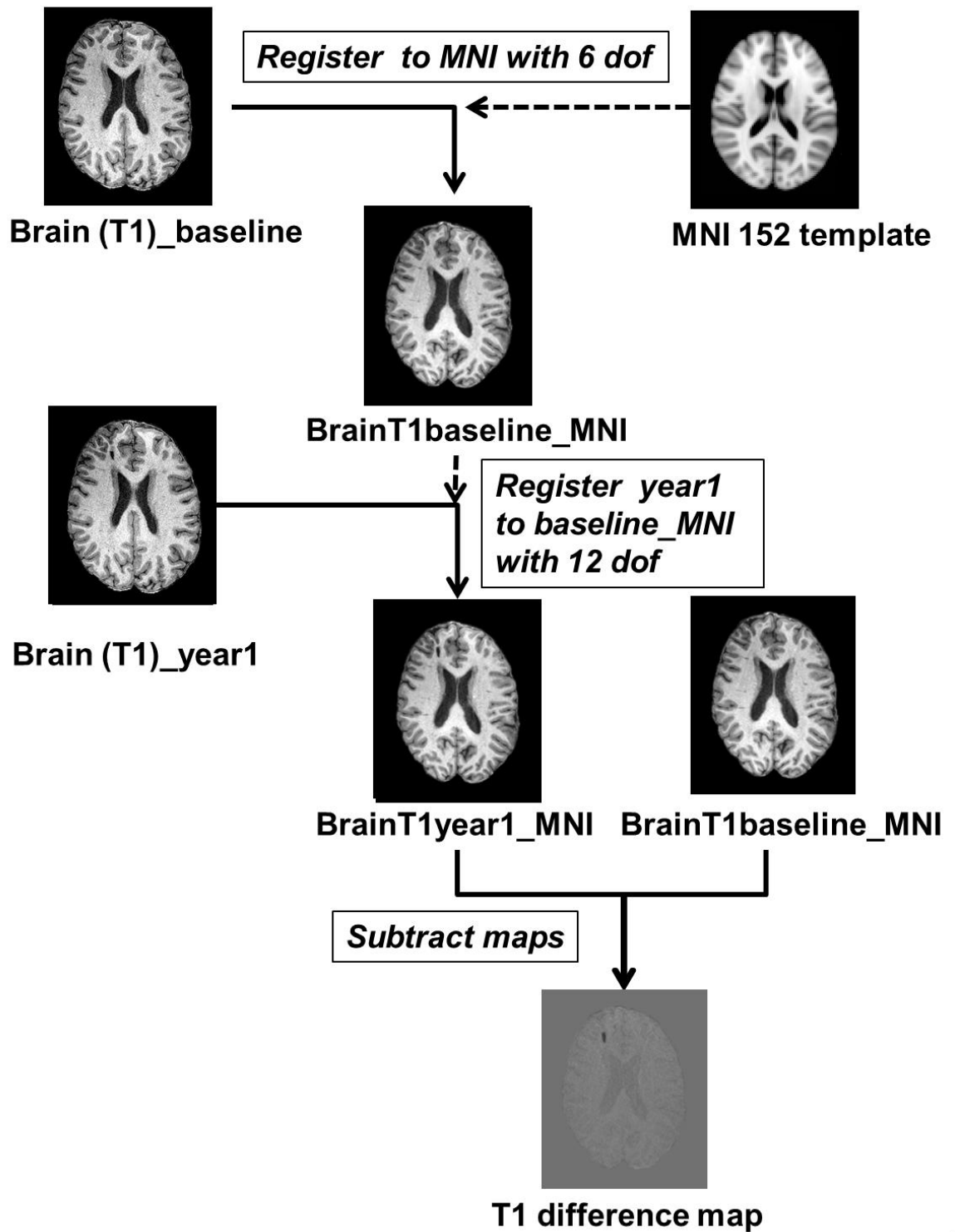


Figure 7-2 Creation of T1 difference maps for new lacune identification
MNI = Montreal Neurological Institute, dof = degrees of freedom

7.2.4.4 Automated SH volume calculation

5 year 1 images were analysed with the baseline method to calculate SH volume, but varying image intensities meant the results were inconsistent. It was therefore decided to use an automated method to avoid error induced by manual correction, and to correct for changes in image intensity.

SH volumes created by thresholding at baseline using the mode of the parenchymal image (see Chapter 2) were affine registered to Montreal Neurological Institute (MNI) standard space to generate a probability map of SH. This map was used in combination with voxel location and intensity on FLAIR to automatically generate SH volumes at baseline and follow-up (coding for this procedure was written by Dr D. Dickie). Once the SH map was created it was then viewed in MRICron whilst overlaid on the FLAIR. The ideal threshold for best delineation of SH was identified and recorded. The SH mask was thresholded to this using FSL maths (ref). The volume of this mask was then calculated and normalised to ICC (NSH, %).

The correlation between the threshold-derived and manually corrected volumes (Chapter 2) and automatically generated volumes was high ($r = 0.952$; $p < 0.001$; Figure 7-3). Example images are shown in Figure 7-4.

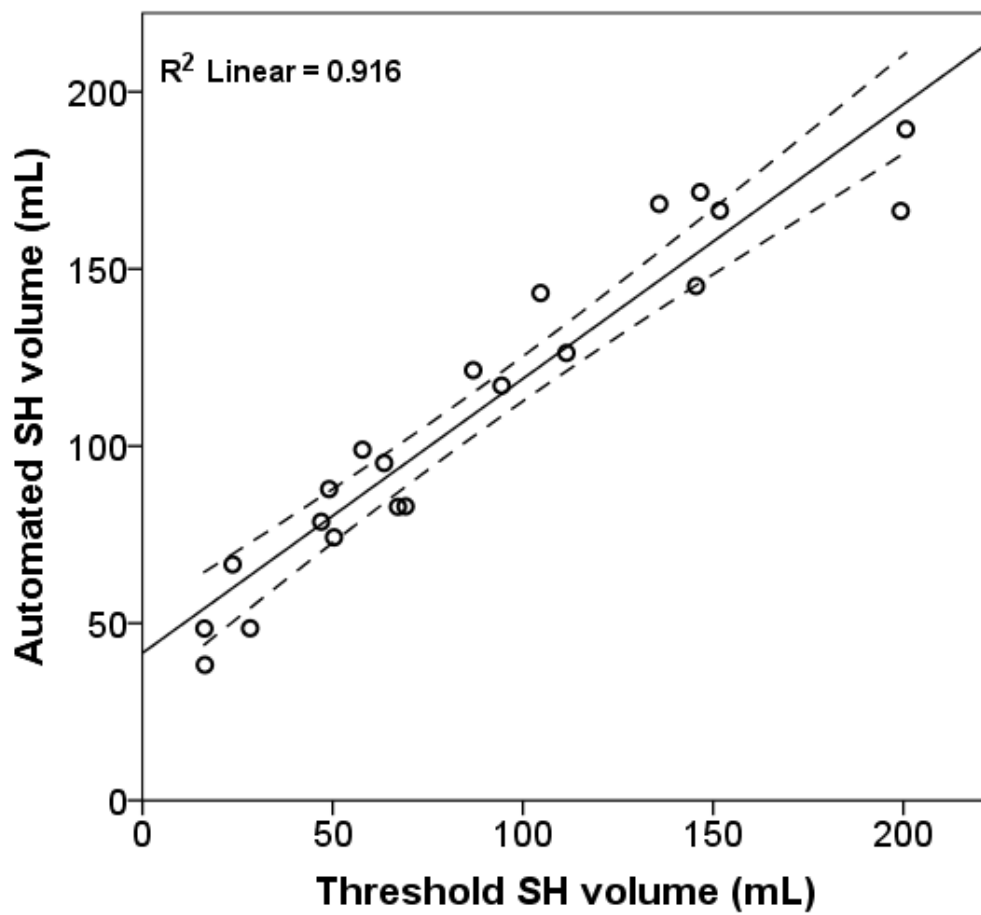


Figure 7-3 Threshold SH volume compared to automated method

The thresholded SH volumes created at baseline were highly correlated to those created by the automated method.

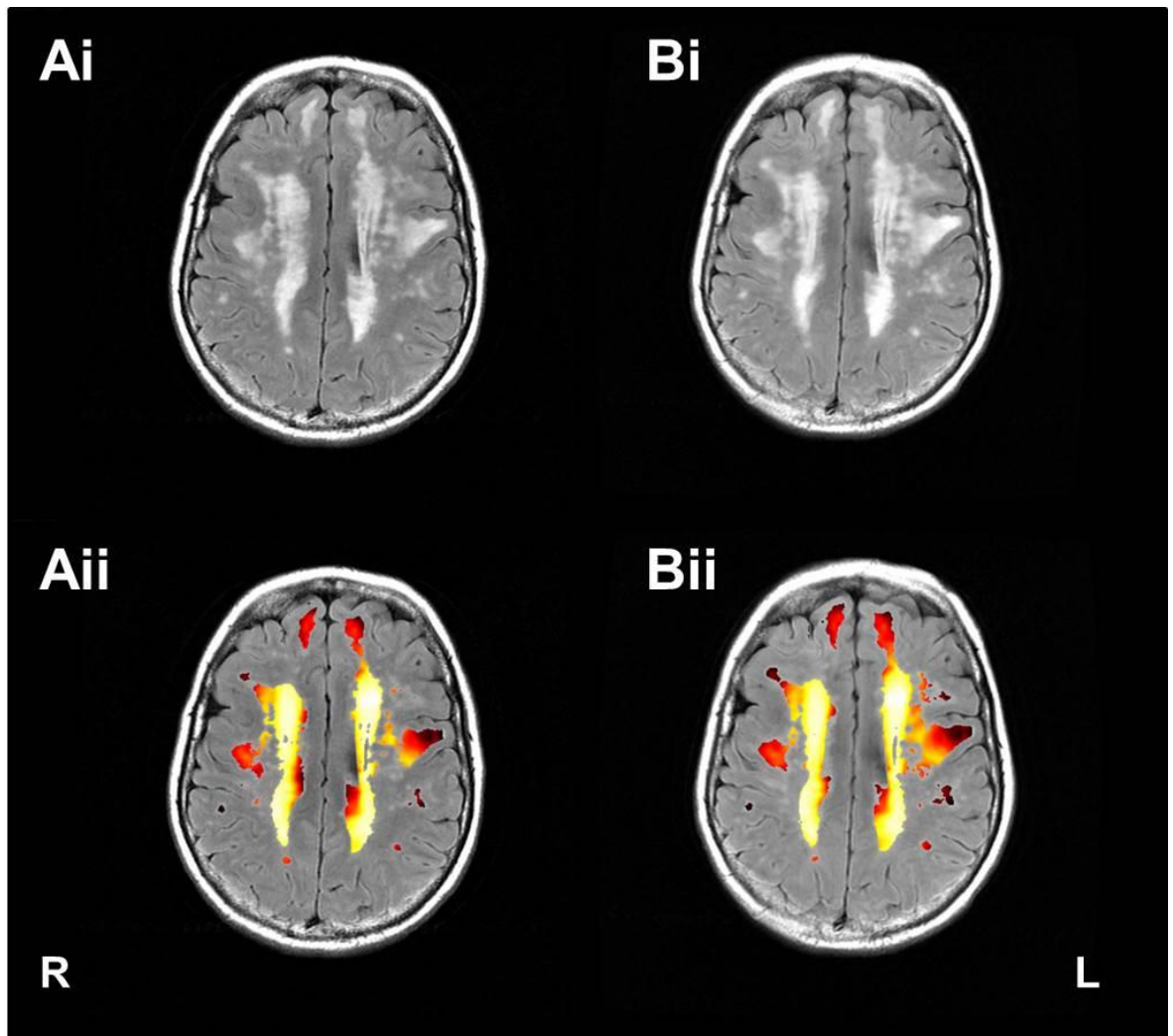


Figure 7-4 Automated subcortical hyperintensity segmentation of baseline and year 1 FLAIR images

Year 1 FLAIR images (Bi) were co-registered to baseline FLAIR (Ai). Overlaid SH masks are shown at a threshold of 0.05. In this subject, at baseline SH volume was 126ml and 143ml at Year 1, an increase of 17ml over 1 year. Areas of previously discontinuous SH at baseline (Aii) have merged to become continuous at Year 1 particularly in the left frontal lobe (Bii).

7.2.4.5 ASL

Masks of whole brain, grey matter, and white matter were created as per Chapter 5. Pixels from SH masks created above were removed from the grey and white matter images. In this chapter only GM mask was used.

Deep white matter masks were created as described in Chapter 6.

Baseline and year 1 masks were applied to their appropriate CBF map and CBF, $\% \Delta \text{CBF}$ and CVR calculated.

7.2.4.6 MRI marker stratification

For analysis, MRI markers were dichotomised either by their median (NLV, NSH, PCBV) or;

- no new lacunes or new lacunes;
- no new microbleeds or new microbleeds.

7.2.5 Baseline predictors

The following factors at baseline were investigated as potential predictors of radiological or neuropsychological decline: age, gender, PWV, CIMT, RHI, FMD, GM CVR, deep WM CVR, and CBF.

7.2.6 Statistics

Statistical analysis was performed with IBM SPSS Version 21 (IBM Corp, Armonk, NY, USA). Results are expressed as mean (SD) unless otherwise stated. Normality was tested with the Shapiro-Wilk test. Continuous variables were compared to by Spearman's rank correlation.

For categorical outcome variables, normally distributed continuous variables were tested with independent t-tests, and non-normally distributed continuous variables with independent samples Mann-Whitney U tests. For the effect of gender and smoking, a Chi-squared test was used.

Significance was set at $p < 0.05$.

7.3 Results

7.3.1 Patient characteristics

All 22 patients were followed up at Year 1 and underwent MRI, neuropsychological testing and vascular tests. 3 patients did not undergo TCD (1

unable to find MCA, 2 declined due to the length of the visit). Vascular parameters at baseline and year 1 are shown in Table 7-1. SBP and BMI increased over 1 year but other parameters did not change.

The time between baseline and year 1 visits was: MRI 350 (25) days; vascular visit 404 (29) days; neuropsychology 398 (96) days.

3 patients had a new stroke or TIA, 3 self-reported new depression and 7 reported worsening cognition. Despite this there was no change in overall HADS depression or anxiety scores. 3 patients had a worsening of their mRS. Due to the small numbers affected by new clinical outcomes at year 1, these were not compared to baseline measures.

Table 7-1 Clinical and vascular measures at baseline and year 1

	Baseline	Year 1	P value
mRS, median (range), n	0 (0-3), 22	0 (0-4), 22	
NIHSS, median (range), n	0 (0-3), 22	0 (0-4), 22	
HADS anxiety, mean (SD), n	8 (5), 21	8 (5), 19	0.554*
HADS depression, mean (SD), n	6 (5)	6 (6)	0.874*
SBP mmHg, mean (SD), n	120 (11), 22	125 (12), 22	0.023
BMI kg/m ² , mean (SD), n	29 (7), 22	29 (7), 21	0.043
AI@75 bpm, mean (SD), n	17 (13), 22	20 (15), 21	0.164*
PWV m/s, mean (SD), n,	7.6 (1.1), 21	7.6 (1.1), 19	0.783
CIMT mm, mean (SD), n	0.64 (0.1), 21	0.64 (0.1), 19	0.190
RHI %, mean (SD), n	2.1 (0.7), 20	2.0 (0.5), 20	0.114
FMD %, mean (SD), n	4.1 (1.9), 18	5.0 (2.6), 17	0.403

*Non-parametric

7.3.2 Radiological change over 1 year

7.3.2.1 Normalised subcortical hyperintensity volume (NSH)

Baseline and year 1 NSH were correlated (n = 21, paired sample correlation = 0.990, p <0.001; Figure 7-5) with an increase of 0.82 % (SD 0.45%, median 0.75%; p = <0.001). 1 patient, who had the highest baseline NSH, showed a reduction in NSH. The probability maps for baseline and year 1 are shown in Figure 7-6.

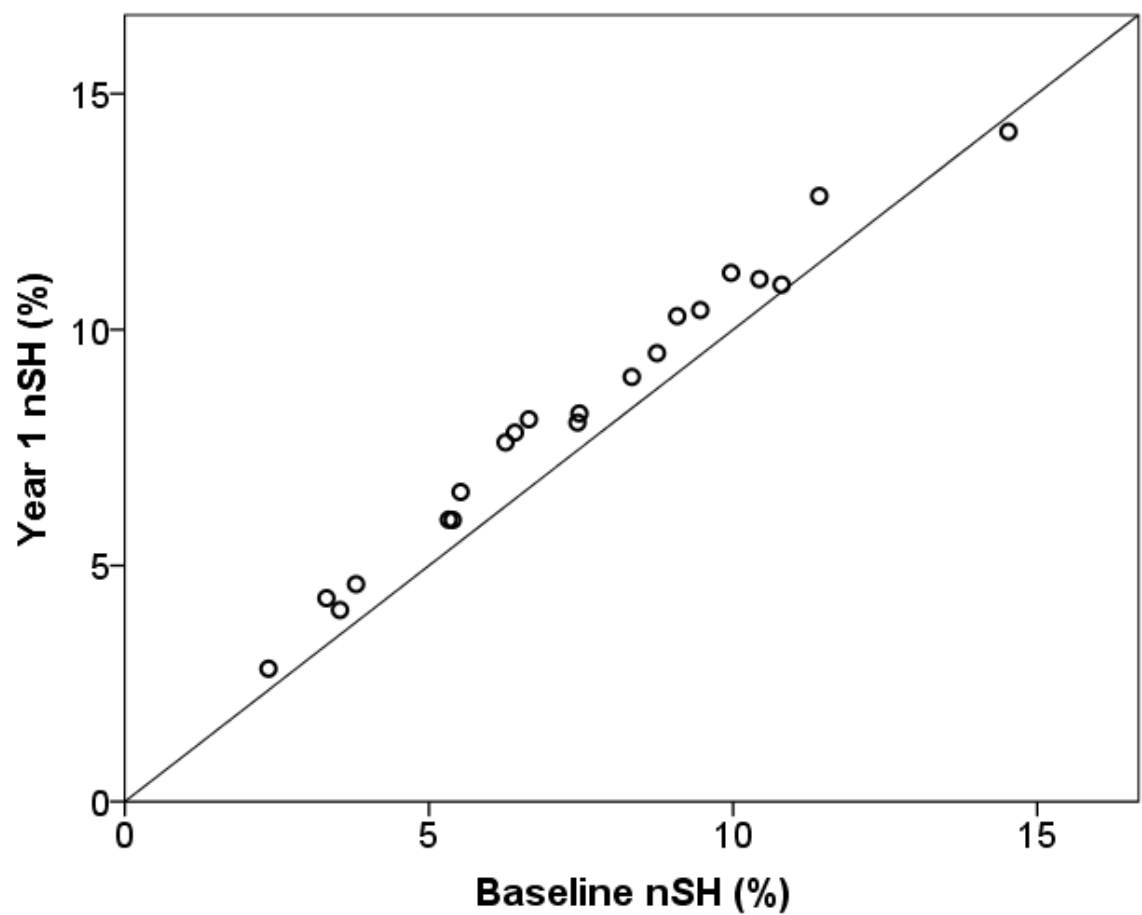


Figure 7-5 Baseline versus Year 1 normalised subcortical hyperintensities
20 patients showed an increase in NSH, 1 a decrease (baseline data missing for one). The solid line represents the reference line $y = x$.

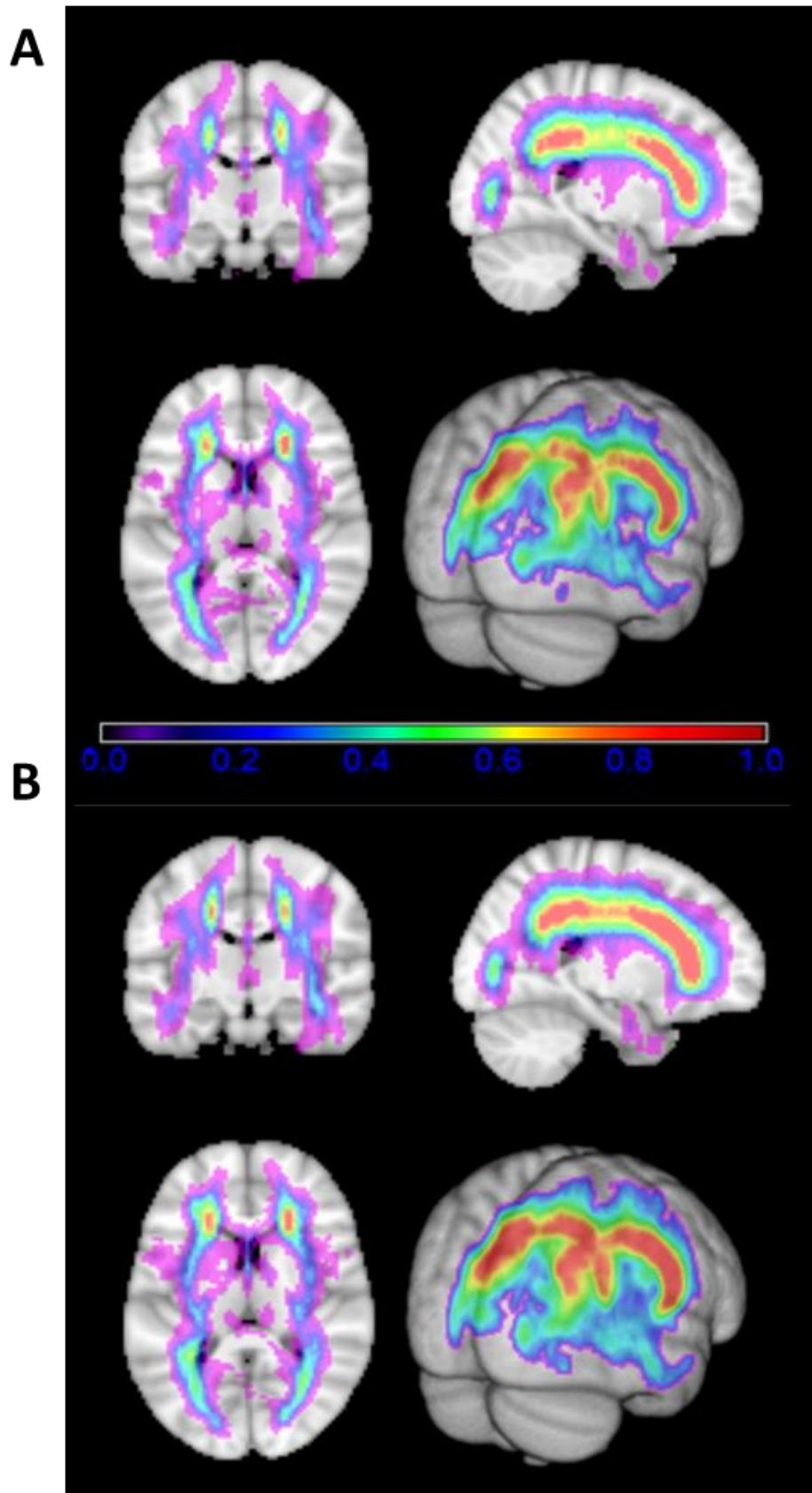


Figure 7-6 Subcortical hyperintensity probability maps
(A) Baseline and (B) year 1, showing increased probability of periventricular hyperintensities at year 1. Hyperintensities involving the anterior temporal lobes can be seen at both time points.

7.3.2.2 Percentage brain volume change (PBVC)

PBVC was -0.44% (0.56; median -0.45, range -1.84 to 1.08). 3 patients showed increase in PBVC and 18 a decrease (1 missing baseline data). Age ($n = 21$, $r_s = -0.276$, $p = 0.225$) and gender (male -0.42% (0.36) v female -0.46% (0.72); $p = 0.896$) did not affect PBVC (Figure 7-7).

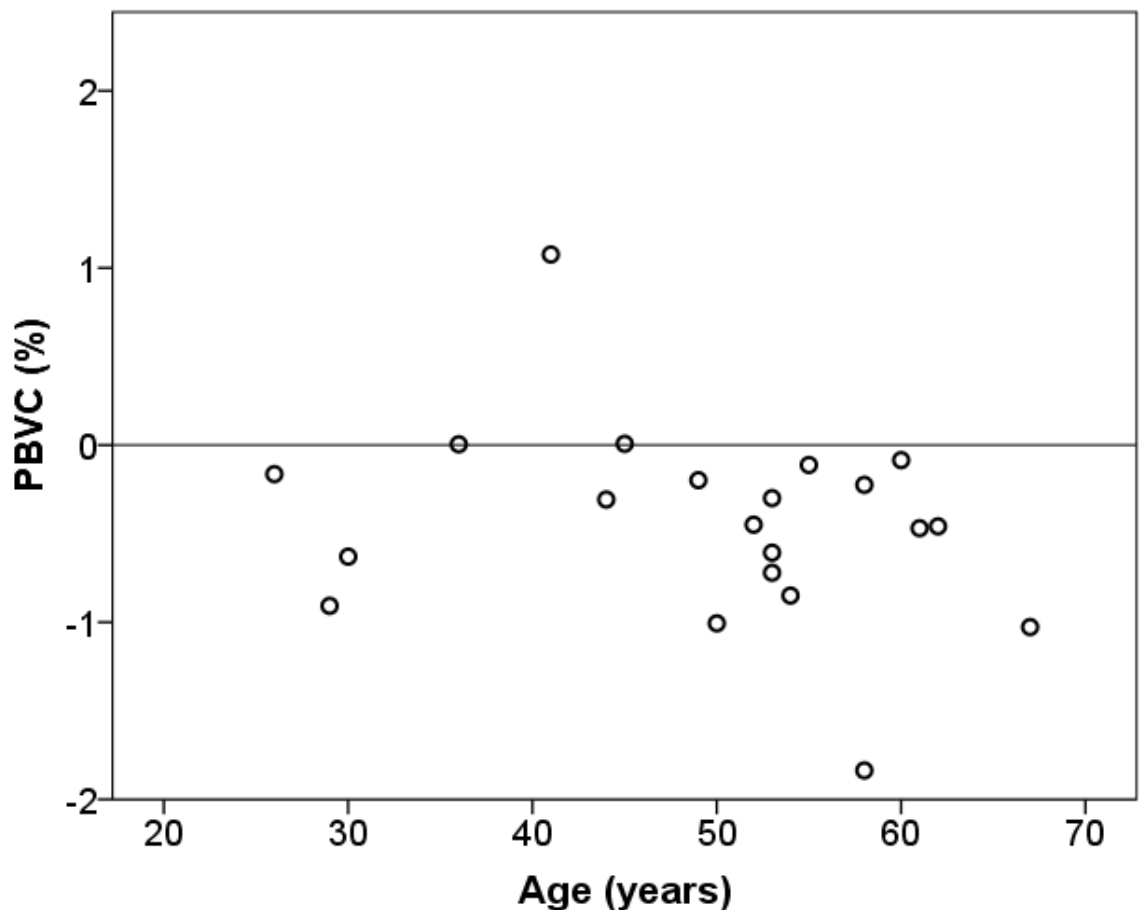


Figure 7-7 Percentage brain volume change (PBVC) over 1 year compared to age

7.3.2.3 Lacune number and volume

11 patients had new lacunes on MRI after 1 year (median 1, range 0 - 7; $p = 0.002$). Examples of lacune difference maps are shown in Figure 7-8. 10 did not have new lacunes, and 1 did not have a scan at baseline to compare. NLV increased by median 0.003% (range 0 - 0.02%; $p = 0.003$). NLV was not dichotomised for testing as it divided subjects the same as lacune number.

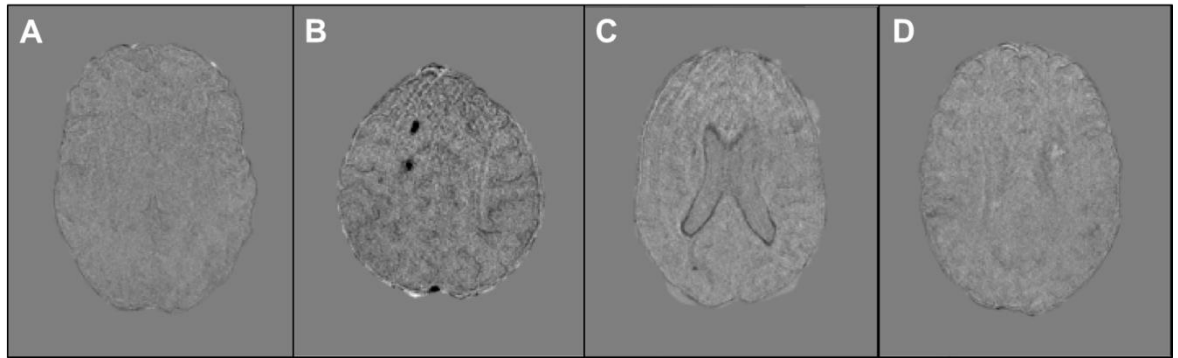


Figure 7-8 T1 difference maps

(A) A difference map with no change between baseline and year 1. (B) New right centrum semiovale lacunes (black areas). (C) Central atrophy shown by increased ventricle size (black rim surrounding ventricles). (D) Lacunes can shrink: a lacune lateral to the left ventricle is shown as white. Whilst present on both images, the lacune at year 1 appeared smaller than at baseline.

7.3.2.4 Microbleed number

7 out of 20 patients had new microbleeds, median 1 (range 0 - 6, $n = 20$; $p = 0.103$). 2 patients had different slice thickness at baseline and year 1 so comparison could not be made.

7.3.3 Change in processing speed and executive function.

Overall there was no significant change over one year in processing speed or executive function. Individual values can be seen in Figure 7 - 9.

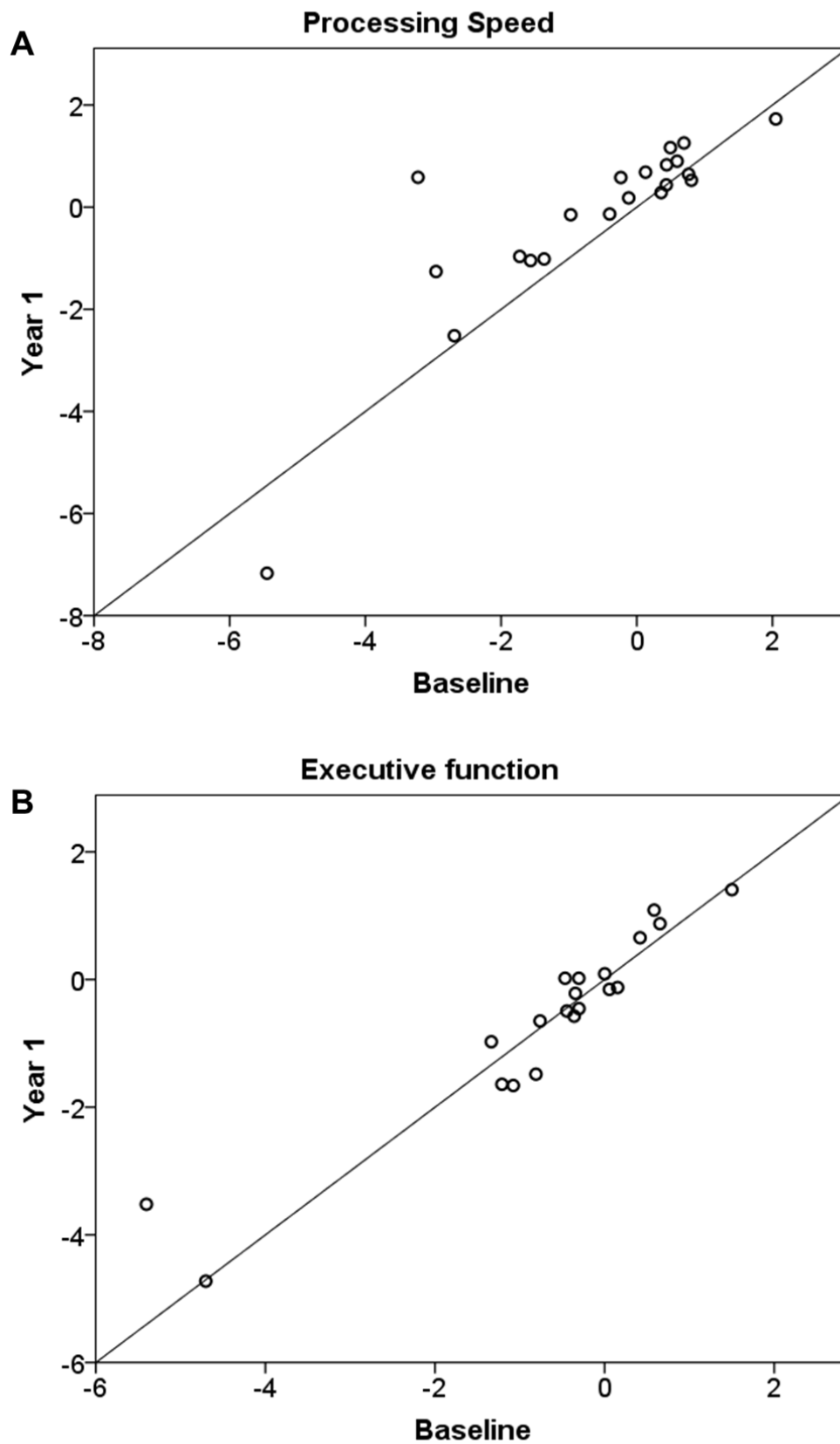


Figure 7-9 Neuropsychological measures
(A) Processing speed and (B) executive function at baseline and year 1. The solid line represents $x = y$.

7.3.4 Predictors of change in MRI markers

No baseline vascular marker significantly predicted change in any MRI marker. Smoking and gender did not have an effect. Patients with new lacunes had higher baseline CIMT than those without new lacunes, but this did not reach significance (no new lacunes 0.59 (0.99); new lacunes 0.68 (0.86); $p = 0.063$).

7.3.5 Vascular predictors of neuropsychological decline

No baseline vascular marker significantly predicted change in processing speed. Patients with deterioration in processing speed had a lower baseline RHI ($n = 6$, 2.4 (0.7)) than those with improved speed ($n = 13$, 1.8 (0.4); $p = 0.087$) but this did not reach significance (Figure 7-10A).

No baseline vascular marker significantly predicted change in executive function parameter over one year. Patients with deterioration in executive function had a lower baseline FMD ($n = 7$, 3.2 (1.8)) than those with improved function ($n = 10$, 14.8 (1.8); $p = 0.070$) but this did not reach significance (Figure 7-10B).

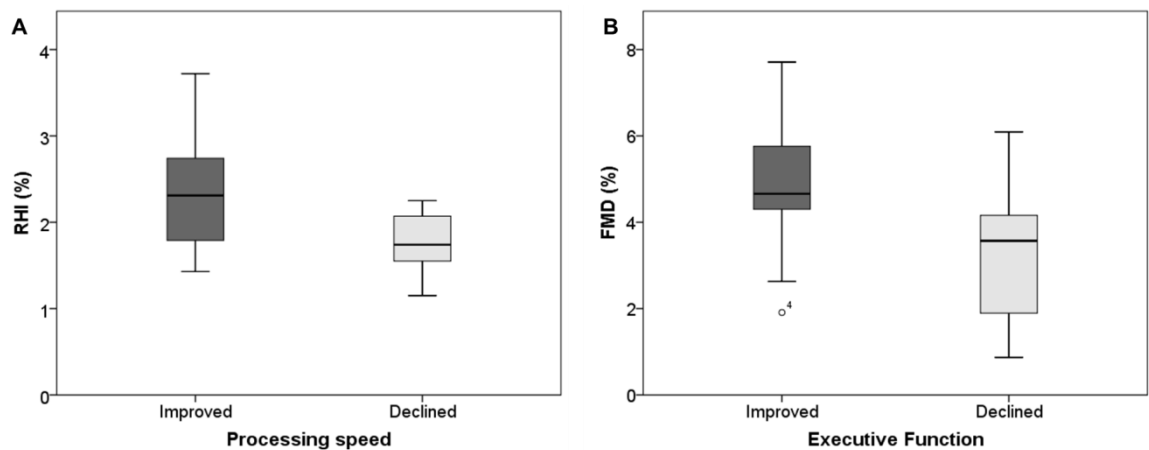


Figure 7-10 Peripheral vasoreactivity and neuropsychological decline

Whilst neither showed a significant relationship, (A) FMD was lower in patients with poorer processing speed over 1 year, and (B) RHI in those with a decline in executive function.

7.3.6 Radiological predictors of neuropsychological decline

Patients with a decline in executive function had lower NBV at baseline. Patients with a decline in processing speed had higher NSH at baseline (see Table 7-2).

Table 7-2 MRI markers and prediction of neuropsychological decline

	Processing speed			Executive function		
	Improved	Declined	p value	Improved	Declined	p value
	Median (IQR)			Median (IQR)		
NLV, %	0.02 (0.04)	0.02 (0.05)	0.733	0.02 (0.04)	0.02 (0.05)	0.393
NSH, %	6.3 (4.4)	9.5 (5.8)	0.033	6.3 (4.9)	7.9 (4.5)	0.604
No. of microbleeds	0 (4)	1 (8)	0.391	0 (2)	3 (6.5)	0.113
No. of lacunes	4 (13)	9 (14)	0.659	2 (15)	7 (12)	0.243
NBV, L	1.57 (0.14)	1.50 (0.23)	1	1.59 (0.14)	1.49 (0.15)	0.013

7.4 Discussion

In this chapter, change in MRI parameters over 1 year has been demonstrated. NSH increased by 0.8%, brain volume decreased by 0.4% and a high number of patients had new lacunes and microbleeds. Vascular measures were not able to predict which patients showed these changes however. In patients with a decline in processing speed, NSH was higher at baseline, and in those with a decline in executive function, NBV was lower.

There was little change in clinical parameters over 1 year. Vascular parameters also showed little change although BMI and blood pressure did increase. Given what is known about the slow progression of CADASIL, these results are not surprising and highlight the need for biomarkers.

As seen in Figure 7-9, many patients showed minimal difference between the two time points. Practice effects, as well as that some patients found testing very tiring, may explain some of the variation. Dichotomising change in neuropsychological measures is a broad way of assessing change particularly when doing being “better” or “worse” may be minimal. Over a longer time period of 2 years, I would expect to see greater change in these variables, which will allow more detailed assessment of which factors relate to cognitive decline.

The mean rate of brain atrophy in this cohort was 0.44%. Peters and colleagues stated the annual rate of atrophy was 0.56%, significantly higher than healthy people of the same age (Peters, 2006). Atrophy is known to be associated with worse cognition in cross-sectional studies (Viswanathan et al., 2010). A recent large longitudinal study of 290 subjects has confirmed that baseline brain volume to be an important predictor of cognitive decline and clinical events (Chabriat et al., 2016). The results of this study relating to executive function, may be consistent with this, but require ongoing assessment over time given the small overall change over one year in cognition.

NSH was associated with a decline in processing speed. Whilst hyperintensities are known to have clinical implications in the general populations, their relevance to the development of disability or dementia in CADASIL remains controversial. Given the small change in processing speed, this result may well be relevant, and it is important to note that, whilst not statistically significant, the number of lacunes and microbleeds were also both higher in patients with declining cognitive functions. Thus further assessment of this is needed.

Difference maps for identification of lacunes has previously been used in CADASIL patients (Duering et al., 2013). This approach offers the advantage of removing some of the manual error that may be associated with re-counting and re-measuring lacunes at two different time points. As median increase in lacunes was only 1, even small errors in lacune identification could be significant. A 3D FLAIR image would have been preferable for identification of lacunes due to enhanced contrast between CSF and tissue, and this scan has been introduced into the final year of this study (Wardlaw et al., 2013).

The SH maps were created using an automated method which used the original maps created at baseline as a template. Its effectiveness at identifying SH is therefore based on the adequacy of the original maps. Whilst manual correction of the original maps was performed, it consisted only of removing cortical pixels or single pixels, rather than adding any missed areas of SH as I felt this would introduce error at later time points. Therefore some small areas which may appear hyperintense will have been missed by the threshold method. However they will have been missed at both time points when using the automated method so this is unlikely to be relevant. Registering year 1 images to baseline

does introduce interpolation error, and in preference both images should have been registered to a different space. This will be done when analysing the year 2 data. Identifying SH rather than WMH may have its drawbacks, as it will include grey matter and therefore may include areas of higher CBF, which may alter results.

Strengths of the study include 100% attendance at all study visits by patients, and image analysis techniques which are repeatable. I undertook all the vascular tests and administered all CO₂ challenges (MRI and TCD). Dr Cullen undertook all neuropsychological assessments. This gave consistency to the testing, although the technical ability in performing some of the assessments may have improved over time.

Limitations include the short period of follow up and the lack of analysis of the effect of drugs. Modelling of the effect of different variables is not possible with these small group numbers.

Use of an independent rater for several of the analyses including lacune identification may have been appropriate. Attempts were made to use automated methods where possible to avoid introducing bias, but as the author was not blinded to knowledge of the expected natural history of the disease, there may have been a tendency to over score radiological progression.

As stated in Chapter 5, the lack of control subjects is a limitation of this study. Although we would not expect to see significant changes in healthy subjects over one year, their inclusion would allow better modelling of whether or not the changes are significant. It would also allow assessment of whether other factors such as techniques used for analysis are producing repeatable results, or whether changes in the scanner itself may affect results.

The study uses multiple statistical tests and multiple comparisons to investigate changes, without Bonferroni correction. This leads to the possibility that any significant results have been produced through chance alone. A more definitive primary hypothesis would have allowed more robust assessment of results.

7.5 Conclusion

Progression of radiological features of CADASIL was evident over one year, with changes in brain volume, subcortical hyperintensities, new lacunes and microbleeds. Vascular measures have not been shown to predict radiological or neuropsychological change over 1 year. A longer period of follow up, as well as more detailed statistical analysis, may allow any potential relevance of these markers to be understood, particularly with regards to peripheral vasoreactivity.

Chapter 8 – Does *ex vivo* myography correlate with *in vivo* vasoreactivity in CADASIL patients?

8.1 Introduction

The NOTCH3 protein is expressed by VSMC throughout the body. Minor vessel wall thickening, GOM deposits and loss of VSMC can be seen in systemic vessels, and this has formed the basis of skin biopsy as a method for CADASIL diagnosis (Ruchoux et al., 1994). Retinal microvascular changes including arteriolar narrowing (Pretegeani et al., 2013), nephroangiosclerosis and renal impairment (Guerrot et al., 2008), peripheral nerve damage (Schröder et al., 2005) and Raynaud's phenomenon (Bartkova et al., 2010), have all been described in CADASIL patients. However systemic clinical effects remain uncommonly reported, with symptoms being largely confined to the brain.

As well as histological changes, there is evidence from *in vivo* testing that peripheral vascular function is impaired. This includes an absence of the nocturnal dipping of blood pressure (Manabe et al., 2001), and abnormal reactive hyperaemia, which may be due to inadequate vasodilatation (Campolo et al., 2011). These tests can vary in response to patient factors such as smoking, caffeine or food, as well as environmental factors such as timing of experiments and room temperature, necessitating strict protocols to enable accurate interpretation.

An alternative is *ex vivo* experimentation. This is conducted on tissue from an organism in an external environment, with minimum alterations of natural conditions. In CADASIL, it is assessment of small arteries that is of most interest. Small arteries with internal diameters less than 500µm are referred to as small resistance arteries (SRAs) as they contribute significantly to peripheral resistance (Mulvany and Aalkjaer, 1990) through their ability to regulate their diameter. Vessels of this diameter are those most affected by CADASIL (Okeda et al., 2002). Whilst brain tissue is difficult to obtain from living CADASIL patients, SRAs can be easily obtained from gluteal or abdominal tissue. Assessment of SRAs has been used in cardiovascular research for many years to examine small vessel remodelling and function (Intengan et al., 1999).

Wire myography is a technique developed to investigate the structure and function of these vessels (Mulvany and Halpern, 1977), independent of factors such as blood flow or the autonomic nervous system. It involves the dissection of vessels from tissue. Vessels are then mounted on a wire myograph and exposed to different experimental conditions. The ability of vessels to contract and relax can be investigated.

One study undertook clinical assessment and gluteal biopsy with myography in 10 CADASIL and 10 control subjects without a history of stroke, matched for age, sex and blood pressure (Hussain et al., 2004). Disease severity was assessed in patients with the expanded disability status scale, and T2 lesion load on brain MRI quantified as a percentage of brain parenchyma. Subjects were asked to discontinue antiplatelets and cholesterol lowering drugs for 72 hours before the biopsy. Resistance arteries were obtained from gluteal biopsy, stored and studied the following day. Concentration response curves to a number of vasoconstrictors and vasodilators were obtained. There was a reduced potency of noradrenaline contraction, but a greater maximal response to angiotensin II. The response to vasorelaxants was similar between controls and patients. Whilst noradrenaline potency was reduced, subjects with higher noradrenaline potency had the more severe disease on the basis of both imaging and disability scores. Conclusions from this study were that vasoconstrictor abnormalities are important in the pathophysiology of CADASIL, and that reduced noradrenaline potency may represent a secondary or compensatory response. This study was therefore in contrast to *in vivo* studies which have suggested an impairment of vasodilatory response (Stenborg et al., 2007).

In vivo and *ex vivo* experimentation may therefore increase our understanding of the pathophysiology of CADASIL, but it is not clear if these techniques relate to each other, and whether either correlates to disease severity.

The main hypothesis is that there will be abnormalities in vessel function in a cohort of CADASIL patients.

The aims of this chapter are therefore to:

- 1) correlate *ex vivo* myography in a group of CADASIL patients to radiological and clinical markers of disease;
- 2) compare *ex vivo* myography in a group of CADASIL patients to *in vivo* vasoreactivity measures;
- 3) examine the effect of anti-oxidants on vessel responsiveness.

8.2 Methods

8.2.1 Funding

The gluteal biopsy study was funded by project grants from the Stroke Association and the Neurosciences Foundation.

8.2.2 Ethics

Ethical approval was obtained for the gluteal biopsy study from the West of Scotland Research Ethics Service; project reference WS/12/0294. The study was sponsored by the NHS Greater Glasgow and Clyde Research and Development Service (GN12NE341). Written informed consent was obtained for all study participants in accordance with the Declaration of Helsinki.

8.2.3 Patient recruitment

Recruitment of subjects to the study took place between September 2013 and July 2015. Patients with genetically confirmed CADASIL from Neurovascular Genetics clinic at the Southern General Hospital, and who fulfilled the inclusion criteria for the study, were considered. Potential participants were approached by letter, then with a follow up telephone call.

8.2.3.1 Inclusion criteria

Inclusion criteria were as follows:

- Diagnosis of CADASIL confirmed with a characteristic mutation in exons 2 - 24 of the *NOTCH3* gene on chromosome 19.
- Over 18 years of age.
- Capacity to give informed consent.
- Able to participate in the study, and willing to comply with all procedures, either alone or with the aid of a responsible care giver.

8.2.3.2 Exclusion criteria

Exclusion criteria were as follows:

- Individuals incapable of giving informed consent.
- Chronic diffuse skin condition without uninvolved areas suitable for biopsy.
- History of keloid scar formation.
- Known diagnosis of hepatitis B, C or HIV.
- Known coagulopathy or history of significant bleeding after injury or operation.
- Known myopathy.
- Known allergy to local anaesthetic.
- Current treatment with warfarin or other anticoagulant medication.

8.2.3.3 Patient consent

Patients who met the inclusion and exclusion criteria were invited to a study visit at the BHF Glasgow Cardiovascular Research Centre (GCRC). Written informed consent was obtained.

8.2.4 Study design

Information including past medical history, demographics, cardiovascular risk factors and medication was collected. Height and weight were obtained. Pulse and supine blood pressure were recorded with an Omron Blood Pressure Monitor (OMRON 705IT, Omron corporation, Kyoto, Japan). A blood sample was obtained and full blood count, urea and electrolytes, HBA1c and cholesterol were analysed by NHS Greater Glasgow and Clyde routine laboratories. Urine protein was measured on a random urine sample.

Neurological disability was assessed with NIH Stroke Scale, and functional disability with modified Rankin scale (see Chapter 2).

8.2.4.1 Gluteal biopsy

Gluteal biopsies were performed by Dr Paul Rocchiccioli and Dr Jane Cannon. Surgeons wore a surgical gown, mask, hat and latex powder-free gloves during the biopsy. Disposable sterile surgical equipment was used. The patient was positioned face down on a bed with the buttocks exposed. The buttock was cleaned with Chlorprep® (CareFusion, UK) to produce a sterile field. A fenestrated drape (Easidrape® Single drape 75 x 75cm) was used to cover the patient but leave the operating field exposed. The upper, outer quadrant of the buttock was selected. Typically the right buttock was used unless the patient requested otherwise. 10ml of 2% lidocaine was injected using a needle and syringe. An incision was made with a scalpel (Disposable Sterile Scalpel, Swann-Morton, No 15), and a biopsy approximately 2cm x 1cm x 1cm of gluteal skin and subcutaneous fat was taken and placed in sterile normal saline solution (NaCl 0.9%; Figure 8-1). Haemostasis was achieved with manual pressure and wound closure. Absorbable sutures (coated VICRYL absorbable sutures, 3/0, 3/8 circle reverse, Ethicon) were used to close under the skin, followed by 4 or 5 non-absorbable sutures (ETHILON non-absorbable sutures, 3/8 circle reverse, Ethicon) to close the skin, using an interrupted mattress technique. A sterile dressing was then placed over the sutures (Mepore®, Mölnlycke Health Care). The biopsy site, volume of local anaesthetic used, number of sutures and any immediate complications were recorded in the case report form.



Figure 8-1 Gluteal tissue sample in normal saline

Patients were observed for one hour following procedure, and then provided with transport home. All patients were given written instructions regarding wound care, and contact details in the event of any complications. Patients either returned to the BHF GCRC one week post biopsy for wound inspection by a member of BHF GCRC nursing or medical staff, or attended their GP and were contacted by telephone. All complications were recorded in the case report form. If there were any complications patients were followed up until these had resolved.

8.2.5 Vessel dissection

Dissection of vessels from the gluteal biopsy specimen was performed by Elisabeth Beattie or Laura Mcpherson, on the day of biopsy. This was undertaken with surgical grade microscopic instruments with the aid of a high powered microscope (Stemi 2000, Zeiss). The biopsy was placed in a petri dish. If required, the biopsy was secured with entomology pins. The dish was filled with physiological salt solution (PSS; 118.4mM NaCl, 4.7mM KCl, 1.2mM MgSO₄.H₂O, 1.2mM KH₂PO₄, 24.9mM NaHCO₃, 2.5mM CaCl₂, 11.1mM glucose, 0.023mM EDTA) which was regularly changed during the dissection process. Dissection took between 30 minutes and 3 hours, and a single biopsy yielded none, one or several vessels. Care was taken to avoid direct contact with the vessels. Vessels were isolated from subcutaneous tissue and placed in a scintillation vial

containing physiological salt solution. Vessel length (in mm) and diameter (in μm) were recorded.

8.2.6 Myography

Myography experiments were performed by Dr Aurelie Nguyen Dinh Cat or Laura McPherson. Wire myography was conducted using a Mulvany-Halpern myograph. Vessel segments (around 2mm long) were mounted on a pressurized myograph (Danish MyoTechnology, Aarhus, Denmark, Figure 8-2). Vessel segments were slipped onto 2 glass microcannulas, one of which was positioned until vessel walls were in parallel. Once in position vessels were washed with PSS and left to equilibrate for 20min to achieve a pH of 7.4 at 37°C.

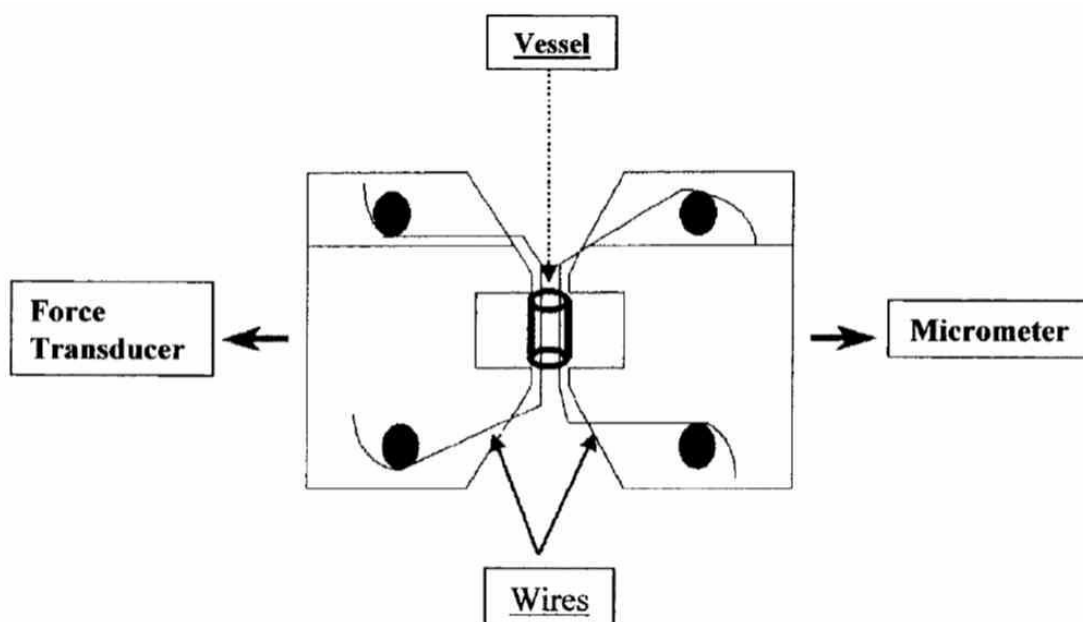


Figure 8-2 Mulvany-Halpern myograph

Reproduced from *Methods in Molecular Medicine*, Vol. 108: Hypertension: Methods and Protocols, 2005, page 94, Chapter 7: A guide to wire myograph, Spiers A and Padmanabhan, N. Figure 1 (© Humana Press Inc., Totowa, NJ), with kind permission from Springer Science and Business Media

Viability of tissue was assessed by testing contractile response to high-potassium depolarisation and noradrenaline. If vessels failed to contract, they were discarded. For vasodilatory studies, arteries were precontracted with phenylephrine to achieve approximately 80% of maximal response. Endothelium-dependent relaxations were measured by dilatory responses to acetylcholine (ACh, 10^{-9} to 10^{-5} mol/L). Endothelium-independent relaxations were assessed with sodium nitroprusside (SNP, 10^{-9} to 10^{-5} mol/L). A contraction curve to

cumulative increasing doses of phenylephrine (Phe, 10^{-9} to 10^{-5} mol/L) was constructed from arteries with intact endothelium.

These experiments produced concentration response curves, which are logarithmic and usually sigmoidal. Between 20 and 80% of the maximal, the response is approximately linear. This protocol was based on that found in “A guide to wire myography” (Spiers and Padmanabhan, 2005).

In patients 13 to 20 the vessels were incubated with the antioxidant N-acetylcysteine (NAC), and the concentration response curves for acetylcholine and phenylephrine were repeated.

8.2.7 Data from longitudinal study

Some patients recruited into the biopsy study had also taken part in the study detailed in Chapter 2 “Cerebral and peripheral perfusion and reactivity in CADASIL: A longitudinal pilot study”. Reactive hyperaemia index, CIMT and FMD results were used from the visit closest to the biopsy. This could have been either the baseline or year 1 study visit.

8.2.8 Imaging data

If an MRI head was available within one year of the biopsy date it was analysed. Hyperintensities were recorded using Scheltens score on the T2 FLAIR. The number of lacunes was also counted on the FLAIR image. If SWI or T2* gradient-echo was available the number of microbleeds was recorded.

8.2.9 Control data

Data from previous studies have been used to illustrate the differences in small vessel vasoreactivity between patients with CADASIL and healthy subjects. There are normal vessel data available, and for this study further sampling of healthy subjects was not undertaken. The paper used was by Glasgow researchers and studied small resistance vessels ($<300\mu\text{m}$) using a similar protocol (Hillier et al., 1999). Precontraction prior to vasodilatation studies was with noradrenaline, not phenylephrine, however, this was to a similar level of vessel contraction.

8.2.10 Statistics

If more than one vessel was tested per patient, the average response was taken. The response of vessels to additives at $\log 10^{-5}$ was chosen for statistical testing, as this should be close to maximal responsiveness. Values were reported as mean (SD) unless otherwise stated. For comparisons of independent categorical data Mann-Whitney tests for independent samples were used. For comparison of related samples Wilcoxon signed rank tests were used. For comparison of continuous variables, a Spearman rank correlation was used. Although there were multiple comparisons, as this was an exploratory study, p value significance was set at $p = 0.05$.

8.3 Results

20 patients (11 female) from 20 pedigrees were recruited to the gluteal biopsy study. Demographics, past medical history and medication are summarised in Table 8-1. 15 subjects had a mutation in exon 4, 3 in exon 5 and one each in exon 2 and 6.

4 patients were on antihypertensive medication but only 1 had a diagnosis of hypertension. The other patients were on propranolol for migraine, a diuretic for polycystic ovarian syndrome, and in 1 individual an ACE-inhibitor and a diuretic since the diagnosis of CADASIL despite never having been hypertensive.

Vessels were obtained in 17 patients. MRI scans were available for 16 patients. 11 patients also took part in the longitudinal study described in Chapter 2.

Table 8-1 Characteristics of gluteal biopsy cohort (n = 20)

Number of patients (female)	20 (11)
Age, years, median (range)	52 (30 - 62)
Modified Rankin Scale, median (range)	0 (0 - 2)
Systolic blood pressure, mmHg, median (range)	129 (100 - 145)
Diastolic blood pressure, mmHg, median (range)	76 (60 - 97)
BMI, kg/m ² , mean (SD)	28 (4.3)
Laboratory	
eGFR >60 mls/min/1.73m ² , n (%)	20 (100)
Cholesterol, mmol/L, mean (SD)	4.3 (0.6)
HbA1c, mmol/mol, mean, (SD)	35 (3)
Urine protein <0.1 g/L, n (%)*	18 (100)
Medical history, n (%)	
Stroke or TIA	10 (50)
Migraine	15 (75)
Depression (patient reported)	9 (45)
Hypertension	1 (5)
Diabetes	1 (5)
Medication, n (%)	
Antiplatelet	18 (90)
Statin	17 (85)
Antihypertensive	4 (20)
Beta-blocker only	1 (5)
Diuretic only	1 (5)
ACE inhibitor and diuretic	2 (10)
Complications	
Minor wound dehiscence only	2 (10)
Infection requiring antibiotics	3 (15)
Radiological characteristics (median (range))	
Number of lacunes, n =15	4 (0-18)
Number of microbleeds, n = 15	0 (0-21)
Modified Schelten's score, n = 16	48 (26-70)
Vessel properties	
Vessel length, mm, mean (SD)	1.9 (0.1)
Vessel diameter, µm, mean (SD)	576 (171)

*2 missing values

8.3.1 Concentration response curves

Examples of curves from healthy patients (in a different study) are shown in Figure 8-3. Mean endothelium-dependent relaxation (A), endothelium-independent relaxation (B), and contraction (C) curves are shown in Figure 8-4 for CADASIL patients. These failed to show a typical sigmoidal shape as maximal responsiveness was limited. Vessels from CADASIL patients failed to obtain 100% relaxation or contraction even at very high concentrations of vasoactive agents.

Significance of differences: * $P < 0.05$.

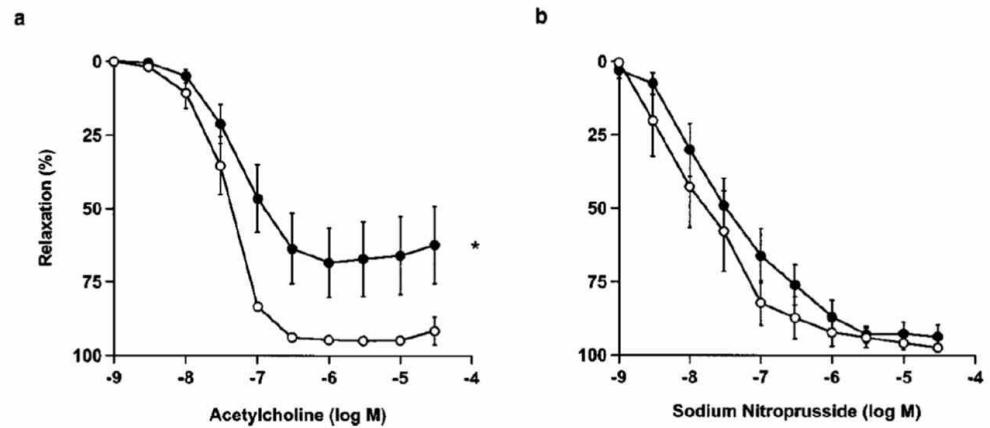


Figure 8-3 Effect of acetylcholine (a) and sodium nitroprusside (b) on isolated resistance arteries from control subjects and patients with chronic heart failure. Control subjects (open circles), CHF patients (dark circles). Reproduced with permission from Clinical Science (1999), 97, 671-679. Hillier et al, Structural and functional assessment of small arteries in patients with chronic heart failure. Significance of difference, * $p < 0.05$

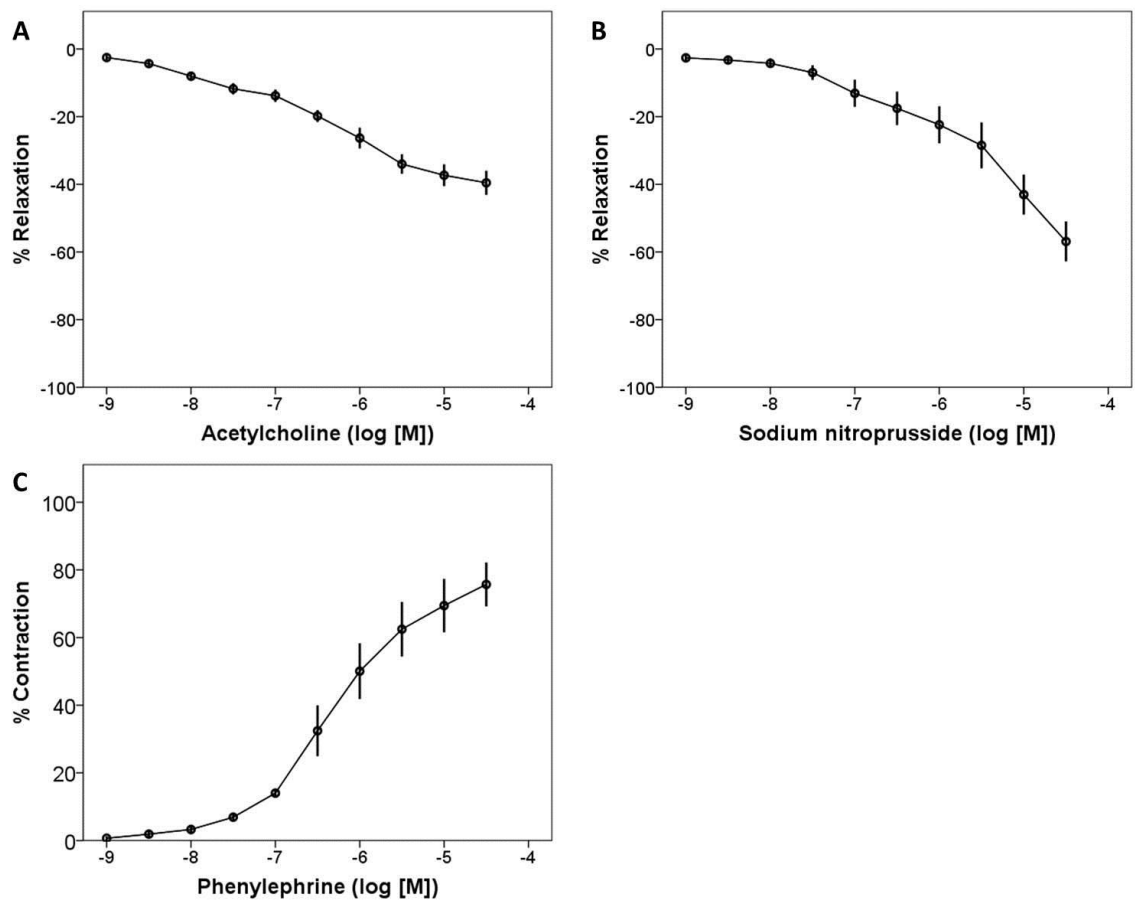


Figure 8-4 Concentration response curves in gluteal resistance arteries (A) Endothelium-dependent relaxation to acetylcholine, $n = 17$; (B) Endothelium-independent relaxation to sodium nitroprusside, $n = 14$; (C) Contraction to phenylephrine, $n = 17$. Expressed as mean \pm standard error of mean. Interpolation line shown.

8.3.2 Effect of NAC

Vessel responsiveness to acetylcholine at 10^{-5} was improved in the presence of NAC (with NAC -53 (13), without NAC -33 (7), $p = 0.017$). Vessel contraction to phenylephrine at 10^{-5} was not statistically improved by NAC (with NAC 55 (16), without NAC 70 (20), $p = 0.208$). Concentration response curves with and without NAC for patients 13-20 are shown in Figure 8-5.

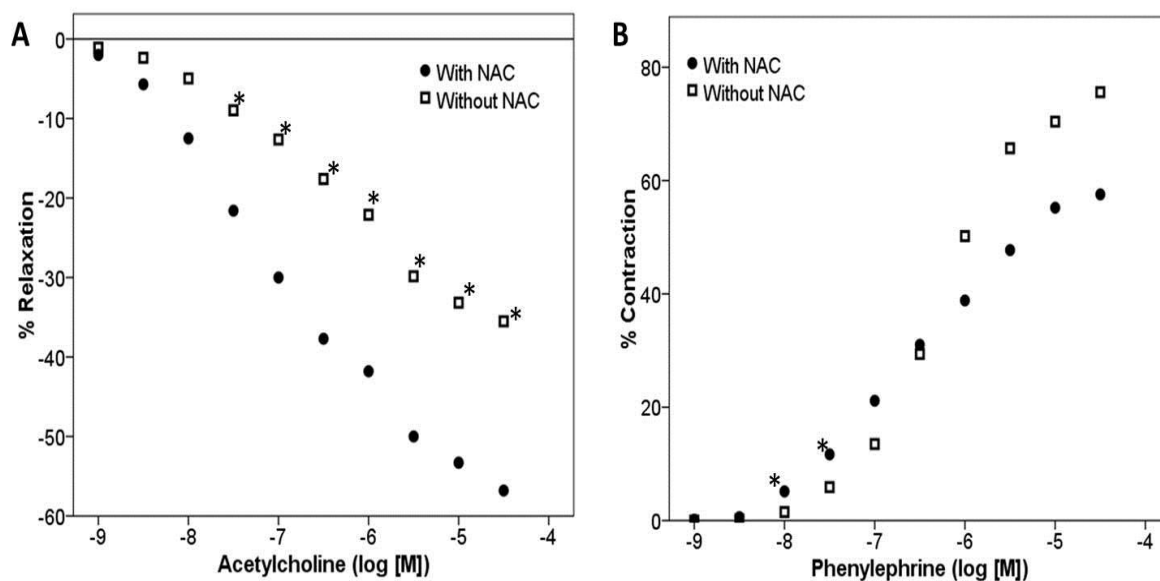


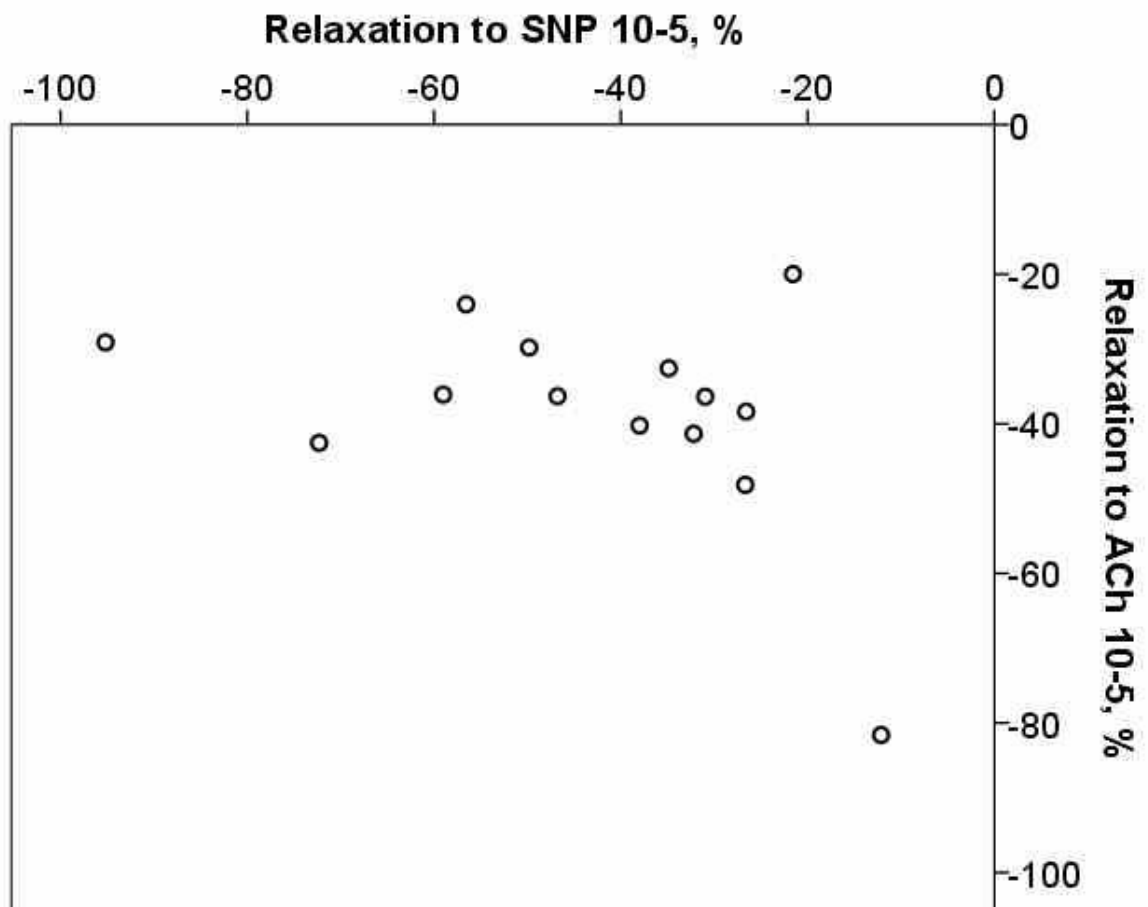
Figure 8-5 Vessel responsiveness with and without N-acetylcysteine (NAC)
(A) Endothelium-dependent relaxation to acetylcholine was improved by the addition of an antioxidant; **(B)** contraction to phenylephrine was unaffected overall. Significant differences shown with *.

8.3.3 Relationship of vasoactive responses

There was no relationship between the responses to acetylcholine, phenylephrine or sodium nitroprusside (see Table 8-2, Figure 8-6). Endothelium-dependent and independent vessel relaxation was independent.

Table 8-2 Relationship of vasoactive responses

		Response at 10^{-5} , %		
		ACh	SNP	Phe
Response at 10^{-5} , %	ACh	r_s	-0.336	-0.188
		Sig (2 tail)	0.240	0.471
		N	14	17
	SNP	r_s	-0.336	0.183
		Sig (2 tail)	0.240	0.532
		N	14	14
	Phe	r_s	-0.188	0.183
		Sig (2 tail)	0.471	0.532
		N	17	14

Figure 8-6 Endothelium-dependent and independent relaxation at 10^{-5}

8.3.4 Vasoactive responses to vessel diameter

Vessel diameter was negatively correlated to contraction in response to phenylephrine ($r_s = -0.652$, $p = 0.005$, $n = 17$; Figure 8-7) but did not affect relaxation.

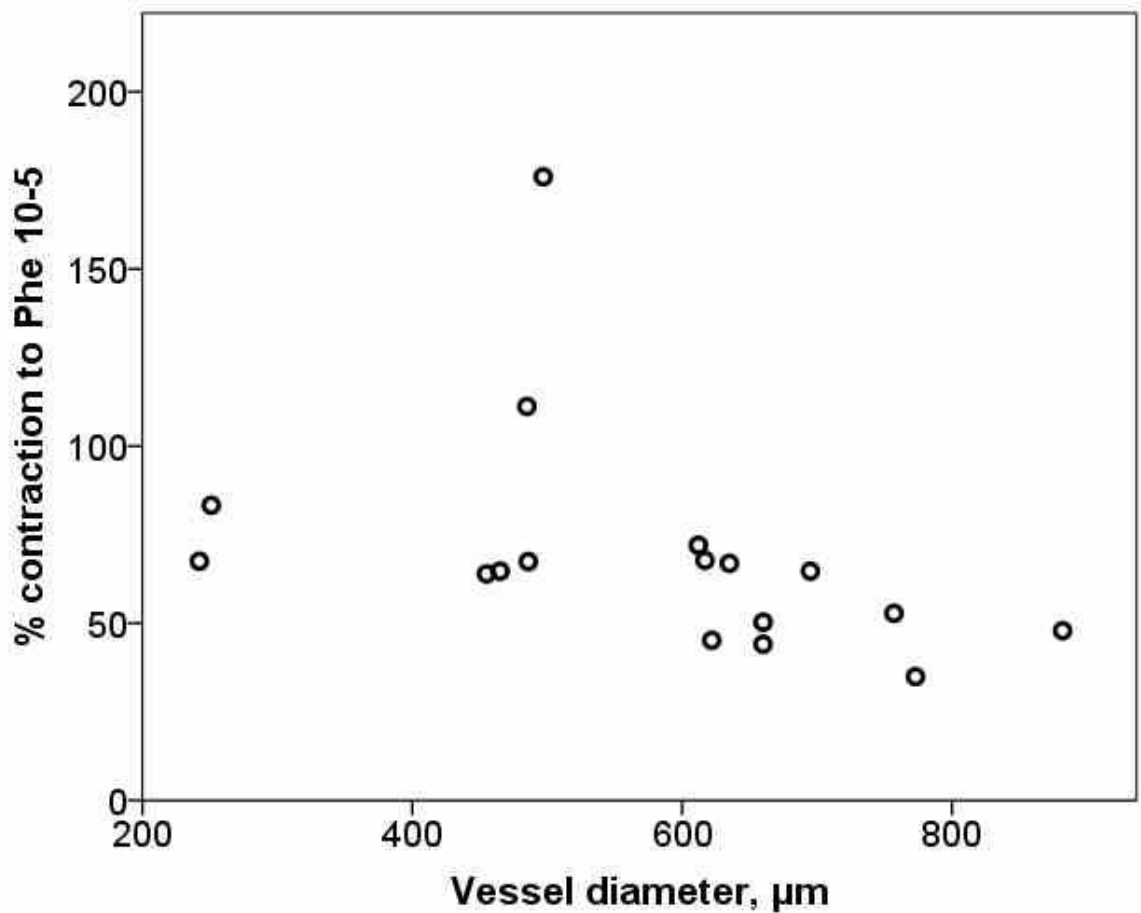


Figure 8-7 Vessel diameter and contraction to phenylephrine

Smaller diameter vessels contracted more in response to phenylephrine.

8.3.5 Vasoactive responses and clinical outcomes

Age was not found to be correlated with any measure of vessel responsiveness (ACh $n = 17$, $r_s = -0.389$, $p = 0.123$; SNP $n = 14$, $r_s = -0.194$, $p = 0.506$; Phe $n = 17$, $r_s = -0.81$, $p = 0.757$). Systolic blood pressure was not found to be correlated with any measure of vessel responsiveness (ACh r_s $n = 17$, 0.207 , $p = 0.425$; SNP $n = 14$, $r_s = 0.108$, $p = 0.714$; Phe $n = 17$, $r_s = -0.169$, $p = 0.517$).

There was no association between gender and either endothelium-dependent vessel relaxation (ACh; male ($n = 6$), $-35\% \pm 7$; female ($n = 11$), $-39\% \pm 16$; $p = 0.961$) or endothelium-independent relaxation (SNP, male ($n = 5$), $-52\% \pm 16$; female ($n = 9$), $-38\% \pm 24$; $p = 0.083$). Females contracted more than males (male ($n = 6$), $51\% \pm 12$; female ($n = 11$), $80\% \pm 36$; $p = 0.007$).

There was no difference in those patients with a history of stroke compared to those without, in any parameters of vessel responsiveness. There was no difference between those with an mRS of 0 or 1 compared to 2 or more, in any parameter of vessel responsiveness (Table 8-3).

Table 8-3 Vessel responsiveness compared to clinical parameters

		Response at 10^{-5} , %		
		ACh	SNP	Phe
		Mean (SD), n	Mean (SD), n	Mean (SD), n
Modified Rankin Scale	0- 1	-34 (8), 11	-42 (18), 9	63 (21), 11
	≥ 2	-44 (19), 6	-45 (31), 5	81 (47), 6
	p value	0.216	1	0.350
Stroke	No stroke	-32 (6)	-33 (11), 5	69 (23), 7
	Stroke	-42 (16), 10	-49 (25), 9	70 (39), 10
	p value	0.088	0.190	0.536

8.3.6 Vasoactive responses and radiological outcomes

16 subjects had MRI scans which took place within 1 year of the date of the biopsy (median 50 days, range 6 - 352).

Table 8-4 Vessel responsiveness compared to radiological measures

		Lacunes, n	Microbleeds, n	Scheltens, n
Response at 10^{-5} , %	ACh	r_s	-0.057	-0.090
		Sig (2 tail)	0.860	0.781
		N	12	12
	SNP	r_s	-0.638	-0.492
		Sig (2 tail)	0.026	0.124
		N	12	11
	Phe	r_s	-0.253	0.141
		Sig (2 tail)	0.427	0.663
		N	12	12

There was no relationship between vessel responsiveness to acetylcholine or phenylalanine and any radiological marker. Vessel responsiveness to sodium nitroprusside was negatively correlated to number of lacunes (see Table 8-4, Figure 8-8).

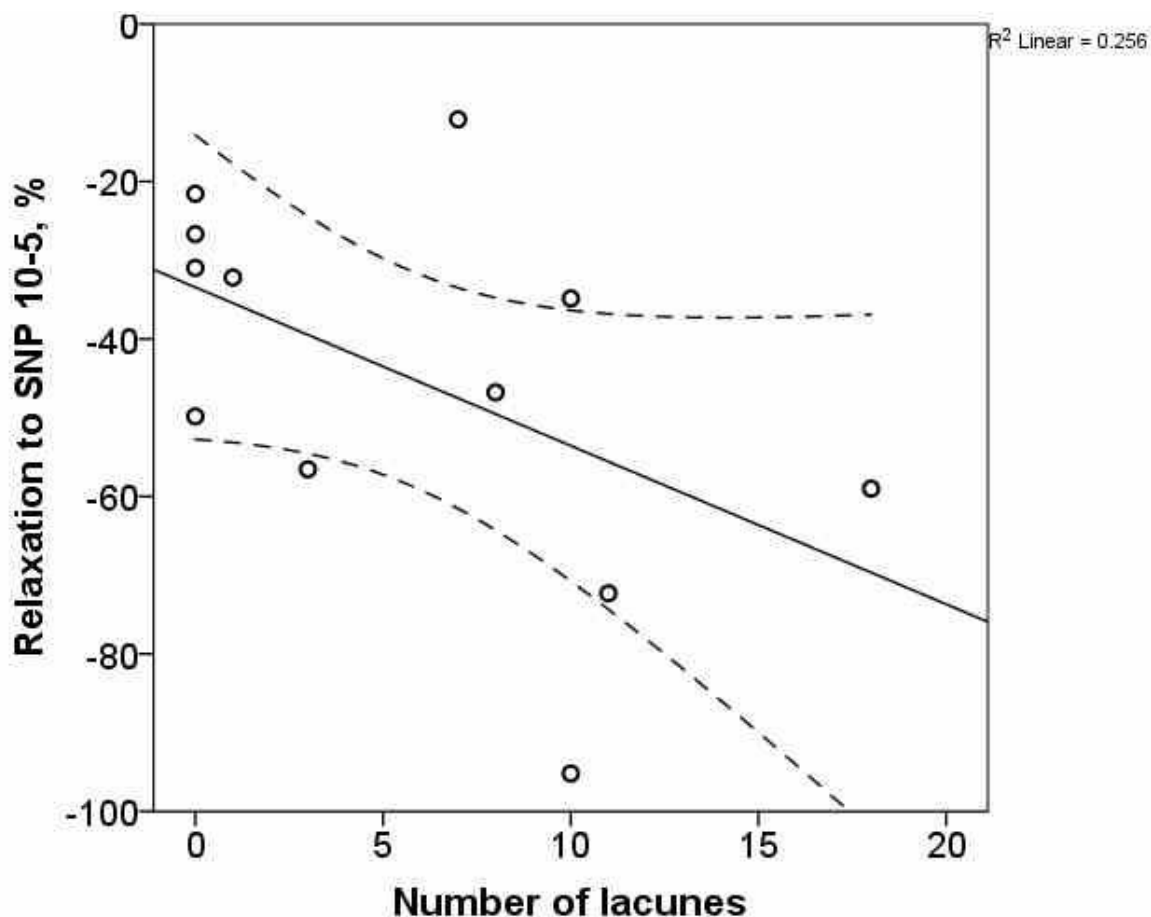


Figure 8-8 Relaxation to sodium nitroprusside in comparison to number of lacunes
 Patients with a higher number of lacunes showed greater relaxation in response to SNP

8.3.7 *Ex vivo* vasoactive responses and *in vivo* vascular assessment

A subset of patients (11) had also undergone *in vivo* vasoreactivity tests. There were 1 and 5 months between the vascular tests and the biopsy. Unfortunately vessels were only available in 8 of these patients. No statistically significant relationship was seen between *ex vivo* vessel responsiveness and FMD, RHI or CIMT (Table 8-5). Patients with higher contraction to phenylephrine did seem to have higher FMD but this was not significant (Figure 8-9).

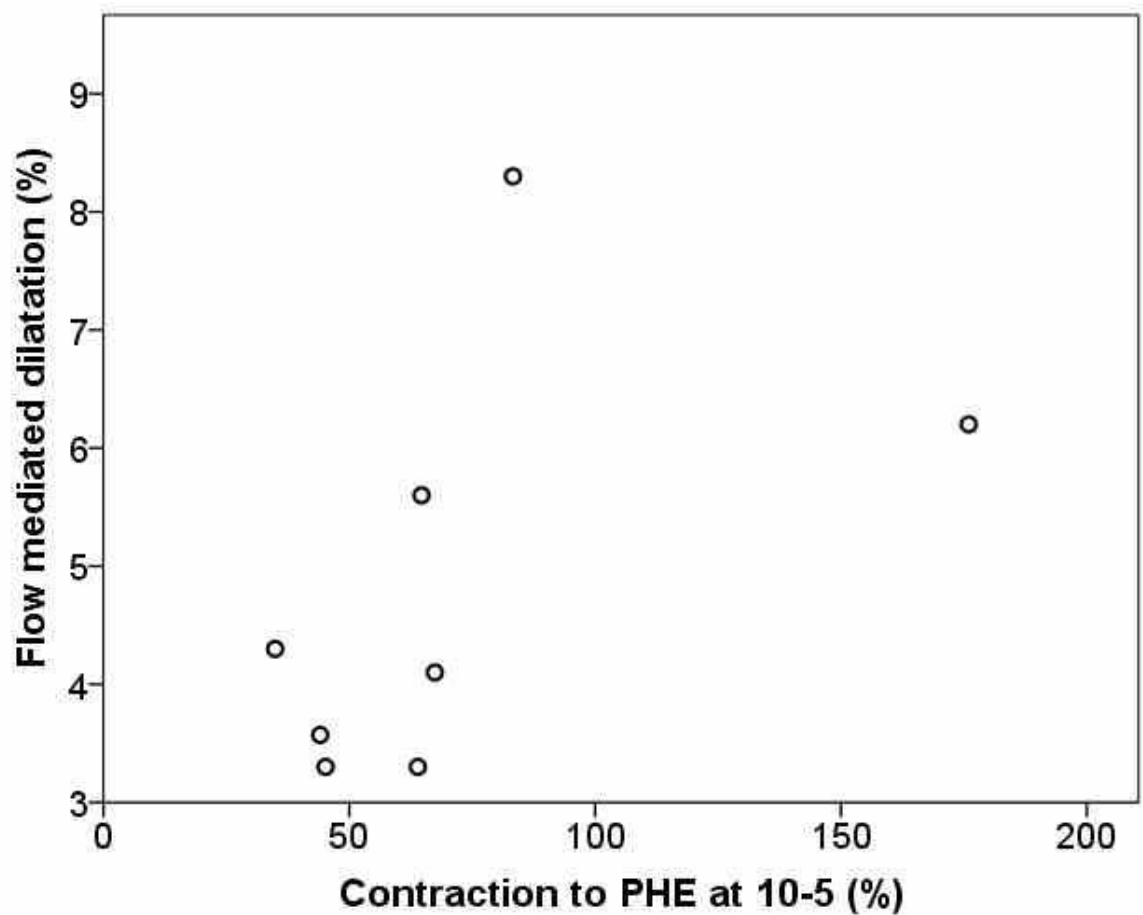


Figure 8-9 Flow mediated dilatation and contraction to phenylephrine

Table 8-5 *Ex vivo* vessel responsiveness compared to *in vivo* vessel reactivity

		FMD, %	RHI, %	CIMT, mm
Response at 10 ⁻⁵ , %	ACh	r _s	0.371	0.179
		Sig (2 tail)	0.365	0.701
		N	8	7
	SNP	r _s	0.198	0.657
		Sig (2 tail)	0.670	0.156
		N	7	6
	Phe	r _s	0.611	r0
		Sig (2 tail)	0.108	1
		N	8	7

8.4 Discussion

This chapter presents the initial results of an ongoing study examining small arteries in patients with CADASIL. Concentration response curves to agents which cause vasodilation and constriction have been produced under standardised

conditions. Whilst at present, control patients collected by the same researchers are not available, comparison of these results to control patients from previous studies shows evidence of markedly impaired vasoreactivity. Both dilation and constriction are affected. These results are in contrast to previous work in CADASIL, where only deficits in vasoconstriction were demonstrated (Hussain et al., 2004). However confirmation of these results with controls is required.

There was improved endothelium-dependent relaxation when NAC was incubated with the vessels. NAC has antioxidant effects and reduces free radicals, and is thought to enhance endothelial function. NAC may improve endothelial dysfunction during myography in oophorectomized rats which display vascular endothelial dysfunction (Delgado et al., 1999). It has also been demonstrated to augment acetylcholine-induced relaxation in human coronary and femoral arteries, in patients both with and without atherosclerosis (Andrews et al., 2001).

No relationship was demonstrated between *in vivo* vasoreactivity measures and *ex vivo* testing. This was however limited by small group numbers. Age and blood pressure did not appear to play a significant role in vasoactive responses. No difference in clinical measures could be detected. Surprisingly the only relationship between vasoreactivity and radiological measures was that patients with more impaired endothelial-independent relaxation had a smaller number of lacunes. This may either reflect small group numbers or multiple testing, or that lacunes are not due to impairment of vasodilatation but that another mechanism is responsible.

NOTCH signalling clearly plays a role in vascular function. *Notch3* null mice display a failure for post-natal arterial remodelling. Arterial vessels at 28 days are enlarged, with a thinner VSMC layer and disorganised VSMC, compared to wildtype littermates (Domenga et al., 2004). Blockage of NOTCH signalling to smooth muscle (all NOTCH receptors) by expression of an inhibitory protein, DNMAML1, leads to decreased VSMC contractile and relaxation responses in mutant mice arteries. This effect was postulated to be at the level of the myofilaments (Basu et al., 2013).

Notch3 mutated mice also demonstrate abnormal vasculature (see Chapter 1). In transgenic *Notch3* Arg90Cys mice, an age-dependent arteriopathy is demonstrated. These mice show attenuated responses to vasodilatory challenges, which stimulate myogenic responses, and altered CBF autoregulation. These findings are present prior to visible brain abnormalities (Lacombe et al., 2005). This mouse model shows GOM and NOTCH3 deposits but does not demonstrate parenchymal pathology or clinical effects in the mouse. Interestingly, the vessels with the most extensive abnormalities are found in the mouse tail, rather than the brain (Ruchoux et al., 2003).

Tail caudal vessels of 10 month old CADASIL mice showed reduced shear-stress induced dilatation. This response is endothelium-dependent. Reduced response may represent either direct endothelial damage, or abnormal myoendothelial communication (Dubroca et al., 2005). Vessels also showed increased myogenic tone, suggesting less effective adaptations to variations in blood pressure, making the brain more vulnerable to periods of hypotension. These findings were detected prior to the detection of GOM. Vessel responses to phenylephrine and acetylcholine were not shown to be impaired however.

Mechanical forces and chemical agents likely function in different pathways, reflected in the lack of relationship between the two. It may be that mechanical dysfunction is present early in the disease, prior to histological abnormalities, but altered responses to chemical agents comes after VSMC degeneration (Dubroca et al., 2005).

The human endothelium both secretes, and is susceptible to, a variety of vasoactive substances. It is vulnerable to damage, and its dysfunction is a marker of vascular risk (Anderson and Phillips, 2015). Endothelial dysfunction is seen in conditions such as hypertension, diabetes and renal impairment. The more severe the hypertension the more impaired endothelial function appears to be (Benjamin et al., 2004). However it remains unclear if endothelial function is a cause, or a consequence, of hypertension (Dharmashankar and Widlansky, 2010). Probably both are over-simplistic, and there is a complex interaction between the two.

Vascular inflammation and oxidative stress are thought to be key in the development of endothelial dysfunction (Brandes, 2014), both of which have been described in CADASIL (Ihalainen et al., 2007, Rafalowska et al., 2004). If the results of this study are valid, and systemic small arteries are affected in CADASIL as profoundly as those in the brain, the question arises as to why other systemic effects are not seen. In this cohort blood pressure was unrelated to all measures of vessel dysfunction, and was generally within normotensive limits. Renal function also appeared unaffected, with no evidence of proteinuria in any patient. Therefore in CADASIL patients, despite abnormal small vessel function, hypertension and renal failure are not seen.

The reasons for this are unclear. Theories have included that as the brain has fewer vascular smooth muscle cells than other organs (Heistad, 2001), and less capacity to regenerate, it may be more vulnerable to their damage (Rafalowska et al., 2004). Another explanation is that endothelial and pericyte dysfunction may lead to the breakdown of the blood brain barrier leading to toxic effects on the brain (Hall et al., 2014). NOTCH3 has been found to be additionally expressed in astroglial progenitors and the choroid plexus (Alberi et al., 2013), and is proposed to have a role in neural stem cell development (Alunni et al., 2013). In RBJK mutations, which lead to loss of NOTCH signalling, there is depletion of neural stem cells and early termination of lineages, although this has not been confirmed in NOTCH3 mutations (Alunni et al., 2013). The brain may therefore be more vulnerable due to co-existent neural cell and vascular damage.

Vessel size varied from 221 to 882µm. Smaller vessels contracted more than larger vessels. This may be because larger vessels are in fact flaccid and lack functioning VSMC. Some of the vessels were larger than the definition of <500µm so this may reflect that smaller vessels are more contractile and the source of vascular resistance.

8.4.1 Strengths

All vascular tests were performed by a single, trained rater. Vascular tests were conducted as per published recommendations and established standardised operating procedures in the BHF GCRC laboratory. The majority of biopsies (18)

were performed by a single surgeon who has completed multiple previous gluteal biopsy procedures. The patients were well phenotyped and included a number of different mutations. The age range was wide and both male and female patients were represented. Very disabled patients were not recruited, usually due to difficulties with informed consent or attending the appointments. However the included participants still had a range of symptoms and disabilities.

The number of subjects is limited due to the invasive and highly technical nature of the biopsy and post-biopsy procedures. However 20 subjects in this sort of study is relatively large (Hussain et al., 2004). Vessels were obtained in 85% (17/20) of patients.

8.4.2 Limitations

This study does not have concurrent healthy control subjects. This is however planned. This will allow more accurate comparison with these subjects as the same protocol, equipment and staff will be used. *In vivo* studies were not undertaken in all subjects, and these did not occur on the same day. At the time of planning the studies, consideration was taken about combining the 2 studies. However some potential participants did not want to take part in a multi visit longitudinal study, whilst others did not want to undergo an invasive procedure.

MRI scans were clinical scans and could be up to a year before or after the biopsy. Progression of microbleeds, lacunes and white matter hyperintensities, as seen in Chapter 7, is generally slow however. Use of the presence or absence of lesions, and the Scheltens score are broad-brush descriptors of radiological disease load. However, they do have greater relevance to the clinician than more complex measures.

Patients were not asked to fast or avoid alcohol or cigarettes prior to the biopsy. All these factors are known to influence vasoreactivity studies (Anderson and Phillips, 2015). It was not considered appropriate to withhold medication in patients with a disease which increases the risk of stroke therefore antiplatelets were not stopped. ACE-inhibitors and statins are thought to improve endothelial function (Dharmashankar and Widlansky, 2010) but given that in general these patients responded poorly, presence of these drugs is unlikely to be relevant. In

this technique vessels are effectively “washed out” of confounding factors in the PSS so reactivity is likely to represent local signalling pathways only.

There are a large number of statistical comparisons in this study and specific primary hypothesis was not established at the start of the study. Using multiple comparisons without a correction for this can be criticised and any significant results may well be through chance.

8.5 Conclusion

Further assessment using myography is needed to establish the vascular abnormalities seen in CADASIL patients, and whether these relate to *in vivo* vascular, clinical and radiological measures of disease.

Chapter 9 – Arterial branch order and lenticulostriate artery territory lacunes in CADASIL

9.1 Introduction

Lacunes are a characteristic manifestation of CADASIL, and cerebral small vessel disease (CSVD) in general. Lacunes are proposed to be due to subcortical infarct or haemorrhage in the territory of a single perforating artery (Wardlaw et al., 2013), and are commonly found in the basal ganglia, subcortical white matter or brainstem (Duering et al., 2013). They are often associated with characteristic neurological syndromes, but can also occur without concurrent clinical manifestations (Fisher, 1982). Most subcortical infarcts are thought to be due to intrinsic abnormalities of cerebral small vessels (Wardlaw, 2008), and this is certainly the proposed cause in CADASIL. Lacunes may also be caused by embolism or intracranial atherosclerosis (Futrell, 2004). Research has focussed on the mechanisms responsible for subcortical infarcts, rather than the size of vessel involved, partly due to limited resolution of *in vivo* imaging.

Contrast injection into the basal ganglia microvasculature of 40 cerebral hemispheres, demonstrated that basal ganglia vasculature is consistent across brains with little overlap between arterial territories (Feekes et al., 2005). The medial and lateral lenticulostriate arteries (LSA) originate from the middle cerebral artery and supply portions of the caudate, putamen, internal capsule and external globus pallidus. These primary vessels subdivide into smaller vessels which terminate in defined territories (Marinković et al., 2001). Investigators have produced a microangiographic template derived from the arterial maps outlined above. This was used to estimate the branching order of vessels related to basal ganglia subcortical infarcts in a general acute stroke population using FLAIR images (Phan et al., 2013). These investigators concluded that the volume and dimensions of subcortical infarct were dependent on the order of artery involved. In a heterogeneous stroke population however, with multiple cardiovascular risk factors, it is not possible to determine whether the infarcts studied were caused solely by CSVD, or whether other mechanisms might be relevant. CADASIL patients offer a more homogenous population with pathologically pure CSVD. CADASIL has similar radiological findings to CSVD but

with a younger age of onset and hence a lower prevalence of confounding pathology such as atheroma or cardioembolism.

The main hypothesis of this chapter is that most lenticulostriate lacunes will be associated with tertiary branching order vessels in CADASIL.

The aims of this chapter are to:

- 1) investigate the size of lacunes in CADASIL;
- 2) correlate this with the branching order of the LSA using a microangiographic template in CADASIL patients.

9.2 Methods

9.2.1 Sample

All subjects underwent imaging, clinical assessment and vascular assessment as stated in Chapter 2.

9.2.2 MRI analysis

Lacunes were defined as in Chapter 2. Each lacune was identified on 3D-T1 image and a seed placed within it using Analyze v 11.0 (Analyze Direct Inc., United States). Seed-based thresholding was used to define the lacune. Segmented lacunes were fused with 3D-T1 scan which was transformed into standard MNI 1mm brain space using FLIRT (FMRIB's Linear Image Registration Tool (Jenkinson and Smith, 2001) from the FMRIB software library (FSL v 5.0, Oxford University, UK).

Individual lacunes were transformed into MNI standard space using the matrix derived above. The transformed lacune volume was measured using the voxel-counting method. Coronal slices 125, 130 and 135 were extracted from the transformed T1 (FSL slicer) and the LSA template created as part of a recent study (Phan et al., 2013) was overlaid onto coronal images using a programme

provided by Dr Richard Beare and Prof Thanh Phan from Monash University (see Figure 9-1).

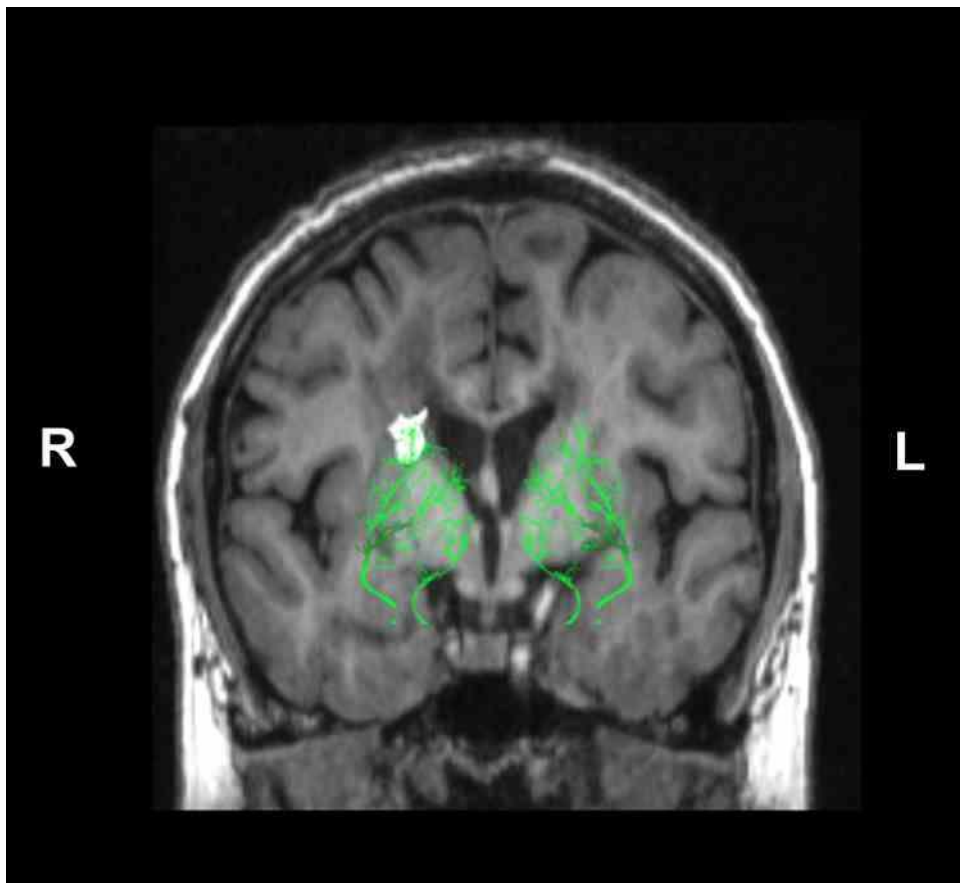


Figure 9-1 Lacune and brain on MNI template with overlaid microangiographic template
A lacune (white area) can be seen on the right with the arterial template overlaid in green.

Lacune dimensions (axial width and anterior-posterior (AP) length) were measured using the boundary of their locations on the standardised brain map. Coronal height was measured on the slice with the arterial map. Coronal height, axial width and AP length were also measured at the geometric centre of the lacune.

Analysis of microbleeds, calculation of subcortical hyperintensity volume, and brain volume has been stated in Chapter 2 and 5.

9.2.3 Clinical rating

4 raters (2 neurologists, 1 geriatrician, 1 neurology trainee) who were blinded to clinical information, were asked to rate infarcts. Raters were provided with all overlaid coronal images where a lacune was visible (see Figure 9-1), along with a standardised rating form (Figure 9-2). The scans were labelled 1 to 16. If a

lacune was visible on more than one slice, all slices were included and scored (but only the slice closest to the centre of the lacune was included in the analysis). Each rater independently assessed whether the vessel likely to have been diseased in relation to the lacune was a primary, secondary, or tertiary branch of the LSA, or out with the LSA territory. Examples from the previous study using the arterial template were provided (see Figure 9-2). Individual ratings were averaged to provide a summary score for each lacune. A summary score of ≤ 1.5 was rounded to 1 (primary), $1.5 < \leq 2.5$ to 2 (secondary) and > 2.5 rounded to 3 (tertiary).

Lacunae were excluded if the coronal height in the overlaid slice was over 50% different from the coronal height in the geometric centre, as it was felt likely that the coronal slice therefore gave an inaccurate visual impression of lacune size.

9.2.4 Statistical analysis

Differences in MRI characteristics, and lacune dimensions in different orders of arteries, were calculated with independent samples Mann-Whitney U Test. The relationship between width and volume was determined with Spearman's correlation. Statistical analysis was performed with IBM SPSS Version 21 (IBM Corp, Armonk, NY, USA). Differences were considered significant at $p < 0.05$. Results are expressed as median (IQR) unless otherwise stated.

Dear Reader,

Please examine the segmented infarcts on the provided images. Please determine if you believe the infarct was caused by disease of a 1st order, 2nd order or 3rd order infarct. Examples are shown below. If you do not think it is in the lenticular artery territory please indicate this along with the order of the infarct.

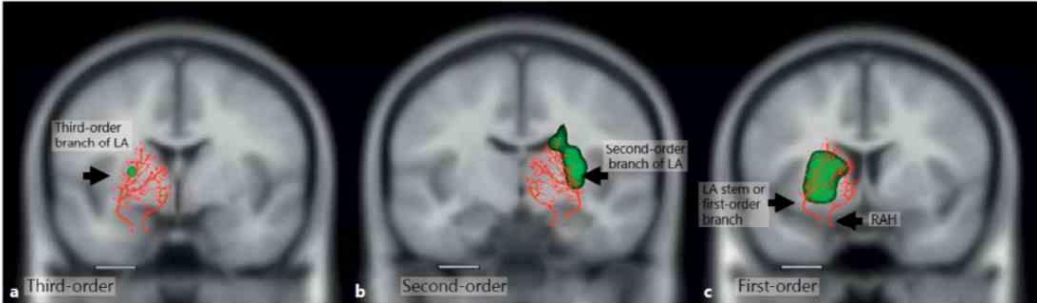


Fig. 1. Microangiography of the LA is superimposed on a third-order (a) second-order (b) and first-order (c) arterial branch infarct. The line bar is 1 cm in length.

Image from Phan et al. *Cerebrovascular Diseases* 2013; 35:262-267

Tick as appropriate

Image	Infarct side	1 st order	2 nd order	3 rd order	Not LA territory
1	Right				
2	Right				
3	Right				
4	Left				
5	Left				
6	Right				
6	Left				
7	Left				
8	Left				
9	Left				
10	Right				
10	Left				
11	Left				
12	Upper left				
12	Lower left				
13	Left				
14	Left				
15	Left				
16	Right				

Figure 9-2 Worksheet for rating of lacunes and arterial branching order
Picture used with permission from Phan et al, “Dimensions of subcortical infarcts associated with first- to third-order branches of the basal ganglia arteries”, *Cerebrovasc Dis* 2014; 35: 262-267. Copyright © 2013 Karger Publishers, Basel, Switzerland.

9.3 Results

9.3.1 Patient information

22 subjects with CADASIL (50% male, median age 53 years, range 26 - 67) were included in the study. 10 subjects had one or more discrete lesions in the territory of the LSA, and none were associated with blood on SWI. 8 of these subjects were male. Subjects with lacunes in LSA territory had a higher total lacunes (10 (12) v 2 (11); $p = 0.051$) compared to subjects without LSA lacunes although this did not quite reach significance. There was no difference in number of microbleeds or NSH.

There was no evidence of extracranial vessel disease on MRA in 20/22 (one patient age 30 years did not undergo MRA and in one patient MRA was degraded by artefact but there was no evidence of vessel abnormalities on carotid ultrasound). One patient had a known patent foramen ovale and another had poor quality 3D T1 scan inadequate for further analysis of lacunes. The demographics and radiological data of the 10 patients with LSA lacunes are shown in Table 9-1.

Table 9-1 Demographics and MRI variables of CADASIL patients with LSA lacunes (n = 10)

CADASIL patients with LSA lacunes	
Age in years, median (IQR)	53 (30 - 67)
Male : Female	8:2
History of stroke or TIA, n (%)	5 (50)
Hyperlipidaemia, n (%)	7 (70)
Ever smoker, n (%)	5 (50)
Hypertension, n (%)*	0 (0)
Diabetes, n (%)	0 (0)
No. of lacunes, median (range)	10 (2 - 29)
NSH %, median (range)	5.3 (1 - 9)
No. of microbleeds, median (range)	0 (0 - 10)

*3 patients were on beta-blockers for anxiety or migraine prevention.

16 lacunes on 16 MRI images were scored. Rating of lacunes by individual raters is shown in Table 9-2. For lacunes present on more than one slice, the image closest to the centre of mass was included in analysis of dimensions. 3 lacunes were excluded as the coronal height on the overlaid slice was more than 50% different from the coronal height at the geometric centre, meaning the image was not representative of the true lacune size for scoring. Thus 13 lacunes were included in analysis of lacune size.

Table 9-2 Rating of each lacune and exclusions

Scan	Lacune position	Rater				Overall Rating	Excluded	Branch Order
		1	2	3	4			
1	Right	2	3	3	2	2.5		2
2	Right	3	3	3	3	3		3
3	Right	3	3	3	3	3		3
4	Left	2	3	3	3	2.75		3
5	Right	2	3	3	2	2.5	Repeated lacune	
6	Right	3	3	3	3	3	Not representative of height	
6	Left	Not LSA	3	3	3	3		3
7	Left	3	3	3	2	2.75		3
8	Left	3	2	3	3	2.75		3
9	Left	2	2	2	2	2		2
10	Right	3	3	3	2	2.75	Not representative of height	
10	Left	2	3	2	3	2.5		2
11	Left	3	3	3	3	3	Not representative of height	
12	Upper left	3	3	3	3	3	Repeated lacune	
12	Lower left	3	2	3	3	2.75		3
13	Left	3	3	3	2	2.75		3
14	Left	3	3	3	2	2.75	Repeated lacune	
15	Left	3	3	Not LSA	3	3		3
16	Right	3	3	3	3	3		3

9.3.2 Lacune dimensions and vessel branching order

The dimensions for all included lacunes are shown in Table 9-3. No lacunes were associated with primary arterial branch vessels, 3 with secondary, and 10 with tertiary. Lacunes associated with secondary arterial branch vessels had a

significantly greater dimensions than those associated with tertiary arterial branch vessels (see Table 9 - 4, Figure 9-3, Figure 9-4).

Table 9-3 Dimensions of all LSA territory lacunes

	Volume (mL)	Axial width (mm)	Coronal height (mm)	AP length (mm)
Median (range)	0.04 (0.01 - 0.65)	5 (3 - 11)	5 (3 - 17)	4 (2 - 15)
Mean (SD)	0.14 (0.21)	6 (3)	7 (5)	6 (4)

Table 9-4 Dimensions in secondary and tertiary arterial branch lacunes

Lacunes	Volume (mL)	Axial width (mm)	Coronal height (mm)	AP length (mm)
Secondary, n = 3, median (range)	0.48 (0.32 - 0.65)	11 (8 - 11)	14 (12 - 17)	10 (9 - 15)
Tertiary, n = 10, median (range)	0.03 (0.01 - 0.14)	4 (3 - 6)	4 (3 - 9)	4 (2 - 7)
p value	0.007	0.007	0.007	0.007

Axial width correlated significantly to lacune volume ($n = 13$, $r_s = 0.630$, $p = 0.021$; Figure 9-4) as did coronal height ($n = 13$, $r_s = 0.900$, $p < 0.001$) and A-P diameter ($n = 13$, $r_s = 0.899$, $p < 0.001$).

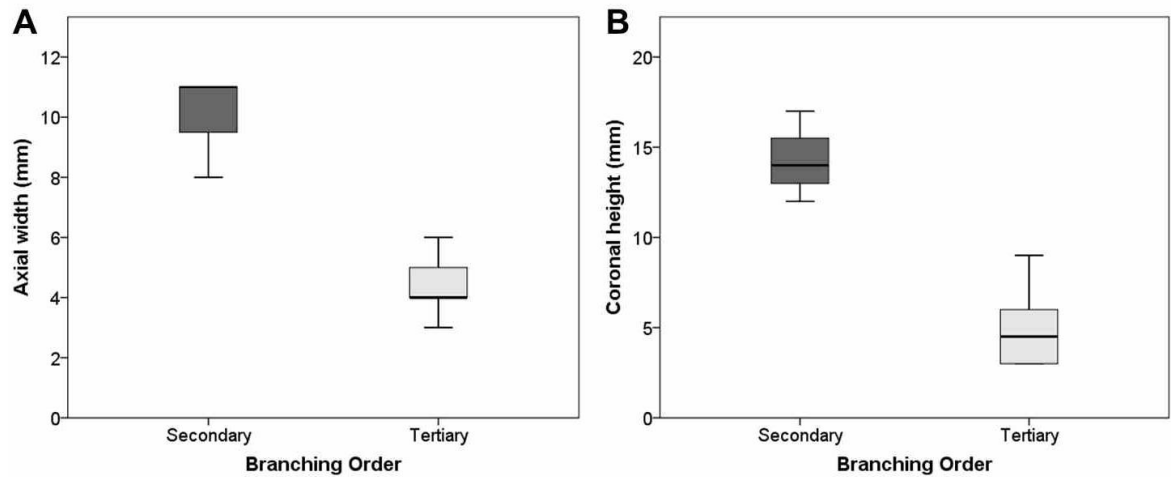


Figure 9-3 Width and height in secondary and tertiary arterial branch lacunes (A) Axial width and (B) coronal height.

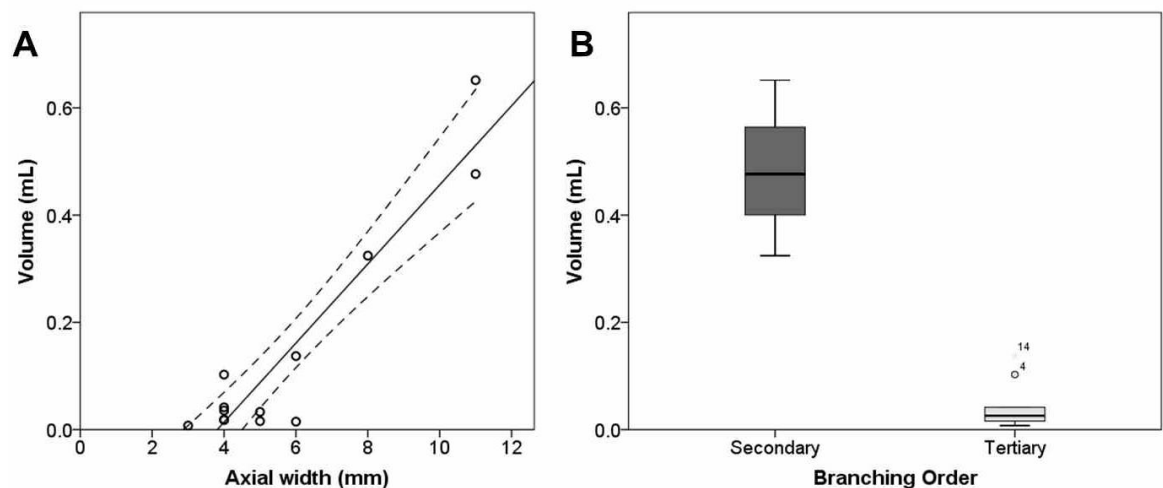


Figure 9-4 Lacune volume (A) Lacune volume was significantly correlated to axial width, and other lacune dimensions. The line of best fit is shown with 95% confidence interval of the mean (dashed lines). The (B) Lacune volume was significantly larger in secondary arterial branch lacunes compared to tertiary.

9.4 Discussion

The diagnosis of CSVD is based upon imaging and clinical syndromes, and up to 20% of incident strokes are attributed to this cause. Imaging does not however always demonstrate acute brain lesions, but instead evidence of previous damage such as lacunes or subcortical hyperintensities. The classification of stroke subtype (e.g. cerebral small vessel disease, cardioembolic, large vessel)

has therapeutic implications, but classification based on clinical syndromes and anatomical imaging cannot always distinguish the diverse aetiologies responsible for stroke. In this cohort of CADASIL patients, the majority of basal ganglia lacunes were small and likely related to tertiary artery branch disease of the perforating vessels. If these lacunes reflect intrinsic vasculopathy due to small order branch disease, then further refinement of the dimensional criterion for chronic lacunes within the basal ganglia, related to intrinsic CSVD, may be required.

Fisher's findings were based on autopsy data well after the acute ischaemic event (Fisher, 1982). As such, his descriptions are more relevant to lacunes than acute subcortical ischaemic events. A range of lacune sizes were observed in his studies, with giant lacunes up to 35mm in diameter noted. In that study, cortical infarctions were documented to co-exist with lacunes in 26% of patients (Fisher, 1965). This frequency of concurrent pathology can cause difficulties in assigning stroke mechanisms. Subsequent to these earlier studies on giant lacunes, investigators suggested these may be the result of embolism (Ay et al., 1999). In this study the chances of other stroke mechanisms being involved were minimised by the fact none of the patients had hypertension or diabetes. None of the patients had documented atrial fibrillation, a known risk factor for cardioembolic disease which, in a recent study, was found in one quarter of subjects with small subcortical infarct. No patient had significant carotid stenosis. One patient had a PFO and had suffered a likely embolic stroke after starting on hormone replacement therapy, but this resulted in cortical infarcts. Therefore it is likely that most, if not all cases in this cohort represent intrinsic CSVD, increasing the confidence in interpreting the involved branching order and dimensions in relation to this particular phenotype of CSVD. Nonetheless, the possibility of other stroke aetiologies being present cannot be excluded, particularly given the high rate of smoking and hypercholesterolaemia. Whether CADASIL can truly represent a "pure" model of intrinsic CSVD is debated, as whilst radiological measures are similar, there are significant histological differences (Pantoni, 2010) which may negate comparisons between groups of subjects. The fact that these patients don't have significant cardiovascular risk factors may also restrict the study generalisability. One may speculate however, that whilst the mechanisms between CADASIL and sporadic CSVD may be

different, the size of the lacune and arterial branch involved are likely to be similar. It has been shown in an autopsy study of 3 subjects with cerebrovascular disease that the observed lacunes were likely to be due to tertiary branch disease (Feekes, 2006).

The mean axial width of lacunes in this study was 6 ± 3 mm far below the current empirical upper limits of 15mm in sporadic CSVD. This finding is in keeping with previous work in CADASIL patients, where 3D segmentation of lacunes showed the majority were small (over 95% had a volume of less than 500mm^3 (0.5mL)) (Hervé et al., 2009). The estimation of coronal heights as 5 ± 2 mm is consistent with that provided in the microangiographic study of the lenticulostriate artery. Those authors gave the coronal dimensions of the tertiary arterioles as between 2 and 12mm but did not provide axial dimensions (Feekes et al., 2005). However it must be noted that dimensions in this study are affected by the transformation of the scans to an MNI template, thereby changing the dimensions of the lacune. This was required in order to apply the template to a standardised brain volume.

9.4.1 Strengths

The principal strength of this study is a carefully phenotyped CADASIL cohort. The arterial template used is derived from preserved and standardized microangiographic maps, and presents a novel, if indirect way of examining small vessels (Phan et al., 2013). In vivo visualisation of the relevant human vasculature requires invasive angiography or high field MRI, but small vessels are beyond the spatial resolution of current routine non-invasive vascular imaging. Co-registration of the map and brain may be preferable to methods which use side-by-side inspection (Duering et al., 2013). The use of 3T MRI gave high resolution 3D images, which leads to excellent visualisation in all planes, although the study would have benefitted from a thinner slice FLAIR sequence.

9.4.2 Limitations

There are several limitations to this study, the most significant being the small numbers of patients and included lenticulostriate artery territory lacunes, which limits the strength of any statistical tests. It would be important to replicate

these findings in a larger cohort of CADASIL patients and CSVD. At present, only a microangiographic template of the LSA is available and hence only lacunes in this territory were assessed. Using the automated overlay method may mean the slice where the lacune is largest in the coronal height is not visualised. A further criticism is whether perivascular spaces and lacunes may have been misclassified as lacunes and vice versa (Cumurciuc et al., 2006), despite using high resolution T1 imaging complimented by T2 FLAIR. As lacunes can shrink over time, a lower size limit for lacunes might not be appropriate. Only a single rater identified lacunes, and this can also be criticised. Using an independent rater, as detailed in other chapters, would have helped prevent bias.

Another caveat is that only the chronic phase of the lacune was studied. Dimensions of acute subcortical infarctions with arterial branching order might be more useful for clinicians in accurately identifying the mechanisms used, and thus the relevance to acute stroke is unclear. Nonetheless, increasing diagnostic use of MRI means that incidental lacunes are a common finding in acute stroke presentations and relevant to mechanistic interpretation and therapeutic decisions. The same technique could be applied to acute lesions, but the low frequency of acute ischaemia in CADASIL means that any acute study in this population would require large numbers of patients.

There are no controls in this study although healthy subjects would be unlikely to have lacunes. Patients with cerebral small vessel disease could be used as an alternative control group, and this could be explored in the future. We cannot be sure that CADASIL patients have the same anatomy as healthy controls as there is a possibility that abnormalities in NOTCH3 leads to different vessel development.

9.5 Conclusion

The dimensions on MRI of LSA lacunes in CADASIL patients are small and likely to involve secondary and tertiary arterial branches of the LSA. If CADASIL represents a “pure” form of typical CSVD, then current dimensions used to define lacunes, at least in the chronic stage, may include infarcts of other

aetiologies. However this study is limited significantly by small study numbers and needs further investigation in larger groups.

Chapter 10 – Conclusions

10.1 Introduction

CADASIL is currently not a treatable condition, and it can rob young adults of their independence, livelihoods and cognition. The burden on families is significant given the age of onset, and the realisation that other family members may be equally affected. Given the age group affected, social care is often arduous to obtain and patients particularly suffer from a lack of awareness of their condition even amongst most medical staff.

As such, further understanding of disease is required and the investigation of vascular dysfunction in this disease was the focus of this thesis. The major findings are reviewed below along with how these fit with recent developments in the field.

10.2 Summary of results

10.2.1 CADASIL is more common than previously thought

CADASIL remains, within EU definitions, a rare disease. However at any one time there may be as many people with CADASIL in Scotland as with motor neurone disease. A prevalence of 11/100,000 adults is likely to still represent an underestimate of the condition, and certainly out-with the Glasgow and Lanarkshire area, there are likely to be many families who have not been diagnosed, with more common conditions like multiple sclerosis and conventional cerebral small vessel disease being thought responsible. Education of clinicians and radiologists will be vital to increase the diagnosis of the disease. Whilst individualised services may not be needed for most CADASIL patients, this may make it easier for them to access what is already available.

10.2.2 Age, impaired vasoreactivity and large vessel disease are related to MRI markers of disease

Impaired cerebral vasoreactivity to hypercapnia, as measured with ASL MRI, was shown to be related to number of lacunes and brain atrophy, important correlates of clinical impairment. Peripheral vasoreactivity was also impaired in those with higher numbers of lacunes. Whether the impaired cerebral vasoreactivity pre-exists, or is subsequent to, the development of lacunes and atrophy is unclear. The finding of co-existent impaired vasoreactivity does suggest that abnormal vessel responsiveness in CADASIL patients is not solely secondary to brain damage. This finding is consistent with evidence that CVR may be impaired in CADASIL patients (Pfefferkorn et al., 2001).

Arterial stiffness and increased carotid intima media thickness were also linked to more extensive brain damage. This suggests that conventional cardiovascular risk factors may contribute to the damaging effects of CADASIL. Smoking and hypertension have been shown to be potential risk factors for stroke in patients with CADASIL (Adib-Samii et al., 2010). The MILES study, a comparison of patients with CADASIL and those with age-related leukoencephalopathy, suggested that when adjustment was made for age and gender, the presence of hypertension was associated with poor cognition (Ciolli et al., 2014). However, blood pressure itself did not show this relationship, suggesting that whilst hypertension is detrimental, blood pressure itself does not have a simple linear relationship with risk in the disease.

Despite limited replication of cerebral vasoreactivity as a biomarker for disease progression, it has been used as an endpoint in therapeutic trials of oral acetazolamide, which improves CVR and CBF in CADASIL patients (Huang et al., 2010) and of high-dose atorvastatin, which did not alter cerebral haemodynamics (Peters et al., 2007). Further studies may need to investigate the role of CVR longitudinally in disease progression before there can be confidence that they truly represent a biomarker that can be used for assessment of therapies.

10.2.3 ASL MRI can be used effectively in CADASIL and shows that cerebral blood flow declines even over 1 year.

This study has demonstrated the effective use of ASL MRI within this cohort of patients. The advantage of not requiring contrast or radiation makes it ideal for longitudinal assessment. I found that ASL was reproducible over one year but was also able to demonstrate change over that time period. The change seen exceeded the change in other MRI markers of disease progression. The quantifiable nature of ASL as shown in this study highlights that it may be useful in multicentre trials. Whilst controversy over the accuracy of white matter measurement remains, obtaining and evaluating these results, along with that of grey matter, could still potentially provide useful information, even if it represents worsening of transit delays. Murphy and colleagues calculated that if a 15% increase or reduction in grey matter CBF was to be detected, 17 subjects would be needed in each group (Murphy et al., 2011). This thesis suggests this could potentially be seen over a 2-3 year period. These numbers fit much more comfortably with any potential trial in a rare disease. ASL should be included in future CADASIL imaging based trials.

10.2.4 Vascular predictors of deterioration remain elusive but warrant further investigation

Whilst change in brain imaging parameters including atrophy and NSH in one year were demonstrated, vascular measures did not predict clinical decline over one year. As expected, more extensive radiological abnormalities at baseline were related to deterioration in cognition, but surprisingly, higher subcortical hyperintensity volume was related to decline in processing speed rather than lacunes or atrophy.

Within population studies, white matter hyperintensities predict an increased risk of stroke, dementia and death (DeBette and Markus, 2010). Within CADASIL the influence of these often extensive abnormalities on patient outcomes remains unclear. Larger volumes of white matter have been seen in patients compared with controls (De Guio et al., 2015) and extensive WMH may be

associated with an increase in brain volume in CADASIL (Yao et al., 2012). This is proposed to be due to intramyelinic oedema, which was shown to be an early change in a mouse model of CADASIL (Cognat et al., 2014). However axons within these areas were generally normal, although there was evidence of impaired clearance of debris. This suggested the white matter could swell without damage to the nerves. The proposed mechanism was a defect in ion and water homeostasis linked to abnormal function of the astrocytic end feet where NOTCH3-expressing pericytes are abundant.

The proposed mechanisms for the development of lacunes and NSH are therefore different. It perhaps makes sense therefore that CVR was related to lacunes and not NSH in Chapter 5. The development of lacunes is more likely related to disease of tertiary arterioles, where failure of autoregulation may lead to tissue hypoperfusion.

10.2.5 Systemic vessels are abnormal and a role for oxidative stress is suggested

Gluteal resistance vessels obtained from CADASIL patients showed evidence of abnormal vasorelaxation and constriction. This is in contrast to a previous biopsy study which showed defects only in constriction (Hussain et al., 2004). Mouse models have failed to show deficits in vessel responsiveness to chemical stimuli. This thesis suggests this is in fact found in CADASIL patients, and therefore is an important direction of research. Whilst it may represent a later stage of the disease than abnormalities in pressure-induced vasodilation, it may therefore be more directly linked to the development of lacunes and clinical effects. The improved response of endothelium-dependent relaxation in the presence of N-acetylcysteine suggested a role for oxidative stress. A recent study of plasma levels of aminothiols showed high levels of antioxidants and low levels of oxidants in CADASIL patients compared with controls (Campolo et al., 2013). Expression of antioxidants may be increased to try and protect the vessels and enhance vasoreactivity.

These results highlight the need for ongoing investigation using human tissue and cells, in order to understand the biology of CADASIL. Mouse models have been

created which show evidence of disease but these often require overexpression of the gene. This study has shown samples are obtainable in CADASIL patients and offer important insights into the disease.

10.3 Place in current literature

Two recent areas of work have furthered our understanding of CADASIL. Joutel et al recently reviewed the role of the “matrisome” - the ensemble of proteins constituting the extracellular matrix, which not only physically anchors cells, but has a multitude of regulatory effects (Joutel et al., 2016). It has been demonstrated that the Notch3 extracellular domain may bind to TIMP3 and promote its upregulation. This in turn recruits additional extracellular matrix proteins to the abnormal toxic aggregate (Monet-Lepretre et al., 2013).

TIMP3 inhibits proteins that are involved in the regulation of specific potassium channels. Upregulation of these channels in the CADASIL mouse model TgNOTCH^{R169C} causes impaired myogenic responses, which may be responsible for altered cerebrovascular reactivity (Dabertrand et al., 2015). This seemed to be a brain specific response. It may therefore offer an explanation as to why different areas are differentially affected in CADASIL, both within the brain and body, as each organ has its own pattern of proteins expressed in the ECM.

In patients, the results of a 2 centre longitudinal study have just been published (Chabriat et al., 2016). 290 patients were recruited over 8 years, and followed up for 3 years. Clinical and radiological data were collected, with completion of the follow up visit in 236 patients. A composite endpoint of incident stroke, incident dementia, moderate or severe disability, or death was observed in 47% of patients, and baseline predictors of this included gait disturbance, atrophy and >3 lacunes. Change in MDRS cognitive scales was predicted by mRS >3, number of lacunes, the presence of microbleeds and brain atrophy. Active smoking more than doubled the risk of stroke and dementia. Age and hypertension were not associated with disease progression. This study highlighted that patients who smoke and are already disabled are likely to do badly. Those patients, whose brain imaging shows multiple lacunes and atrophy, are also likely to deteriorate.

Results of this thesis provide a pathophysiological bridge between these two papers. I have shown evidence that reduced vasoreactivity in humans may be linked to important MRI markers specifically lacunes and brain atrophy. Recent studies show these factors are linked to disease progression. Cerebral blood flow decreases over time both in grey and deep white matter to a degree that may be measurable in multicentre trials. This thesis also provided evidence that addressing cardiovascular risk factors is important (see Figure 10-1).

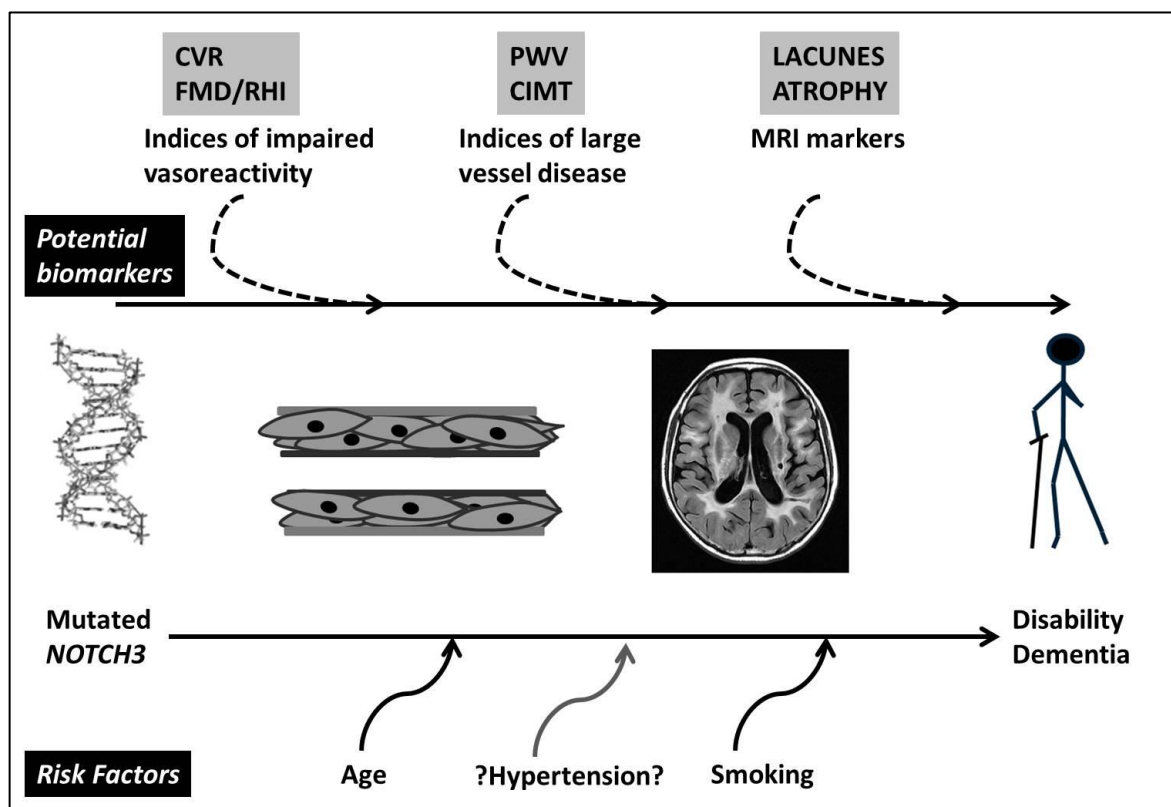


Figure 10-1 Risk factors and potential biomarkers in CADASIL
Potential biomarkers in grey boxes.

The role of hypertension remains unclear, and whilst significant hypertension is likely to have deleterious systemic effects, it is postulated that hypotension may also be undesirable, given the reduction in cerebral blood flow seen in the condition. This area needs further investigation as to the optimal management of blood pressure in these patients.

10.4 Future directions

The second year of the longitudinal study from which much of this thesis data has been derived is due to be completed in February 2016. Analysis of this data may reveal more statistically significant results with regards to prediction of

deterioration than those seen in Chapter 7. Such evidence would suggest that measures including those of cardiovascular dysfunction and small vessel reactivity should be included in therapeutic trials to potentially reduce the numbers required. The decline in cerebral blood flow will be characterised in more detail.

The gluteal biopsy study has recently been extended to healthy controls and hypertensive patients. All these patients will also undergo a comprehensive range of peripheral vascular tests including PWA, PWV, Endo-PAT®, FMD and CIMT. The 9 CADASIL patients who did not previously undergo vascular tests will also be invited back to have these tests conducted. This will allow us to relate *ex vivo* myography results with more confidence *to in vivo* tests. It will also allow more direct assessment of how impaired CADASIL vessels are in comparison to healthy or hypertensive vessels.

It would be important to ensure all future studies are aligned with clinical trial methodology, such as those outlined by the Consolidated Standards of Reporting Trials (CONSORT) group in order to ensure as reliable and stringent scientific methodology as possible (Schulz et al., 2010).

The advantage of such collaborative work with experts in the field of systemic small vessel disease is that there is extensive experience working with these vessels and cells. Proteomic characterisation of vascular smooth muscle cells is part of the work being undertaken on these samples, and will hopefully reveal more biological insights into the pathomechanism of CADASIL.

Skin samples collected from the patients described in Chapter 8 included fibroblasts, which will be transformed into induced pluripotent stem cells. Induced pluripotent stem cells are adult cells that have been genetically reprogrammed into an embryonic stem cell-like state which are capable of propagating indefinitely. They potentially provide an unlimited number of cells with which to investigate the disease or to test therapeutics, although, as has been shown in other stroke trials, close collaboration between bench and bedside is needed for this to be successful.

10.5 Closing remarks

The work detailed in this thesis studies the prevalence of CADASIL and the use of a variety of techniques to assess vascular function. Abnormalities in vessel function both *ex vivo* and *in vivo* have been demonstrated. Whilst longer follow up will provide more clarity on potential risk factors, it is clear both conventional cardiovascular risk and vasoreactivity have a role to play in CADASIL. Understanding of this area will contribute to the development of potential therapeutics, and vascular measures should be included in any clinical trials.

Appendix 1

Cerebral hyperperfusion on arterial spin labelling MRI during CADASIL migrainous encephalopathy

Authors: Fiona C Moreton, Celestine Santosh, Kate McArthur, Keith W. Muir

Reproduced from *Neurology*: Dec 2015 - Volume 85 - Issue 24 - p 2177 - 2179.
Wolters Kluwer Health Lippincott Williams & Wilkins© No modifications will be permitted.

Migrainous encephalopathy is a rare and poorly understood manifestation of the inherited vasculopathy cerebral autosomal dominant arteriopathy with subcortical infarcts and leukoencephalopathy (CADASIL). Patients may present with migraine with aura, complicated by confusion, fever, and decreased conscious level.¹ In this case, a patient with migrainous encephalopathy underwent cerebral perfusion imaging with arterial spin labelling (ASL) MRI before, during, and following admission.

Case report

A 27-year-old man with CADASIL associated with the NOTCH3 mutation pArg133Cys, diagnosed in 2011, noticed his vision to the right side was like “looking through a hole.” Over the next 30 minutes, complete distortion of vision to the right along with altered sensation and reduced power in his right arm occurred, followed by a severe pulsating bilateral frontal headache associated with nausea.

After 3 hours, he was admitted to the hospital and was drowsy with symmetrical weakness in all limbs. Speech was slow but there was no dysphasia, eye movement abnormality, or ataxia. Headache was ongoing. Systemic examination was normal. He was afebrile and normotensive. Full blood count, erythrocyte sedimentation rate, C-reactive protein, urea, and electrolytes were normal. CT head showed no evidence of acute intracranial pathology. CSF examination was not performed.

The following morning, the patient had disconjugate and slowed eye movements, profound motor and cognitive slowing, extensor plantars, and global motor weakness. CT angiogram was normal. Diffusion-weighted MRI demonstrated no evidence of acute ischemia. MRI was unchanged from imaging 4 months previously, with subcortical and deep white matter T2 hyperintensities in both cerebral hemispheres consistent with CADASIL.

He had a history of migraines with visual aura since age 8 years, but had experienced none for several years since starting propranolol, which had been stopped recently. He had depression at age 18 years, but had no history of stroke or seizure. He was diagnosed with viral meningitis in 2009 (CSF leukocyte count 100, no organisms). He was taking part in an observational research study examining perfusion in CADASIL (UKCRN ID 13794) and had a normal neurologic examination 1 month prior to this admission.

ASL MRI showed both global and focal hyperperfusion compared to imaging 3 months previously (gray matter blood flow increased by 34%), with marked hyperperfusion in the left parietal lobe (127% increase on left compared to 40% on right), left occipital (107% vs 18%), and left posterior temporal lobe (64% vs 39%).

The patient's headache fluctuated during admission, and increasing severity of the headaches was followed by deterioration in conscious level. The headache was partly relieved by dihydrocodeine, and improved over 5 days.

At discharge, speech remained slow but the patient was mobile with 2 sticks. Repeat MRI on discharge showed no new ischemic lesions and resolution of the hyperperfusion. Six weeks later, the patient continued to have speech hesitancy but MRI showed no new ischemic lesions. Propranolol was restarted.

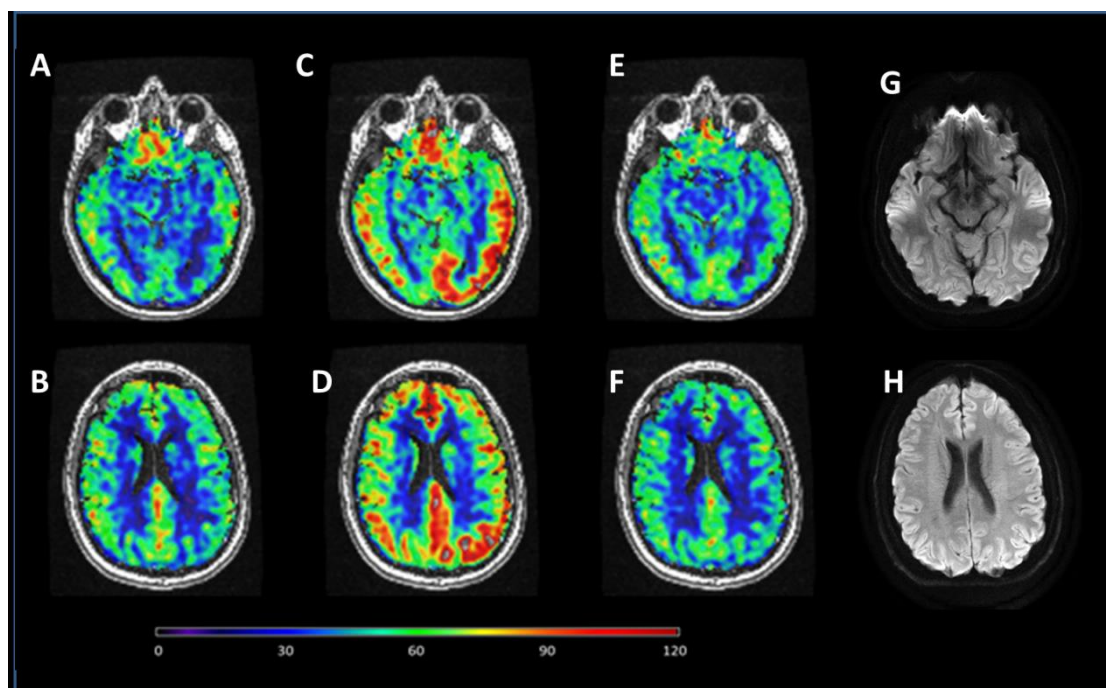


Figure 1 Cerebral blood flow in migrainous encephalopathy
Cerebral blood flow (CBF) measured by arterial spin labeling (ASL) 3 months prior to admission (A, B), during illness (C, D), and 6 days following presentation (E, F). Hyperperfusion particularly in the left occipital, parietal, and posterior temporal lobe is evident (C, D), which settled during admission (E, F). Diffusion-weighted imaging showed no evidence of acute infarction (G, H). ASL was analyzed using an in-house macro written for ImageJ (NIH). Scale bar shows CBF in mL/100 g/min.

Discussion

Migrainous encephalopathy, or CADASIL coma, presents as an acute encephalopathic illness, usually in patients with a history of migraine.¹ Migraine prevalence in CADASIL is significantly higher than in the general population at around 40%, with the majority having an associated aura, which is often atypical, characterized by prolonged or severe neurologic disturbance.² Encephalopathic features are rare, but are often preceded by headache.¹ Susceptibility to severe migraines in CADASIL is unlikely to be related to chronic hypoperfusion or cortical damage, as migraine occurs early in the natural history, and appears to recede in patients after the onset of cerebrovascular events.² Instead, NOTCH3 mutations may influence cortical excitability, with transgenic mouse models demonstrating enhanced susceptibility to cortical spreading depression (CSD).³ Impaired capillary flow regulation as an early and diffuse feature of CADASIL may mediate liability to CSD⁴, and may underpin the more extensive propagation and pronounced clinical features compared to migraine with aura in the general population.

SPECT perfusion imaging of a patient with CADASIL with prolonged aphasic aura has identified increased relative blood flow in the left hemisphere⁵, similar to changes seen in hemiplegic migraine.⁶ The notable advantages of ASL MRI over alternative perfusion methods are lack of requirement for contrast or radiation, and quantification. It is therefore ideal for conditions requiring repeated measurements.⁷ By using ASL, we were able to demonstrate regional hyperperfusion, which temporally and anatomically correlated with the right-sided visual aura, in addition to a generalized hyperperfusion compared to our patient's premigraine state. Increases in cerebral blood flow are associated with encephalopathic features in other hyperperfusion encephalopathies⁷ and hyperperfusion may offer a marker for these conditions.

Migrainous encephalopathy in CADASIL is associated with hyperperfusion, which can be identified and monitored with ASL MRI. Such techniques may allow the further investigation of the pathophysiology and response to treatments.

Acknowledgments

Acknowledgment: The authors thank Dr. Rosario Lopez Gonzalez for writing the in house macro to allow quantitative analysis of ASL.

Footnotes

Author contributions: Dr. Moreton drafted the manuscript, analyzed the data, and obtained funding. Dr. Santosh reported the imaging, revised the manuscript, and obtained funding. Dr. McArthur managed the patient and revised the manuscript. Prof. Muir managed the patient, revised the manuscript, and obtained funding.

Study funding: The first MRI scan was funded by a project grant award from the Chief Scientists Office (ETM/244).

Disclosure: The authors report no disclosures relevant to the manuscript. Go to Neurology.org for full disclosures.

1. Schon F, Martin RJ, Prevett M, Clough C, Enevoldson TP, Markus HS. CADASIL coma: an underdiagnosed acute encephalopathy. *Journal of Neurology, Neurosurgery & Psychiatry* 2003;74:249-252.
2. Liem MK, Oberstein SAL, van der Grond J, Ferrari MD, Haan J. CADASIL and migraine: A narrative review. *Cephalalgia* 2010;30:1284-1289.
3. Eikermann-Haerter K, Yuzawa I, Dilekoz E, Joutel A, Moskowitz MA, Ayata C. Cerebral autosomal dominant arteriopathy with subcortical infarcts and leukoencephalopathy syndrome mutations increase susceptibility to spreading depression. *Annals of Neurology* 2011;69:413-418.
4. Østergaard L, Dreier JP, Hadjikhani N, Jespersen SN, Dirnagl U, Dalkara T. Neurovascular Coupling During Cortical Spreading Depolarization and - Depression. *Stroke* 2015;46:1392-1401.
5. Tfelt-Hansen P, Thorbjørn Jensen L, Olesen J. Delayed hyperperfusion following migraine with a prolonged aphasic aura in a patient with CADASIL. *Cephalalgia* 2008;28:899-902.
6. Lindahl AJ, Allder S, Jefferson D, Allder S, Moody A, Martel A. Prolonged hemiplegic migraine associated with unilateral hyperperfusion on perfusion weighted magnetic resonance imaging. *Journal of Neurology, Neurosurgery & Psychiatry* 2002;73:202-203.
7. Deibler AR, Pollock JM, Kraft RA, Tan H, Burdette JH, Maldjian JA. Arterial Spin-Labeling in Routine Clinical Practice, Part 3: Hyperperfusion Patterns. *American Journal of Neuroradiology* 2008;29:1428-1435.

Appendix 2

Transcranial Doppler Ultrasound (with Carbon Dioxide challenge) Standard Operating Procedure.

Scope and application

This standard operating procedure describes the procedure for the operation of the transcranial Doppler ultrasound system with carbon dioxide challenge. Transcranial Doppler ultrasound allows the assessment of blood flow velocity in the intracranial blood vessels, and when combined with administration of carbon dioxide it allows to measurement of cerebrovascular reactivity.

Summary of method

The patient lies supine. Pulse, blood pressure and oxygen saturation is recorded. Ultrasound jelly is applied to the temples. The middle cerebral artery is identified bilaterally and the ultrasound probes are secured with the head harness. An oxygen mask is applied to the patient, and the gas monitoring line is attached to the remote monitor.

3 minutes of blood flow is recorded whilst the patient breathes normal air. Carbon dioxide mixture is then administered to the patient for 3 minutes, with continuous recording of blood flow. Pulse and blood pressure is also measured half way through and at the end of 3 minutes. Then the patient breathes air for a further 3 minutes.

Equipment and Supplies

Transcranial Doppler ultrasound machine
 2 ultrasound 4Hz probes
 Ultrasound jelly
 Head harness
 6% CO₂/air mixture (BOC Medical, Manchester, UK, Medical Special's Licence Number ML/0735/01).
 Capnograph or Philips monitor
 Blood pressure cuff
 Pulse oximeter
 Gas monitoring line
 Oxygen bubble tubing
 Anaesthetic mask
 Oxygen connector
 Anaesthetic mask harness
 External USB/CD/hard drive
 Timer

Duration of test

Preparation: 10min

Normocapnia: 3min, Hypercapnia 3min, Normocapnia 3min

Health and Safety

This is a non-invasive procedure and transcranial ultrasound is safe. Administration of carbon dioxide can cause anxiety, headache and nausea in a small number of patients.

Quality Control

The TCD is maintained by the Clinical Physics Department of the Southern General Hospital.

Medical gases are the responsibility of the Pharmacy Department.

Procedure

Pre patient arrival

Set up carbon dioxide cylinder as instructed

Ensure patient monitoring equipment is available.

Attach catheter mount to hypercapnia circuit.

Attach cylinder to circuit via oxygen tubing and an oxygen stem connector.

Patient Positioning

Perform with the patient semi-supine.

Allow the patient to rest in this position for 5min.

Setting up patient monitoring

Attach the patient to the observation machine.

Attach blood pressure cuff to patient's non-dominant arm.

Attach pulse oximeter to patient's other finger.

Record a baseline BP, pulse rate and oxygenation.

Identifying the cerebral vessels

Start the Examination

Press POWER button

Press START (Change patient info/Begin exam)

Select NEW PATIENT and press ENTER.

Type in the patient information (initials, study number...CAD001)

Press ENTER when finished entering patient information.

Select BEGIN EXAM.

Set POWER to 50%.

Set DEPTH to 50mm.

Locate the blood vessel

Apply ultrasound gel to patient's temples.

Place probe above right zygomatic arch and aim slightly upward and anterior to the contralateral ear/window.

Identify MCA flow (toward, 32-82cm/s, depth 45-65mm).

Adjust DEPTH into the desired flow band.

Label the vessel with the VESSEL button. Press ENTER to select the desired vessel.

Fix probes to the harness and ensure position is maintained.

Mark the position on the CRF of the MCA.

Repeat to identify the left MCA.

Increase or decrease POWER as needed but try and use minimum necessary to achieve a good signal.

Selecting trend data

SETUP

Setup / Analog Output

Datastream Output Submenu

Enable "CSV File Output" feature.

The datastream for the entire exam will be saved as a CSV file.

Recording a Study

Attach the mask (and filter) to the patient with the harness.

Attach gas sampling line to filter to record inspired and expired gases.

Normocapnia Baseline

Go to recording screen.

Note the time.

Ensure both MCAs are seen and a steady baseline is being achieved.

Note the time and set a timer for 3min (3min of **NORMOCAPNIA**).

Record a blood pressure during this time.

Hypercapnia Trial

Connect the mask to the circuit.

Warn the patient you will be starting carbon dioxide.

Switch on the cylinder and note time.

Give carbon dioxide and record **3 MINUTES OF HYPERCAPNIA**.

Measure BP at 90 seconds and 3min.

Observe heart rate and oxygenation during this time.

Ask the patient how they feel and stop if they feel unwell.

Stop carbon dioxide at 3minutes.

Normocapnia Baseline 2

Keep mask on but disconnect circuit.

Record data for a further **3 MINUTES OF NORMOCAPNIA**

Finish

Remove the mask and the TCD.

Allow the patient to recover.

Decide on the basis of patient's tolerance, BP and pulse whether the patient should undergo MRI with TCD.

Data Collection

Saving the TCD data

Go to the FILES list and ensure internal disk is highlighted.

Highlight the file you wish to export.

Press EXPORT.

Follow the instructions on the system.

Export to a CD-R.

Label CD with subject number and visit number (baseline, Y1 or Y2).

List of References

- AASLID, R., LINDEGAARD, K. F., SORTEBERG, W. & NORNES, H. 1989. Cerebral autoregulation dynamics in humans. *Stroke*, 20, 45-52.
- ADDICOTT, M. A., YANG, L. L., PEIFFER, A. M., BURNETT, L. R., BURDETTE, J. H., CHEN, M. Y., HAYASAKA, S., KRAFT, R. A., MALDJIAN, J. A. & LAURIENTI, P. J. 2009. The effect of daily caffeine use on cerebral blood flow: How much caffeine can we tolerate? *Human Brain Mapping*, 30, 3102-14.
- ADIB-SAMII, P., BRICE, G., MARTIN, R. J. & MARKUS, H. S. 2010. Clinical Spectrum of CADASIL and the Effect of Cardiovascular Risk Factors on Phenotype. *Stroke*, 41, 630-634.
- AINSLIE, P. N. & DUFFIN, J. 2009. Integration of cerebrovascular CO₂ reactivity and chemoreflex control of breathing: mechanisms of regulation, measurement, and interpretation. *American Journal of Physiology - Regulatory, Integrative and Comparative Physiology*, 296, R1473-R1495.
- ALBERI, L., HOEY, S. E., BRAI, E., SCOTTI, A. L. & MARATHE, S. 2013. Notch signaling in the brain: In good and bad times. *Ageing Research Reviews*, 12, 801-814.
- ALUNNI, A., KRECSMARIK, M., BOSCO, A., GALANT, S., PAN, L., MOENS, C. B. & BALLY-CUIF, L. 2013. Notch3 signaling gates cell cycle entry and limits neural stem cell amplification in the adult pallium. *Development*, 140, 3335-3347.
- AMBERLA, K., WÄLJAS, M., TUOMINEN, S., ALMKVIST, O., PÖYHÖNEN, M., TUISKU, S., KALIMO, H. & VIITANEN, M. 2004. Insidious Cognitive Decline in CADASIL. *Stroke*, 35, 1598-1602.
- ANDERSON, T. J. & PHILLIPS, S. A. 2015. Assessment and Prognosis of Peripheral Artery Measures of Vascular Function. *Progress in Cardiovascular Diseases*, 57, 497-509.
- ANDREWS, N. P., PRASAD, A. & QUYYUMI, A. A. 2001. N-acetylcysteine improves coronary and peripheral vascular function. *Journal of the American College of Cardiology*, 37, 117-123.
- ANNUNEN-RASILA, J., FINNILÄ, S., MYKKÄNEN, K., MOILANEN, J., VEIJOLA, J., PÖYHÖNE, M., VIITANEN, M., KALIMO, H. & MAJAMAA, K. 2006. Mitochondrial DNA sequence variation and mutation rate in patients with CADASIL. *Neurogenetics*, 7, 185-194.
- AOYAMA, T., TYNAN, K., DIETZ, H. C., FRANCKE, U. & FURTHMAYR, H. 1993. Missense mutations impair intracellular processing of fibrillin and microfibril assembly in Marfan syndrome. *Human Molecular Genetics*, 2, 2135-2140.
- ARBOLEDA-VELASQUEZ, J. F., LOPERA, F., LOPEZ, E., FROSCH, M. P., SEPULVEDA-FALLA, D., GUTIERREZ, J. E., VARGAS, S., MEDINA, M., MARTINEZ DE ARRIETA, C., LEBO, R. V., SLAUGENHAUPT, S. A., BETENSKY, R. A., VILLEGAS, A., ARCOS-BURGOS, M., RIVERA, D., RESTREPO, J. C. & KOSIK, K. S. 2002. C455R notch3 mutation in a Colombian CADASIL kindred with early onset of stroke. *Neurology*, 59, 277-279.
- ARBOLEDA-VELASQUEZ, J. F., MANENT, J., LEE, J. H., TIKKA, S., OSPINA, C., VANDERBURG, C. R., FROSCH, M. P., RODRÍGUEZ-FALCÓN, M., VILLEN, J., GYGI, S., LOPERA, F., KALIMO, H., MOSKOWITZ, M. A., AYATA, C., LOUVI, A. & ARTAVANIS-TSAKONAS, S. 2011. Hypomorphic Notch 3 alleles link Notch signaling to ischemic cerebral small-vessel disease. *Proceedings of the National Academy of Sciences*.

- ARBOLEDA-VELASQUEZ, J. F., RAMPAL, R., FUNG, E., DARLAND, D. C., LIU, M., MARTINEZ, M. C., DONAHUE, C. P., NAVARRO-GONZALEZ, M. F., LIBBY, P., D'AMORE, P. A., AIKAWA, M., HALTIWANGER, R. S. & KOSIK, K. S. 2005. CADASIL mutations impair Notch3 glycosylation by Fringe. *Human Molecular Genetics*, 14, 1631-1639.
- ARTAVANIS-TSAKONAS, S., RAND, M. D. & LAKE, R. J. 1999. Notch Signaling: Cell Fate Control and Signal Integration in Development. *Science*, 284, 770-776.
- AUER, D. P., SCHIRMER, T., HEIDENREICH, J. O., HERZOG, J., PÜTZ, B. & DICHGANS, M. 2001. Altered white and gray matter metabolism in CADASIL. *Neurology*, 56, 635-642.
- AY, H., OLIVEIRA-FILHO, J., BUONANNO, F. S., EZZEDDINE, M., SCHAEFER, P. W., RORDORF, G., SCHWAMM, L. H., GONZALEZ, R. G. & KOROSHETZ, W. J. 1999. Diffusion-Weighted Imaging Identifies a Subset of Lacunar Infarction Associated With Embolic Source. *Stroke*, 30, 2644-2650.
- AYATA, C. 2010. CADASIL: Experimental insights from animal models. *Stroke*, 41, S129-S134.
- BARTELINK, M. L., WOLLERSHEIM, H., THEEUWES, A., VAN DUREN, D. & THIEN, T. 1990. Changes in skin blood flow during the menstrual cycle: the influence of the menstrual cycle on the peripheral circulation in healthy female volunteers. *Clinical Science*, 78, 527-532.
- BARTKOVA, A., OPAVSKY, R., SANTAVA, A., HLUSTIK, P., HERZIG, R., OBEREIGNERU, K., VLACHOVA, I., SANAK, D. & KANOVSKY, P. 2010. CADASIL: Migraine with aura, stroke like episodes and Reynaud's phenomenon in the clinical picture. *European Journal of Neurology*, 17, 610.
- BASTOS-LEITE, A. J., KUIJER, J. P. A., ROMBOUTS, S. A. R. B., SANZ-ARIGITA, E., VAN STRAATEN, E. C., GOUW, A. A., VAN DER FLIER, W. M., SCHELTENS, P. & BARKHOF, F. 2008. Cerebral Blood Flow by Using Pulsed Arterial Spin-Labeling in Elderly Subjects with White Matter Hyperintensities. *American Journal of Neuroradiology*, 29, 1296-1301.
- BASU, S., SRINIVASAN, D. K., YANG, K., RAINA, H., BANERJEE, S., ZHANG, R., FISHER, S. A. & PROWELLER, A. 2013. Notch Transcriptional Control of Vascular Smooth Muscle Regulatory Gene Expression and Function. *Journal of Biological Chemistry*, 288, 11191-11202.
- BATTISTI-CHARBONNEY, A., FISHER, J. & DUFFIN, J. 2011. The cerebrovascular response to carbon dioxide in humans. *The Journal of Physiology*, 589, 3039-3048.
- BAUDRIMONT, M., DUBAS, F., JOUTEL, A., TOURNIER-LASSERVE, E. & BOUSSER, M. G. 1993. Autosomal dominant leukoencephalopathy and subcortical ischemic stroke. A clinicopathological study. *Stroke*, 24, 122-125.
- BEN-SHLOMO, Y., SPEARS, M., BOUSTRED, C., MAY, M., ANDERSON, S. G., BENJAMIN, E. J., BOUTOUYRIE, P., CAMERON, J., CHEN, C.-H., CRUICKSHANK, J. K., HWANG, S.-J., LAKATTA, E. G., LAURENT, S., MALDONADO, J., MITCHELL, G. F., NAJJAR, S. S., NEWMAN, A. B., OHISHI, M., PANNIER, B., PEREIRA, T., VASAN, R. S., SHOKAWA, T., SUTTON-TYRELL, K., VERBEKE, F., WANG, K.-L., WEBB, D. J., WILLUM HANSEN, T., ZOUNGAS, S., MCENIERY, C. M., COCKCROFT, J. R. & WILKINSON, I. B. 2014. Aortic Pulse Wave Velocity Improves Cardiovascular Event Prediction: An Individual Participant Meta-Analysis of Prospective Observational Data From 17,635 Subjects. *Journal of the American College of Cardiology*, 63, 636-646.

- BENGTSSON, J., BAKE, B., JOHANSSON, Å. & BENGTSON, J. P. 2001. End-tidal to arterial oxygen tension difference as an oxygenation index. *Acta Anaesthesiologica Scandinavica*, 45, 357-363.
- BENJAMIN, E. J., LARSON, M. G., KEYES, M. J., MITCHELL, G. F., VASAN, R. S., KEANEY, J. F., LEHMAN, B. T., FAN, S., OSYPIUK, E. & VITA, J. A. 2004. Clinical Correlates and Heritability of Flow-Mediated Dilation in the Community: The Framingham Heart Study. *Circulation*, 109, 613-619.
- BIOMARKERS DEFINITIONS WORKING GROUP 2001. Biomarkers and surrogate endpoints: Preferred definitions and conceptual framework. *Clinical Pharmacology & Therapeutics*, 69, 89-95.
- BOTS, M. L., HOES, A. W., KOUDSTAAL, P. J., HOFMAN, A. & GROBBEE, D. E. 1997. Common Carotid Intima-Media Thickness and Risk of Stroke and Myocardial Infarction. *Circulation*, 96, 1432-1437.
- BOULOS, N., HELLE, F., DUSSAULE, J. C., PLACIER, S., MILLIEZ, P., DJUDJAJ, S., GUERROT, D., JOUTEL, A., RONCO, P., BOFFA, J. J. & CHATZIANTONIOU, C. 2011. Notch3 Is Essential for Regulation of the Renal Vascular Tone. *Hypertension*, 57, 1176-1182.
- BRANDES, R. P. 2014. Endothelial Dysfunction and Hypertension. *Hypertension*, 64, 924-928.
- BRIAN, J. E. J. 1998. Carbon Dioxide and the Cerebral Circulation. *Anesthesiology*, 88, 1365-1386.
- BRIGHT, M. G. & MURPHY, K. 2013. Reliable quantification of BOLD fMRI cerebrovascular reactivity despite poor breath-hold performance. *NeuroImage*, 83, 559-568.
- BROTT, T., ADAMS, H. P., OLINGER, C. P., MARLER, J. R., BARSAN, W. G., BILLER, J., SPILKER, J., HOLLERAN, R., EBERLE, R. & HERTZBERG, V. 1989. Measurements of acute cerebral infarction: a clinical examination scale. *Stroke*, 20, 864-870.
- BRUENING, R., DICHGANS, M., BERCHTENBREITER, C., YOUSRY, T., SEELOS, K. C., WU, R. H., MAYER, M., BRIX, G. & REISER, M. 2001. Cerebral Autosomal Dominant Arteriopathy with Subcortical Infarcts and Leukoencephalopathy: Decrease in Regional Cerebral Blood Volume in Hyperintense Subcortical Lesions Inversely Correlates with Disability and Cognitive Performance. *American Journal of Neuroradiology*, 22, 1268-1274.
- BRULIN, P., GODFRAIND, C., LETEURTRE, E. & RUCHOUX, M. M. 2002. Morphometric analysis of ultrastructural vascular changes in CADASIL: analysis of 50 skin biopsy specimens and pathogenic implications. *Acta Neuropathologica*, 104, 241-248.
- BUFFON, F., PORCHER, R., HERNANDEZ, K., KURTZ, A., POINTEAU, S., VAHEDI, K., BOUSSER, M. G. & CHABRIAT, H. 2006. Cognitive profile in CADASIL. *Journal of Neurology, Neurosurgery & Psychiatry*, 77, 175-180.
- BULTE, D. P., CHIARELLI, P. A., WISE, R. G. & JEZZARD, P. 2006. Cerebral perfusion response to hyperoxia. *Journal of Cerebral Blood Flow & Metabolism*, 27, 69-75.
- BUTLER, P. M. 2013. A Stroke of Bad Luck: CADASIL and Friedrich Nietzsche's "Dementia" or Madness. In: MCNAMARA, P. (ed.) *Dementia: History and Incidence*. Oxford: ABC-CLIO, LLC.
- CAMPBELL, I. D. & BORK, P. 1993. Epidermal growth factor-like modules. *Current Opinion in Structural Biology*, 3, 385-392.
- CAMPOLO, J., DE MARIA, R., FRONTALI, M., TARONI, F., INZITARI, D., FEDERICO, A., ROMANO, S., PUCA, E., MARIOTTI, C., TOMASELLO, C., PANTONI, L., PESCHINI, F., DOTTI, M. T., STROMILLO, M. L., DE STEFANO, N., TAVANI, A.

- & PARODI, O. 2011. Impaired vasoreactivity in mildly disabled CADASIL patients. *Journal of Neurology, Neurosurgery & Psychiatry*.
- CAMPOLO, J., DE MARIA, R., MARIOTTI, C., TOMASELLO, C., PAROLINI, M., FRONTALI, M., INZITARI, D., VALENTI, R., FEDERICO, A., TARONI, F. & PARODI, O. 2013. Is the oxidant/antioxidant status altered in CADASIL patients? *PLoS ONE [Electronic Resource]*, 8, e67077.
- CANTIN, S., VILLIEN, M., MOREAUD, O., TROPRES, I., KEIGNART, S., CHIPON, E., LE BAS, J. F., WARNKING, J. & KRAINIK, A. 2011. Impaired cerebral vasoreactivity to CO₂ in Alzheimer's disease using BOLD fMRI. *Neuroimage*, 58, 579-587.
- CAPLAN, L. R. 1995. Binswanger's disease--revisited. *Neurology*, 45, 626-633.
- CARARE, R. O., HAWKES, C. A., JEFFREY, M., KALARIA, R. N. & WELLER, R. O. 2013. Review: Cerebral amyloid angiopathy, prion angiopathy, CADASIL and the spectrum of protein elimination failure angiopathies (PEFA) in neurodegenerative disease with a focus on therapy. *Neuropathology and Applied Neurobiology*, 39, 593-611.
- CELERMAJER, D. S., SORENSEN, K. E., GOOCH, V. M., MILLER, SULLIVAN, I. D., LLOYD, J. K., DEANFIELD, J. E. & SPIEGELHALTER, D. J. 1992. Non-invasive detection of endothelial dysfunction in children and adults at risk of atherosclerosis. *The Lancet*, 340, 1111-1115.
- CHABRIAT, H., BOUSSER, M. & PAPPATA, S. 1995. Cerebral autosomal dominant arteriopathy with subcortical infarcts and leukoencephalopathy: a positron emission tomography study in two affected family members. *Stroke*, 26, 1729-1730.
- CHABRIAT, H., HERVÉ, D., DUERING, M., GODIN, O., JOUVENT, E., OPHERK, C., ALILI, N., REYES, S., JABOULEY, A., ZIEREN, N., GUICHARD, J.-P., PACHAI, C., VICAUT, E. & DICHGANS, M. 2016. Predictors of Clinical Worsening in Cerebral Autosomal Dominant Arteriopathy With Subcortical Infarcts and Leukoencephalopathy: Prospective Cohort Study. *Stroke*, 47, 4-11.
- CHABRIAT, H., JOUTEL, A., DICHGANS, M., TOURNIER-LASSERVE, E. & BOUSSER, M. G. 2009. Cadasil. *The Lancet Neurology*, 8, 643-653.
- CHABRIAT, H., LEVY, C., TAILLIA, H., IBA-ZIZEN, M. T., VAHEDI, K., JOUTEL, A., TOURNIER-LASSERVE, E. & BOUSSER, M. G. 1998. Patterns of MRI lesions in CADASIL. *Neurology*, 51, 452-457.
- CHABRIAT, H., MARISSA, R., LEVY, C., VAHEDI, K., TAILLIA, H., IBA-ZIZEN, M. T., JOUTEL, A., TOURNIER-LASSERVE, E. & BOUSSER, M. G. 1999a. Brain stem MRI signal abnormalities in CADASIL. *Stroke*, 30, 457-459.
- CHABRIAT, H., PAPPATA, S., ØSTERGAARD, L., CLARK, C. A., PACHOT-CLOUARD, M., VAHEDI, K., JOBERT, A., LE BIHAN, D. & BOUSSER, M. G. 2000. Cerebral Hemodynamics in CADASIL Before and After Acetazolamide Challenge Assessed With MRI Bolus Tracking. *Stroke*, 31, 1904-1912.
- CHABRIAT, H., PAPPATA, S., POUPON, C., CLARK, C. A., VAHEDI, K., POUPON, F., MANGIN, J. F., PACHOT-CLOUARD, M., JOBERT, A., LE BIHAN, D. & BOUSSER, M. G. 1999b. Clinical Severity in CADASIL Related to Ultrastructural Damage in White Matter : In Vivo Study With Diffusion Tensor MRI. *Stroke*, 30, 2637-2643.
- CHARIDIMOU, A., JÄGER, H. R. & WERRING, D. J. 2012. Cerebral microbleed detection and mapping: Principles, methodological aspects and rationale in vascular dementia. *Experimental Gerontology*.
- CHARLTON, R. A., MORRIS, R. G., NITKUNAN, A. & MARKUS, H. S. 2006. The cognitive profiles of CADASIL and sporadic small vessel disease. *Neurology*, 66, 1523-1526.

- CHEN, C. H., NEVO, E., FETICS, B., PAK, P. H., YIN, F. C. P., MAUGHAN, W. L. & KASS, D. A. 1997. Estimation of Central Aortic Pressure Waveform by Mathematical Transformation of Radial Tonometry Pressure. *Circulation*, 95, 1827-1836.
- CHOI, J. C., KANG, S. Y., KANG, J. H. & PARK, J. K. 2006. Intracerebral hemorrhages in CADASIL. *Neurology*, 67, 2042-2044.
- CHOKSI, V., HUGHES, M., SELWA, L. & HOEFFNER, E. 2005. Transient Neurologic Deficit After Acetazolamide Challenge for Computed Tomography Perfusion Imaging. *Journal of Computer Assisted Tomography*, 29, 278-280.
- CHOWDHURY, T., PETROPOLIS, A., WILKINSON, M., SCHALLER, B., SANDU, N. & CAPPELLANI, R. B. 2014. Controversies in the Anesthetic Management of Intraoperative Rupture of Intracranial Aneurysm. *Anesthesiology Research and Practice*, 2014, 10.
- CIOLLI, L., PESCHINI, F., SALVADORI, E., DEL BENE, A., PRACUCCI, G., POGGESI, A., NANNUCCI, S., VALENTI, R., BASILE, A. M., SQUARZANTI, F., BIANCHI, S., DOTTI, M. T., ADRIANO, E., BALESTRINO, M., FEDERICO, A., GANDOLFO, C., INZITARI, D. & PANTONI, L. 2014. Influence of vascular risk factors and neuropsychological profile on functional performances in CADASIL: results from the Microvascular Leukoencephalopathy Study (MILES). *European Journal of Neurology*, 21, 65-71.
- COGNAT, E., CLEOPHAX, S., DOMENGA-DENIER, V. & JOUTEL, A. 2014. Early white matter changes in CADASIL: evidence of segmental intramyelinic oedema in a pre-clinical mouse model. *Acta Neuropathologica Communications*, 2, 49.
- COLASANTI, A., ESQUIVEL, G., SCHRUERS, K. & GRIEZ, E. 2012. On the psychotropic effects of carbon dioxide. *Current Pharmaceutical Design*, 18, 5627-5637.
- CONNELLY, P. M. 1984. Huntington disease: genetics and epidemiology. *American Journal of Human Genetics*, 36, 506-526.
- CORRETTI, M. C., ANDERSON, T. J., BENJAMIN, E. J., CELERMAJER, D., CHARBONNEAU, F., CREAGER, M. A., DEANFIELD, J., DREXLER, H., GERHARD-HERMAN, M., HERRINGTON, D., VALLANCE, P., VITA, J. & VOGEL, R. 2002. Guidelines for the ultrasound assessment of endothelial-dependent flow-mediated vasodilation of the brachial artery: A report of the International Brachial Artery Reactivity Task Force. *Journal of the American College of Cardiology*, 39, 257-265.
- COVERDALE, N. S., GATI, J. S., OPALEVYCH, O., PERROTTA, A. & SHOEMAKER, J. K. 2014. Cerebral blood flow velocity underestimates cerebral blood flow during modest hypercapnia and hypocapnia. *Journal of Applied Physiology*, 117, 1090-1096.
- CUMURCIUC, R., GUICHARD, J. P., REIZINE, D., GRAY, F., BOUSSER, M. G. & CHABRIAT, H. 2006. Dilation of Virchow-Robin spaces in CADASIL. *European Journal of Neurology*, 13, 187-190.
- D'AGOSTINO, D. P., OLSON, J. E. & DEAN, J. B. 2009. Acute hyperoxia increases lipid peroxidation and induces plasma membrane blebbing in human U87 glioblastoma cells. *Neuroscience*, 159, 1011-1022.
- DABERTRAND, F., KRØIGAARD, C., BONEV, A. D., COGNAT, E., DALSGAARD, T., DOMENGA-DENIER, V., HILL-EUBANKS, D. C., BRAYDEN, J. E., JOUTEL, A. & NELSON, M. T. 2015. Potassium channelopathy-like defect underlies early-stage cerebrovascular dysfunction in a genetic model of small vessel disease. *Proceedings of the National Academy of Sciences*, 112, E796-E805.

- DANI, K. A., SANTOSH, C., BRENNAN, D., MCCABE, C., HOLMES, W. M., CONDON, B., HADLEY, D. M., MACRAE, I. M., SHAW, M. & MUIR, K. W. 2010. T2*-weighted magnetic resonance imaging with hyperoxia in acute ischemic stroke. *Annals of Neurology*, 68, 37-47.
- DAVIS, W. B., RENNARD, S. I., BITTERMAN, P. B. & CRYSTAL, R. G. 1983. Pulmonary Oxygen Toxicity. *New England Journal of Medicine*, 309, 878-883.
- DE GUIO, F., MANGIN, J. F., DUERING, M., ROPELE, S., CHABRIAT, H. & JOUVENT, E. 2015. White matter edema at the early stage of cerebral autosomal-dominant arteriopathy with subcortical infarcts and leukoencephalopathy. *Stroke*, 46, 258-61.
- DE STROOPER, B., ANNAERT, W., CUPERS, P., SAFTIG, P., CRAESSAERTS, K., MUMM, J. S., SCHROETER, E. H., SCHRIJVERS, V., WOLFE, M. S., RAY, W. J., GOATE, A. & KOPAN, R. 1999. A presenilin-1-dependent [gamma]-secretase-like protease mediates release of Notch intracellular domain. *Nature*, 398, 518-522.
- DE VIS, J. B., PETERSEN, E. T., BHOGAL, A., HARTKAMP, N. S., KLIJN, C. J. M., KAPPELLE, L. J. & HENDRIKSE, J. 2015. Calibrated MRI to evaluate cerebral hemodynamics in patients with an internal carotid artery occlusion. *Journal of Cerebral Blood Flow & Metabolism*, 35, 1015-1023.
- DEBETTE, S. & MARKUS, H. S. 2010. The clinical importance of white matter hyperintensities on brain magnetic resonance imaging: systematic review and meta-analysis. *BMJ*, 341.
- DELGADO, J. L., LANDERAS, J., CARBONELL, L. F., PARILLA, J. J., ABAD, L., QUESADA, T., FIOL, G. & HERNÁNDEZ, I. 1999. Effect of N-Acetylcysteine on Vascular Endothelium Function in Aorta from Oophorectomized Rats. *General Pharmacology: The Vascular System*, 32, 23-27.
- DEMCHENKO, I. T., BOSO, A. E., O'NEILL, T. J., BENNETT, P. B. & PIANTADOSI, C. A. 2000. Nitric oxide and cerebral blood flow responses to hyperbaric oxygen. *Journal of Applied Physiology*, 88, 1381-1389.
- DEMPSEY, M. F. & CONDON, B. 2001. Thermal Injuries Associated with MRI. *Clinical Radiology*, 56, 457-465.
- DEPARTMENT OF HEALTH 2007. The National Service Framework for Long-term Conditions.
- DHARMASHANKAR, K. & WIDLANSKY, M. 2010. Vascular Endothelial Function and Hypertension: Insights and Directions. *Current Hypertension Reports*, 12, 448-455.
- DICHGANS, M. 2009. Cognition in CADASIL. *Stroke*, 40, S45-S47.
- DICHGANS, M., FILIPPI, M., BRÜNING, R., IANNUCCI, G., BERCHTENBREITER, C., MINICUCCI, L., UTTNER, I., CRISPIN, A., LUDWIG, H., GASSER, T. & YOUSRY, T. A. 1999. Quantitative MRI in CADASIL. *Neurology*, 52, 1361-1361.
- DICHGANS, M., HOLTMANNSPÖTTER, M., HERZOG, J., PETERS, N., BERGMANN, M. & YOUSRY, T. A. 2002. Cerebral Microbleeds in CADASIL. *Stroke*, 33, 67-71.
- DICHGANS, M., LUDWIG, H., MÜLLER-HÖCKER, J., MESSERSCHMIDT, A. & GASSER, T. 2000. Small in-frame deletions and missense mutations in CADASIL: 3D models predict misfolding of Notch3 EGF-like repeat domains. *European Journal of Human Genetics*, 8, 280-285.
- DICHGANS, M., MAYER, M., UTTNER, I., BRÜNING, R., MÜLLER-HÖCKER, J., RUNGGER, G., EBKE, M., KLOCKGETHER, T. & GASSER, T. 1998. The phenotypic spectrum of CADASIL: Clinical findings in 102 cases. *Annals of Neurology*, 44, 731-739.

- DOMENGA, V. R., FARDOUX, P., LACOMBE, P., MONET, M., MACIAZEK, J., KREBS, L. T., KLONJKOWSKI, B., BERROU, E., MERICKSKAY, M., LI, Z., TOURNIER-LASSERVE, E., GRIDLEY, T. & JOUTEL, A. 2004. Notch3 is required for arterial identity and maturation of vascular smooth muscle cells. *Genes & Development*, 18, 2730-2735.
- DONAHUE, M. J., STROTHER, M. K. & HENDRIKSE, J. 2012. Novel MRI Approaches for Assessing Cerebral Hemodynamics in Ischemic Cerebrovascular Disease. *Stroke*, 43, 903-915.
- DONAHUE, M. J., VAN LAAR, P. J., VAN ZIJL, P. C., STEVENS, R. D. & HENDRIKSE, J. 2009. Vascular space occupancy (VASO) cerebral blood volume-weighted MRI identifies hemodynamic impairment in patients with carotid artery disease. *Journal of Magnetic Resonance Imaging*, 29, 718-724.
- DOTTI, M. T., DE STEFANO, N., BIANCHI, S., MALANDRINI, A., BATTISTI, C., CARDAIOLI, E. & FEDERICO, A. 2004. A Novel NOTCH3 Frameshift Deletion and Mitochondrial Abnormalities in a Patient With CADASIL. *Archives of Neurology*, 61, 942-945.
- DUBROCA, C., LACOMBE, P., DOMENGA, V. R., MACIAZEK, J., LEVY, B., TOURNIER-LASSERVE, E., JOUTEL, A. & HENRION, D. 2005. Impaired Vascular Mechanotransduction in a Transgenic Mouse Model of CADASIL Arteriopathy. *Stroke*, 36, 113-117.
- DUERING, M., CSANADI, E., GESIERICH, B., JOUVENT, E., HERVÉ, D., SEILER, S., BELAROUSSI, B., ROPELE, S., SCHMIDT, R., CHABRIAT, H. & DICHGANS, M. 2013. Incident lacunes preferentially localize to the edge of white matter hyperintensities: insights into the pathophysiology of cerebral small vessel disease. *Brain*, 136, 2717-2726.
- DUERING, M., ZIEREN, N., HERVÉ, D., JOUVENT, E., PETERS, N., PACHAI, C., OPPERK, C., CHABRIAT, H. & DICHGANS, M. 2011. Strategic role of frontal white matter tracts in vascular cognitive impairment: a voxel-based lesion-symptom mapping study in CADASIL. *Brain*.
- DUGGAN, M. & KAVANAGH, B. 2005. Pulmonary Atelectasis: A Pathogenic Perioperative Entity. *American Society of Anesthesiologists*, 102, 838 - 854.
- DUNNEN, J. T. D. & ANTONARAKIS, S. E. 2000. Mutation nomenclature extensions and suggestions to describe complex mutations: A discussion. *Human Mutation*, 15, 7-12.
- EDVINSSON, L. & KRAUSE, D. N. 2002. *Cerebral blood flow and metabolism*, Philadelphia; London, Lippincott Williams & Wilkins.
- ELLINGSEN, I., HAUGE, A., NICOLAYSEN, G., THORESEN, M. & WALLOE, L. 1987. Changes in human cerebral blood flow due to step changes in PAO₂ and PACO₂. *Acta Physiologica Scandinavica*, 129, 157-163.
- ENGEDAL, T. S., MORETON, F. C., CULLEN, B., BOLDSSEN, J. K., ESKILDSEN, S. F., MIKKELSEN, I. K., HANSEN, M. B., MOURIDSEN, K., MUIR, K. W. & OSTERGAARD, L. 2015. The role of microvascular dysfunction in CADASIL. *European Stroke Organisation Conference*. Glasgow: International Journal of Stroke.
- ENZINGER, C., FAZEKAS, F., MATTHEWS, P. M., ROPELE, S., SCHMIDT, H., SMITH, S. & SCHMIDT, R. 2005. Risk factors for progression of brain atrophy in aging. *Neurology*, 64, 1704-1711.
- ESKEY, C. J. & SANELLI, P. C. 2005. Perfusion Imaging of Cerebrovascular Reserve. *Neuroimaging Clinics of North America*, 15, 367-381.
- EUROPEAN COMMISSION 2008. Communication on Rare Diseases: Europe's challenges. Brussels.

- FARACO, C. C., STROTHER, M. K., DETHRAGE, L. M., JORDAN, L., SINGER, R., CLEMMONS, P. F. & DONAHUE, M. J. 2015. Dual Echo Vessel-Encoded ASL for Simultaneous BOLD and CBF Reactivity Assessment in Patients with Ischemic Cerebrovascular Disease. *Magnetic resonance in medicine*, 73, 1579-1592.
- FARLING, P., BULLEN, K., BRITTON, J., DARWENT, G., DEWILDE, J., GILES, S., GODDARD, P., KING, S., MCBRIEN, M., MCDONALD, P., MENON, D., RIDGWAY, J., SURY, M. & WILSON, S. 2002. *Provision of anaesthetic services in magnetic resonance units*, London, The Association of Anaesthetists of Great Britain and Ireland.
- FARLING, P. A., FLYNN, P. A., DARWENT, G., DE WILDE, J., GRAINGER, D., KING, S., MCBRIEN, M. E., MENON, D. K., RIDGWAY, J. P., SURY, M., THORNTON, J. & WILSON, S. R. 2010. Safety in magnetic resonance units: an update. *Anaesthesia*, 65, 766-770.
- FEDERICO, A., BIANCHI, S. & DOTTI, M. T. 2005. The spectrum of mutations for CADASIL diagnosis. *Neurological Sciences*, 26, 117-124.
- FEEKES, J. A., HSU, S.-W., CHALOUPEK, J. C. & CASSELL, M. D. 2005. Tertiary microvascular territories define lacunar infarcts in the basal ganglia. *Annals of Neurology*, 58, 18-30.
- FIERSTRA, J., CONKLIN, J., KRINGS, T., SLESSAREV, M., HAN, J. S., FISHER, J. A., TERBRUGGE, K., WALLACE, M. C., TYMIANSKI, M. & MIKULIS, D. J. 2011. Impaired peri-nidal cerebrovascular reserve in seizure patients with brain arteriovenous malformations. *Brain*, 134, 100-109.
- FIERSTRA, J., SOBCZYK, O., BATTISTI-CHARBONNEY, A., MANDELL, D. M., POUBLANC, J., CRAWLEY, A. P., MIKULIS, D. J., DUFFIN, J. & FISHER, J. A. 2013. Measuring cerebrovascular reactivity: what stimulus to use? *The Journal of Physiology*, 591, 5809-5821.
- FILIPPI, M. & GROSSMAN, R. I. 2002. MRI techniques to monitor MS evolution. *Neurology*, 58, 1147-1153.
- FILIPPI, M., INGLESE, M., ROVARIS, M., SORMANI, M. P., HORSFIELD, M. A., IANNUCCI, G., COLOMBO, B. & COMI, G. 2000. Magnetization transfer imaging to monitor the evolution of MS. *Neurology*, 55, 940-946.
- FIRBANK, M. J., HE, J., BLAMIRE, A. M., SINGH, B., DANSON, P., KALARIA, R. N. & O'BRIEN, J. T. 2011. Cerebral blood flow by arterial spin labeling in poststroke dementia. *Neurology*, 76, 1478-1484.
- FISHER, C. M. 1965. Lacunes: Small, deep cerebral infarcts. *Neurology*, 15, 774-784.
- FISHER, C. M. 1982. Lacunar strokes and infarcts: a review. *Neurology*, 32, 871-876.
- FOUILLADE, C., CHABRIAT, H., RIAANT, F., MINE, M. L., ARNOUD, M., MAGY, L., BOUSSER, M. G., TOURNIER-LASSERVE, E. & JOUTEL, A. 2008. Activating NOTCH3 mutation in a patient with small-vessel-disease of the Brain. *Human Mutation*, 29, 452-452.
- FUJIWARA, Y., MIZUNO, T., OKUYAMA, C., NAGAKANE, Y., WATANABE-HOSOMI, A., KONDO, M., KURIYAMA, N., TOKUDA, T., MATSUSHIMA, S., NISHIMURA, T. & NAKAGAWA, M. 2012. Simultaneous Impairment of Intracranial and Peripheral Artery Vasoreactivity in CADASIL Patients. *Cerebrovascular Diseases*, 33, 128-134.
- FUTRELL, N. 2004. Lacunar Infarction: Embolism is the Key. *Stroke*, 35, 1778-1779.
- GAO, Y.-Z., ZHANG, J.-J., LIU, H., WU, G.-Y., XIONG, L. & SHU, M. 2013. Regional cerebral blood flow and cerebrovascular reactivity in alzheimer's

- disease and vascular dementia assessed by arterial spinlabeling magnetic resonance imaging. *Current Neurovascular Research*, 10, 49-53.
- GESIERICH, B., OPPERK, C., ROSAND, J., GONIK, M., MALIK, R., JOUVENT, E., HERVÉ, D., ADIB-SAMII, P., BEVAN, S., PIANESE, L., SILVESTRI, S., DOTTI, M. T., DE STEFANO, N., VAN DER GROND, J., BOON, E. M. J., PESCHINI, F., ROST, N., PANTONI, L., LESNIK OBERSTEIN, S. A., FEDERICO, A., RAGNO, M., MARKUS, H. S., TOURNIER-LASSERVE, E., CHABRIAT, H., DICHGANS, M., DUERING, M. & EWERS, M. 2016. APOE ϵ 2 is associated with white matter hyperintensity volume in CADASIL. *Journal of Cerebral Blood Flow & Metabolism*, 36, 199-203.
- GLODZIK, L., RUSINEK, H., BRYNS, M., TSUI, W. H., SWITALSKI, R., MOSCONI, L., MISTUR, R., PIRRAGLIA, E., DE, S. S., LI, Y., GOLDSKY, A. & DE LEON, M. J. 2011. Framingham cardiovascular risk profile correlates with impaired hippocampal and cortical vasoreactivity to hypercapnia. *Journal of Cerebral Blood Flow & Metabolism*, 31, 671-679.
- GOBRON, C., VAHEDI, K., VICAUT, E., STUCKER, O., LAEMMEL, E., BAUDRY, N., BOUSSER, M. G. & CHABRIAT, H. 2006. Characteristic features of in vivo skin microvascular reactivity in CADASIL. *Journal of Cerebral Blood Flow & Metabolism*, 27, 250-257.
- GOLANOV, E. V. & REIS, D. J. 1997. Oxygen and Cerebral Blood Flow. In: CAPLAN, L., REIS, D., SIESJO, B., WEIR, B. & WELCH, K. M. (eds.) *Primer on Cerebrovascular Diseases*. Academic Press.
- GREENBERG, S. M., SALMAN, R. A.-S., BIESSELS, G. J., VAN BUCHEM, M., CORDONNIER, C., LEE, J.-M., MONTANER, J., SCHNEIDER, J. A., SMITH, E. E., VERNOOIJ, M. & WERRING, D. J. 2014. Outcome markers for clinical trials in cerebral amyloid angiopathy. *The Lancet Neurology*, 13, 419-428.
- GREENBERG, S. M., VERNOOIJ, M. W., CORDONNIER, C., VISWANATHAN, A., AL-SHAHI SALMAN, R., WARACH, S., LAUNER, L. J., VAN BUCHEM, M. A. & BRETELER, M. M. 2009. Cerebral microbleeds: a guide to detection and interpretation. *The Lancet Neurology*, 8, 165-174.
- GREGOIRE, S. M., CHAUDHARY, U. J., BROWN, M. M., YOUSRY, T. A., KALLIS, C., JÄGER, H. R. & WERRING, D. J. 2009. The Microbleed Anatomical Rating Scale (MARS): Reliability of a tool to map brain microbleeds. *Neurology*, 73, 1759-1766.
- GRUBB, R. L., RAICHLE, M. E., EICHLING, J. O. & TER-POGOSSIAN, M. M. 1974. The Effects of Changes in PaCO₂ Cerebral Blood Volume, Blood Flow, and Vascular Mean Transit Time. *Stroke*, 5, 630-639.
- GUARANHA, M. S. B., GARZON, E., BUCHPIGUEL, C. A., TAZIMA, S., YACUBIAN, E. M. T. & SAKAMOTO, A. C. 2005. Hyperventilation Revisited: Physiological Effects and Efficacy on Focal Seizure Activation in the Era of Video-EEG Monitoring. *Epilepsia*, 46, 69-75.
- GUERROT, D., FRANCOIS, A., BOFFA, J. J., BOULOS, N., HANOY, M., LEGALLICIER, B., TRIQUENOT-BAGAN, A., GUYANT-MARECHAL, L., LAQUERRIERE, A., FREQUIN-BOUILLAND, C., RONCO, P. & GODIN, M. 2008. Nephroangiosclerosis in Cerebral Autosomal Dominant Arteriopathy With Subcortical Infarcts and Leukoencephalopathy: Is NOTCH3 Mutation the Common Culprit? *American Journal of Kidney Diseases*, 52, 340-345.
- GUEY, S., MAWET, J., HERVÉ, D., DUERING, M., GODIN, O., JOUVENT, E., OPPERK, C., ALILI, N., DICHGANS, M. & CHABRIAT, H. 2015. Prevalence and characteristics of migraine in CADASIL. *Cephalalgia*.
- GUNDA, B., HERVÉ, D., GODIN, O., BRUNO, M., REYES, S., ALILI, N., OPPERK, C., JOUVENT, E., DUERING, M., BOUSSER, M. G., DICHGANS, M. & CHABRIAT, H. 2011. Effects of Gender on the Phenotype of CADASIL. *Stroke*.

- GUNDERSEN, H., VAN WAGENINGEN, H. & GRÜNER, R. 2013. Alcohol-Induced Changes in Cerebral Blood Flow and Cerebral Blood Volume in Social Drinkers. *Alcohol and Alcoholism*, 48, 160-165.
- GUO, Z., VIITANEN, M., FRATIGLIONI, L. & WINBLAD, B. 1996. Low blood pressure and dementia in elderly people: the Kungsholmen project. *British Medical Journal*, 312, 805-808.
- HACHINSKI, V., IADECOLA, C., PETERSEN, R. C., BRETELER, M. M., NYENHUIS, D. L., BLACK, S. E., POWERS, W. J., DECARLI, C., MERINO, J. G., KALARIA, R. N., VINTERS, H. V., HOLTZMAN, D. M., ROSENBERG, G. A., WALLIN, A., DICHGANS, M., MARLER, J. R. & LEBLANC, G. G. 2006. National Institute of Neurological Disorders and Stroke-Canadian Stroke Network Vascular Cognitive Impairment Harmonization Standards. *Stroke*, 37, 2220-2241.
- HADDAD, N., IKARD, C., HIATT, K., SHANMUGAM, V. & SCHMIDLEY, J. 2015. Recurrent status epilepticus as the primary neurological manifestation of CADASIL: A case report. *Epilepsy & Behavior Case Reports*, 3, 26-29.
- HALL, C. N., REYNELL, C., GESSLEIN, B., HAMILTON, N. B., MISHRA, A., SUTHERLAND, B. A., O'FARRELL, F. M., BUCHAN, A. M., LAURITZEN, M. & ATTWELL, D. 2014. Capillary pericytes regulate cerebral blood flow in health and disease. *Nature*, 508, 55-60.
- HALL, E. L., DRIVER, I. D., CROAL, P. L., FRANCIS, S. T., GOWLAND, P. A., MORRIS, P. G. & BROOKES, M. J. 2011. The effect of hypercapnia on resting and stimulus induced MEG signals. *NeuroImage*, 58, 1034-1043.
- HAN, J. S., ABOU-HAMDEN, A., MANDELL, D. M., POUBLANC, J., CRAWLEY, A. P., FISHER, J. A., MIKULIS, D. J. & TYMIANSKI, M. 2011. Impact of extracranial-intracranial bypass on cerebrovascular reactivity and clinical outcome in patients with symptomatic moyamoya vasculopathy. *Stroke*, 42, 3047-3054.
- HARITOGLOU, C., HOOPS, J. P., STEFANI, F. H., MEHRAEIN, P., KAMPIK, A. & DICHGANS, M. 2004. Histopathological abnormalities in ocular blood vessels of CADASIL patients. *American Journal of Ophthalmology*, 138, 302-305.
- HARITUNIAN, T., BOULTER, J., HICKS, C., BUHRMAN, J., DISIBIO, G., SHAWBER, C., WEINMASTER, G., NOFZIGER, D. & SCHANEN, C. 2002. CADASIL Notch3 Mutant Proteins Localize to the Cell Surface and Bind Ligand. *Circulation Research*, 90, 506-508.
- HARPER, P. 2002. The epidemiology of Huntington's disease. In: BATES, G., HARPER, P. & JONES, L. (eds.) *Huntington's Disease*. 3 ed. Oxford: Oxford University Press.
- HARPER, P. S., LIM, C. & CRAUFURD, D. 2000. Ten years of presymptomatic testing for Huntington's disease: the experience of the UK Huntington's Disease Prediction Consortium. *Journal of Medical Genetics*, 37, 567-571.
- HARRIS, J. & CHRISTOPHER, C. 2001. CADASIL: Neuropsychological findings in three generations of an affected family. *Journal of the International Neuropsychological Society*, 7, 768-774.
- HEADACHE CLASSIFICATION COMMITTEE OF THE INTERNATIONAL HEADACHE SOCIETY 2013. The International Classification of Headache Disorders, 3rd edition (beta version). *Cephalalgia*, 33, 629-808.
- HEISTAD, D. D. 2001. What's New in the Cerebral Microcirculation? *Microcirculation*, 8, 366-375.
- HEMELSOET, D., HEMELSOET, K. & DEVREESE, D. 2008. The neurological illness of Friedrich Nietzsche. *Acta Neurologica Belgica*, 108, 9-16.
- HENSHALL, T. L., KELLER, A., HE, L., JOHANSSON, B. R., WALLGARD, E., RASCHPERGER, E., MÄE, M. A., JIN, S., BETSHOLTZ, C. & LENDAHL, U.

2015. Notch3 Is Necessary for Blood Vessel Integrity in the Central Nervous System. *Arteriosclerosis, Thrombosis, and Vascular Biology*, 35, 409-420.
- HERRMANN, C. 1997. International experiences with the Hospital Anxiety and Depression Scale-A review of validation data and clinical results. *Journal of Psychosomatic Research*, 42, 17-41.
- HERVÉ, D., GODIN, O., DUFOUIL, C., VISWANATHAN, A., JOUVENT, E., PACHAÏ, C., GUICHARD, J.-P., BOUSSER, M.-G., DICHGANS, M. & CHABRIAT, H. 2009. Three-Dimensional MRI Analysis of Individual Volume of Lacunes in CADASIL. *Stroke*, 40, 124-128.
- HETZEL, A., BRAUNE, S., GUSCHLBAUER, B. & DOHMS, K. 1999. CO₂ Reactivity Testing Without Blood Pressure Monitoring? *Stroke*, 30, 398-401.
- HEYN, C., POUBLANC, J., CRAWLEY, A., MANDELL, D., HAN, J. S., TYMIANSKI, M., TERBRUGGE, K., FISHER, J. A. & MIKULIS, D. J. 2010. Quantification of cerebrovascular reactivity by blood oxygen level - Dependent MR imaging and correlation with conventional angiography in patients with moyamoya disease. *American Journal of Neuroradiology*, 31, 862-867.
- HILLIER, C., COWBURN, P. J., MORTON, J. J., DARGIE, H. J., CLELAND, J. G. F., MCMURRAY, J. J. V. & MCGRATH, J. C. 1999. Structural and functional assessment of small arteries in patients with chronic heart failure. *Clinical Science*, 97, 671-679.
- HOFMANN, J. J. & IRUELA-ARISPE, M. L. 2007. Notch Signaling in Blood Vessels. *Circulation Research*, 100, 1556-1568.
- HOLTMANNSPOTTER, M., PETERS, N., OPPERK, C., MARTIN, D., HERZOG, J., BRUCKMANN, H., SAMANN, P., GSCHWENDTNER, A. & DICHGANS, M. 2005. Diffusion magnetic resonance histograms as a surrogate marker and predictor of disease progression in CADASIL: a two-year follow-up study. *Stroke*, 36, 2559-2565.
- HSU, Y. Y., KUANG, W. C., LIM, K. E. & LIU, H. L. 2010. Breathhold-regulated blood oxygenation level-dependent (BOLD) MRI of human brain at 3 tesla. *Journal of Magnetic Resonance Imaging*, 31, 78-84.
- HUANG, L., YANG, Q., ZHANG, L., CHEN, X., HUANG, Q. & WANG, H. 2010. Acetazolamide improves cerebral hemodynamics in CADASIL. *Journal of the Neurological Sciences*, 292, 77-80.
- HUDAK, M. L., KOEHLER, R. C., ROSENBERG, A. A., TRAYSTMAN, R. J. & JONES, M. D. 1986. Effect of hematocrit on cerebral blood flow. *American Journal of Physiology - Heart and Circulatory Physiology*, 251, H63-H70.
- HUSSAIN, M. B., SINGHAL, S., MARKUS, H. S. & SINGER, D. R. J. 2004. Abnormal Vasoconstrictor Responses to Angiotensin II and Noradrenaline in Isolated Small Arteries From Patients With Cerebral Autosomal Dominant Arteriopathy With Subcortical Infarcts and Leukoencephalopathy (CADASIL). *Stroke*, 35, 853-858.
- IADECOLA, C. 2013. The Pathobiology of Vascular Dementia. *Neuron*, 80, 844-866.
- IANNUCCI, G., DICHGANS, M., ROVARIS, M., BRÜNING, R., GASSER, T., GIACOMOTTI, L., YOUSRY, T. A. & FILIPPI, M. 2001. Correlations Between Clinical Findings and Magnetization Transfer Imaging Metrics of Tissue Damage in Individuals With Cerebral Autosomal Dominant Arteriopathy With Subcortical Infarcts and Leukoencephalopathy. *Stroke*, 32, 643-648.
- IHALAINEN, S., SOLIYMANI, R., IIVANAINEN, E., MYKKANEN, K., SAINIO, A., POYHONEN, M., ELENIS, K., JARVELAINEN, H., KALIMO, H. & BAUMANN, M. 2007. Proteome Analysis of Cultivated Vascular Smooth Muscle Cells from a CADASIL Patient. *Molecular Medicine*, 15, 305-314.

- INTENGAN, H. D., DENG, L. Y., LI, J. S. & SCHIFFRIN, E. L. 1999. Mechanics and Composition of Human Subcutaneous Resistance Arteries in Essential Hypertension. *Hypertension*, 33, 569-574.
- ISHIKO, A., SHIMIZU, A., NAGATA, E., TAKAHASHI, K., TABIRA, T. & SUZUKI, N. 2006. Notch3 ectodomain is a major component of granular osmiophilic material (GOM) in CADASIL. *Acta Neuropathologica*, 112, 333-339.
- ITAMER. 2015. <http://www.itamar-medical.com/EndoScore> [Online]. [Accessed 22/11/2015].
- ITO, H., TAKAHASHI, K., HATAZAWA, J., KIM, S.-G. & KANNO, I. 2001. Changes in Human Regional Cerebral Blood Flow and Cerebral Blood Volume During Visual Stimulation Measured by Positron Emission Tomography. *Journal of Cerebral Blood Flow & Metabolism*, 21, 608-612.
- ITO, S., MARDIMAE, A., HAN, J., DUFFIN, J., WELLS, G., FEDORKO, L., MINKOVICH, L., KATZNELSON, R., MEINER, M., ARENOVICH, T., KESSLER, C. & FISHER, J. A. 2008. Non-invasive prospective targeting of arterial PCO₂ in subjects at rest. *The Journal of Physiology*, 586, 3675-3682.
- JACKSON, R. M. 1985. Pulmonary oxygen toxicity. *Chest*, 88, 900-905.
- JAIN, K. 2013. Biomarkers of Neurological Disorders. *Applications of Biotechnology in Neurology*. Humana Press.
- JAMIESON, D., CHANCE, B., CADENAS, E. & BOVERIS, A. 1986. The Relation of Free Radical Production to Hyperoxia. *Annual Review of Physiology*, 48, 703-719.
- JARRIAULT, S., BROU, C., LOGEAT, F., SCHROETER, E. H., KOPAN, R. & ISRAEL, A. 1995. Signalling downstream of activated mammalian Notch. *Nature*, 377, 355-358.
- JENKINSON, M. & SMITH, S. 2001. A global optimisation method for robust affine registration of brain images. *Medical Image Analysis*, 5, 143-156.
- JESPERSEN, S. N. & ØSTERGAARD, L. 2012. The roles of cerebral blood flow, capillary transit time heterogeneity, and oxygen tension in brain oxygenation and metabolism. *Journal of Cerebral Blood Flow & Metabolism*, 32, 264-277.
- JIN, S., HANSSON, E. M., TIKKA, S., LANNER, F., SAHLGREN, C., FARNEBO, F., BAUMANN, M., KALIMO, H. & LENDAHL, U. 2008. Notch Signaling Regulates Platelet-Derived Growth Factor Receptor-Expression in Vascular Smooth Muscle Cells. *Circulation Research*, 102, 1483-1491.
- JOUTEL, A. 2013. Loss-of-function mutation in the NOTCH3 gene: simply a polymorphism? *Human Mutation*, 34, v.
- JOUTEL, A., ANDREUX, F. D., GAULIS, S., DOMENGA, V. R., CECILLON, M., BATTAIL, N., PIGA, N., CHAPON, F. O., GODFRAIN, C. & TOURNIER-LASSERVE, E. 2000a. The ectodomain of the Notch3 receptor accumulates within the cerebrovasculature of CADASIL patients. *The Journal of Clinical Investigation*, 105, 597-605.
- JOUTEL, A., CHABRIAT, H., VAHEDI, K., DOMENGA, V., VAYSSIERE, C., RUCHOUX, M. M., LUCAS, C., LEYS, D., BOUSSER, M. G. & TOURNIER-LASSERVE, E. 2000b. Splice site mutation causing a seven amino acid Notch3 in-frame deletion in CADASIL. *Neurology*, 54, 1874-1875.
- JOUTEL, A., CORPEchot, C., DUCROS, A., VAHEDI, K., CHABRIAT, H., MOUTON, P., ALAMOWITCH, S., DOMENGA, V., CECILLION, M., MARECHAL, E., MACIAZEK, J., VAYSSIERE, C., CRUAUD, C., CABANIS, E. A., RUCHOUX, M. M., WEISSENBAACH, J., BACH, J. F., BOUSSER, M. G. & TOURNIER-LASSERVE, E. 1996. Notch3 mutations in CADASIL, a hereditary adult-onset condition causing stroke and dementia. *Nature*, 383, 707-710.

- JOUTEL, A. & FARACI, F. M. 2014. Cerebral Small Vessel Disease: Insights and Opportunities From Mouse Models of Collagen IV-Related Small Vessel Disease and Cerebral Autosomal Dominant Arteriopathy With Subcortical Infarcts and Leukoencephalopathy. *Stroke*, 45, 1215-1221.
- JOUTEL, A., FAVROLE, P., LABAUGE, P., CHABRIAT, H., LESCOAT, C., ANDREUX, F., DOMENGA, V., CECILLON, M., VAHEDI, K., DUCROS, A., CAVE-RIANT, F., BOUSSER, M. G. & TOURNIER-LASSERVE, E. 2001. Skin biopsy immunostaining with a Notch3 monoclonal antibody for CADASIL diagnosis. *Lancet*, 358, 2049-2051.
- JOUTEL, A., HADDAD, I., RATELADE, J. & NELSON, M. T. 2016. Perturbations of the cerebrovascular matrisome: A convergent mechanism in small vessel disease of the brain? *Journal of Cerebral Blood Flow & Metabolism*, 36, 143-157.
- JOUTEL, A., MONET-LEPRETRE, M., GOSELE, C., BARON-MENGUY, C., HAMMES, A., SCHMIDT, S., LEMAIRE-CARRETTE, B., DOMENGA, V., SCHEDL, A., LACOMBE, P. & HUBNER, N. 2010. Cerebrovascular dysfunction and microcirculation rarefaction precede white matter lesions in a mouse genetic model of cerebral ischemic small vessel disease. *The Journal of Clinical Investigation*, 120, 433-445.
- JOUTEL, A., MONET, M., DOMENGA, V., RIAANT, F. & TOURNIER-LASSERVE, E. 2004. Pathogenic Mutations Associated with Cerebral Autosomal Dominant Arteriopathy with Subcortical Infarcts and Leukoencephalopathy Differently Affect Jagged1 Binding and Notch3 Activity via the RBP/JK Signaling Pathway. *American journal of human genetics*, 74, 338-347.
- JOUVENT, E., VISWANATHAN, A., MANGIN, J. F. O., O'SULLIVAN, M., GUICHARD, J. P., GSCHWENDTNER, A., CUMURCIUC, R., BUFFON, F. D. R., PETERS, N., PACHAÏ, C., BOUSSER, M. G., DICHGANS, M. & CHABRIAT, H. 2007. Brain Atrophy Is Related to Lacunar Lesions and Tissue Microstructural Changes in CADASIL. *Stroke*, 38, 1786-1790.
- KALAMANGALAM, G. P., NELSON, J. T., ELLMORE, T. M. & NARAYANA, P. A. 2012. Oxygen-enhanced MRI in temporal lobe epilepsy: diagnosis and lateralization. *Epilepsy Research*, 98, 50-61.
- KANAL, E., BARKOVICH, A. J., BELL, C., BORGSTEDE, J. P., BRADLEY, W. G., FROELICH, J. W., GIMBEL, J. R., GOSBEE, J. W., KUHN-KAMINSKI, E., LARSON, P. A., LESTER, J. W., NYENHUIS, J., SCHAEFER, D. J., SEBEK, E. A., WEINREB, J., WILKOFF, B. L., WOODS, T. O., LUCEY, L. & HERNANDEZ, D. 2013. ACR guidance document on MR safe practices: 2013. *Journal of Magnetic Resonance Imaging*, 37, 501-530.
- KARLSTROM, H., BEATUS, P., DANNAEUS, K., CHAPMAN, G., LENDAHL, U. & LUNDKVIST, J. 2002. A CADASIL-mutated Notch 3 receptor exhibits impaired intracellular trafficking and maturation but normal ligand-induced signaling. *Proceedings of the National Academy of Sciences*, 99, 17119-17124.
- KASTRUP, A., LI, T. Q., GLOVER, G. H. & MOSELEY, M. E. 1999. Cerebral blood flow-related signal changes during breath-holding. *American Journal of Neuroradiology*, 20, 1233-1238.
- KEMPSTER, P. A. & ALTY, J. E. 2008. John Ruskin's relapsing encephalopathy. *Brain*, 131, 2520-2525.
- KETY, S. S. & SCHMIDT, C. F. 1948a. The effects of altered arterial tensions of carbon dioxide and oxygen on cerebral blood flow and cerebral oxygen consumption of normal young men. *Journal of Clinical Investigation*, 27, 484-492.

- KETY, S. S. & SCHMIDT, C. F. 1948b. The nitrous oxide method for the quantitative determination of cerebral blood flow in man: theory, procedure and normal values. *Journal of Clinical Investigation*, 27, 476-483.
- KOMIYAMA, M., NISHIKAWA, M., YASUI, T. & SAKAMOTO, H. 1997. Reversible pontine ischemia caused by acetazolamide challenge. *American Journal of Neuroradiology*, 18, 1782-4.
- KREBS, L. T., XUE, Y., NORTON, C. R., SUNDBERG, J. P., BEATUS, P., LENDAHL, U., JOUTEL, A. & GRIDLEY, T. 2003. Characterization of Notch3-deficient mice: Normal embryonic development and absence of genetic interactions with a Notch1 mutation. *Genesis*, 37, 139-143.
- KULUZ, J. W., PRADO, R., CHANG, J., GINSBERG, M. D., SCHLEIEN, C. L. & BUSTO, R. 1993. Selective brain cooling increases cortical cerebral blood flow in rats. *American Journal of Physiology - Heart and Circulatory Physiology*, 265, H824-H827.
- KURIDZE, N., CZERNICKI, Z., JARUS-DZIEDZIC, K., JURKIEWICZ, J. & CERVOS-NAVARRO, J. 2000. Regional differences of cerebrovascular reactivity effected by calcium channel blocker - Dotarizine. *Journal of the Neurological Sciences*, 175, 13-16.
- KUVIN, J. T., PATEL, A. R., SLINEY, K. A., PANDIAN, N. G., SHEFFY, J., SCHNALL, R. P., KARAS, R. H. & UDELSON, J. E. 2003. Assessment of peripheral vascular endothelial function with finger arterial pulse wave amplitude. *American Heart Journal*, 146, 168-174.
- LACOMBE, P., OLIGO, C., DOMENGA, V., TOURNIER-LASSERVE, E. & JOUTEL, A. 2005. Impaired Cerebral Vasoreactivity in a Transgenic Mouse Model of Cerebral Autosomal Dominant Arteriopathy With Subcortical Infarcts and Leukoencephalopathy Arteriopathy. *Stroke*, 36, 1053-1058.
- LAGAS, P. A. & JUVONEN, V. 2001. Schizophrenia in a patient with cerebral autosomally dominant arteriopathy with subcortical infarcts and leucoencephalopathy (CADASIL disease). *Nordic Journal of Psychiatry*. Informa Scandinavian.
- LAURENT, S., BOUTOUYRIE, P., ASMAR, R., GAUTIER, I., LALOUX, B., GUIZE, L., DUCIMETIERE, P. & BENETOS, A. 2001. Aortic Stiffness Is an Independent Predictor of All-Cause and Cardiovascular Mortality in Hypertensive Patients. *Hypertension*, 37, 1236-1241.
- LAURENT, S., COCKCROFT, J., VAN BORTEL, L., BOUTOUYRIE, P., GIANNATTASIO, C., HAYOZ, D., PANNIER, B., VLACHOPOULOS, C., WILKINSON, I. & STRUIJKER-BOUDIER, H. 2006. Expert consensus document on arterial stiffness: methodological issues and clinical applications. *European Heart Journal*, 27, 2588-2605.
- LAVY, S., STERN, S., MELAMED, E., COOPER, G., KEREN, A. & LEVY, P. 1980. Effect of chronic atrial fibrillation on regional cerebral blood flow. *Stroke*, 11, 35-38.
- LEENDERS, K. L., PERANI, D., LAMMERTSMA, A. A., HEATHER, J. D., BUCKINGHAM, P., JONES, T., HEALY, M. J. R., GIBBS, J. M., WISE, R. J. S., HATAZAWA, J., HEROLD, S., BEANEY, R. P., BROOKS, D. J., SPINKS, T., RHODES, C. & FRACKOWIAK, R. S. J. 1990. Cerebral blood flow, blood volume and oxygen utilization: Normal values and effect of age. *Brain*, 113, 27-47.
- LESNIK OBERSTEIN, S. A. J., VAN DEN BOOM, R., VAN BUCHEM, M. A., VAN HOUWELINGEN, H. C., BAKKER, E., VOLLEBREGT, E., FERRARI, M. D., BREUNING, M. H., HAAN, J. & GROUP*, F. T. D. C. R. 2001. Cerebral microbleeds in CADASIL. *Neurology*, 57, 1066-1070.

- LEVY, M. & FEINGOLD, J. 2000. Estimating prevalence in single-gene kidney diseases progressing to renal failure. *Kidney International*, 58, 925-943.
- LIEM, M. K., LESNIK OBERSTEIN, S. A. J., HAAN, J., BOOM, R., FERRARI, M. D., BUCHEM, M. A. & GROND, J. 2009a. Cerebrovascular Reactivity Is a Main Determinant of White Matter Hyperintensity Progression in CADASIL. *American Journal of Neuroradiology*, 30, 1244-1247.
- LIEM, M. K., LESNIK OBERSTEIN, S. A. J., HAAN, J., VAN DER NEUT, I. L., FERRARI, M. D., VAN BUCHEM, M. A., MIDDELKOOP, H. A. M. & VAN DER GROND, J. 2009b. MRI correlates of cognitive decline in CADASIL. *Neurology*, 72, 143-148.
- LIEM, M. K., LESNIK OBERSTEIN, S. A. J., HAAN, J., VAN DER NEUT, I. L., VAN DEN BOOM, R., FERRARI, M. D., VAN BUCHEM, M. A. & VAN DER GROND, J. 2008. Cerebral Autosomal Dominant Arteriopathy with Subcortical Infarcts and Leukoencephalopathy: Progression of MR Abnormalities in Prospective 7-year Follow-up Study1. *Radiology*, 249, 964-971.
- LIEM, M. K., OBERSTEIN, S. A. L., VAN DER GROND, J., FERRARI, M. D. & HAAN, J. 2010. CADASIL and migraine: A narrative review. *Cephalalgia*, 30, 1284-1289.
- LIEM, M. K., VAN DER GROND, J., HAAN, J., VAN DEN BOOM, R., FERRARI, M. D., KNAAP, Y. M., BREUNING, M. H., VAN BUCHEM, M. A., MIDDELKOOP, H. A. M. & LESNIK OBERSTEIN, S. A. J. 2007. Lacunar Infarcts Are the Main Correlate With Cognitive Dysfunction in CADASIL. *Stroke*, 38, 923-928.
- LINDER, V., BOOTH, C., PRUDOVSKY, I., SMALL, D., MACAIG, T. & LIAW, L. 2001. Members of the *Jagged/Notch* Gene Families Are Expressed in Injured Arteries and Regulate Cell Phenotype via Alterations in Cell Matrix and Cell-Cell Interaction. *American Journal of Pathology*, 159, 875-883.
- LORENZ, M. W., MARKUS, H. S., BOTS, M. L., ROSVALL, M. & SITZER, M. 2007. Prediction of Clinical Cardiovascular Events With Carotid Intima-Media Thickness. *Circulation*, 115, 459-467.
- LOW, W. C., JUNNA, M., BÖRJESSON-HANSON, A., MORRIS, C. M., MOSS, T. H., STEVENS, D. L., ST CLAIR, D., MIZUNO, T., ZHANG, W. W., MYKKÄNEN, K., WAHLSTROM, J., ANDERSEN, O., KALIMO, H., VIITANEN, M. & KALARIA, R. N. 2007. Hereditary multi-infarct dementia of the Swedish type is a novel disorder different from NOTCH3 causing CADASIL. *Brain*, 130, 357-367.
- LUNT, M. J., RAGAB, S., BIRCH, A. A., SCHLEY, D. & JENKINSON, D. F. 2004. Comparison of caffeine-induced changes in cerebral blood flow and middle cerebral artery blood velocity shows that caffeine reduces middle cerebral artery diameter. *Physiological Measurement*, 25, 467-74.
- MACLEAN, A. V., WOODS, R., ALDERSON, L. M., SALLOWAY, S. P., CORREIA, S., CORTEZ, S. & STOPA, E. G. 2005. Spontaneous lobar haemorrhage in CADASIL. *Journal of Neurology, Neurosurgery & Psychiatry*, 76, 456-457.
- MANABE, Y., MURAKAMI, T., IWATSUKI, K., NARAI, H., WARITA, H., HAYASHI, T., SHOJI, M., IMAI, Y. & ABE, K. 2001. Nocturnal blood pressure dip in CADASIL. *Journal of the Neurological Sciences*, 193, 13-16.
- MANCIA, G., DE, B. G., DOMINICZAK, A., CIFKOVA, R., FAGARD, R., GERMANO, G., GRASSI, G., HEAGERTY, A. M., KJELDSSEN, S. E., LAURENT, S., NARKIEWICZ, K., RUILOPE, L., RYNKIEWICZ, A., SCHMIEDER, R. E., STRUIJKER BOUDIER, H. A., ZANCHETTI, A., VAHANIAN, A., CAMM, J., DE, C. R., DEAN, V., DICKSTEIN, K., FILIPPATOS, G., FUNCK-BRENTANO, C., HELLEMANS, I., KRISTENSEN, S. D., MCGREGOR, K., SECHTEM, U., SILBER, S., TENDERA, M., WIDIMSKY, P., ZAMORANO, J. L., KJELDSSEN, S. E., ERDINE, S., NARKIEWICZ, K., KIOWSKI, W., AGABITI-ROSEI, E., AMBROSIONI, E., CIFKOVA, R., DOMINICZAK, A., FAGARD, R., HEAGERTY,

- A. M., LAURENT, S., LINDHOLM, L. H., MANCIA, G., MANOLIS, A., NILSSON, P. M., REDON, J., SCHMIEDER, R. E., STRUIJKER-BOUDIER, H. A., VIIGIMAA, M., FILIPPATOS, G., ADAMOPOULOS, S., AGABITI-ROSEI, E., AMBROSIONI, E., BERTOMEU, V., CLEMENT, D., ERDINE, S., FARSANG, C., GAITA, D., KIOWSKI, W., LIP, G., MALLION, J. M., MANOLIS, A. J., NILSSON, P. M., O'BRIEN, E., PONIKOWSKI, P., REDON, J., RUSCHITZKA, F., TAMARGO, J., VAN, Z. P., VIIGIMAA, M., WAEBER, B., WILLIAMS, B. & ZAMORANO, J. L. 2007. 2007 Guidelines for the management of arterial hypertension: The Task Force for the Management of Arterial Hypertension of the European Society of Hypertension (ESH) and of the European Society of Cardiology (ESC). *European Heart Journal*, 28, 1462-1536.
- MANCIA, G., LAURENT, S., AGABITI-ROSEI, E., AMBROSIONI, E., BURNIER, M., CAULFIELD, M. J., CIFKOVA, R., CLEMENT, D., COCA, A., DOMINICZAK, A., ERDINE, S., FAGARD, R., FARSANG, C., GRASSI, G., HALLER, H., HEAGERTY, A., KJELDSSEN, S. E., KIOWSKI, W., MALLION, J. M., MANOLIS, A., NARKIEWICZ, K., NILSSON, P., OLSEN, M. H., RAHN, K. H., REDON, J., RODICIO, J., RUILOPE, L., SCHMIEDER, R. E., STRUIJKER-BOUDIER, H. A., VAN ZWIETEN, P. A., VIIGIMAA, M., ZANCHETTI, A. & HYPERTENSION, E. S. O. 2009. Reappraisal of European guidelines on hypertension management: a European Society of Hypertension Task Force document. *Journal of Hypertension*, 27, 2121-2158.
- MANDELL, D. M., HAN, J. S., POUBLANC, J., CRAWLEY, A. P., FIERSTRA, J., TYMIANSKI, M., FISHER, J. A. & MIKULIS, D. J. 2011. Quantitative Measurement of Cerebrovascular Reactivity by Blood Oxygen Level-Dependent MR Imaging in Patients with Intracranial Stenosis: Preoperative Cerebrovascular Reactivity Predicts the Effect of Extracranial-Intracranial Bypass Surgery. *American Journal of Neuroradiology*, 32, 721-727.
- MANDELL, D. M., HAN, J. S., POUBLANC, J., CRAWLEY, A. P., STAINSBY, J. A., FISHER, J. A. & MIKULIS, D. J. 2008. Mapping cerebrovascular reactivity using blood oxygen level-dependent MRI in Patients with arterial stenocclusive disease: comparison with arterial spin labeling MRI. *Stroke*, 39, 2021-2028.
- MARINKOVIĆ, S., GIBO, H., MILISAVLJEVIĆ, M. & ČETKOVIĆ, M. 2001. Anatomic and clinical correlations of the lenticulostriate arteries. *Clinical Anatomy*, 14, 190-195.
- MARKUS, H. S. & HARRISON, M. J. 1992. Estimation of cerebrovascular reactivity using transcranial Doppler, including the use of breath-holding as the vasodilatory stimulus. *Stroke*, 23, 668-673.
- MARKUS, H. S., MARTIN, R. J., SIMPSON, M. A., DONG, Y. B., ALI, N., CROSBY, A. H. & POWELL, J. F. 2002. Diagnostic strategies in CADASIL. *Neurology*, 59, 1134-1138.
- MARTIN, D. S. & GROCOTT, M. P. W. 2013. Oxygen Therapy in Critical Illness: Precise Control of Arterial Oxygenation and Permissive Hypoxemia. *Critical Care Medicine*, 41, 423-432.
- MAWET, J., VAHEDI, K., AOUT, M., VICAUT, E., DUERING, M., TOUBOUL, P. J., DICHGANS, M. & CHABRIAT, H. 2011. Carotid Atherosclerotic Markers in CADASIL. *Cerebrovascular Diseases*, 31, 246-252.
- MAZZEI, R., GUIDETTI, D., UNGARO, C., CONFORTI, F. L., MUGLIA, M., CENACCHI, G., LANZA, P. L., PATITUCCI, A., SPROVIERI, T., RIGUZZI, P., MAGARIELLO, A., GABRIELE, A. L., CITRIGNO, L., PREDA, P. & QUATTRONE, A. 2008. First evidence of a pathogenic insertion in the

- NOTCH3 gene causing CADASIL. *Journal of Neurology, Neurosurgery & Psychiatry*, 79, 108-110.
- MCGRATH, J., SAHA, S., CHANT, D. & WELHAM, J. 2008. Schizophrenia: A Concise Overview of Incidence, Prevalence, and Mortality. *Epidemiologic Reviews*, 30, 67-76.
- MCROBBIE, D. W., MOORE, E. A., GRAVES, M. J. & PRINCE, M. R. 2007. *MRI From Picture to Proton*, Cambridge, Cambridge University Press.
- MEDICAL IMAGING APPLICATIONS 2006. Vascular Research Tools 5 Documentation. Medical Imaging Applications, LLC.
- MELLIES, J. K., BAUMER, T., MULLER, J. A., TOURNIER-LASSERVE, E., CHABRIAT, H., KNOBLOCH, O., HACKELOER, H. J., GOEBEL, H. H., WETZIG, L. & HALLER, P. 1998. SPECT study of a German CADASIL family: a phenotype with migraine and progressive dementia only. *Neurology*, 50, 1715-1721.
- MIAO, Q., PALONEVA, T., TUOMINEN, S., PÖYHÖNEN, M., TUISKU, S., VIITANEN, M. & KALIMO, H. 2004. Fibrosis and Stenosis of the Long Penetrating Cerebral Arteries: the Cause of the White Matter Pathology in Cerebral Autosomal Dominant Arteriopathy with Subcortical Infarcts and Leukoencephalopathy. *Brain Pathology*, 14, 358-364.
- MIKULIS, D. J., KROLczyk, G., DESAL, H., LOGAN, W., DEVEBER, G., DIRKS, P., TYMIANSKI, M., CRAWLEY, A., VESELY, A., KASSNER, A., PREISS, D., SOMOGYI, R. & FISHER, J. A. 2005. Preoperative and postoperative mapping of cerebrovascular reactivity in moyamoya disease by using blood oxygen level-dependent magnetic resonance imaging. *Journal of Neurosurgery*, 103, 347-355.
- MOCCIA, M., MOSCA, L., ERRO, R., CERVASIO, M., ALLOCCA, R., VITALE, C., LEONARDI, A., CARANCI, F., DEL BASSO-DE CARO, M. L., BARONE, P. & PENCO, S. 2015. Hypomorphic NOTCH3 mutation in an Italian family with CADASIL features. *Neurobiology of Aging*, 36, 547.e5-11.
- MOHR, O. L. 1919. Character Changes Caused by Mutation of an Entire Region of a Chromosome in *Drosophila*. *Genetics*, 4, 275-282.
- MOLKO, N., PAPPATA, S., MANGIN, J. F., POUPON, C., VAHEDI, K., JOBERT, A., LEBIHAN, D., BOUSSER, M. G. & CHABRIAT, H. 2001. Diffusion Tensor Imaging Study of Subcortical Gray Matter in CADASIL. *Stroke*, 32, 2049-2054.
- MOLKO, N., PAPPATA, S., MANGIN, J. F. O., POUPON, F., LEBIHAN, D., BOUSSER, M. G. & CHABRIAT, H. 2002. Monitoring Disease Progression in CADASIL With Diffusion Magnetic Resonance Imaging. *Stroke*, 33, 2902-2908.
- MONET-LEPRETRE, M., BARDOT, B., LEMAIRE, B., DOMENGA, V., GODIN, O., DICHGANS, M., TOURNIER-LASSERVE, E., COHEN-TANNOUDJI, M., CHABRIAT, H. & JOUTEL, A. 2009. Distinct phenotypic and functional features of CADASIL mutations in the Notch3 ligand binding domain. *Brain*, 132, 1601-1612.
- MONET-LEPRETRE, M., HADDAD, I., BARON-MENGUY, C., FOUILLOT-PANCHAL, M., RIANI, M., DOMENGA-DENIER, V., DUSSAULE, C., COGNAT, E., VINH, J. & JOUTEL, A. 2013. Abnormal recruitment of extracellular matrix proteins by excess Notch3ECD: a new pathomechanism in CADASIL. *Brain*, 136, 1830-1845.
- MONET, M., DOMENGA, V., LEMAIRE, B., SOUILHOL, C., LANGA, F., BABINET, C., GRIDLEY, T., TOURNIER-LASSERVE, E., COHEN-TANNOUDJI, M. & JOUTEL, A. 2007. The archetypal R90C CADASIL–NOTCH3 mutation retains NOTCH3 function in vivo. *Human Molecular Genetics*, 16, 982-992.
- MORROW, D., SWEENEY, C., BIRNEY, Y. A., CUMMINS, P. M., WALLS, D., REDMOND, E. M. & CAHILL, P. A. 2005. Cyclic Strain Inhibits Notch

- Receptor Signaling in Vascular Smooth Muscle Cells In Vitro. *Circulation Research*, 96, 567-575.
- MULVANY, M. J. & AALKJAER, C. 1990. Structure and function of small arteries. *Physiological Reviews*, 70, 921-961.
- MULVANY, M. J. & HALPERN, W. 1977. Contractile properties of small arterial resistance vessels in spontaneously hypertensive and normotensive rats. *Circulation Research*, 41, 19-26.
- MURAKAMI, M., FUJIOKA, S., HIRATA, Y. & KURATSU, J.-I. 2008. Low-dose of Statin Treatment Improves Cerebrovascular Reactivity in Patients With Ischemic Stroke: Single Photon Emission Computed Tomography Analysis. *Journal of stroke and cerebrovascular diseases : the official journal of National Stroke Association*, 17, 16-22.
- MURPHY, K., HARRIS, A. D., DIUKOVA, A., EVANS, C. J., LYTHGOE, D. J., ZELAYA, F. & WISE, R. G. 2011. Pulsed arterial spin labeling perfusion imaging at 3 T: estimating the number of subjects required in common designs of clinical trials. *Magnetic Resonance Imaging*, 29, 1382-1389.
- MURRAY, C. J. D., LOPEZ, A. D. & EDS. 1996. The global burden of disease: a comprehensive assessment of mortality and disability from diseases, injuries and risk factors in 1990 and projected to 2020. In: MURRAY, C. J. D. & LOPEZ, A. D. (eds.) *Global Burden of Disease and Injury Series, Vol 1*. Cambridge.
- MUTCH, W. A., MANDELL, D. M., FISHER, J. A., MIKULIS, D. J., CRAWLEY, A. P., PUCCI, O. & DUFFIN, J. 2012. Approaches to Brain Stress Testing: BOLD Magnetic Resonance Imaging with Computer-Controlled Delivery of Carbon Dioxide. *PLoS ONE*, 7, e47443.
- MUTSAERTS, H. J. M. M., RICHARD, E., HEIJTEL, D. F. R., VAN OSCH, M. J. P., MAJOIE, C. B. L. M. & NEDERVEEN, A. J. 2014. Gray matter contamination in arterial spin labeling white matter perfusion measurements in patients with dementia. *NeuroImage : Clinical*, 4, 139-144.
- NAGANAWA, S., NORRIS, D. G., ZYSSET, S. & MILDNER, T. 2002. Regional differences of fMR signal changes induced by hyperventilation: comparison between SE-EPI and GE-EPI at 3-T. *Journal of Magnetic Resonance Imaging*, 15, 23-30.
- NARAYAN, S. K., GORMAN, G., KALARIA, R. N., FORD, G. A. & CHINNERY, P. F. 2012. The minimum prevalence of CADASIL in northeast England. *Neurology*, 78, 1025-1027.
- NATIONAL RECORDS OF SCOTLAND 2012. Mid-2011 population estimates Scotland. Scotland: National Records of Scotland.
- NOSEDA, M., FU, Y., NIESSEN, K., WONG, F., CHANG, L., MCLEAN, G. & KARSAN, A. 2006. Smooth Muscle alpha-Actin Is a Direct Target of Notch/CSL. *Circulation Research*, 98, 1468-1470.
- NOTH, U., KOTAJIMA, F., DEICHMANN, R., TURNER, R. & CORFIELD, D. R. 2008. Mapping of the cerebral vascular response to hypoxia and hypercapnia using quantitative perfusion MRI at 3 T. *NMR in Biomedicine*, 21, 464-472.
- NOVACK, P., SHENKIN, H. A., BORTIN, L., GOLUBOFF, B., SOFFE, A. M., BATSON, P. & GOLDEN, D. 1953. The effects of carbon dioxide inhalation upon the cerebral blood flow and cerebral oxygen consumption in vascular disease. *Journal of Clinical Investigation*, 32, 696 - 702.
- O'LEARY, D. H. & BOTS, M. L. 2010. Imaging of atherosclerosis: carotid intima-media thickness. *European Heart Journal*, 31, 1682-1689.
- O'ROURKE, M. F. & GALLAGHER, D. E. 1996. Pulse wave analysis. *Journal of hypertension. Supplement : official journal of the International Society of Hypertension*, 14, S147-S157.

- O'SULLIVAN, M., BARRICK, T. R., MORRIS, R. G., CLARK, C. A. & MARKUS, H. S. 2005. Damage within a network of white matter regions underlies executive dysfunction in CADASIL. *Neurology*, 65, 1584-1590.
- O'SULLIVAN, M., JAROSZ, J. M., MARTIN, R. J., DEASY, N., POWELL, J. F. & MARKUS, H. S. 2001. MRI hyperintensities of the temporal lobe and external capsule in patients with CADASIL. *Neurology*, 56, 628-634.
- O'SULLIVAN, M., RICH, P. M., BARRICK, T. R., CLARK, C. A. & MARKUS, H. S. 2003. Frequency of Subclinical Lacunar Infarcts in Ischemic Leukoaraiosis and Cerebral Autosomal Dominant Arteriopathy with Subcortical Infarcts and Leukoencephalopathy. *American Journal of Neuroradiology*, 24, 1348-1354.
- O'SULLIVAN, M., SINGHAL, S., CHARLTON, R. & MARKUS, H. S. 2004. Diffusion tensor imaging of thalamus correlates with cognition in CADASIL without dementia. *Neurology*, 62, 702-707.
- OBERSTEIN, S., VAN DEN BOOM, R., MIDDELKOOP, H. M. & ET AL. 2003. Incipient cadasil. *Archives of Neurology*, 60, 707-712.
- OH, S., KIM, S. & KIM, H. 2014. MASSive pontine microbleeds in a patient with cadasil. *JAMA Neurology*, 71, 1048-1049.
- OHKURA, T., TESHIMA, Y., ISSE, K., MATSUDA, H., INOUE, T., SAKAI, Y., IWASAKI, N. & YAOI, Y. 1995. Estrogen Increases Cerebral and Cerebellar Blood Flows in Postmenopausal Women. *Menopause*, 2, 13-18.
- OKEDA, R., ARIMA, K. & KAWAI, M. 2002. Arterial Changes in Cerebral Autosomal Dominant Arteriopathy With Subcortical Infarcts and Leukoencephalopathy (CADASIL) in Relation to Pathogenesis of Diffuse Myelin Loss of Cerebral White Matter. *Stroke*, 33, 2565-2569.
- OLESEN, S. P., CLAPHAMT, D. & DAVIES, P. 1988. Haemodynamic shear stress activates a K⁺ current in vascular endothelial cells. *Nature*, 331, 168-170.
- OMAE, T., IBAYASHI, S., KUSUDA, K., NAKAMURA, H., YAGI, H. & FUJISHIMA, M. 1998. Effects of High Atmospheric Pressure and Oxygen on Middle Cerebral Blood Flow Velocity in Humans Measured by Transcranial Doppler. *Stroke*, 29, 94-97.
- OPHERK, C., DUERING, M., PETERS, N., KARPINSKA, A., ROSNER, S., SCHNEIDER, E., BADER, B., GIESE, A. & DICHGANS, M. 2009. CADASIL mutations enhance spontaneous multimerization of NOTCH3. *Human Molecular Genetics*, 18, 2761-2767.
- OPHERK, C., GONIK, M., DUERING, M., MALIK, R., JOUVENT, E., HERVE, D., ADIB-SAMII, P., BEVAN, S., PIANESE, L., SILVESTRI, S., DOTTI, M. T., DE STEFANO, N., LIEM, M., BOON, E. M., PESCHINI, F., PACHAI, C., BRACOD, L., MULLER-MYHSOK, B., MEITINGER, T., ROST, N., PANTONI, L., LESNIK OBERSTEIN, S., FEDERICO, A., RAGNO, M., MARKUS, H. S., TOURNIER-LASSERVE, E., ROSAND, J., CHABRIAT, H. & DICHGANS, M. 2014. Genome-wide genotyping demonstrates a polygenic risk score associated with white matter hyperintensity volume in CADASIL. *Stroke*, 45, 968-72.
- OPHERK, C., PETERS, N., HERZOG, J., LUEDTKE, R. & DICHGANS, M. 2004. Long-term prognosis and causes of death in CADASIL: a retrospective study in 411 patients. *Brain*, 127, 2533-2539.
- ØSTERGAARD, L., ENGEDAL, T. S., MORETON, F., HANSEN, M. B., WARDLAW, J. M., DALKARA, T., MARKUS, H. S. & MUIR, K. W. 2015. Cerebral small vessel disease: Capillary pathways to stroke and cognitive decline. *Journal of Cerebral Blood Flow & Metabolism*.
- PANTONI, L. 2010. Cerebral small vessel disease: from pathogenesis and clinical characteristics to the therapeutic challenges. *Lancet Neurol.*, 9, 689-701.

- PANTONI, L., PESCHINI, F., INZITARI, D. & DOTTI, T. 2005. Postpartum psychiatric disturbances as an unrecognized onset of CADASIL. *Acta Psychiatrica Scandinavica*, 112, 241-241.
- PARKES, L. M., RASHID, W., CHARD, D. T. & TOFTS, P. S. 2004. Normal cerebral perfusion measurements using arterial spin labeling: Reproducibility, stability, and age and gender effects. *Magnetic Resonance in Medicine*, 51, 736-743.
- PARKS, A. L., KLUEG, K. M., STOUT, J. R. & MUSKAVITCH, M. A. 2000. Ligand endocytosis drives receptor dissociation and activation in the Notch pathway. *Development*, 127, 1373-1385.
- PETERS, N., FREILINGER, T., OPPERK, C., PFEFFERKORN, T. & DICHGANS, M. 2007. Effects of short term atorvastatin treatment on cerebral hemodynamics in CADASIL. *Journal of the Neurological Sciences*, 260, 100-105.
- PETERS, N., FREILINGER, T., OPPERK, C., PFEFFERKORN, T. & DICHGANS, M. 2008. Enhanced L-arginine-induced vasoreactivity suggests endothelial dysfunction in CADASIL. *Journal of Neurology*, 255, 1203-1208.
- PETERS, N., HERZOG, J., OPPERK, C. & DICHGANS, M. 2004a. A Two-Year Clinical Follow-Up Study in 80 CADASIL Subjects. *Stroke*, 35, 1603-1608.
- PETERS, N., HOLTMANNSPOTTER, M., OPPERK, C., GSCHWENDTNER, A., HERZOG, J., SAMANN, P. & DICHGANS, M. 2006. Brain volume changes in CADASIL. *Neurology*, 66, 1517-1522.
- PETERS, N., OPPERK, C., ZACHERLE, S., CAPELL, A., GEMPEL, P. & DICHGANS, M. 2004b. CADASIL-associated Notch3 mutations have differential effects both on ligand binding and ligand-induced Notch3 receptor signaling through RBP-Jk. *Experimental Cell Research*, 299, 454-464.
- PETERS, N., ZIEREN, N., DUERING, M., OPPERK, C. & DICHGANS, M. 2010. Effects of clinical depression on cognitive function in subcortical ischemic vascular dementia: Results from a cross-sectional study in CADASIL. *Stroke*, 41, e324-e324.
- PETERSEN, P., KASTRUP, J., VIDEBAEK, R. & BOYSEN, G. 1989. Cerebral Blood Flow Before and After Cardioversion of Atrial Fibrillation. *Journal of Cerebral Blood Flow & Metabolism*, 9, 422-425.
- PFEFFERKORN, T., VON, S. S.-B., HERZOG, J., GASSER, T., HAMANN, G. F. & DICHGANS, M. 2000. Reduced Cerebrovascular CO₂ Reactivity in CADASIL. *Abstracts of the International Stroke Conference*, 32, 339.
- PFEFFERKORN, T., VON STUCKRAD-BARRE, S., HERZOG, J., GASSER, T., HAMANN, G. F. & DICHGANS, M. 2001. Reduced Cerebrovascular CO₂ Reactivity in CADASIL : A Transcranial Doppler Sonography Study. *Stroke*, 32, 17-21.
- PHAN, T. G., VAN DER VOORT, S., BEARE, R., CLISSOLD, B., HOLT, M., LY, J., FOSTER, E., THONG, E., STUCKEY, S., CASSELL, M. D. & SRIKANTH, V. 2013. Dimensions of Subcortical Infarcts Association with First- to Third Order Branches of the Basal Ganglia Arteries. *Cerebrovascular Diseases*, 35, 262 - 267.
- PHILLIPS, J. S., KING, J. A., CHANDRAN, S., PRINSLEY, P. R. & DICK, D. 2005. Cerebral autosomal dominant arteriopathy with subcortical infarcts and leukoencephalopathy (CADASIL) presenting with sudden sensorineural hearing loss. *The Journal of Laryngology & Otology*, 119, 148-151.
- PILKINTON, D. T., HIRAKI, T., DETRE, J. A., GREENBERG, J. H. & REDDY, R. 2012. Absolute cerebral blood flow quantification with pulsed arterial spin labeling during hyperoxia corrected with the simultaneous measurement of the longitudinal relaxation time of arterial blood. *Magnetic Resonance in Medicine*, 67, 1556-1565.

- POHL, U., HOLTZ, J., BUSSE, R. & BASSENGE, E. 1986. Crucial role of endothelium in the vasodilator response to increased flow in vivo. *Hypertension*, 8, 37-44.
- POTTER, G., MORRIS, Z. & WARDLAW, J. M. 2014. *Enlarged perivascular spaces (EPVS): a visual rating scale and user guide*. <http://www.sbirc.ed.ac.uk/documents/epvs-rating-scale-user-guide.pdf> [Online]. University of Edinburgh. 2013].
- POULIN, M. J., LIANG, P. J. & ROBBINS, P. A. 1996. Dynamics of the cerebral blood flow response to step changes in end-tidal PCO₂ and PO₂ in humans. *Journal of Applied Physiology*, 81, 1084-1095.
- PRADOTTO, L., ORSI, L., DANIELE, D., CAROPPO, P., LAURO, D., MILESI, A., SELLITTI, L. & MAURO, A. 2012. A new NOTCH3 mutation presenting as primary intracerebral haemorrhage. *Journal of the Neurological Sciences*, 315, 143-145.
- PRAKASH, K., CHANDRAN, D. S., KHADGAWAT, R., JARYAL, A. K. & DEEPAK, K. K. 2014. Correction for Blood Pressure Improves Correlation between Cerebrovascular Reactivity Assessed by Breath Holding and 6% CO₂ Breathing. *Journal of Stroke and Cerebrovascular Diseases*, 23, 630-635.
- PRETEGIANI, E., ROSINI, F., DOTTI, M. T., BIANCHI, S., FEDERICO, A. & RUFA, A. 2013. Visual System Involvement in CADASIL. *Journal of Stroke and Cerebrovascular Diseases*, 22, 1377-1384.
- PRETNAR-OBLAK, J., SABOVIC, M., SEBESTJEN, M., POGACNIK, T. & ZALETEL, M. 2006. Influence of Atorvastatin Treatment on L-Arginine Cerebrovascular Reactivity and Flow-Mediated Dilatation in Patients With Lacunar Infarctions. *Stroke*, 37, 2540-2545.
- QUINN, T. J., DAWSON, J., WALTERS, M. R. & LEES, K. R. 2009. Reliability of the Modified Rankin Scale. *Stroke*, 40, 3393-3395.
- RAFALOWSKA, J., DZIEWULSKA, D. & FIDZIANSKA, A. 2004. CADASIL: what component of the vessel wall is really a target for Notch 3 gene mutations? *Neurological Research*, 26, 558-562.
- RAICHLE, M. E. & PLUM, F. 1972. Hyperventilation and Cerebral Blood Flow. *Stroke*, 3, 566-575.
- RANKIN, J. 1957. Cerebral vascular accidents in patients over the age of 60. II. Prognosis. *Scottish Medical Journal*, 2, 200-215.
- RATNATUNGA, C. & ADISESHIAH, M. 1990. Increase in middle cerebral artery velocity on breath holding: A simplified test of cerebral perfusion reserve. *European Journal of Vascular Surgery*, 4, 519-523.
- RAZVI, S. S. M., DAVIDSON, R., BONE, I. & MUIR, K. W. 2005a. Is inadequate family history a barrier to diagnosis in CADASIL? *Acta Neurologica Scandinavica*, 112, 323-326.
- RAZVI, S. S. M., DAVIDSON, R., BONE, I. & MUIR, K. W. 2005b. The prevalence of cerebral autosomal dominant arteriopathy with subcortical infarcts and leucoencephalopathy (CADASIL) in the west of Scotland. *Journal of Neurology, Neurosurgery & Psychiatry*, 76, 739-741.
- REIVICH, M. 1964. Arterial PCO₂ and cerebral hemodynamics. *American Journal of Physiology*, 206, 25-35.
- REYES, S., VISWANATHAN, A., GODIN, O., DUFOUIL, C., BENISTY, S., HERNANDEZ, K., KURTZ, A., JOUVENT, E., O'SULLIVAN, M., CZERNECKI, V., BOUSSER, M. G., DICHGANS, M. & CHABRIAT, H. 2009. Apathy: a major symptom in CADASIL. *Neurology*, 72, 905-910.
- RINGELSTEIN, E. B., KAHLSCHEUER, B., NIGGEMEYER, E. & OTIS, S. M. 1990. Transcranial doppler sonography: Anatomical landmarks and normal velocity values. *Ultrasound in Medicine & Biology*, 16, 745-761.

- ROGERS, S., WELLS, R. & RECHSTEINER, M. 1986. Amino acid sequences common to rapidly degraded proteins: the PEST hypothesis. *Science*, 234, 364-368.
- ROOB, G., SCHMIDT, R., KAPPELLER, P., LECHNER, A., HARTUNG, H. P. & FAZEKAS, F. 1999. MRI evidence of past cerebral microbleeds in a healthy elderly population. *Neurology*, 52, 991-991.
- RORDEN, C., KARNATH, H.-O. & BONILHA, L. 2007. Improving Lesion-Symptom Mapping. *Journal of Cognitive Neuroscience*, 19, 1081-1088.
- ROSTRUP, E., KNUDSEN, G. M., LAW, I., HOLM, S., LARSSON, H. B. & PAULSON, O. B. 2005. The relationship between cerebral blood flow and volume in humans. *Neuroimage*, 24, 1-11.
- RUBIO, A., RIFKIN, D., POWERS, J. M., PATEL, U., STEWART, J., FAUST, P., GOLDMAN, J. E., MOHR, J. P., NUMAGUCHI, Y. & JENSEN, K. 1997. Phenotypic variability of CADASIL and novel morphologic findings. *Acta Neuropathologica*, 94, 247-254.
- RUCHOUX & MAURAGE 1998. Endothelial changes in muscle and skin biopsies in patients with CADASIL. *Neuropathology and Applied Neurobiology*, 24, 60-65.
- RUCHOUX, M. M., CHABRIAT, H., BOUSSER, M. G., BAUDRIMONT, M. & TOURNIER-LASSERVE, E. 1994. Presence of ultrastructural arterial lesions in muscle and skin vessels of patients with CADASIL. *Stroke*, 25, 2291-2292.
- RUCHOUX, M. M., DOMENGA, V. R., BRULIN, P., MACIAZEK, J., LIMOL, S., TOURNIER-LASSERVE, E. & JOUTEL, A. 2003. Transgenic Mice Expressing Mutant Notch3 Develop Vascular Alterations Characteristic of Cerebral Autosomal Dominant Arteriopathy with Subcortical Infarcts and Leukoencephalopathy. *The American Journal of Pathology*, 162, 329-342.
- RUCHOUX, M. M. & MAURAGE, C. A. 1997. CADASIL: Cerebral Autosomal Dominant Arteriopathy with Subcortical Infarcts and Leukoencephalopathy. *Journal of Neuropathology & Experimental Neurology*, 56, 947-964.
- RUFA, A. 2004. Hemodynamic evaluation of the optic nerve head in cerebral autosomal dominant arteriopathy with subcortical infarcts and leukoencephalopathy. *Archives of Neurology*, 61, 1230-1233.
- RUFA, A., DOTTI, M. T., FRANCHI, M., STROMILLO, M. L., CEVENINI, G., BIANCHI, S., DE STEFANO, N. & FEDERICO, A. 2005. Systemic Blood Pressure Profile in Cerebral Autosomal Dominant Arteriopathy With Subcortical Infarcts and Leukoencephalopathy. *Stroke*, 36, 2554-2558.
- RUFA, A., GUIDERI, F., ACAMPA, M., CEVENINI, G., BIANCHI, S., DE STEFANO, N., STROMILLO, M. L., FEDERICO, A. & DOTTI, M. T. 2007. Cardiac Autonomic Nervous System and Risk of Arrhythmias in Cerebral Autosomal Dominant Arteriopathy With Subcortical Infarcts and Leukoencephalopathy (CADASIL). *Stroke*, 38, 276-280.
- RUFA, A., PRETEGIANI, E., FREZZOTTI, P., DE STEFANO, N., CEVENINI, G., DOTTI, M. T. & FEDERICO, A. 2011. Retinal Nerve Fiber Layer Thinning in CADASIL: An Optical Coherence Tomography and MRI Study. *Cerebrovascular Diseases*, 31, 77-82.
- RUTTEN, J. W., BOON, E. M. J., LIEM, M. K., DAUWERSE, J. G., PONT, M. J., VOLLEBREGT, E., MAAT-KIEVIT, A. J., GINJAAR, H. B., LAKEMAN, P., VAN DUINEN, S. G., TERWINDT, G. M. & LESNIK OBERSTEIN, S. A. J. 2013. Hypomorphic NOTCH3 Alleles Do Not Cause CADASIL in Humans. *Human Mutation*, 34, 1486-1489.
- SAEKI, N., SATO, M., KUBOTA, M., UCHINO, Y., MURAI, H., NAGAI, Y., ISHIKURA, H., NOMURA, S., MATSUURA, I. & YAMAURA, A. 2005. MR Imaging of

- Normal Perivascular Space Expansion at Midbrain. *American Journal of Neuroradiology*, 26, 566-571.
- SALVI, F., MICHELUCCI, R., PLASMATI, R., PARMEGGIANI, L., ZONARI, P., MASCALCHI, M. & TASSINARI, C. A. 1992. Slowly progressive familial dementia with recurrent strokes and white matter hypodensities on CT scan. *The Italian Journal of Neurological Sciences*, 13, 135-140.
- SAUNDERS, K. B. 1980. Methods in the assessment of the control of breathing. *British Journal of Clinical Pharmacology*, 9, 3-9.
- SAVER, J. L., FILIP, B., HAMILTON, S., YANES, A., CRAIG, S., CHO, M., CONWIT, R., STARKMAN, S. & COORDINATORS, F. T. F.-M. I. A. 2010. Improving the Reliability of Stroke Disability Grading in Clinical Trials and Clinical Practice. *Stroke*, 41, 992-995.
- SAX, L. 2003. What was the cause of Nietzsche's dementia? *Journal of Medical Biography*, 11, 47-54.
- SCHEID, R., PREUL, C., LINCKE, T., MATTHES, G., SCHROETER, M. L., GUTHKE, T., YVES VON, C. D. & SABRI, O. 2006. Correlation of cognitive status, MRI- and SPECT-imaging in CADASIL patients. *European Journal of Neurology*, 13, 363-370.
- SCHELTENS, P., BARKHOF, F., LEYS, D., PRUVO, J. P., NAUTA, J. J. P., VERMERSCH, P., STEINLING, M. & VALK, J. 1993. A semiquantitative rating scale for the assessment of signal hyperintensities on magnetic resonance imaging. *Journal of the Neurological Sciences*, 114, 7-12.
- SCHIAVONE, F., CHARLTON, R. A., BARRICK, T. R., MORRIS, R. G. & MARKUS, H. S. 2009. Imaging age-related cognitive decline: A comparison of diffusion tensor and magnetization transfer MRI. *Journal of Magnetic Resonance Imaging*, 29, 23-30.
- SCHMIDT, R., ENZINGER, C., ROPELE, S., SCHMIDT, H. & FAZEKAS, F. 2003. Progression of cerebral white matter lesions: 6-year results of the Austrian Stroke Prevention Study. *The Lancet*, 361, 2046-2048.
- SCHON, F., MARTIN, R. J., PREVETT, M., CLOUGH, C., ENEVOLDSON, T. P. & MARKUS, H. S. 2003. CADASIL coma: an underdiagnosed acute encephalopathy. *Journal of Neurology, Neurosurgery & Psychiatry*, 74, 249-252.
- SCHRÖDER, J. M., ZÜCHNER, S., DICHGANS, M., NAGY, Z. & MOLNAR, M. J. 2005. Peripheral nerve and skeletal muscle involvement in CADASIL. *Acta Neuropathologica*, 110, 587-599.
- SCHULZ, K. F., ALTMAN, D. G. & MOHER, D. 2010. CONSORT 2010 Statement: updated guidelines for reporting parallel group randomised trials. *BMJ*, 340.
- SCHWARZBAUER, C. & DEICHMANN, R. 2012. Vascular component analysis of hyperoxic and hypercapnic BOLD contrast. *NeuroImage*, 59, 2401-2412.
- SCOUTEN, A. & SCHWARZBAUER, C. 2008. Paced respiration with end-expiration technique offers superior BOLD signal repeatability for breath-hold studies. *NeuroImage*, 43, 250-257.
- SELIM, M., JONES, R., NOVAK, P., ZHAO, P. & NOVAK, V. 2008. The effects of body mass index on cerebral blood flow velocity. *Clinical Autonomic Research*, 18, 331-338.
- SHEN, Y., AHEARN, T., CLEMENCE, M. & SCHWARZBAUER, C. 2011. Magnetic resonance imaging of the mean venous vessel size in the human brain using transient hyperoxia. *NeuroImage*, 55, 1063-1067.
- SHIINO, A., MORITA, Y., TSUJI, A., MAEDA, K., ITO, R., FURUKAWA, A., MATSUDA, M. & INUBUSHI, T. 2003. Estimation of cerebral perfusion reserve by blood oxygenation level-dependent imaging: comparison with

- single-photon emission computed tomography. *Journal of Cerebral Blood Flow & Metabolism*, 23, 121-135.
- SHIINO, A., YAMAUCHI, H., MORIKAWA, S. & INUBUSHI, T. 2012. Mapping of cerebral metabolic rate of oxygen using DSC and BOLD MR imaging: a preliminary study. *Magnetic Resonance in Medical Sciences*, 11, 109-115.
- SHINOHARA, T., NAGATA, K., YOKOYAMA, E., SATO, M., MATSUOKA, S., KANNO, I., HATAZAWA, J. & DOMINO, E. F. 2006. Acute effects of cigarette smoking on global cerebral blood flow in overnight abstinent tobacco smokers. *Nicotine and Tobacco Research*, 8, 113-121.
- SINGHAL, S., BEVAN, S., BARRICK, T., RICH, P. & MARKUS, H. S. 2004. The influence of genetic and cardiovascular risk factors on the CADASIL phenotype. *Brain*, 127, 2031-2038.
- SINGHAL, S. & MARKUS, H. S. 2005. Cerebrovascular reactivity and dynamic autoregulation in nondemented patients with CADASIL (cerebral autosomal dominant arteriopathy with subcortical infarcts and leukoencephalopathy). *Journal of Neurology*, 252, 163-167.
- SKINNER, S. L., BARIN, E., GALLERY, E. D. M., BEATTIE, J., AVOLIO, A. & KARMEN, P. A *Clinical Guide: Pulse Wave Analysis*, AtCor Medical Pty Ltd.
- SLESSAREV, M., HAN, J., MARDIMAE, A., PRISMAN, E., PREISS, D., VOLGYESI, G., ANSEL, C., DUFFIN, J. & FISHER, J. A. 2007. Prospective targeting and control of end-tidal CO₂ and O₂ concentrations. *The Journal of Physiology*, 581, 1207-1219.
- SLOAN, M. A., ALEXANDROV, A. V., TEGELER, C. H., SPENCER, M. P., CAPLAN, L. R., FELDMANN, E., WECHSLER, L. R., NEWELL, D. W., GOMEZ, C. R., BABIKIAN, V. L., LEFKOWITZ, D., GOLDMAN, R. S., ARMON, C., HSU, C. Y. & GOODIN, D. S. 2004. Assessment: Transcranial Doppler ultrasonography: Report of the Therapeutics and Technology Assessment Subcommittee of the American Academy of Neurology. *Neurology*, 62, 1468-1481.
- SMART, S. D., FIRBANK, M. J. & O'BRIEN, J. T. 2011. Validation of Automated White Matter Hyperintensity Segmentation. *Journal of Aging Research*, 2011, 5.
- SMITH, S. M. 2002. Fast robust automated brain extraction. *Human Brain Mapping*, 17, 143-155.
- SMITH, S. M., JENKINSON, M., WOOLRICH, M. W., BECKMANN, C. F., BEHRENS, T. E. J., JOHANSEN-BERG, H., BANNISTER, P. R., DE LUCA, M., DROBNJAK, I., FLITNEY, D. E., NIAZY, R., SAUNDERS, J., VICKERS, J., ZHANG, Y., DE STEFANO, N., BRADY, J. M. & MATTHEWS, P. M. 2004. Advances in functional and structural MR image analysis and implementation as FSL. *NeuroImage*, 23, 208-219.
- SNAITH, R. P. & ZIGMOND, A. S. 1994. *The Hospital Anxiety and Depression Scale Manual*, London, GL Assessment.
- SONNINEN, V. & SAVONTAUS, M. L. 1987. Hereditary Multi-Infarct Dementia. *European Neurology*, 27, 209-215.
- SOURANDER, P. & WALINDER, J. 1977. Hereditary multi-infarct dementia. Morphological and clinical studies of a new disease. *Acta Neuropathologica*, 39, 247-254.
- SPALLETTA, G., BOSSU, P., CIARAMELLA, A., BRIA, P., CALTAGIRONE, C. & ROBINSON, R. G. 2006. The etiology of poststroke depression: a review of the literature and a new hypothesis involving inflammatory cytokines. *Molecular Psychiatry*, 11, 984-991.
- SPANO, V. R., MANDELL, D. M., POUBLANC, J., SAM, K., BATTISTI-CHARBONNEY, A., PUCCI, O., HAN, J. S., CRAWLEY, A. P., FISHER, J. A. & MIKULIS, D. J. 2013. CO₂ blood oxygen level-dependent MR mapping of cerebrovascular

- reserve in a clinical population: safety, tolerability, and technical feasibility. *Radiology*, 266, 592-598.
- SPIERS, A. & PADMANABHAN, N. 2005. A guide to wire myography. *Methods in Molecular Medicine*.
- ST CLAIR, D., BOLT, J., MORRIS, S. & DOYLE, D. 1995. Hereditary multi-infarct dementia unlinked to chromosome 19q12 in a large Scottish pedigree: evidence of probable locus heterogeneity. *Journal of Medical Genetics*, 32, 57-60.
- STEIN, J. H., KORCARZ, C. E., HURST, R. T., LONN, E., KENDALL, C. B., MOHLER, E. R., NAJJAR, S. S., REMBOLD, C. M. & POST, W. S. 2008. Use of Carotid Ultrasound to Identify Subclinical Vascular Disease and Evaluate Cardiovascular Disease Risk: A Consensus Statement from the American Society of Echocardiography Carotid Intima-Media Thickness Task Force Endorsed by the Society for Vascular Medicine. *Journal of the American Society of Echocardiography*, 21, 93-111.
- STENBORG, A., KALIMO, H., VIITANEN, M., TERENT, A. & LIND, L. 2007. Impaired Endothelial Function of Forearm Resistance Arteries in CADASIL Patients. *Stroke*, 38, 2692-2697.
- STROHM, J., DUFFIN, J. & FISHER, J. A. 2014. Circadian cerebrovascular reactivity to CO₂. *Respiratory Physiology & Neurobiology*, 197, 15-18.
- STROMILLO, M. L., DOTTI, M. T., BATTAGLINI, M., MORTILLA, M., BIANCHI, S., PLEWNIA, K., PANTONI, L., INZITARI, D., FEDERICO, A. & DE STEFANO, N. 2009. Structural and metabolic brain abnormalities in preclinical cerebral autosomal dominant arteriopathy with subcortical infarcts and leucoencephalopathy. *Journal of Neurology, Neurosurgery & Psychiatry*, 80, 41-47.
- SWEENEY, C., MORROW, D., BIRNEY, Y. A., COYLE, S., HENNESSY, C., SCHELLER, A., CUMMINS, P. M., WALLS, D., REDMOND, E. M. & CAHILL, P. A. 2004. Notch 1 and 3 receptor signaling modulates vascular smooth muscle cell growth, apoptosis, and migration via a CBF-1/RBP-Jk dependent pathway. *The FASEB Journal*, 18, 1421-1423.
- TAKAHASHI, K., ADACHI, K., YOSHIZAKI, K., KUNIMOTO, S., KALARIA, R. N. & WATANABE, A. 2010. Mutations in NOTCH3 cause the formation and retention of aggregates in the endoplasmic reticulum, leading to impaired cell proliferation. *Human Molecular Genetics*, 19, 79-89.
- TATSCH, K., KOCH, W., LINKE, R., POEPPERL, G., PETERS, N., HOLTMANN-SPOETTER, M. & DICHGANS, M. 2003. Cortical Hypometabolism and Crossed Cerebellar Diaschisis Suggest Subcortically Induced Disconnection in CADASIL: An 18F-FDG PET Study. *Journal of Nuclear Medicine*, 44, 862-869.
- TAYLOR, N. J., BADDELEY, H., GOODCHILD, K. A., POWELL, M. E., THOUMINE, M., CULVER, L. A., STIRLING, J. J., SAUNDERS, M. I., HOSKIN, P. J., PHILLIPS, H., PADHANI, A. R. & GRIFFITHS, J. R. 2001. BOLD MRI of human tumor oxygenation during carbogen breathing. *Journal of Magnetic Resonance Imaging*, 14, 156-163.
- THE NEUROLOGICAL ALLIANCE 2003. Neuro Numbers: A brief review of the numbers of people in the UK with a neurological condition.
- THOMASON, M. E., BURROWS, B. E., GABRIELI, J. D. & GLOVER, G. H. 2005. Breath holding reveals differences in fMRI BOLD signal in children and adults. *Neuroimage*, 25, 824-837.
- THOMASON, M. E., FOLAND, L. C. & GLOVER, G. H. 2007. Calibration of BOLD fMRI using breath holding reduces group variance during a cognitive task. *Human Brain Mapping*, 28, 59-68.

- THOMASON, M. E. & GLOVER, G. H. 2008. Controlled inspiration depth reduces variance in breath-holding-induced BOLD signal. *Neuroimage*, 39, 206-214.
- TIKKA, S., MYKKANEN, K., RUCHOUX, M. M., BERGHOLM, R., JUNNA, M., POYHONEN, M., YKI-JARVINEN, H., JOUTEL, A., VIITANEN, M., BAUMANN, M. & KALIMO, H. 2009. Congruence between NOTCH3 mutations and GOM in 131 CADASIL patients. *Brain*, 132, 933-939.
- TOPAKIAN, R., BARRICK, T. R., HOWE, F. A. & MARKUS, H. S. 2010. Blood brain barrier permeability is increased in normal-appearing white matter in patients with lacunar stroke and leucoaraiosis. *Journal of Neurology, Neurosurgery & Psychiatry*, 81, 192-197.
- TOURNIER-LASSERVE, E., IBA-ZIZEN, M. T., ROMERO, N. & BOUSSER, M. G. 1991. Autosomal dominant syndrome with strokelike episodes and leukoencephalopathy. *Stroke*, 22, 1297-1302.
- TSAI, W.-C., LI, Y.-H., LIN, C.-C., CHAO, T.-H. & CHEN, J.-H. 2004. Effects of oxidative stress on endothelial function after a high-fat meal. *Clinical Science*, 106, 315-319.
- TUOMINEN, S., MIAO, Q., KURKI, T., TUISKU, S., PÖYHÖNEN, M., KALIMO, H., VIITANEN, M., SIPILÄ, H., BERGMAN, J. & RINNE, J. O. 2004. Positron Emission Tomography Examination of Cerebral Blood Flow and Glucose Metabolism in Young CADASIL Patients. *Stroke*, 35, 1063-1067.
- VAGAL, A. S., LEACH, J. L., FERNANDEZ-ULLOA, M. & ZUCCARELLO, M. 2009. The acetazolamide challenge: techniques and applications in the evaluation of chronic cerebral ischemia. *American Journal of Neuroradiology*, 30, 876-884.
- VALENTI, R., PESCHINI, F., ANTONINI, S., CASTELLINI, G., POGGESI, A., BIANCHI, S., INZITARI, D., PALLANTI, S. & PANTONI, L. 2011. Major depression and bipolar disorders in CADASIL: a study using the DSM-IV semi-structured interview. *Acta Neurologica Scandinavica*, no-no.
- VALENTI, R., POGGESI, A., PESCHINI, F., INZITARI, D. & PANTONI, L. 2008. Psychiatric disturbances in CADASIL: a brief review. *Acta Neurologica Scandinavica*, 118, 291-295.
- VAN BOGAERT, L. 1955. Encephalopathie sous-corticale progressive (Binswanger) a evolution rapide chez deux soeurs. *Med Hellen*, 24, 961-972.
- VAN BORTEL, L., DUPREZ, D., STARMANS-KOOL, M., SAFAR, M., GIANNATTASIO, C., COCKCROFT, J., KAISER, D. & THUILLEZ, C. 2002. Clinical applications of arterial stiffness, Task Force III: recommendations for user procedures. *American Journal of Hypertension*, 15, 445-452.
- VAN DEN BOOM, R., LESNICK OBERSTEIN, S. A. J., BERG-HUYSMANS, A. A., FERRARI, M. D., VAN BUCHEM, M. A. & HAAN, J. 2006. Cerebral Autosomal Dominant Arteriopathy with Subcortical Infarcts and Leukoencephalopathy: Structural MR Imaging Changes and Apolipoprotein E Genotype. *American Journal of Neuroradiology*, 27, 359-362.
- VAN DEN BOOM, R., LESNIK OBERSTEIN, S. A., SPILT, A., BEHLOUL, F., FERRARI, M. D., HAAN, J., WESTENDORP, R. G. & VAN BUCHEM, M. A. 2003a. Cerebral Hemodynamics and White Matter Hyperintensities in CADASIL. *Journal of Cerebral Blood Flow & Metabolism*, 23, 599-604.
- VAN DEN BOOM, R., LESNIK OBERSTEIN, S. A. J., FERRARI, M. D., HAAN, J. & VAN BUCHEM, M. A. 2003b. Cerebral Autosomal Dominant Arteriopathy with Subcortical Infarcts and Leukoencephalopathy: MR Imaging Findings at Different Ages —3rd –6th Decades. *Radiology*, 229, 683-690.
- VAN DEN BOOM, R., LESNIK OBERSTEIN, S. A. J., VAN DUINEN, S. G., BORNEBROEK, M., FERRARI, M. D., HAAN, J. & VAN BUCHEM, M. A. 2002. Subcortical Lacunar Lesions: An MR Imaging Finding in Patients with

- Cerebral Autosomal Dominant Arteriopathy with Subcortical Infarcts and Leukoencephalopathy¹. *Radiology*, 224, 791-796.
- VAN GELDEREN, P., DE ZWART, J. A. & DUYN, J. H. 2008. Pitfalls of MRI measurement of white matter perfusion based on arterial spin labeling. *Magnetic Resonance in Medicine*, 59, 788-795.
- VAN SWIETEN, J. C., KOUDSTAAL, P. J., VISSER, M. C., SCHOUTEN, H. J. & VAN GIJN, J. 1988. Interobserver agreement for the assessment of handicap in stroke patients. *Stroke*, 19, 604-7.
- VESELY, A., SASANO, H., VOLGYESI, G., SOMOGYI, R., TESLER, J., FEDORKO, L., GRYNSPAN, J., CRAWLEY, A., FISHER, J. A. & MIKULIS, D. 2001. MRI mapping of cerebrovascular reactivity using square wave changes in end-tidal PCO₂. *Magnetic Resonance in Medicine*, 45, 1011-1013.
- VISWANATHAN, A. & CHABRIAT, H. 2006. Cerebral Microhemorrhage. *Stroke*, 37, 550-555.
- VISWANATHAN, A., GODIN, O., JOUVENT, E., O'SULLIVAN, M., GSCHWENDTNER, A., PETERS, N., DUERING, M., GUICHARD, J. P., HOLTMANNSPÖTTER, M., DUFOUIL, C., PACHAI, C., BOUSSER, M. G., DICHGANS, M. & CHABRIAT, H. 2010. Impact of MRI markers in subcortical vascular dementia: A multi-modal analysis in CADASIL. *Neurobiology of Aging*, 31, 1629-1636.
- VISWANATHAN, A., GRAY, F., BOUSSER, M. G., BAUDRIMONT, M. & CHABRIAT, H. 2006a. Cortical Neuronal Apoptosis in CADASIL. *Stroke*, 37, 2690-2695.
- VISWANATHAN, A., GSCHWENDTNER, A., GUICHARD, J.-P., BUFFON, F., CUMURCIUC, R., O'SULLIVAN, M., HOLTMANNSPÖTTER, M., PACHAI, C., BOUSSER, M.-G., DICHGANS, M. & CHABRIAT, H. 2007. Lacunar lesions are independently associated with disability and cognitive impairment in CADASIL. *Neurology*, 69, 172-179.
- VISWANATHAN, A., GUICHARD, J. P., GSCHWENDTNER, A., BUFFON, F., CUMURCIUC, R., BOUTRON, C., VICAUT, E., HOLTMANNSPÖTTER, M., PACHAI, C., BOUSSER, M. G., DICHGANS, M. & CHABRIAT, H. 2006b. Blood pressure and haemoglobin A1c are associated with microhaemorrhage in CADASIL: a two-centre cohort study. *Brain*, 129, 2375-2383.
- VOGT, K. M., IBINSON, J. W., SCHMALBROCK, P. & SMALL, R. H. 2011. Comparison between end-tidal CO₂ and respiration volume per time for detecting BOLD signal fluctuations during paced hyperventilation. *Magnetic Resonance Imaging*, 29, 1186-1194.
- VORSTRUP, S., HENRIKSEN, L. & PAULSON, O. B. 1984. Effect of acetazolamide on cerebral blood flow and cerebral metabolic rate for oxygen. *Journal of Clinical Investigation*, 74, 1634-1639.
- WALTERS, M., MUIR, S., SHAH, I. & LEES, K. 2004. Effect of Perindopril on Cerebral Vasomotor Reactivity in Patients With Lacunar Infarction. *Stroke*, 35, 1899-1902.
- WANG, Z., YUAN, Y., ZHANG, W., LV, H., HONG, D., CHEN, B., LIU, Y., LUAN, X., XIE, S. & WU, S. 2011. NOTCH3 mutations and clinical features in 33 mainland Chinese families with CADASIL. *Journal of Neurology, Neurosurgery & Psychiatry*, 82, 534-539.
- WARDLAW, J. M. 2008. What Is a Lacune? *Stroke*, 39, 2921-2922.
- WARDLAW, J. M., SMITH, E. E., BIESSELS, G. J., CORDONNIER, C., FAZEKAS, F., FRAYNE, R., LINDLEY, R. I., O'BRIEN, J. T., BARKHOF, F., BENAVENTE, O. R., BLACK, S. E., BRAYNE, C., BRETELER, M., CHABRIAT, H., DECARLI, C., DE LEEUW, F. E., DOUBAL, F., DUERING, M., FOX, N. C., GREENBERG, S., HACHINSKI, V., KILIMANN, I., MOK, V., OOSTENBRUGGE, R. V., PANTONI, L., SPECK, O., STEPHAN, B. C. M., TEIPEL, S., VISWANATHAN, A., WERRING, D., CHEN, C., SMITH, C., VAN BUCHEM, M., NORRVING, B.,

- GORELICK, P. B. & DICHGANS, M. 2013. Neuroimaging standards for research into small vessel disease and its contribution to ageing and neurodegeneration. *The Lancet Neurology*, 12, 822-838.
- WASHINGTON STATE DEPARTMENT OF HEALTH 2002. Guidelines for using confidence intervals for public health assessment.
- WATANABE-HOSOMI, A., WATANABE, Y., TANAKA, M., NAKAGAWA, M. & MIZUNO, T. 2012. Transendocytosis is impaired in CADASIL-mutant NOTCH3. *Experimental Neurology*.
- WATSON, N. A., BEARDS, S. C., ALTAFF, N., KASSNER, A. & JACKSON, A. 2000. The effect of hyperoxia on cerebral blood flow: a study in healthy volunteers using magnetic resonance phase-contrast angiography. *European Journal of Anaesthesiology*, 17, 152-159.
- WEI, E. P., KONTOS, H. A. & PATTERSON, J. L. 1980. Dependence of pial arteriolar response to hypercapnia on vessel size. *American Journal of Physiology*, 238, 697-702.
- WEIMAR, C., KÖNIG, I. R., KRAYWINKEL, K., ZIEGLER, A., DIENER, H. C. & ON BEHALF OF THE GERMAN STROKE STUDY COLLABORATION 2004. Age and National Institutes of Health Stroke Scale Score Within 6 Hours After Onset Are Accurate Predictors of Outcome After Cerebral Ischemia. *Stroke*, 35, 158-162.
- WERBROUCK, B. F. & DE BLEECKER, J. L. 2006. Intracerebral haemorrhage in CADASIL. A case report. *Acta Neurologica Belgica*, 106, 219-221.
- WESTBROOK, C., KAUT ROTH, C. & TALBOT, J. 2011. *MRI in Practice*, UK, Blackwell Publishing Ltd.
- WILSON, J. T. L., HAREENDRAN, A., GRANT, M., BAIRD, T., SCHULZ, U. G. R., MUIR, K. W. & BONE, I. 2002. Improving the Assessment of Outcomes in Stroke: Use of a Structured Interview to Assign Grades on the Modified Rankin Scale. *Stroke*, 33, 2243-2246.
- WINTERMARK, M., SESAY, M., BARBIER, E., BORBÉLY, K., DILLON, W. P., EASTWOOD, J. D., GLENN, T. C., GRANDIN, C. B., PEDRAZA, S., SOUSTIEL, J.-F., NARAI, T., ZAHARCHUK, G., CAILLÉ, J.-M., DOUSSET, V. & YONAS, H. 2005. Comparative Overview of Brain Perfusion Imaging Techniques. *Stroke*, 36, e83-e99.
- WISE, R. G., PATTINSON, K. T., BULTE, D. P., CHIARELLI, P. A., MAYHEW, S. D., BALANOS, G. M., O'CONNOR, D. F., PRAGNELL, T. R., ROBBINS, P. A., TRACEY, I. & JEZZARD, P. 2007. Dynamic forcing of end-tidal carbon dioxide and oxygen applied to functional magnetic resonance imaging. *Journal of Cerebral Blood Flow & Metabolism*, 27, 1521-1532.
- WOLLENWEBER, F. A., HANECKER, P., BAYER-KARPINSKA, A., MALIK, R., BÄZNER, H., MORETON, F., MUIR, K. W., MÜLLER, S., GIESE, A., OPPERK, C., DICHGANS, M., HAFFNER, C. & DUERING, M. 2015. Cysteine-Sparing CADASIL Mutations in NOTCH3 Show Proaggregatory Properties In Vitro. *Stroke*, 46, 786-792.
- WORLD HEALTH ORGANISATION 2006. Neurological Disorders: Public Health Challenges. Switzerland.
- WU, B., LOU, X., WU, X. & MA, L. 2014. Intra- and interscanner reliability and reproducibility of 3D whole-brain pseudo-continuous arterial spin-labeling MR perfusion at 3T. *Journal of Magnetic Resonance Imaging*, 39, 402-409.
- XU, F., LIU, P., PASCUAL, J. M., XIAO, G. & LU, H. 2012. Effect of hypoxia and hyperoxia on cerebral blood flow, blood oxygenation, and oxidative metabolism. *Journal of Cerebral Blood Flow & Metabolism*, 32, 1909-1918.

- XU, G., ROWLEY, H. A., WU, G., ALSOP, D. C., SHANKARANARAYANAN, A., DOWLING, M., CHRISTIAN, B. T., OAKES, T. R. & JOHNSON, S. C. 2010. Reliability and precision of pseudo-continuous arterial spin labeling perfusion MRI on 3.0 T and comparison with 15O-water PET in elderly subjects at risk for Alzheimer's disease. *NMR in Biomedicine*, 23, 286-293.
- YAO, M., JOUVENT, E., DURING, M., GODIN, O., HERVE, D., GUICHARD, J. P., ZHU, Y. C., GSCHWENDTNER, A., OPPERK, C., DICHGANS, M. & CHABRIAT, H. 2012. Extensive white matter hyperintensities may increase brain volume in cerebral autosomal-dominant arteriopathy with subcortical infarcts and leukoencephalopathy. *Stroke*, 43, 3252-3257.
- YEBOAH, J., FOLSOM, A. R., BURKE, G. L., JOHNSON, C., POLAK, J. F., POST, W., LIMA, J. A., CROUSE, J. R. & HERRINGTON, D. M. 2009. Predictive Value of Brachial Flow-Mediated Dilation for Incident Cardiovascular Events in a Population-Based Study: The Multi-Ethnic Study of Atherosclerosis. *Circulation*, 120, 502-509.
- YETKIN, F. Z. & MENDELSON, D. 2002. Hypoxia imaging in brain tumors. *Neuroimaging Clinics of North America*, 12, 537 - 552.
- ZHANG, Y., BRADY, M. & SMITH, S. 2001. Segmentation of brain MR images through a hidden Markov random field model and the expectation-maximization algorithm. *Medical Imaging, IEEE Transactions on*, 20, 45-57.
- ZHAO, P., ALSOP, D. C., ABDULJALIL, A., SELIM, M., LIPSITZ, L., NOVAK, P., CAPLAN, L., HU, K. & NOVAK, V. 2009. Vasoreactivity and peri-infarct hyperintensities in stroke. *Neurology*, 72, 643-649.
- ZHU, Y. C., DUFOUIL, C., MAZOYER, B., SOUMARÉ, A., RICOLFI, F., TZOURIO, C. & CHABRIAT, H. 2011. Frequency and Location of Dilated Virchow-Robin Spaces in Elderly People: A Population-Based 3D MR Imaging Study. *American Journal of Neuroradiology*, 32, 709-713.
- ZIGMOND, A. S. & SNAITH, R. P. 1983. The Hospital Anxiety and Depression Scale. *Acta Psychiatrica Scandinavica*, 67, 361-370.